UNIVERSITÀ DEGLI STUDI DI UDINE
hic sunt futura

www.uniud.it

Corso di dottorato di ricerca in:

"Scienze Biomediche e Biotecnologiche"

XXXII Ciclo

Titolo della tesi

"Endocrine and nutritional factors promoting WAT to BAT conversion"

Dottorando
dott. Tommaso Montanari

Supervisore
prof. Monica Colitti

Co-supervisore
prof. Luisa Dalla Valle

Anno 2020

To my dad, the strongest part of my heart

To my mum, the brightest side of my mind

To Tania and Laura, the eyes that showed me the world

Abstract

The process of white adipose tissue (WAT) browning has become a key focus topic in adipobiology research, due to its fat burning potential in obesity treatment. The interest in brown adipose tissue (BAT) derives from its unique ability to generate heat by adaptive thermogenesis. This process mediates the catabolism of energy substrates without the generation of ATP. Therefore, energy dissipation by BAT can control obesity by leading excess fat towards heat production. While brown adipocytes are rich in mitochondria and small lipid droplets (multilocular adipocytes), white adipocytes have few mitochondria and a single large lipid droplet (unilocular adipocytes). Moreover, uncoupling protein 1, the main driver of thermogenesis, is present only on the inner mitochondrial membrane of brown adipocytes, where it uncouples the oxidative phosphorylation from ATP synthesis.

The research presented in this doctoral thesis involves the administration of endogenous and nutritional compounds to *in vitro* adipocyte models to evaluate their potential in inducing WAT browning. The chosen compounds are two myokines (β-aminoisobutyric acid and brain-derived neurotrophic factor) and two nutritional molecules (capsaicin and *cis*-9 retinoic acid). The effectiveness and the long-term effects of these biocompounds were here investigated in terms of lipid droplets and mitochondria structural changes on different cellular models.

The results hereby discussed confirmed the potential of these bioactive compounds in inducing WAT browning, in agreement with previous knowledge and bringing new insights in this research field. Novel observations concerning doses and time-dependent effects of these browning fac-

tors could direct future research towards a correct and effective implementation of anti-obesity therapies.

Contents

Part I

Introduction

Chapter 1

The adipose tissue

Adipose tissue (AT) is a connective tissue composed by different cell types. The main cells constituting AT are the lipid-accumulating adipocytes. Other cell types include preadipocytes, macrophages, endothelial cells, stem cells and nerve endings. Taken together, these cell types represent the stromal-vascular fraction (SVF) [1].

Conventionally, AT is divided into two different subtypes: white adipose tissue (WAT) and brown adipose tissue (BAT).

1.1 White adipose tissue

In past decades, WAT was associated to the sole function of passive storage of excess energy coming from food in form of triacylglycerols (TAGs). Afterwards, researches described the endocrine function of white adipocytes, able to produce a great variety of adipose-derived hormones and cytokines, named adipokines, and to participate in the metabolism of sex hormones [1].

From a histological point of view, WAT is composed by large adipocytes (around 100 µm diameter) whose cytoplasm is almost entirely filled with a unilocular lipid droplet (LD) that pushes the nucleus against the plasma membrane. WAT forms depots in different parts of the body and the distribution of mass in each depot depends on genetics, age and sensitivity to

glucocorticoids and other hormones [2]. According to the impact of WAT depots on metabolic health, WAT can be divided into visceral WAT (vWAT) and subcutaneous WAT (scWAT). Visceral WAT is associated to metabolic disease, such as dyslipidemia, obesity, type 2 diabetes mellitus, cardiovascular disease, hepatic steatosis and some forms of cancer; scWAT is associated with a decreased risk of developing metabolic syndrome [3].

Anatomically, WAT depots can be classified in mice as follows, according to Waldén and colleagues [4] (Figure 1.1):

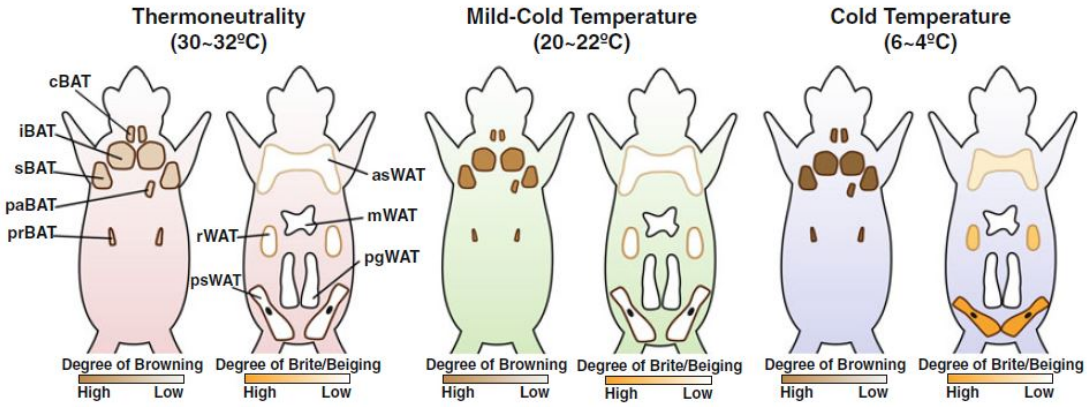

Figure 1.1: Localization of WAT and BAT depots in mouse, modified from Jung *et al.* [5]

- anterior subcutaneous WAT (asWAT), which includes axillary and interscapular fat;
- inguinal WAT (iWAT), dorsal to the pelvis;
- perigonadal WAT (pgWAT), which surroundes epididymis and testes in male, ovaries and uterus in female;
- retroperitoneal WAT (rpWAT), which is in the abdominal cavity behind kidneys;
- mesenteric WAT (mWAT), which surroundes visceral organs.

A similar classification is proposed for human WAT depots by Wronska *et al.* [6] (Figure 1.2):

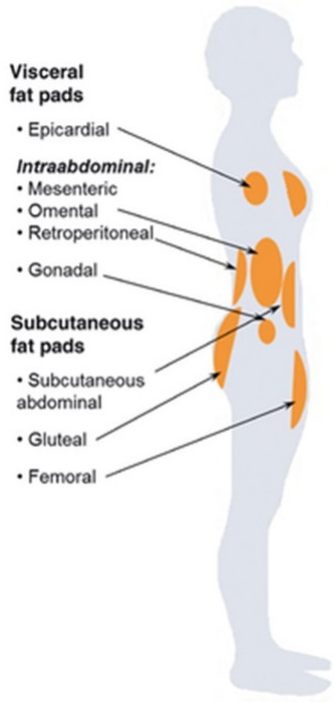

Figure 1.2: Localization of WAT fat pads in human, modified from Wronska *et al.* [6]

- scWAT depots: subcutaneous abdominal, gluteal and femoral;
- vWAT depots: epicardial, mesenteric, omental, retroperitoneal and gonadal.

The cellularity of WAT is determined in early life and renewal of senescent adipocytes occurs constantly during lifetime [7], although the rate of adipocyte turnover is still matter of debate [8–10]. Albeit adipocyte age and turnover are not affected by body mass index (BMI) [9], cellular growth and expansion are depot-specific and respond differently to high-fat diet [11]. AT expansion by hyperplasia (i.e. increase of cellular number) is a feature of scWAT in femoral and gluteal depots, while vWAT is more prone to hypertrophy (i.e. increase of cellular volume) [12].

The excessive expansion of WAT depots is a pathological state known as obesity, whose deleterious effects on whole body health state are a consequence of the changes in adipocyte number and size [13]. Abdominal adipocytes can increase their volume until they reach a critical size [14]

before cell death occurs. When this happens, new preadipocytes are stimulated to differentiate from SVF into mature adipocytes to increase the storage capacity of the WAT depot. Adipocyte death recruits macrophages, which remove the cellular debrits [15]. When multiple adipocytes reach their critical size and face apoptosis, a high number of macrophages is recruited and an inflammatory response is triggered in the depot [16]. This causes the release of proinflammatory cytokines that alter the functionality of living adipocytes and promote the synthesis of lipid mediators. These molecules interfere with insulin signaling, eventually leading to the insurgence of insulin resistance and type 2 diabetes mellitus [16].

1.1.1 Origins of white adipocytes

Since mature adipocytes cannot divide by mitosis, the development of new adipocytes involves progenitor cells located in SVF [2]. The presence of different cell surface markers on SVF stem cells allows to distinguish populations with the ability to give rise to functional adipocytes from those which will not committ into fat cells; moreover, most of these markers are depot-specific [11].

In past decades, it was rather spreaded the simplistic convintion that, at embryonal level, adipocyte precursors were of exclusively mesodermic origin [17]. Recent findings confirmed that adipocytes forming depots in the cephalic area derive from at least two kinds of precursors in the neural crest [18]. The neural crest $Sox10^{+}$ adipogenic lineage is the main contributor to the cephalic depots [19]. Since they decrease with age, they are replaced by another lineage who shares similar metabolic profiles, hence the derived differentiated adipocytes have the same characteristics [18]. Moreover, also bone marrow is a source of adipogenic precursors: experiments of bone marrow transplants revealed that hematopoietic cells turned into adipocytes in several depots in mice [20].

In adult AT, the main adipose progenitors are mesenchymal stem cells

(MSCs) expressing platelet-derived growth factor receptor α (PDGFRα). These cells can be either positive or negative for CD24. MSCs CD24$^+$ appear to be more committed to the adipogenic lineage, despite they are much less frequent than CD24$^-$ ones [21, 22]. A subpopulation of perivascular MSCs PDGFRα^+ may give rise to both white and brown adipocytes. They express Sca1 and CD34, but are negative for other pericyte markers [21].

Endothelial cells may become white or brown adipocytes as well: ZFP423$^+$ cells can give rise to mature adipocytes [23]. Also VE-cadherin$^+$ endothelial cells may become adipogenic, but they are not evenly distributed [24]. An important study identified PDGFRβ^+ mural cells in adipose SVF as adipose progenitors, individuating the endothelium of adipose blood vessels as a niche of future adipocytes [25]. These cells are committed to become fat cells during embryonic life or in the perinatal period [25].

1.1.2 White adipogenesis

In many species, WAT formation begins before birth and then rapidly increases in the post-natal life [26]. Adipose precursors are recruited from stem cells and then differentiate into mature adipocytes through a process named adipogenesis. The presence of different types of precursors in various WAT depots explains the depot-specific metabolic and growth differences [11]. The adipogenic machinery can be activated by different stimuli, such as a number of extracellular factors including bone morphogenetic proteins (BMPs), transforming growth factor β (TGFβ), insulin-like growth factor 1 (IGF1) and different fibroblast growth factors (FGFs) [27]. The inhibition of anti-adipogenic Wnt [28] and hedgehog [29] signaling pathways can also trigger adipogenesis (Figure 1.3). Moreover, intracellular pathways and regulators, such as glutathione, Janus kinase-signal transducer and activator of transcription 3 (JAK-STAT3) and insulin transduction cascade, have a role in favoring adipogenesis [27].

Pro-adipogenic stimuli upregulate the transcription of early adipogenic

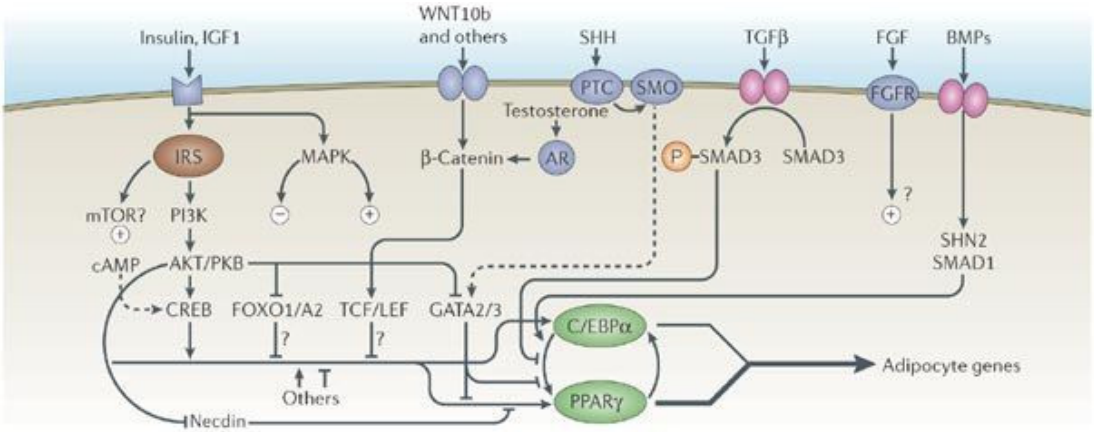

Figure 1.3: Transcriptional networks regulating adipogenesis in white fat cells. IGF1: insulin-like growth factor; WNT10b: Wnt family member 10B; SHH: sonic hedgehog signaling molecule; PTC: protein patched homolog 1; SMO: smoothened; TGFβ: transforming growth factor β; SMAD: mothers against decapentaplegic homolog; FGF: fibroblast growth factor; FGFR: FGF receptor; BMPs: bone morphogenetic proteins; IRS: insulin receptor substrate; MAPK: mitogen-activated protein kinase; AR: androgen receptor; SHN2: schnurri-2; mTOR: mammalian target of rapamycin; PI3K: phosphoinositide 3-kinase; cAMP: cyclic adenosine monophosphate; AKT/PKB: protein kinase B; CREB: cAMP-responsive element-binding protein; FOXO1: forkhead box protein O1; FOXA2: forkhead box protein A2; TCF/LEF: T-cell factor/lymphoid enhancer-binding factor; C/EBPα: CAAT/enhancer-binding protein α; PPARγ: peroxisome proliferator-activated receptor γ; GATA: globin transcription factor. From Rosen & MacDougald [30].

factors CAAT/enhancer-binding protein β (C/EBPβ) and C/EBPδ. These two proteins promote the synthesis of key adipogenic transcription factors C/EBPα, peroxisome proliferator-activated receptor γ (PPARγ), and of sterol regulatory element binding protein 1 (SREBP1), which positively regulate lipogenic genes. C/EBPα enhances PPARγ expression and vice versa in a positive feedback loop (Figure 1.3). These elements are key regulators of adipogenesis because they affect the expression of a wide spectrum of genes involved in lipid metabolism and insulin sensitivity [27]. In particular, PPARγ recruits different histone deacetylases (HDACs) and histone acetyltransferases (HATs) that have multiple effects on adipogenesis-related genes [31].

The pro-adipogenic transcriptional network is tightly regulated by a number of enhancing and inhibiting genes and factors, as reported in Figure 1.3, some of which have not been identified yet.

The epigenetic control of adipogenesis involves many histone-modificator enzymes and a complex net of adipose-specific micro RNAs (miRNAs), including both positive and negative regulators, as extensively reviewed by Engin [32].

The transcriptional machinery that controls adipogenesis may slightly vary between different depots: the ablation of certain adipogenic genes may impair adipogenesis in some depots, while other ones are uneffected. The only factor whose deletion is detrimental for all depots is PPARγ [7].

1.2 Brown adipose tissue

Numerous and important differences distinguish WAT from BAT. Indeed, brown adipocytes have many unique morphological and phenotypic characteristics. These cells are far smaller than white adipocytes (about 40 µm of diameter), with a circular central nucleus and lipids that are accumulated in a high number of small LDs surrounded by a branched network of mitochondria [33].

Among Mammals, BAT has a very different distribution, being mostly displayed in rodents and hibernating animals. In humans, BAT was believed to be widespread in neonatal period and to disappear while going through adult life. Only recently, active BAT has been observed in adult humans following ^{18}F-deoxyglucose positron emission tomography (^{18}FDG PET) combined with X-ray computerized tomography (CT) imaging [34–36]. Unlike WAT depots, BAT is accumulated in few discrete regions in adult human (Figure 1.4), which are richer in blood vessels and nerve endings [37]. Subcutaneous BAT is present in the cervical area, flanking anterior neck muscles, in the anterior abdominal wall and in the inguinal region. A perivascular portion is also present around common carotid artery,

aorta, brachiocephalic artery and epicardial coronary artery. Moreover, visceral BAT depots are present in close proximity of pericardium, kidneys, adrenal glands, pancreas and liver.

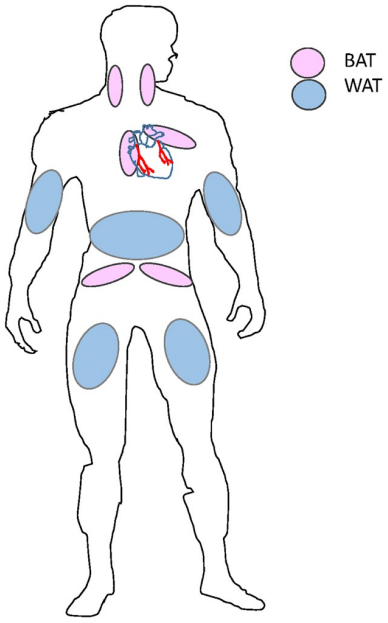

Figure 1.4: Distribution of BAT depots compared to WAT ones in adult humans. From Jeremic *et al.* [37].

In mice, BAT depots are found in interscapular, subscapular and cervical regions and surround portions of aorta and kidneys [2], as displayed in Figure 1.1.

The functional significance of BAT resides in its ability to perform thermogenesis, a process by which the catabolism of high energy substrates, like fatty acids (FAs) or carbohydrates, is uncoupled from the synthesis of ATP in mitochondria, hence the energy of these molecules is released in form of heat [33]. The main driver of this process is the uncoupling protein 1 (UCP1), expressed in the inner mitochondrial membrane of brown adipocytes [38].

1.2.1 Development of brown adipocytes

The main precursor of brown adipocytes is the same that can differentiate into myocytes, but not into white fat cells [2]. These precursors express

a whole set of pro-myogenic factors, including the myogenic factor 5 (Myf5) [39]. The paired box factors 3 and 7 (Pax3 and Pax7) also contribute normally to myogenesis, thus are expressed in the BAT-committed progenitors as well [40]. According to these observations, the developmental routes that contribute to the formation of WAT and BAT depots are completely different and brown adipocytes appear to be closer to myocytes than to white adipocytes (Figure 1.5).

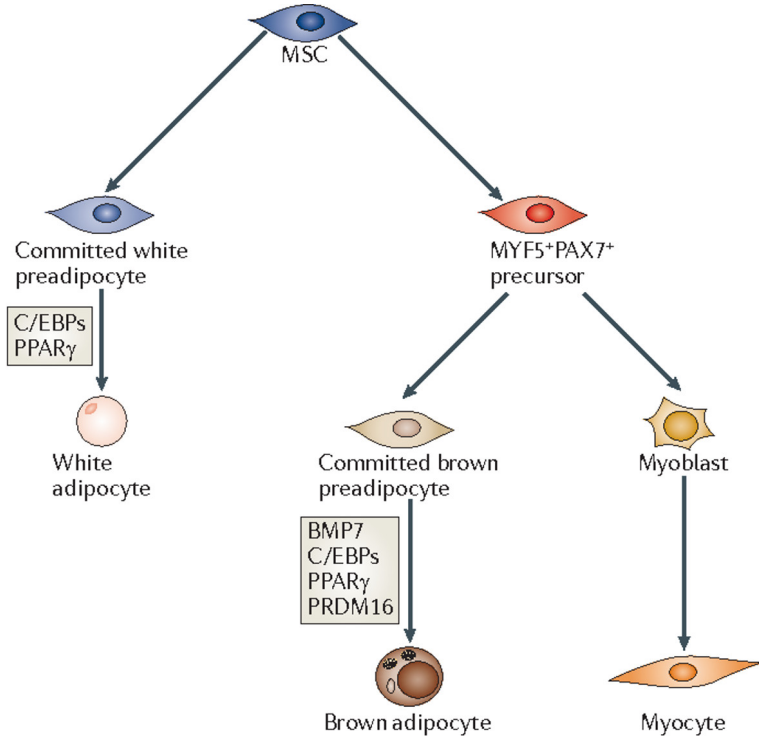

Figure 1.5: Pathways to the development of white and brown adipocytes. Modified from Cristancho *et al.* [41].

Novel findings have refuted this hypothesis [42] and led to the formulation of two different models for Myf5$^+$ cells contribution to the development of adipocytes. According to the first model, proposed in [42], Myf5$^+$ (and possibly Pax3$^+$) cells are spatially mixed with Myf5$^-$ precursors in the same depots. The relative abundance of the two cell types is a function of the depot itself. For instance, in murine BAT depots will preveal Myf5$^+$ progenitors and in inguinal WAT the Myf5$^-$ lineage will be the most abundant. In other WAT depots, like subcutaneous one, the two populations

are more equally distributed. Despite this heterogeneity, the recruitment of adipocyte progenitors is quite selective: while in BAT and subcutaneous WAT the Myf5^{+} will differentiate into mature adipocytes, in inguinal WAT the Myf5^{-} is favored. The second model described in [42] proposes that the expression of Myf5 and Pax3 might occur later in time, during recruitment or differentiation, hence the majority of adipogenic precursors in different depots should be Myf5^{-} [2].

The recruited brown preadipocytes differentiate into mature fat cells with a transduction cascade mostly similar to that previously described for WAT. PPARγ remains the key transcription factor of adipogenesis, but C/EBPα is not as fundamental as it is in white adipocytes [43]. Nevertheless, PPARγ function is supported by important brown-specific factors during adipogenesis, which are PPARγcoactivator 1α (PGC-1α) and PRD1-BF-1-RIZ1 homologous domain containing protein 16 (PRDM16). PGC-1α has a crucial role in the development of mature brown adipocytes, as it positively induces mitochondrial biogenesis and oxidative metabolism and upregulates many thermogenic genes, including UCP1 [44]. Despite its role in promoting thermogenesis, the ablation of PGC-1α has no effect on total BAT mass [43]. PRDM16 is a key determinant of brown fat fate. When expressed in preadipocytes and myoblasts, it can induce a complete brown adipose phenotype [45]. Its effects are achieved by the physical interaction with several DNA-binding factors (including PPARs, PGC-1α and C/EBPs), rather than the direct interaction with DNA [45]. Its depletion from brown preadipocytes induces the emergence of a muscular phenotype [46]. The differentiation of novel brown adipocytes is timed by the induction of PRDM16: despite its regulatory pathway is mostly unknown, BMPs have been recently found to be involved in this regulation. The most critical member seems to be BMP7, which can induce PRDM16 enhancing brown, but not white, adipogenesis [47].

1.3 Thermogenesis

As mentioned above, thermogenesis is the physiological process that enables brown adipocytes to produce heat instead of ATP following the catabolism of high energy substrates. It is also called non-shivering thermogenesis because the spastic contraction of subcutaneous muscles is not involved in heat generation [33].

The so-called cold-induced thermogenesis is the response of the body to a decrease in external temperature and is triggered by the hypothalamus (Figure 1.6) to counterbalance the loss of energy induced by the variation in the thermal condition [48]. The perception of a modification in external temperature is sensed by thermal sensory receptors on skin, which transmit a signal to primary sensory neurons in dorsal root ganglia, which in turn transfer the information to the dorsal horn. A glutamatergic signal is sent to subnuclei of the lateral parabrachial nucleus and then to the preoptic area of the hypothalamus. Here, a stimulatory response activates W-S neurons in the dorsomedial hypothalamus which in turn stimulate BAT sympathetic premotor neurons in rostral raphe pallidus. This signal propagates to BAT sympathetic preganglionic neurons in the intermediolateral nucleus, activating the peripheral release of norepinephrine (NE) in BAT nerve ends [49].

The brown adipocyte expresses membrane β_3-adrenoreceptors (β_3-ARs) activated by the NE surge caused by cold exposure. The entity of heat production depends on the level of sympathetic activation, the quantity of released NE and the amount of NE efficiently binding β_3-ARs [50]. The activated β_3-ARs stimulate the production of cyclic adenosine monophosphate (cAMP) by the enzyme adenylyl cyclase (AC) via the activity of associated stimulatory G protein. The elevated cAMP intracellular level is important for the activation of protein kinase A (PKA), a key enzyme with multiple targets involved in the activation of thermogenesis [51]. PKA phosphorylates the cAMP response element-binding (CREB) transcription fac-

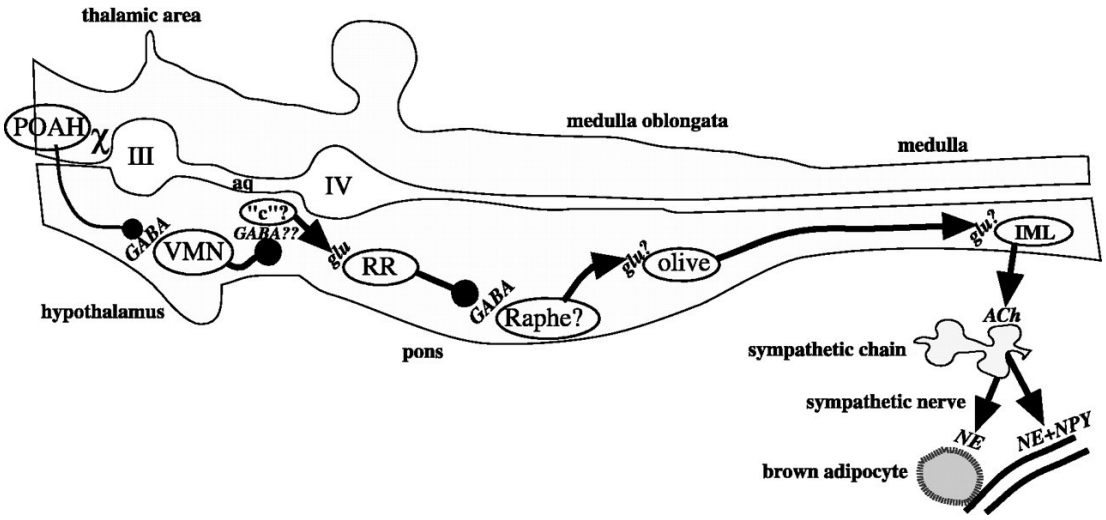

Figure 1.6: Central pathway leading to sympathetic activation and NE release in mice. POAH: preoptic chiasma/anterior hypothalamus; GABA: γ-aminobutyric acid; VMN: ventromedial nucleus; c: unidentified stimulus converter; aq; aquaduct; glu: glutamate; RR: retrorubral field; IML: intermediolateral neurons; ACh: acetylcholine; NE: norepinephrine; NPY: neuropepdite Y. From Cannon & Nedergaard [33].

tor, which upregulates several genes, including *UCP1* [52] and activates the p38 mitogen-activated protein kinase (MAPK) signaling cascade. p38 MAPK has a key role in phosphorylating the activated transcription factor 2 (ATF2) and PGC-1α, which in turn positively regulate the expression of UCP1 [53]. Moreover, ATF2 also upregulates PGC-1α expression. Moreover, PKA activation promotes lipolytic pathways in brown adipocytes.

1.3.1 The role of lipolysis in thermogenesis

Thermogenesis and lipolysis are two intimately related processes. Indeed, thermogenesis cannot occur without the onset of lipolysis, besides lipolysis itself represents a sufficient event to activate thermogenesis [33]. In brown adipocytes, lipolysis is mediated by adrenergic stimulation and cAMP-mediated PKA activation. The central event is the phosphorylation of hormone-sensitive lipase (HSL) and of perilipins. Perilipin (PLIN) is a family of proteins found in the phospholipid monolayer that envelops LDs. Among different types, PLIN1 and PLIN5 are present in fat-storing,

grown LDs and have the most prominent protective role, while others are mostly expressed in growing LDs [54]. The PKA-mediated phosphorylation of Ser660 in HSL translocates the enzyme from the cytosol to the LD [55]. Hyperphosphorylation of PLIN1, which is supported by optic atrophy 1 (OPA1) [56], inactivates its protective funtion and exposes TAGs to active lipases, which release glycerol and FAs [54].

The products of lipolysis are then intercepted by fatty acid binding protein 4 (FABP4) and chaperoned towards mitochondria [57]. Like in any other cell, FAs enter mitochondria via the carnithine palmitoyltransferase (CPI) proteins and undergo canonical steps of β-oxidation and the resulting acetyl-CoA enters the citric acid cycle. Another possible fate for FAs in mitochondria is the direct activation of UCP1 [33].

1.3.2 Regulation of UCP1 expression and thermogenesis

The activation of thermogenesis and, consequently, the expression of UCP1 are NE-dependent. The transcriptional regulation of UCP1 is committed by the 5' non-coding region of *UCP1* gene, which shares sequence homology in humans and rodents [58]. This portion of the gene contains a proximal regulatory region, which is immediately before the transcription initiation site, containing a number of transcription factor binding site. The distal enhancer is another important regulatory site, as it promotes *UCP1* expression when interacts with activated nuclear receptors.

Positive regulation

The proximal regulatory region contains the cAMP response element (CRE), targeted by the active CREB, whose phosphorylation is under direct control of cAMP [59]. The zinc finger protein 516 (Zfp516) has been recently described as a cold-induced transcription factor which can directly bind to the proximal regulatory region of *UCP1* promoter to increase its expres-

sion. The interaction involves the physical association with PRDM16 [60]. Other important regulatory sites present in this region are the elements that interact with C/EBPα and β, previously described as pro-adipogenic factors, which bind to the promoter following the physical interaction with PRDM16 [45, 61].

The distal enhancer of *UCP1* promoter contains another CRE and many sites targeted by hormone- and nuclear receptors-mediated transcription factors. PPARα and PPARγ directly interact with *UCP1* enhancer to promote its expression while forming a heterodimer with retinoid X receptors (RXRs) [62]. Unlike PPARγ, PPARα is selectively expressed in BAT and promotes thermogenic activity, as many of its target genes are oxidative enzymes [62].

Isomers of retinoic acid can promote UCP1 synthesis binding to different nuclear receptors. Specifically, *all*-trans retinoic acid (atRA) binds to retinoic acid receptors (RARs), while *cis*-9 retinoic acid (c9RA) binds to both RAR and RXRs. Activated retinoid receptors directly promote *UCP1*: RXRs forms heterodimers with RARs and PPARs that interact with the distal enhancer [63].

Also hormone-mediated regulation of *UCP1* expression occurs through the distal enhancer. Thyroid hormones triiodothyronine (T_3) and thyroxine (T_4) are involved in the upregulation of *UCP1* thanks to the interaction of T_3 with the nuclear thyroid receptor (TR), which directly binds to its responsive element on the enhancer [64]. T_4 indirectly promotes gene expression because it is converted to active T_3 by the type II iodothyronine 5'-deiodinase (DIO2) prior to the bond with its receptor [65]. Estrogens participate in *UCP1* expression because activated estrogen-related receptors (ERRs) α, β and γ can bind to an ERR responsive element in distal enhancer; moreover, a number of pro-thermogenic actions have been recently described for estrogen in brown and white adipocytes [66].

Negative regulation

Receptor interacting protein 140 (RIP140) is a repressor that alters thermogenesis by inhibiting PGC-1α activity, inducing a downregulation of downstream genes (i.e. *PPARG*, *PPARA* and *ERRA*) and decreasing *UCP1* expression [67].

The liver X receptor α (LXRα) directly inhibits *UCP1* transcription by forming a complex with RIP140 that ablates PPARγ from the gene promoter [68].

The activated receptor for vitamin D also acts as a repressor of UCP1 and thermogenesis, but its mechanism of action is still matter of debate [69].

The retinoblastoma protein (pRb) is a tumor-suppressing protein with a key role in differentiating preadipocytes into white adipocytes and acts as a thermogenic repressor by inhibiting the expression of *PGC1A* gene [70] and hindering PPARγ activity [71].

The twist basic helix-loop-helix transcription factor 1 (Twist1) is a negative regulator of thermogenesis induced by PPARδ which inhibits PGC-1α at a transcriptional level [72].

The two members of steroid receptor coactivator (SRC) family SRC2 and SRC3 negatively regulate thermogenesis by acting on PGC-1α through different mechanisms [68]. In particular, SRC2 blocks the interaction between PPARγ and PGC-1α, thus the expression of *UCP1* is reduced [73]. Conversely, SRC3 impairs the transcriptional activity of PGC-1α by recruiting an acetyltransferase which inactivates PGC-1αby its acetylation [74].

The transient receptor potential cation channel subfamily V member 4 (TRPV4), also known as vanilloid-receptor related osmotically activated channel, is a membrane ion channel. Its activation by endogenous or exogenous agonists triggers a Ca^{2+} influx that, via ERK 1/2 pathway, inhibits PGC-1α expression and its downstream thermogenic targets [75]. Moreover, TRPV4 activation promotes the production of proinflammatory

chemokines that favor the onset of insulin resistance [75].

1.3.3 The function of UCP1

UCP1 is located in the inner mitochondrial membrane and belongs to the SLC25 family of mitochondrial solute carriers [76]. Its role in thermogenesis is to uncouple the oxidative phosphorylation from the synthesis of ATP. To do this, UCP1 breaks the proton gradient existing in mitochondria inducing a leakage of H^+ in the intermembrane space; in this way, the electrochemical gradient is converted into heat and cannot fuel ATP synthesis [77]. When brown adipocytes are inactive, UCP1 does not perform thermogenesis because either exposed to the inhibitory action of purine nucleotides or lacks of activating cofactors, i.e. FAs [33]. In fact, UCP1 activity is positively regulated by FAs and negatively regulated by purine nucleotides. The way FAs activate UCP1 is still matter of debate [33, 77], as high UCP1 activity has been observed also in absence of stimulatory FAs [78]. The models proposed for FA-induced UCP1 activation have been reviewed by Cannon and Nedergaard [33].

1.4 Recruitable thermogenic adipocytes

The canonical classification of AT into WAT and BAT became too simplistic in recent years, as it has been observed that populations of thermogenic adipocytes may appear into WAT depots. They were first identified by Lazar in 2008 [79] and extensively described in both mouse and human in 2012 by Wu and colleagues [80]. These inducible fat cells were named beige or brite (brown-in-white) adipocytes. These cells are recruitable from white adipocytes that may acquire the thermogenic ability after proper stimulation. The conversion of white adipocytes into beige/brite cells is called browning (Figure 1.7).

The most powerful browning stimulus is the sympathetic response to

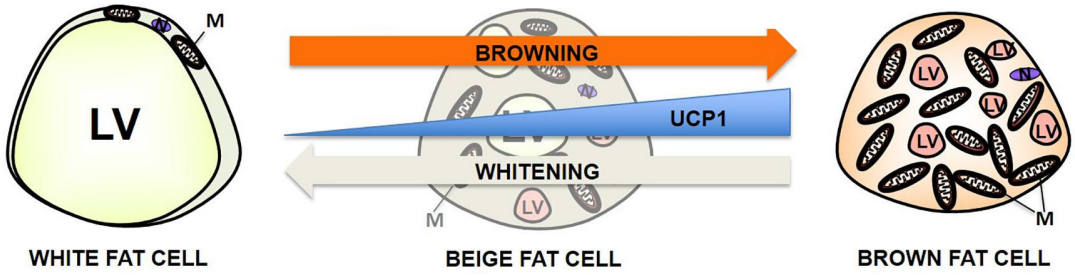

Figure 1.7: Conversion of white adipocytes to brown adipocytes. LV: lipid vacuole; M: mitochondrion; N: nucleus. Modified from Ro *et al.* [81].

cold exposure which, as described for BAT, triggers a peripheral release of NE also in WAT depots [82], despite their lower innervation in comparison to BAT ones [83]. Also in white adipocytes, the surge of NE activates β_3-ARs which, through the signaling cascade already described for brown fat cells, stimulate the expression of *UCP1* and other thermogenic genes. Therefore, PGC-1α synthesis is increased and mitochondrial biogenesis is enhanced. These changes are flanked by a dynamic remodeling of lipid stores, as the big LD that characterizes white adipocytes is fragmented into multiple, smaller LDs and lipolysis is empowered.

WAT depots do not respond to cold exposure with the same extent, as acute cold exposure induces a rapid response mainly in inguinal and retroperitoneal depots. Visceral and perigonadal depots are less prone to recruit brite adipocytes and they need a chronic exposure to induce browning [4]. The response of mature white adipocytes to cold exposure depends also on the proximity to noradrenergic sympathetic nerve ends, depot vascularization and the exposure to favorable micro-environmental conditions. When the browning stimulation ceases, brite adipocytes acquire a typical white phenotype; this does not occur in canonical brown adipocytes, as even when they are inactive their phenotypic characteristics and molecular signature do not change.

1.4.1 Origin of brite adipocytes

Browning of white adipocytes is not the only way to recruit brite cells in WAT depots. Indeed, brite adipocytes may arise from precursors not shared with white adipocytes. WAT browning and differentiation of *de novo* brite adipocytes coexist with depot-specific differences [2]. Since brite adipocytes are recruited in WAT depots, their precursors should be Myf5$^-$. Actually, they can be either Myf5$^+$ or Myf5$^-$, according to the anatomical fat pad from which they originate.

A recent study showed that adipose progenitors PDGFRα^+, Sca-1$^+$ and CD34$^+$ in murine abdominal fat depots can differentiate into both white and brite adipocytes following a moderate β_3-adrenergic activation [21]. It has also been demonstrated that brite cell precursors may lack a number of surface markers present in the precursors of other adipocytes [2].

It is now ascertained that PDGFRα^+ adipose progenitors can differentiate into white or brite adipocytes regardless of Myf5 expression. The two phenotypes are interchangeable according to the degree of sympathetic activation without any impact on the expression of surface markers [2].

1.4.2 Molecular signature of brite adipocytes

The first studies on brite adipocytes demonstrated that these cells have comparable expression profiles with both brown and white adipocytes. However, these cells also express a spectrum of brite-specific genes that can be treated as distinctive markers. The first genes recognized as selective brite markers were the developmental transcription factor TBX1, the transmembrane protein TMEM26 and the tumor necrosis factor receptor superfamily member CD137 [80]. Their expression was elevated in inguinal subcutaneous WAT of mice [80], which is a notable source of recruitable thermogenic adipocytes. Nonetheless, *in vivo* β_3-adrenergic activation of murine inguinal white adipocytes did not evoke an increase of *Tbx1* and *Tmem26* expression, while other putative surface markers were selectively upregu-

lated [84]. These genes, namely *Pat2* and *P2rx5*, were selectively upregulated in brown and brite adipocytes, with *Pat2* being more close to brite adipocyte markers [84]. Notably, the markers characterized in this research partly or totally lost their discriminating ability when isolated preadipocytes were immortalized and differentiated into mature fat cells. This study also pointed neuregulin 4 (NRG4) as an adipose-specific potential marker, despite no differences were found between white and brown adipocytes [84]. Later research stated that actually the specificity for NRG4 expression exists for brite adipocytes and the gene has been proposed as a brite marker both in mice [85] and in humans [86].

A massive up-regulation of *Tbx1* was demonstrated in recruited murine thermogenic cells, while *Tmem26* was induced just in SVF [87].

Primary murine adipocytes treated with rosiglitazone, a PPARγ agonist, became brite and exhibited an upregulation of canonical thermogenic genes and putative brite markers, with the exception of *Tmem26* [88]. Adrenergic stimulation of these brite adipocytes lowered the expression of some markers, including *Tbx1* and *P2rx5*, which lost their discriminating ability compared to control white adipocytes. The characterization of SVF adipocyte precursors demonstrated the highest levels of specific markers (TBX1 and TMEM26) compared to mature adipocytes [88]. Taken together, these results show that the accuracy of putative brite markers depends on many factors. For instance, *in vivo* and *in vitro* models differently express TBX1 and CD137 [88]. *In vivo*, CD137 does not meet the marker criteria because its levels are regulated by other physiological processes different from browning [89]. Moreover, immortalized cell lines might lose the expression of some biomarkers [84, 88], and *in vitro* adrenergic stimulation might downregulate the expression of a number of biomarkers [88]. In light of these findings, unambiguous validated brite biomarkers are limited to fibroblast growth factor 21 (FGF21), carbonic anhydrase 4 (CAH4) and Cbp/P300-interacting transactivator 1 (CITED1), even if the last one is negatively affected by adrenergic activation [88].

1.4.3 Dynamic of LD remodeling during browning

Lipid droplets are organelles with a dynamic nature, since they undergo several important changes during cell life and in response to metabolic variations. LDs are organelles generated via the endoplasmic reticulum (ER) through a seipin-mediated complex machinery that allows intraluminal lipid synthesis and budding from the ER membrane of the nascent LD [90, 91]. Cytoplasmic LDs are packed within a phospholipid monolayer that includes a mosaic of LD membrane-associated proteins [90].

The enlargement of LDs in differentiating adipocytes occurs via *de novo* lipogenesis and LD fusion. This process takes place when two LDs begin a mutual contact and the smaller droplet transfers its lipid content in the larger one [91]. In the contact site between two fusing LDs, a trans homodimer between cell death-inducing DNA fragmentation factor alpha-like effector A (CIDEA) and CIDEC (also known as fat-specific protein 27, FSP27) is formed. The protein complex forms a channel through which lipids are slowly transferred to the large LD, driven by a pressure gradient [91].

LD-associated proteins are differentially expressed among different fat depots. A study demonstrated that most LD-associated proteins are particularly enriched in murine interscapular BAT [92]. Interestingly, CIDEA has been found overexpressed only in BAT, while different WAT depots express only CIDEC; this is true in mouse [93], since human WAT expresses CIDEA as well [94]. This finding has led the use of CIDEA as a selective BAT marker in mouse experiments and pointed out a different role of CIDEA and CIDEC in LD remodeling. CIDEA is a mediator of LD fusion, as stated above, but CIDEA alone cannot achieve an unilocular phenotype, typical of WAT [95]. To obtain large LDs as in white adipocytes, CIDEC's activity is compulsory. Its lipid transfer efficiency can be improved by the interaction with PLIN1, despite this is not strictly necessary to achieve the unilocular phenotype [96]. This explains why, at least in mouse, *Cidea* expression is limited to BAT and *Fsp27* is conversely more expressed in WAT.

Recently, a differential role for FSP27 in BAT and WAT has been described in mouse. A new isoform of FSP27, alternatively transcribed by the same gene, has been found in liver and BAT. This isoform, known as FSP27β, is synthesized through the activation of a different promoter [97]. The native form, namely FSP27α, is expressed in white adipocytes and dimerizes to promote LD fusion towards the unilocular phenotype. The role of FSP27β is not clear. Nevertheless, a model for its function in LD dynamic has been proposed. The interaction of FSP27β with CIDEA should prevent the formation of the heterodimer that promotes LD fusion. In this way, fusion is prevented and LDs maintain a small size [94].

In human, both CIDEA and CIDEC are expressed in all types of AT and their expression level is positively correlated with insulin sensitivity [98]. They are supposed to have a beneficial role, since they are overexpressed to reduce ectopic accumulation of fat, storing it in adipocytes, and thus to improve insulin sensitivity [94].

When browning occurs, a change in LD morphology can be appreciated [92, 99]. A significant β_3-adrenergic activation in white adipocytes switches the unilocular phenotype to a multilocular one. Stimulated cells decrease the dimensions of their LDs due to the NE-dependent activation of lipolysis. Concurrently, *de novo* lipid synthesis is also stimulated: existing LDs become surrounded by a multitude of micro LDs which are enlarged as a consequence of lipogenesis and CIDE's activity [92]. This physiological response is achieved to improve the efficiency of lipolysis: smaller LDs increase the total surface accessible to lipases, so a higher mass of TAGs is oxidized to fuel mitochondrial thermogenesis [92, 99]. The adrenergic stimulus can also trigger energy-consuming metabolic pathways, included a lipolysis/lipogenesis futile cycle involved in LD remodeling and reducing lipid content in a UCP1-independent way [100].

1.4.4 Mitochondrial dynamics during browning

Mitochondria are also dynamic organelles in cells, as they undergo continuous episodes of fusion and fission. Fusion produces complex and highly interconnected mitochondrial networks composed by elongated, tubular mitochondria. These interconnected mitochondrial networks are important for communication between organelles and transfer of mitochondrial DNA gene products [101]. The elongated mitochondrial shape is associated with highly energy demanding conditions, as tubular mitochondria are more efficient in ATP synthesis [102]. For instance, interconnected mitochondrial networks have been observed in white pre-adipocytes at the beginning of their differentiation into mature cells [99].

During mitochondrial fission, the elongated networks splinter into discrete, circular mitochondria which eventually can show swelling. Fissed mitochondria can be more easily distributed in the cytoplasm [101]. Despite fission has been frequently associated with apoptosis [103], it has a precise physiological meaning in thermogenic adipocytes. Mitochondrial fission has been proven to be associated with low energy demanding situations, like thermogenesis [103], in which the catabolism of high energy substrates does not fuel the production of ATP.

The molecular machinery driving fusion and fission involves the activity of dynamin-related proteins (DRPs), which can remodel mitochondrial membranes thanks to their GTPasic activity [101]. Fusion is mediated by two sets of proteins: mitofusins (MFN) 1 and 2 join together the outer membranes of mitochondria, while the fusion of inner membranes is achieved by OPA1, which also maintains the architecture of cristae [104]. Little is known about factors regulating mitochondrial fission. DRP1 is, thus far, the only described protein involved in fission [104].

In brown adipocytes, fission is stimulated by β_3-adrenergic activation, thus it is narrowly coupled with thermogenesis. NE has a role in stimulating fission by activating PKA, which in turn phosphorylates DRP1,

turning it in an active form [103]. Fission produces small globular mitochondria. Once the thermogenic stimulus ceases, the mitochondrial architecture returns to an elongated, interconnected web of tubular mitochondria [103]. NE favors mitochondrial fission by enhancing DRP1 activity in a PKA-dependent way and prevents mitochondrial fusion by abrogating mitochondria-bound OPA1 [105]. OPA1 inhibition also provokes mitochondrial swelling [106]. NE-induced fission is functional for energy expenditure, because fragmented mitochondria surrounding LDs become more sensitive to FAs. As a consequence, UCP1 activation is improved and mitochondria oxidize FAs more efficiently [103].

This physiological model occurs also during browning, as the NE-driven mitochondrial biogenesis is flanked by DRP1-mediated fission and remodeling of LDs. The difference in mitochondrial architecture between brown and brite adipocytes lies in the behavior of the cells after the ending of the thermogenic stimulus. Unstimulated brown adipocytes fuse their mitochondria into native interconnected webs [103] and, moreover, maintain a constitutively high level of mitochondrial biogenesis [107]. Unstimulated brite adipocytes come back to a white phenotype in a process that involves both the decline of mitochondrial biogenesis and the stimulation of mitophagy, i.e. the controlled disruption of mitochondria [107]. Mitophagy is activated when mitochondria lose their membrane potential and recruit the parkin protein [108]. The proton leakage promoted by UCP1 prevents mitophagy and parkin is strongly repressed by β_3-adrenergic activation. The NE withdrawal allows parkin expression, promoting mitophagy in brite adipocytes [107].

Chapter 2

Browning as a therapeutic strategy

The physiological changes induced in WAT by browning opened new perspectives in adipobiology and obesity research. In particular, there is growing interest in the induction of WAT browning in obese patients as a therapy for obesity and related co-morbidities.

2.1 An overview on obesity

Obesity is a complex disease in which excess energy is accumulated. The BMI is the parameter of choice to discriminate between normal weight, overweight and obese individuals: people with a BMI between 25 and 30 kg m^{-2} are overweight, while individuals with a BMI that exceeds 30 kg m^{-2} are obese [109]. Nevertheless, this parameter does not take into account the dishomogeneous distribution of fat mass across different depots. The severity of obesity depends on the degree of fat accumulation in different depots [110]. An excess of fat in the upper part of the body (i.e. abdominal obesity) is a typical feature of obese men and is highly correlated with diabetes and cardiovascular disease. Conversely, when fat mostly accumulates in the lower part of the body (mostly in the gluteo-femoral depot), the correlation with severe morbidities is much lower. This phenotype is

widespread among obese women.

Obesity has gained a worldwide epidemic distribution, with nearly one billion of individuals being obese [109]. The treatment of obesity becomes then a primary concern in global health, but the traditional approaches (i.e. modification of dietary habits, physical exercise) are not always effective, since the regain of fat mass is a likely feature [111]. Bariatric surgery is an interesting alternative, but is not available in all cases [109]. In this scenario, WAT browning is claimed as a promising alternative therapeutic tool.

2.2 Therapeutic significance of browning

The interest of the scientific community about WAT browning derives from the high metabolic capacity of BAT in dissipating energy as heat. Being highly vascularized and innervated, BAT can respond promptly to thermogenic stimuli and mobilize energy substrates to be oxidized. This interest further grew after the discovery of functional BAT in adult humans and of brite adipocytes enclosed in WAT depots [112]. The activation of thermogenesis in brown and brite fat cells should lead to the depletion of cellular lipid stores. Consequently, a flow of glucose and FAs should be mobilized towards these cells to fuel the thermogenic machinery, leading to a decrease of ectopic fat depots and an increase in AT insulin sensitivity [112].

Unlike rodents, BAT in adult humans represents only 2.7% of total body weight (5.5% in women, 1.3% in men) and its content is inversely correlated to BMI [113]. PET-CT measurements and mathematical models estimated that mass and volume of functional BAT in adult humans are respectively 50 g and 137 cm^3 [114]. In terms of metabolic contribution, adaptive thermogenesis in thermoneutral conditions represents 5% of basal metabolic rate (BMR) [114]. A 4% increase of BMR through adaptive thermogenesis, with the contribution of recruited brite adipocytes, could produce a

3% reduction of total body weight per year, assuming that the activation is chronically sustained [115]. This can be true if functional tolerance is avoided [116] and if thermogenesis is not impaired and compensated by an increase in food assumption [117].

The administration of the β_3-adrenergic agonist mirabegron caused a 13% increase in BMR [118]; if chronically sustained, this activation could induce an 8% decrease in total body weight per year. It has to be stressed that the chronic thermogenic activation induced by exogenous substances has been only assumed in the cited researches and it deserves further elucidation [112].

These results assume that brite adipocytes contribute to metabolic rate to the same extent of brown fat cells, although a basal thermogenesis in BAT in absence of thermal challenges may occur [119]. Moreover, there is growing evidence that thermogenesis in brite adipocytes can occur through alternative processes that do not involve *UCP1* expression, like the futile lipolysis and lipogenesis cycle [100, 120]. Taken together, all these statements show a complex panorama that still needs deeper understanding to translate the results of scientific research about adipobiology and physiology of browning into routinary clinical practice.

2.3 Inducing WAT browning

The activation of BAT and the recruitment of brite adipocytes, in terms of *UCP1* expression and modifications of intracellular architecture as described above, can occur through a number of different pathways involving a number of signaling cascades and transcription factors. The main molecular hallmark is β_3-AR, which responds to NE surges following thermal challenges. Cold exposure is the most effective way to activate thermogenesis in AT [121].

Other endogenous mechanisms can produce browning. These processes can be driven by hormonal compounds or by other molecular mediators

acting directly on *UCP1* promoter or on upstream transcription factors. Some of these molecules are centrally active and can activate sympathetic nervous system to produce a peripheral release of NE. Among endogenous factors, myokines produced by contracting skeletal muscles are gaining interest because their browning activity could strengthen the existing link between weight loss and physical exercise. For instance, studies on the browning activity of β-aminoisobutyric acid [122] and brain-derived neurotrophic factor [123] have been performed with interesting results, but further characterization is needed, since their molecular mechanisms and the effect on LD and mitochondrial dynamics are mostly unknown. A plethora of such endogenous browning factor have been reviewed in [109, 124].

Browning can be also induced by external molecules. Historically, a number of anti-obesity drugs were present; many of them have been withdrawn because of their deleterious side effects [112]. Nevertheless, studies about different pharmacological molecules have shown interesting browning effects, despite their primary target is not AT, like selective serotonin re-uptake inhibitors and tamoxifen [109]. Concerning exogenous molecules, the attention is now focused on the study of bioactive compounds found in nature (e.g. nutraceuticals from plants). Among these, capsaicin can induce WAT browning by directly activating adipocyte transcriptional program and by triggering a central stimulation that ends up in the peripheral release of NE. Despite the molecular pathway activated by capsaicin has been characterized [125, 126], little is known about long term effects of capsaicin administration and its effects on structural variations. The β-carotene-derived retinoic acid is another bioactive compound with browning activity, but only the effect of the *all*-trans isomer has been extensively described [63], as its *cis*-9 isomer has not been fully characterized yet. A high number of bioactive molecules deserves deeper studies to better exploit the way they can induce browning and to which extent.

Chapter 3

Aim of the thesis

This thesis aims to gain new insight about the principal features of WAT browning. The effects of chosen bioactive compounds on cells was evidenced in terms of gene expression and modifications of the structure of lipid droplets and mitochondria. The attention was focused on delineating the browning effect of selected endogenous and nutraceutical molecules, such as β-aminoisobutyric acid, capsaicin, brain-derived neurotrophic factor and *cis*-9 retinoic acid, on white and brite preadipocytes and differentiated adipocytes. Simpson-Golabi-Behmel syndrome cell strain, a human model of white preadipocytes, was also investigated in order to characterize their transient unstimulated browning.

Part II

Materials and methods

Chapter 4

Chemicals and culture media

The chemicals and culture media used in the experiments presented in this thesis, together with the buffers and solvents, have been listed in Table 4.1. Kits and chemicals for RNA extraction, cDNA synthesis and amplification were listed in Table 4.2, together with products and dyes used in structural analyses, immunofluorescence and in-cell Western.

Table 4.1: Reagents and media for cell cultures and for buffer preparation. DMEM/F12: Dulbecco's modified Eagle medium/Ham's F12; HEPES: 4-(2-hydroxyethyl)-1-piperazine ethanesulfonic acid.

Cell culture media and reagents		
Product	*Identifier*	*Source*
DMEM/F12 (1:1)	31330038	Thermo Fisher Scientific
High glucose DMEM, GlutaMAX™ supplement	10566016	Thermo Fisher Scientific
Biotin	B4639	Sigma-Aldrich
D-pantothenic acid hemicalcium salt	P5155	Sigma Aldrich
Penicillin-streptomycin	15140122	Thermo Fisher Scientific
Amphotericin B	15290026	Thermo Fisher Scientific
Fetal bovine serum	10270106	Thermo Fisher Scientific
Human apo-Transferrin	T2252	Sigma-Aldrich
Human insulin	I1507	Sigma-Aldrich
Hydrocortisone	H0888	Sigma-Aldrich
3,3',5-Triiodo-L-thyronine sodium salt	T6397	Sigma-Aldrich
Dexamethasone	D1756	Sigma-Aldrich
3-Isobutyl-1-methylxanthine	I5879	Sigma-Aldrich
Rosiglitazone	71740	Cayman Chemical
Indomethacin	70270	Cayman Chemical
3-Aminoisobutyric acid	AG-CR1-3596	AdipoGen Life Sciences
Capsaicin	92350	Cayman Chemical
Brain-derived neurotrophic factor	4004	BioVision Inc.
9-*cis*-Retinoic acid	14587	Cayman Chemical
L-(–)-norepinephrine bitartrate hydrate	16673	Cayman Chemical
(–)-Isoproterenol hydrochloride	I6504	Sigma-Aldrich
Thiazolyl blue tetrazolium bromide (MTT)	M5655	Sigma-Aldrich
Oil red O solution	O1391	Sigma-Aldrich
Salts, buffers and solvents		
Sodium chloride	S7653	Sigma-Aldrich
Potassium chloride	P9333	Sigma-Aldrich
Sodium phosphate dibasic	S7907	Sigma-Aldrich
Potassium phosphate monobasic	P5655	Sigma-Aldrich
Hank's balanced salt solution	ECM0507L	Euroclone S.p.A.
HEPES buffer	ECM0180D	Euroclone S.p.A.
TWEEN® 20	P7949	Sigma-Aldrich
Absolute ethanol	3086052	Carlo Erba Reagents S.r.l.
2-Propanol	I9516	Sigma-Aldrich
Dimethyl sulphoxide	D2650	Sigma-Aldrich
Buffered neutral 10% formalin	05-01004F	Bio-Optica S.p.A.

Table 4.2: Reagents and kits for molecular biology protocols, structural analyses, immunofluorescence and in-cell Western. TBE: tris/borate/EDTA; DAPI: 4',6-diamidino-2-phenylindole.

Products for molecular biology		
Product	*Identifier*	*Source*
TRIzol™ reagent	15596026	Thermo Fisher Scientific
Chloroform	C2432	Sigma-Aldrich
PureLink™ RNA Mini Kit	12183018A	Thermo Fisher Scientific
SuperScript™ III one-step RT-PCR system	12574026	Thermo Fisher Scientific
Agarose	EMR010001	Euroclone S.p.A.
GelRed®	41003	Biotium
1 kb DNA ladder	31022	Biotium
TBE	AM9863	Thermo Fisher Scientific
ImProm-II™ Reverse Transcription System	A3800	Promega Corporation
Transcriptor High Fidelity cDNA Synthesis Kit	5091284001	Roche Diagnostics
Platinum™ SYBR™ Green qPCR SuperMix-UDG	11733046	Thermo Fisher Scientific
Fluorescent dyes		
BODIPY™ 493/503	D3922	Thermo Fisher Scientific
MitoTracker™ Orange CMTMRos	M7510	Thermo Fisher Scientific
Fluo-8 AM	ab142773	Abcam
Protein expression reagents		
Triton™ X-100	T9284	Sigma-Aldrich
Glycine	G8898	Sigma-Aldrich
Ammonium chloride	A9434	Sigma-Aldrich
Normal goat	S-1000	Vector Laboratories
Bovine serum albumin fraction V	10738328103	Roche Diagnostics
Anti-rabbit AlexaFluor® 555	ab150078	Abcam
Anti-rabbit fluorescein IgG	FI-1000	Vector Laboratories
Anti-mouse fluorescein IgM	FI-2020	Vector Laboratories
Anti-rabbit IRDye® 800CW	925-32211	LI-COR Inc.
Fluoroshield mounting medium with DAPI	ab104139	Abcam

Chapter 5

Preliminary methodological assessment

5.1 Establishing culture media formulation

The experiments presented in this doctoral thesis have been performed on different adipose cell lines: Simpson-Golabi-Behmel syndrome (SGBS) human preadipocytes, 3T3-L1 murine preadipocytes and X9 murine preadipocytes. These cells need different formulations to achieve satisfactory growth and differentiation rate, but they show common features in the culture protocol.

After thawing, cells are plated on culture dishes or microscopy slides and are cultured in a growth medium to reach a confluence rate close to or equal to 100%. The exact time each cell type requires for clonal expansion varies according to: i) seeding density; ii) desired confluence rate; iii) cell viability. In general, for all cell types used, clonal expansion from the seeding day to reach 90% confluence requires 5-8 days, starting from 5,000 cells/cm^2.

When cells reached a satisfactory confluence rate, differentiation has been induced with differently formulated differentiation media according to cell type. The differentiation medium formulation is critical for the

successful achievement of cell differentiation, hence this aspect has been carefully studied and different formulations have been tested to find the optimal differentiation conditions.

The incubation with differentiation medium normally lasted from 2 to 4 days and was followed by the administration of the maintenance medium, which is formulated in a way that keeps cells in their differentiated state, allowing fat accumulation in their LDs until they become fully differentiated adipocytes. The administration of the maintenance medium lasts until cell sampling for analyses and its formulation depends on the differentiation medium, so different formulation have been tested accordingly.

For all the experiments reported in this doctoral thesis, cells were grown in a Forma™ Steri-Cycle™ i160 CO_2 incubator (51030301 Thermo Fisher Scientific) at 37°C, with 5% CO_2 and 95% relative humidity.

5.1.1 SGBS cells

A stock of SGBS human preadipocytes has been kindly provided by prof. Martin Wabitsch (University of Ulm). The culture media formulation for SGBS cells has been described by Wabitsch and colleagues, who first isolated this model and implemented their *in vitro* growth [127]. The suggested media formulation has been reported in Table 5.1.

The media presented in Tabel 5.1 achieved satisfactory results in terms of cell expansion and differentiation. Nevertheless, we observed a significant decline in LD formation in SGBS cultures at high passage number. For this reason, being hydrocortisone recognized as a powerful lipogenic and antilipolitic factor [128], the differentiation and maintenance media have been reinforced with additional 150 nM hydrocortisone, to a final concentration of 250 nM. The duration of cell incubation with differentiation and maintenance media did not change from how suggested by Wabitsch and colleagues [127]: after two washes with phosphate buffer saline (PBS) 1X, 90% confluent cells were incubated with the differentiation medium for

4 days. The incubation with maintenance medium, refreshed every 4 days, lasted until cell sampling. This growth protocol has been adopted in the results presented in Chapter 11.

Table 5.1: Formulation of SGBS cells culture media as reported by Wabitsch *et al.* [127]. DMEM/F12: Dulbecco's modified Eagle medium/Ham's F12; FBS: fetal bovine serum; P/S: penicillin/streptomycin; IBMX: isobutylmethylxanthine.

Reagent	**Growth medium**	**Differentiation medium**	**Maintenance medium**
Basal medium	DMEM/F12	DMEM/F12	DMEM/F12
FBS	10%	–	–
P/S	1%	1%	1%
Biotin	33 µM	33 µM	33 µM
Panthotenic acid	17 µM	17 µM	17 µM
Human transferrin	–	10 µg/mL	10 µg/mL
Triiodothyronine	–	0.2 nM	0.2 nM
Hydrocortisone	–	100 nM	100 nM
Human insulin	–	20 nM	20 nM
Dexamethasone	–	25 nM	–
IBMX	–	250 µM	–
Rosiglitazone	–	2 µM	–

5.1.2 3T3-L1 cells

Unlike SGBS cells, 3T3-L1 murine preadipocytes (SP-L1-F ZenBio Inc.) are a worldwide commonly used cell model for adipobiology study, as they represent an accurate model of WAT depots with visceral features. Different laboratories adopted differentiation medium formulations that varied in composition and reagent concentration, but the gold standard for 3T3-L1 is the insulin-dexamethasone-IBMX (isobutylmethylxanthine) cocktail [129].

The adopted media for culturing 3T3-L1 cells in our laboratory changed during the 3 years of doctoral studies. This was due to a decline in differentiation outcome probably linked to cell aging during routinary cell culture practice [130]. It has to be underlined that all 3T3-L1 cells used in the studies reported in the present thesis derive from a single stock of 3T3-L1 cells purchased at the beginning of the first year of doctoral study.

Hence, the variations of the culture media experienced during the research period come from the time course-dependent need to implement cell differentiation to counteract the unavoidable throwbacks caused by cell senescence. While differentiation media underwent some changes throughout time, clonal expansion was always performed in high glucose Dulbecco's modified Eagle medium (DMEM) with 10% fetal bovine serum (FBS), 1% penicillin/streptomycin solution (P/S) and 1% amphotericin B. To inhibit fibroblast mitosis, 100% confluent cells were switched to the differentiation cocktail only 48 hours after reaching full confluence.

The first differentiation cocktail adopted in our laboratory has been described by Asano and colleagues [131] and has been slightly modified in reagents' concentration. The formulation of differentiation and maintenance cocktails are reported in Table 5.2. This formulation has been used in experiments reported in Chapter 12. The incubation with the differentiation medium lasted three days and the replacement with maintenance medium was performed until cell sampling.

Table 5.2: Formulation of 3T3-L1 cells culture media modified from Asano *et al.* [131]. DMEM/F12: Dulbecco's modified Eagle medium/Ham's F12; FBS: fetal bovine serum; P/S: penicillin/streptomycin; IBMX: isobutylmethylxanthine.

Reagent	**Differentiation medium**	**Maintenance medium**
Basal medium	DMEM/F12	DMEM/F12
FBS	10%	10%
P/S	1%	1%
Amphotericin B	1%	1%
Triiodothyronine	1 nM	1 nM
Human insulin	0.5 µg/mL	0.5 µg/mL
Dexamethasone	5 µM	–
IBMX	0.5 mM	–
Rosiglitazone	1 µM	–

This first differentiation cocktail has been switched to a formulation closer to the gold standard proposed in late '70s [132]. This formulation has been used in experiments described in Chapters 13 and 15 and produced good differentiation outcomes. Also in this case, the differentiation

medium was administered for three days and the maintenance lasted until cell sampling. Used reagents and their concentrations are reported in Table 5.3.

Table 5.3: Formulation of 3T3-L1 cells culture media modified from Rubin *et al.* [132]. DMEM/F12: Dulbecco's modified Eagle medium/Ham's F12; FBS: fetal bovine serum; P/S: penicillin/streptomycin; IBMX: isobutylmethylxanthine.

Reagent	**Differentiation medium**	**Maintenance medium**
Basal medium	DMEM/F12	DMEM/F12
FBS	10%	10%
P/S	1%	1%
Amphotericin B	1%	1%
Human insulin	1 µg/mL	1 µg/mL
Dexamethasone	0.5 µM	–
IBMX	0.5 mM	–

The final differentiation cocktail tested for 3T3-L1 culture is currently in use in our experiments and is achieving excellent differentiation rates. The formulation has been derived from Zebisch and colleagues [133] without modifications and it has been used for experiments described in Chapter 14. The incubation with the differentiation cocktail lasted two days, while maintenance was administered to cell cultures until cell sampling. The list of reagents and their concentration are indicated in Table 5.4.

Table 5.4: Formulation of 3T3-L1 cells culture media modified from Zebisch *et al.* [133]. HG DMEM: high glucose Dulbecco's modified Eagle medium; FBS: fetal bovine serum; P/S: penicillin/streptomycin; IBMX: isobutylmethylxanthine.

Reagent	**Differentiation medium**	**Maintenance medium**
Basal medium	HG DMEM	HG DMEM
FBS	10%	10%
P/S	1%	1%
Amphotericin B	1%	1%
Human insulin	1 µg/mL	1 µg/mL
Dexamethasone	0.25 µM	–
IBMX	0.5 mM	–
Rosiglitazone	2 µM	–

5.1.3 X9 cells

Experiments on 3T3-L1 cells and X9 cells (CRL-3282 ATCC) are reported in Chapter 13. These two murine models are different in their metabolic profile, as X9 cells have been isolated from the subcutaneous inguinal white fat pad, which is more prone to browning than other depots [80]. Researches using these cell line are lacking in literature, so the choice of the most appropriate culture medium required a deep study and comparison between various formulations.

When differentiated with the cocktail recommended by Wu and Xu [134], the differentiation rate of X9 cells was very low, as about 85% cells preserved a fibroblast-like aspect after the incubation with both differentiation and maintenance media. The formulation proposed for the media in [134] has been reported in Table 5.5.

Table 5.5: Formulation of X9 cells culture media as reported by Wu & Xu [134]. DMEM/F12: Dulbecco's modified Eagle medium/Ham's F12; HG DMEM: high glucose Dulbecco's modified Eagle medium; FBS: fetal bovine serum; P/S: penicillin/streptomycin; IBMX: isobutylmethylxanthine.

Reagent	**Growth medium**	**Differentiation medium**	**Maintenance medium**
Basal medium	DMEM/F12	DMEM/F12	DMEM/F12
FBS	15%	10%	10%
P/S	1%	1%	1%
Amphotericin B	1%	1%	1%
Triiodothyronine	–	1 nM	1 nM
Human insulin	–	0.5 µg/mL	0.5 µg/mL
Dexamethasone	–	5 µM	–
IBMX	–	0.5 mM	–
Rosiglitazone	–	1 µM	–

For X9 cells, four different media formulations have been tested. They were taken from [133] and [135] and differed not only in the reagents' nature and concentration, but also in basal medium composition and FBS level. Different media will be called to hereafter Formulation (F) 1, F2, F3 and F4 and their reagents' concentrations are reported in Table 5.6.

To test the effectiveness of each formulation, cells were grown for 2 and

Table 5.6: Formulation of X9 cells culture media F1, F2, F3 and F4. DMEM/F12: Dulbecco's modified Eagle medium/Ham's F12; FBS: fetal bovine serum; P/S: penicillin/streptomycin; IBMX: isobutylmethylxanthine.

	Reagent	**F1**	**F2**	**F3**	**F4**
Growth medium	Basal medium	DMEM/F12	HG DMEM	DMEM/F12	HG DMEM
	FBS	15%	10%	15%	10%
	P/S	1%	1%	1%	1%
	Amphotericin B	1%	1%	1%	1%
Differentiation medium	Basal medium	DMEM/F12	HG DMEM	DMEM/F12	HG DMEM
	FBS	10%	10%	10%	10%
	P/S	1%	1%	1%	1%
	Amphotericin B	1%	1%	1%	1%
	IBMX	0.5 mM	0.5 mM	0.5 mM	0.5 mM
	Human insulin	10 ng/mL	10 ng/mL	1 µg/mL	1 µg/mL
	Dexamethasone	1 µM	1 µM	0.25 µM	0.25 µM
	Triiodothyronine	1 nM	1 nM	1 nM	1 nM
	Rosiglitazone	1 µM	1 µM	2 µM	2 µM
	Indomethacin	125 µM	125 µM	–	–
Maintenance medium	Basal medium	DMEM/F12	HG DMEM	DMEM/F12	HG DMEM
	FBS	10%	10%	10%	10%
	P/S	1%	1%	1%	1%
	Amphotericin B	1%	1%	1%	1%
	Human insulin	10 ng/mL	10 ng/mL	1 µg/mL	1 µg/mL
	Triiodothyronine	1 nM	1 nM	1 nM	1 nM
Reference	modified from	[135]	[135]	[133]	[133]

6 days post-differentiation induction and lipid accumulation was evaluated through oil red O (ORO) staining quantification, according to Mehlem's protocol [136]. ORO staining is a protocol that allows the quantification of the TAG accumulation in cultured cells through a colorimetric measurement of absorbance.

ORO was filtered with 0.2 µm filters and mixed with H_2O in a 6:4 ratio. The mixture was incubated at room temperature (RT) for 20 minutes and then filtered again with 0.2 µm filters. In the meantime, cells plated in 96-well plates were fixed with formalin 10% for 5 minutes at RT. Formalin was then refreshed for a second incubation lasting 90 minutes at RT. Next, cells were rinsed with 60% isopropanol and wells were let to completely air dry. ORO:H_2O working solution was then added to well and incubated for 10 minutes at RT. After ORO removal, cells were immediately washed 5 times with H_2O; following the last cleansing, wells were let to completely air dry. ORO accumulated in adipocytes was eluted with a 15 minutes incubation with 100% isopropanol at RT, followed by absorbance detection with a Spark multimode microplate reader (Tecan Trading AG). Prior to ORO elution, cells were imaged with a DM4 B optical microscope (Leica Microsystems GmbH).

ORO internalization by differentiating X9 cells is shown in Figure 5.1. At 2d, most of X9 cells preserved a fibroblast morphology, but a certain level of ORO internalization was displayed. At this time point, the formulation which guaranteed the best lipid accumulation is F4 (Figure 5.1, a). The presence of a high glucose level in the basal medium has probably been useful for cell expansion and differentiation, as glucose was internalized and accumulated in form of triglycerides. At 6d, cells were more differentiated with all media formulations and a higher quantity of ORO was internalized in LDs (Figure 5.1). Nevertheless, F4 medium, which achieved the best lipid accumulation at 2d, resulted the least efficient medium at 6d (Figure 5.1, b), while the most effective media were found to be F1 and F3.

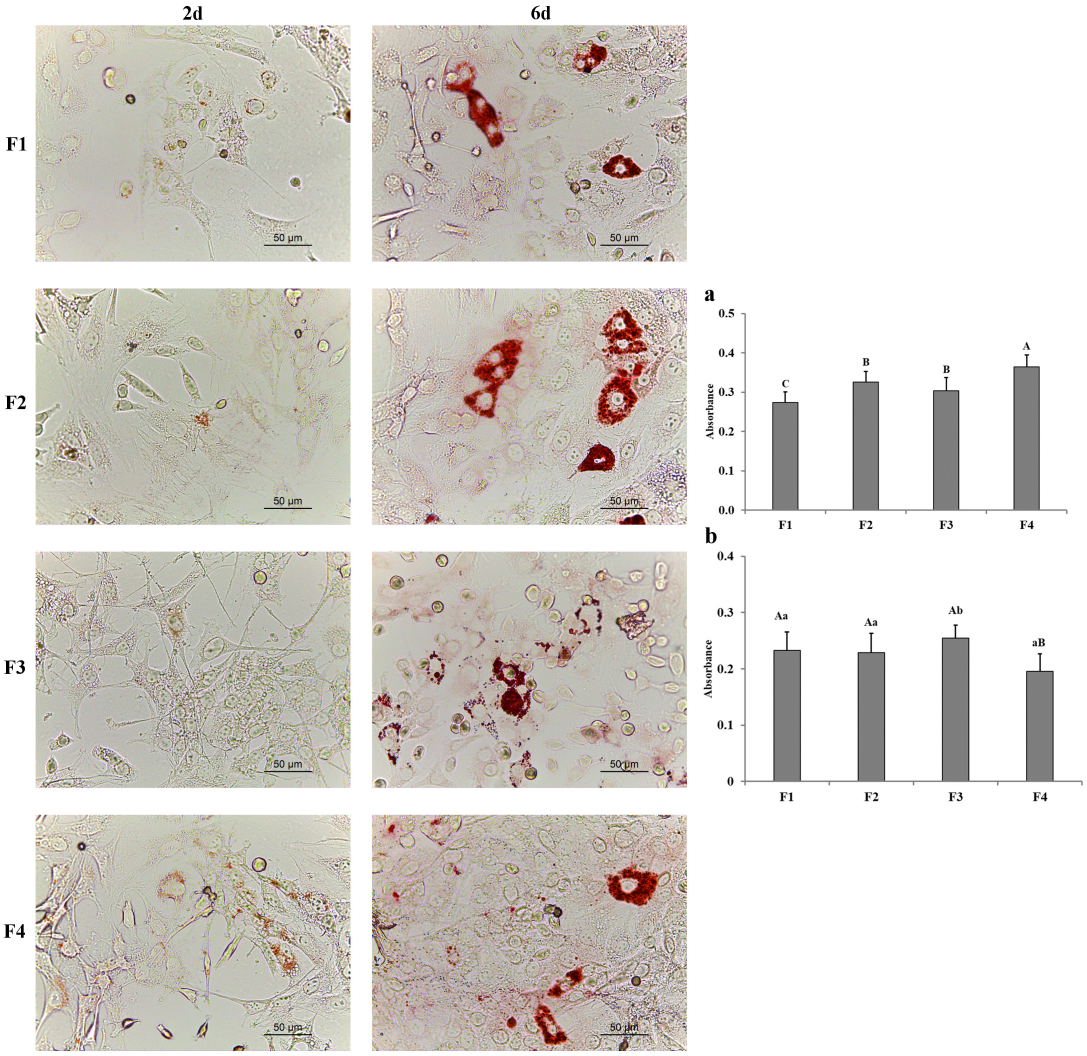

Figure 5.1: ORO uptake by X9 cells at 2 (2d) and 6 (6d) days of differentiation with differently formulated differentiation media and its quantification at 2d **(a)** and 6d **(b)**. Absorbance data are expressed as means ± SEM from one-way ANOVA. Capital letters indicate $p < 0.0001$, small letters indicate $p < 0.05$.

5.1.4 IMBAT cells

A preliminary methodological study has been performed also on IMBAT cells, which are immortalized brown adipocytes isolated from the intrascapular fat pad of mice kindly gifted by prof. Mark Christian (Nottingham Trent University).

The culture of IMBAT cells presents some substantial differences with other models, as the initial clonal expansion phase should occur at 33°C. After the incubation in the differentiation cocktail recommended by prof.

Christian, cell culture is continued at 37°C. The culture media have been tested in our laboratory and they gave satisfactory growth and differentiation performances; their formulation is reported in Table 5.7.

Table 5.7: Formulation of IMBAT cells culture media as reported by prof. Christian. DMEM/F12: Dulbecco's modified Eagle medium/Ham's F12; FBS: fetal bovine serum; P/S: penicillin/streptomycin; IBMX: isobutylmethylxanthine.

Reagent	**Growth medium**	**Differentiation medium**	**Maintenance medium**
Basal medium	DMEM/F12	DMEM/F12	DMEM/F12
FBS	10%	10%	10%
P/S	1%	1%	1%
Amphotericin B	1%	1%	1%
Triiodothyronine	–	1 nM	1 nM
Human insulin	–	1 µg/mL	1 µg/mL
Dexamethasone	–	250 nM	–
IBMX	–	0.5 mM	–
Rosiglitazone	–	2.5 µM	–
Indomethacin	–	125 µM	–

The use of this model will have interesting applications for the current studies, as they both serve as a reliable positive control in comparison to treated white and brite cells and can further strengthen data about the induction of thermogenesis produced by tested bioactive compounds.

Chapter 6

Structural analyses

6.1 Lipid droplets analysis

6.1.1 BODIPY staining

4,4-difluoro-1,3,5,7,8-pentamethyl-4-bora-3a,4a-diaza-*s*-indacene (BODIPY) 493/503 is a fluorescent dye that stains neutral lipids in biological samples. This has been chosen to perform ultrastructural studies on adipocytes imaged at epifluorescence Axio Observer Z1 microscope (Carl Zeiss GmbH) or SP8 confocal microscope (Leica Microsystems GmbH) equipped with LAS X software, version 3.1.5.16308.

To perform BODIPY staining, cells grown on microscopy slides were fixed with a 2% formalin solution diluted in PBS 1X at RT for 15 minutes. Fixed cells were then rinsed in PBS 1X and incubated with 1 µg/µL BODIPY for 45 minutes at RT in dark. Stained cells were rinsed three times with PBS 1X and mounted with a Fluoroshield mounting medium with 4',6-diamidino-2-phenylindole (DAPI).

6.1.2 LD dynamic analysis

A comprehensive and descriptive system to obtain reliable morphological data about browning of white adipocytes is the analysis of LD dynamic in cells. For this purpose, the colorimetric ORO assay cannot provide useful

data, because it is used mainly to understand the differentiation level of adipocytes, as it gives a global quantitation of the concentration of TAGs without distinguishing the contribution of each LD. For this reason, the morphology of LDs in this thesis was measured with the MRI_Lipid Droplets macro for ImageJ software (http://rsb.info.nih.org/ij/) [137], following the acquisition of images of BODIPY-stained adipocytes. The macro applied a bandpass filter to the input image by using a Gaussian filter and then scaling the image down and up again with increasing scale. This procedure allowed to apply an automatic threshold to the image, which produced a mask that removed artefacts. Objects that appeared smaller than a given size chosen by the user were considered artefacts and consequently removed from the count. Contacting lipid droplets are separated by a binary watershed transformation. Finally, individual LDs in every field are enclosed in single regions of interest (ROI) for which the software measures the area surface (Figure 6.1).

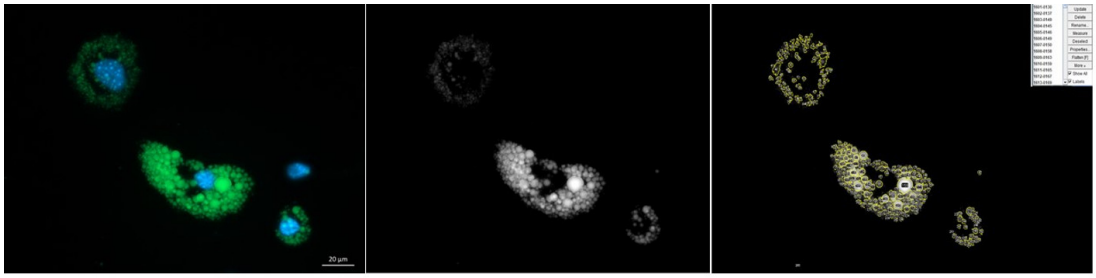

Figure 6.1: MRI_Lipid Droplets macro for ImageJ measures simultaneously all LDs present in the input micrography by enclosing them in discrete ROIs.

As a raw output, the macro provided a number of data, including the number of LDs in the input image, their area surface, maximum Feret diameter (MFD) and integrate optical density (IOD). MFD estimated the diameter of irregularly shaped objects [138], while IOD indicated the triglyceride content, as a linear correlation between IOD and lipid content of LDs has been described [139]. Total area surface occupied by LDs in each input image has been calculated as the sum of single LD area surfaces. The cell count allowed the calculation of area surface and number of LDs per cell.

The average area surface of a single LD was calculated by dividing the area surface of LDs/cells by the number of LDs/cell.

Morphological data were produced for at least 15 images per experimental condition and were analyzed as non-parametric data, since they did not follow the normal Gaussian distribution. Thus, statistical analyses of LD data were performed with Kruskal-Wallis or Mann-Whitney tests with *post hoc* Bonferroni correction of significance, run on SPSS or XLSTAT statistical softwares. A non-parametric representation of the LD size probability density function (kernel) was also applied to avoid making assumptions about the distribution of the data; the kernel size distribution was produced by a routine written in Matlab 7.1.

6.2 Mitochondrial morphology analysis

6.2.1 MitoTracker staining

MitoTracker® Orange CMTMRos is a selective mitochondrial fluorescent dye whose accumulation depends upon membrane potential. The working solution of choice was prepared by diluting MitoTracker stock solution in cell growth medium to a final concentration of 100 nM. The incubation with the dye was performed on live cells prior fixation with formalin. Cells treated with MitoTracker working solution were incubated in the CO_2 incubator for 30 minutes. After the incubation, fixation with 2% of formalin, washing with PBS 1X and mounting with DAPI-Fluoroshield were performed prior imaging at the epifluorescence Axio Observer Z1 microscope.

6.2.2 Analysis of mitochondrial dynamic

The analysis of mitochondrial morphology has been performed with the ImageJ macro Mito-Morphology [140] for experiments in Chapter 11. 10 images per time point underwent mitochondrial morphology analysis: the intensity of mitochondria-specific fluorescence produced by MitoTracker

Orange staining was adjusted with contrast-limited adaptive histogram equalization (CLAHE) to optimally resolve the pixel constituting each mitochondrion. Measurements produced data about mitochondrial content (% of cytosol occupied by mitochondria), the area/perimeter ratio (a parameter that described the level of interconnectivity between mitochondria) and the area/perimeter ratio normalized to the minor axis, which in turn described the degree of swelling.

Later investigations unveiled some limitations of this tool. A more comprehensive analysis was provided by the stand-alone software MicroP, whose functionality has been described by Peng and colleagues [141]. Images of MitoTracker-stained cells used as input were semi-automatically segmented to distinguish mitochondria from nuclei. Each mitochondria-background image was subsequently segmented to extract mitochondria with local normalization and Otsu's thresholding. After this final segmentation step, mitochondria appeared as binary objects which can be extracted by standard object labeling. Postprocessing of these images removed objects with low intensity and small area surface, which are likely artefacts.

For each segmented mitochondrion, structural data were produced, including area surface, solidity and ratio of skeleton. Solidity has been described as the ratio of the mitochondrial area and the area of the virtual box enclosing the mitochondria: the more this value is close to 1, the more compact is the mitochondrion. Values close to 0 indicate a twisted structure. The ratio of skeleton indicated the ratio between mitochondrial major and minor axes and it can be interpreted as an elongation index. The whole set of quantitative data per each mitochondrion allowed their clustering and classification into six discrete morphological subtypes (Figure 6.2):

1. small globules: round-shaped mitochondria, that are likely a product of mitochondrial fission;

2. large globules: swollen globules with a larger area;

3. simple tubules: straight, elongated mitochondria with no branches;
4. twisted tubules: elongated tubules with a non-linear development in the cytoplasm;
5. donuts: elongated tubules whose ends fused with each other;
6. branched tubules: complex interconnected mitochondrial structure with a web-like organization.

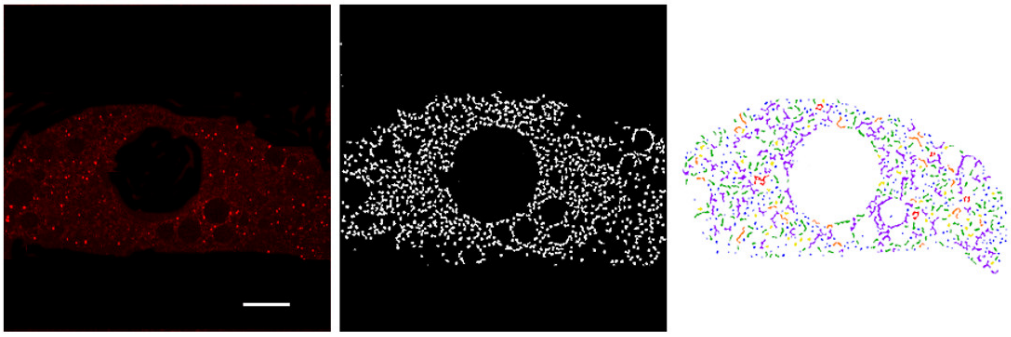

Figure 6.2: From an image of MitoTracker Orange-stained cells (left), MicroP software perform a segmentation with Otsu's thresholding (middle) and classifies detected mitochondria into morphological subtypes (right) as follows: blue: small globules; yellow: large globules; green: straight tubules; orange: twisted tubules; red: donuts; purple: branched tubules. Scale bar: 10 µm.

This set of morphological data was more descriptive and has been adopted in our experiments to quantify the impact of browning treatments on cell cultures, as presented in Chapter 14. The quantitative data were elaborated to evaluate the frequency of each mitochondrial subtype in differentially treated cells, their cumulative area surface and their cumulative skeletal ratio to effectively present how mitochondrial dynamic was affected by browning-inducing treatments.

Chapter 7

Cell viability

Different treatments administered to cultured cells might affect their viability. To pinpoint the best concentration of bioactive compounds to be administerd to cells, the MTT colorimetric viability assay has been chosen. After removal of culture medium from treated cells, an incubation with 5 mg/mL MTT solution in Hank's balanced salt solution (HBSS) was performed after a wash in PBS 1X. The incubation was carried out at 37°C for 4 h. During this period, living cells convert water-soluble, yellow MTT into a water-insoluble, purple metabolite named formazan; this conversion is catalyzed by mitochondrial reductases [142]. Accumulated formazan is dissolved in dimethyl sulfoxide (DMSO) and incubated overnight at 37°C. The optical density at 550 nm is measured to calculate cell viability, which is directly proportional to the quantity of formazan produced during incubation with MTT. Statistical differences between differentially treated cells are evaluated through one-way analysis of variance (ANOVA) with *post hoc* Bonferroni correction.

Chapter 8

Gene expression analysis

All gene expression experiments were performed on purified RNA isolated from cell culture. RNA isolation was achieved by cell lysis with 1 mL/10 cm^2 TRIzol reagent, which induced a severe breakdown of cellular structures and preserved the integrity of nucleic acids for a long time, if stored at –80°C. Cell lysates were then processed with the PureLink™ RNA Mini Kit following the producer's protocol to purify the isolated RNA. The concentration and quality of isolated RNA were measured with a NanoDrop 1000 spectrophotometer (Thermo Fisher Scientific) or with the Spark multiplate reader.

Gene expression was analyzed either by RT-PCR amplification, followed by agarose gel band quantification, or by retrotranscription of RNA into cDNA which was subsequently amplified with real time PCR. The required primers for PCR amplification were designed on Primer3 Input web tool [143].

8.1 RT-PCR

RT-PCR was the technique of choice in gene expression analysis of the experiment presented in Chapter 11, involving the use of human SGBS adipocytes. β-actin was the housekeeping gene of choice and preliminary trials displayed that its expression was more stable than other housekeeping ge-

nes in human adipocytes. Moreover, the quantification of its amplicon band in the agarose gel was more robust and accurate among replicates than fluorescence quantitation in real time PCR. RT-PCR was performed using the SuperScript™ III one-step RT-PCR system. A list of primers designed on human gene sequences is reported in Table 8.1.

Total RNA is reverse-transcribed and amplified in a PTC-100 thermal cylcer (MJ Research) with the following reaction conditions:

- cDNA synthesis: 50°C, 30 minutes;
- reverse transcriptase inhibition: 94°C, 2 minutes;
- cDNA amplification: 40 cycles of:
    1. cDNA denaturation, 94°C, 30 seconds;
    2. primers annealing at different temperatures according to Table 8.1, 30 seconds;
    3. primers elongation, 72°C, 30 seconds;
- termination: 72°C, 5 minutes.

Amplified cDNA was then quantified by 1% agarose gel electrophoresis with GelRed and normalized against β-actin expression. Agarose bands were measured with the Gel analysis method in ImageJ, which returned absolute density values. Relative density was subsequently calculated by dividing the absolute value of the gene of interest for the density of the housekeeping.

The gene expression analysis was performed on three biological replicates and at least three technical replicates. These expression data accepted the null hypothesis of Kolmogorov-Smirnov statistical test of normality, so they were treated as normal parametric values. For this reason, the statistical significance of differences between genes in each experimental pipeline was analyzed through one-way ANOVA with *post hoc* Bonferroni correction.

Table 8.1: List of primers used in RT-PCR for human gene amplification. *ACTB*: β-actin; *PPARG1*: peroxisome proliferator-activated receptor γ, variant 1; *PPARG2*: peroxisome proliferator-activated receptor γ, variant 2; *PPARA*: peroxisome proliferator-activated receptor α; *PRDM16*: PR domain containing 16; *PPARGC1A*: PPARγ coactivator 1α; *UCP1*: uncoupling protein 1; *LEP*: leptin; *ADIPOQ*: adiponectin; *LIPE*: lipase E.

Gene	GenBank accession	Sequence	Amplicon length (bp)	T_m (°C)
ACTB	JN038572.1	Forward: 5'-CTCTTCCAGCCTTCCTTCCT-3' Reverse: 5'-AGCACTGTGTTGGCGTACAG-3'	116	59.4
PPARG1	NM_138712.3	Forward: 5'-GCCGCCAGATTTGAAAGAAGC-3' Reverse: 5'-TGGCATCTCTGTGTCAACCA-3'	110	57.3
PPARG2	NM_015869.4	Forward: 5'-TACAGCAAACCCCTATTCCA-3' Reverse: 5'-GAGAAGTCAACAGTAGTGAAG-3'	240	55.6
PPARA	NM_005036.4	Forward: 5-TCTGTCGGGATGTCACACAA-3' Reverse: 5'-CGGGCTTTGACCTTGTTCAT-3'	191	57.3
PRDM16	AF294478.1	Forward: 5'-GAGGAGGACGATGAGGACAG-3' Reverse: 5'-GCTCCTCATCCTCCTCATCC-3'	103	61.4
PPARGC1A	NM_001330751	Forward: 5'-GCCCAGGTACAGTGAGTCTT-3' Reverse: 5'-GTGAGGACTGAGGACTTGCT-3'	105	59.4
UCP1	NM_021833.4	Forward: 5'-GCGGATGAAACTCTACAGCG-3' Reverse: 5'-GTTTCTTTCCCTGCGGTGAG-3'	117	59.4
LEP	D63519.2	Forward: 5'-ACCAAGGTCTTCAGCCATCA-3' Reverse: 5'-CCCTCTGCCCTCTCTGAAAT-3'	108	58.4
ADIPOQ	EU420013.1	Forward: 5'-CCTAAGGGAGACATCGGTGA-3' Reverse: 5'-GTAAAGCGAATGGGCATGTT-3'	173	57.4
LIPE	NM_005357.3	Forward: 5'-CTCTGGTCTACTACGCCCAG-3' Reverse: 5'-CATCCCTTATGCAGCGTGAC-3'	121	60.4

8.2 Real time PCR

Real time PCR was chosen for murine samples following multiple housekeeping genes analysis. TATA box-binding protein (*Tbp*), glyceraldehyde 3-phosphate dehydrogenase (*Gapdh*) and RPLP0 ribosomal protein (*36b4*) were found to be excellent housekeeping genes for murine 3T3-L1 and X9 adipocytes. Their amplification with real time PCR was more effective and raw expression data were constant and stable among replicates and between different days of differentiation.

To perform real time PCR, purified RNA was retrotranscribed with either ImProm-II™ Reverse Transcription System or Transcriptor High Fidelity cDNA Synthesis Kit. Aliquots of the synthesized cDNA have been pooled and diluted in serial dilutions to perform standard curves in order to optimize PCR conditions, such as the concentration of both cDNA and primers. A comprehensive list of primers used in all experiments involving murine genes is reported in Tables 8.2 and 8.3. Real time PCR was performed with the Platinum™ SYBR™ Green qPCR SuperMix-UDG in a 96-well spectrofluorimetric CFX thermal cycler (Bio-Rad Laboratories, Inc.) with the following reaction conditions:

- Platinum™ Taq polymerase activation: 50°C, 2 minutes;
- first cDNA denaturation: 95°C, 10 minutes;
- cDNA amplification: 45 cycles of:
    1. cDNA denaturation, 95°C, 10 seconds;
    2. primers annealing at different temperatures according to Tables 8.2 and 8.3, 30 seconds;
    3. primers elongation, 72°C, 30 seconds;
- termination: 72°C, 5 minutes;
- melting curve construction: 0.5°C increments from 65 to 95°C, 5 seconds per each increment.

Table 8.2: List of primers used in real time PCR. **Housekeeping genes:** *Tbp*: TATA box-binding protein; *Gapdh*: glyceraldehyde 3-phosphate dehydrogenase; *36b4*: RPLP0 ribosomal protein. **Brown & brite fat markers:** *Ucp1*: uncoupling protein 1; *Tbx1*: T-box1; *Prdm16*: proline rich domain containing 16; *Elovl3*: elongase of very long chain fatty acids 3; *Ppara*: peroxisome proliferator-activated receptor α; *Ppargc1a*: PPARγ coactivator 1α. **Mitochondrial genes:** *Mfn2*: mitofusin 2; *Drp1*: dynamin-related protein 1; *Cyc1*: cytochrome C1.

Gene	GenBank accession	Sequence	Amplicon length (bp)	T_m (°C)
Tbp	NM_013684.3	Forward: 5'-CCAATGACTCCTATGACCCCTA-3' Reverse: 5'-CAGCCAAGATTCACGGTAGAT-3'	104	58.5
Gapdh	NM_008084	Forward: 5'-AATGTGTCCGTCGTGGATCTGA-3' Reverse: 5'-AGTGTAGCCCAAGATGCCCTTC-3'	117	60.0
36b4	BC099384.1	Forward: 5'-GAAACTGCTGCCTCACATCC-3' Reverse: 5'-AGGTCTTCTCGGGTCCTAGA-3'	179	59.0
Ucp1	NM_009463.3	Forward: 5'-CTTTGCCTCACTCAGGATTGG-3' Reverse: 5'-ACTGCCACACCTCCAGTCATT-3'	123	59.8
Tbx1	NM_011532.2	Forward: 5'-AGGCGGAAGGAAGTGGTATT-3' Reverse: 5'-TACCAGTATCTACACCGCCC-3'	118	58.4
Prdm16	NM_027504.3	Forward: 5'-CCACCAGCGAGGACTTCAC-3' Reverse: 5'-GGAGGACTCTCGTAGCTCGAA-3'	107	61.4
Elovl3	NM_007703.2	Forward: 5'-TTCTCACGCGGGTTAAAAATGG-3' Reverse: 5'-GGCCAACAACGATGAGCAAC-3'	139	58.9
Ppara	NM_011144.6	Forward: 5'-TCTGTCGGGATGTCACACAA-3' Reverse: 5'-CGGGCTTTGACCTTGTTCAT-3'	191	57.3
Ppargc1a	NM_008904.2	Forward: 5-TATGGAGTGACATAGAGTGTGCT-3' Reverse: 5'-CTGGGCAAAGAGGCTGGTC-3'	191	60.0
Mfn2	AY123975.1	Forward: 5'-TGTAGCAGGAGGAATGGTGG-3' Reverse: 5'-TTGTAGCAAGGCAGGGATGA-3'	139	58.4
Drp1	AB079133.1	Forward: 5'-TATGCCAGCAAGTCCACAGA-3' Reverse: 5'-CACAATCTCGCTGTTCTCGG-3'	98	58.4
Cyc1	NM_025567.3	Forward: 5'-GGCATCAGAACCAGAGCATG-3' Reverse: 5'-CTGACCACTTATGCCGCTTC-3'	110	59.4

Table 8.3: List of primers used in real time PCR (continues). **Lipid droplets-associated genes:** *Cidea*: cell death-inducing DFFA-like effector A; *Cidec*: cell death-inducing DFFA-like effector C; *Plin1*: perilipin 1. **Receptors:** *Adrb3*: β_3 adrenoreceptor; *Trpv1*: transient receptor potential vanilloid 1; *Rara*: retinoic acid receptor α; *Rarb*: retinoic acid receptor β; *Rxra*: retinoid X receptor α; *Rxrb*: retinoid X receptor β. **Other genes:** *Adipoq*: adiponectin; *Bdnf*: brain-derived neurotrophic factor; *Lipe*: lipase E.

Gene	GenBank accession	Sequence	Amplicon length (bp)	T_m (°C)
Cidea	NM_007702.2	Forward: 5'-ATCACAACTGGCCTGGTTACG-3' Reverse: 5'-TACTACCCGGTGTCCATTTCT-3'	136	58.9
Cidec	NM_178373.4	Forward: 5'-ACCTTCGACCTGTACAAGCT-3' Reverse: 5'-GTGCAGGTCATAGGAAAGCG-3'	99	58.4
Plin1	NM_175640.2	Forward: 5'-TGGACCACCTGGAGGAAAAG-3' Reverse: 5'-CTTCGAAGGCGGGTAGAGATG-3'	94	60.6
Adrb3	NM_013462.3	Forward: 5'-CCAATGACTCCTATGACC-3' Reverse: 5'-TTCTGGAGCGTTGGAGAGTT-3'	89	57.3
Trpv1	AY445519.1	Forward: 5'-CGAGATAGGCATAGCACCCA-3' Reverse: 5'-TGCTTCATGGTGTCCCTCAT-3'	130	58.4
Rara	BC010216.1	Forward: 5'-CCGACTTGGTCTTTGCCTTC-3' Reverse: 5'-TCTCAGCATCGTCCATCTCC-3'	60	59.4
Rarb	BC076597.1	Forward: 5'-TTCCTGGATCAATGCCACCT-3' Reverse: 5'-TTGGGGTCAAGGGTTCATGT-3'	72	57.3
Rxra	M84817.1	Forward: 5-TCAGGCAAACACTATGGGGT-3' Reverse: 5'-GCAGGTGTAGGTCAGGTCTT-3'	87	58.4
Rxrb	M84818.1	Forward: 5'-AGACAGCTCCTCCCCAAATC-3' Reverse: 5'-GTGCTGAAGGGGTAAGAGGT-3'	80	59.4
Adipoq	BC028770.1	Forward: 5'-AGGGAGAGAAAGGAGATGCAG-3' Reverse: 5'-AGTCCCGGAATGTTGCAGTA-3'	81	60.0
Bdnf	NM_007540.4	Forward: 5'-ATTACCTGGATGCCGCAAAC-3' Reverse: 5'-CCTTCCTTGGTGTAACCCAT-3'	241	58.5
Lipe	NM_010719.5	Forward: 5'-GACAGAGGCAGAGGACCATT-3' Reverse: 5'-TGAGGAACAGCGAAGTGTCT-3'	86	59.0

Gene expression was calculated with the $\Delta\Delta$Ct method [144]: the cycle threshold (Ct) of amplified genes was normalized against the geometric mean of Ct of selected housekeeping genes (ΔCt) and then the ΔCt of control samples was subtracted to the ΔCt of treated samples ($\Delta\Delta$Ct). Relative fold change of analyzed genes was obtained by calculating $2^{-\Delta\Delta Ct}$.

Expression data were generated from biological triplicates and represented similar results from at least three independent experiments. As for gel band quantitation, the relative fold change data were analyzed as parametric data with one- or two-ways ANOVA, followed by *post hoc* Bonferroni correction or Tukey's range test.

In Chapter 13, gene expression data underwent enrichment analysis through FunRich 3.1.3 tool [145]. This software clustered the input expression data into biological processes (BPs), calculating the percentage of annotated protein and the p-value in each BP after Bonferroni correction. The raw list of BPs was screened and most significant ones, with a relevance for the browning study, were extracted and further analyzed with a principal component analysis (PCA). The output of PCA was a distance biplot that clustered significant BPs with relative fold change data per each sample to show correlations among each others.

Chapter 9

Protein expression

The detection of expressed proteins in cellular specimens was mainly performed through immunofluorescence, which allowed to observe positive immunoreaction and the cellular localization of proteins. During the last year of Ph.D, it has been studied and delineated a protocol for in-cell Western (ICW), a protein detection technique that merged the immunofluorescence protocol with the protein quantification that is made possible by Western blot analysis.

9.1 Immunofluorescence

Cells grown on slides were rinsed in PBS 1X and fixed with 2% formalin. After fixation, cells were washed twice with PBS 1X supplemented with 0.05% TWEEN 20 (PBST) and permeabilized for 10 minutes at RT with 0.1% Triton X-100. Autofluorescence induced by the aldehyde-based fixative has been quenched with 0.3 M glycine or 50 mM ammonium chloride for 15 minutes at RT. Then, an incubation for 1 hour at RT with a blocking solution containing 10% FBS and 5% normal goat (NG) serum was performed to avoid the background labeling of secondary antibody. The slides were then incubated with the primary antibody diluted in blocking solution overnight at 4°C in a moist chamber. A list of used primary antibodies has been reported in Table 9.1. The following day, cells were washed in

PBST 1X and incubated for 45 minutes at RT in dark with a fluorescently-labeled secondary antibody. These antibodies included anti-rabbit AlexaFluor® 555 and anti-rabbit fluorescein made in goat for the reaction with primary antibodies, and anti-mouse fluorescein IgM against secondary antibodies. Labeled cells were then washed in PBST 1X and mounted with DAPI-Fluoroshield. The subsequent imaging was performed with the epifluorescence Axio Observer Z1 microscope.

9.2 In-cell Western analysis

Quantification of proteins through ICW was performed on cells plated on a 96-well plate. After culture medium removal, cells were rinsed once in PBS 1X and fixed with 2% formalin for 15 minutes at RT. Cells were then washed in PBST 1X for 5 minutes while shaking and subsequently permeabilized with 0.1% Triton X-100 for 5 minutes. Following four washes in PBST 1X, cells were incubated with a blocking solution containing 1% (bovine serum albumin) BSA and 5% NG. The incubation with primary antibodies (reported in Table 9.1) lasted 2 hours at RT while shaking. A background control was established by incubating selected wells with blocking solution. After four washes in PBST 1X, cells were incubated with the secondary antibody for 1 hour at RT in dark. The secondary antibody was an anti-rabbit IRDye® 800CW labeled IgG made in goat and specific for near infrared detection of protein positivity during ICW imaging.

The detection of fluorescence was performed on an Odyssey® CLx imaging system (LI-COR Inc.) for Western blot equipped with Image Studio™ software. Data have been acquired and analyzed by running an automatic routine specific for ICW.

The relative protein % produced by Image Studio™ was normalized against the expression of a housekeeping protein (α-tubulin) and data were analyzed through one-way ANOVA with *post hoc* Tukey's range test.

Table 9.1: List of primary antibodies used in immunofluorescence and ICW experiments. PPARγ: peroxisome proliferator-activated receptor γ; PLIN1: perilipin 1; UCP1: uncoupling protein 1; TRPV1: transient receptor potential vanilloid 1; PGC-1α: PPARγ coactivator 1 α.

Antibody	Type	Synthesis	Code	Purchased from
Anti-PPARγ	Rabbit polyclonal	Raised against C-terminal amino acids 311-500 of bovine PPARγ.	PAA886Bo01	Cloud-Clone Corp.
Anti-PLIN1	Rabbit polyclonal	Raised against N-terminal amino acids 1-300 of human PLIN1.	sc-67164	Santa Cruz Biotechnology
Anti-UCP1	Rabbit polyclonal	Raised against amino acids 145-159 of human UCP1.	ab10983	Abcam
Anti-TRPV1	Mouse monoclonal	Generated against N-terminal amino acids 1-130 of rat TRPV1.	sc-398417	Santa Cruz Biotechnology
Anti-UCP1	Rabbit polyclonal	Raised against amino acid sequence from 1 to 299 of human UCP1	PA5-29575	Thermo Fisher Scientific
Anti-PGC-1α	Rabbit polyclonal	Raised against a 17 amino acid sequence close to the N-terminus of human PGC-1α	GTX31921	GeneTex
Anti-α tubulin	Rabbit polyclonal	Generated from an amino acid sequence within residues 400 to the C-terminus of human α tubulin.	ab18251	Abcam

Chapter 10

Intracellular calcium analysis

The measurement of intracellular Ca^{2+} in cells has been performed when analyzing samples treated with capsaicin, because its membrane receptor TRPV1, when activated, triggers a Ca^{2+} influx (see Chapter 13). To measure intracellular Ca^{2+}, the calcium probe Fluo-8 AM has been chosen. Live cells were incubated with the probe that, once uptaken by cells, was cleaved of its amphipathic region and became active, emitting fluorescence when associated to a Ca^{2+} ion [146]. It was excited at 490 nm and emitted at 520 nm.

After culture medium removal, the staining with a 4 µM Fluo-8 AM working solution in HBSS supplemented with 15 mM HEPES was performed for 1 h at 37°C. Stained cells were then rinsed with HEPES-HBSS and immediately imaged.

The acquisition of Fluo-8-treated cells was performed as a time lapse imaging at the epifluorescence Axio Observer Z1 microscope, which produced a movie that lasted 180 seconds. This experiment required a first acquisition of untreated Fluo-8-stained cells to acquire the baseline fluorescence, followed by the administration of the treatment during the acquisition itself (12-14 seconds after the beginning of the acquisition) to appreciate real time changes in cellular fluorescence induced by Ca^{2+} movements across plasma membrane.

The analysis of fluorescence signals was performed with ImageJ soft-

ware, which separated the single frames of the movie creating a stack. To visualize the fluorescence signal, the brightness and contrast of the stack were automatically corrected. By creating a Z-projection of the standard deviation of all the frames composing the stack, the user appreciated which cells displayed a variation in fluorescence intensity. Those cells showing a significant signal were manually added to the ROI manager tool for the measurement. The standard deviation was the parameter of choice because it displayed the intensity of the variation of fluorescence only in cells that actually showed such variation. Cells that did not respond to either the treatment or the staining with Fluo-8 did not display a difference in fluorescence intensity, so their standard deviation equaled to 0.

The ratio between the maximum fluorescence intensity emitted after the addition of the compound (F) and the average of baseline fluorescence (F_0) was plotted to visually describe the cell-specific variations in fluorescence signal, according to the protocol stated by Muto and colleagues [147].

Part III

Results and discussion

Chapter 11

SGBS cells as a browning model

The Simpson-Golabi-Behmel syndrome (SGBS) cell strain is an *in vitro* model of human white preadipocytes. This strain has been established in 2001 by Wabitsch and colleagues, who isolated preadipocytes from the subcutaneous adipose tissue of a SGBS-affected pediatric patient [127].

SGBS is caused by deletions or point mutations of the X-linked glypican 3 gene (*GPC3*), located in Xq26. The causative mutations may also involve the gene glypican 4 (*GPC4*), which is 120 kb downstream from *GPC3* [148]. The different levels of mutation that can affected these genes produce a variable range of symptoms: while the mild form is associated with long-term survival, more aggressive forms of this syndrome cause early death [149]. These forms are characterized by pre- and post-natal macrosomia, coarse facial features and different levels of skeletal, visceral and neurological abnormalities. A number of cases of SGBS-associated gastrointestinal anomalies, renal malformations, hepatocellular carcinoma, Wilms tumor and mental retardation have been reported [149–151].

The singular behavior of SGBS cells relies on the *GPC3* mutation: it has been reported that cells mutated for this gene show enhanced hedgehog signaling pathway [152], a positive regulator of body growth, and dipeptidyl peptidasic activity of CD26, which is positively correlated to cell proliferation [153]. In fact, despite these cells are neither immortalized nor transformed, they retain the ability to expand and differentiate into ma-

ture adipocytes for a high number of generations. For this reason, SGBS cells are an excellent model for the study of obesity and cancer and have been extensively used in recent years [154].

More recently, another unique feature of SGBS cells has been described. During differentiation, these adipocytes exploit a transient brown-like phenotype without any kind of stimulation [155, 156]. Around the 14^{th} day of differentiation, the expression of canonical BAT markers, such as *UCP1*, sharply increases. The expression levels of these markers decreases around the 28^{th} day of differentiation, when the original white phenotype is restored [155].

The aim of the present research is to gain further knowledge of the phenotypic switch that characterizes these cells by analyzing the dynamic changes in LD and mitochondrial morphology. This aspect, despite not being investigated in previous studies, is of outstanding importance because one of the main features of WAT browning is a dynamic reorganization of LDs and mitochondria. This investigation is corroborated with the expression analysis of selected browning markers.

SGBS cells were grown as described in Section 5.1.1 and cell sampling occurred at 0, 7, 14 and 21 days following the induction of differentiation (D0, D7, D14 and D21). The results of this research have been published in Histochemistry and Cell Biology in 2018 as an original research article [99]. Briefly, this study confirmed previous findings about the changeful phenotype of SGBS cells [155, 156], corroborating them with a structural analysis of changes in LD and mitochondrial morphology. Both organelles display structural variations coherently with the onset of a brown fat-like phenotype [92, 103]. In conclusion, this research work provided a new insight of SGBS cells browning attitude, stressing the need to pay attention in their use as a model when testing browning factors [99].

Chapter 12

The browning factor BAIBA

Physical exercise has been shown to have many health benefits, as it increases metabolic rate, improves glucose homeostasis and increases insulin sensitivity. Recently, endocrine factors called myokines, produced by skeletal muscles and released during their contraction, have been described and actively participate in the loss of fat mass through thermogenesis[109, 157].

The β-aminoisobutyric acid (BAIBA) is a non-protein amino acid derived by the catabolism of thymine and valine [158] and has the following structure:

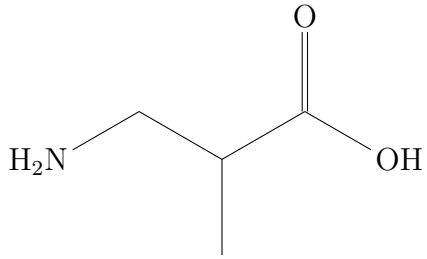

Recently, it has been demonstrated that BAIBA promotes browning of white adipocytes, lipid oxidation in hepatocytes and has a protective role against insulin resistance [122]. Moreover, it preserves osteocytes from reactive oxygen species (ROS)-induced apoptosis [159]. The role of myokines in enhancing lipid metabolism and promoting the recruitment of thermogenic adipocytes has been deeply studied and reviewed [109, 160]. Nevertheless, the cellular pathways in adipocytes activated by the interaction

with circulating myokines is still mostly unknown. Roberts and colleagues proposed a PPARα-dependent pathway through which BAIBA achieves its positive effects on adipocytes and hepatocytes [122]. Despite this observation, the exact signaling pathway involving BAIBA needs further investigation, as well as the role that BAIBA has on affecting LD dynamic in adipocytes. This research aims to elucidate the browning effect of BAIBA on 3T3-L1 preadipocytes during their differentiation into mature fat cells by analyzing the modifications of cytomorphological parameters of LDs and the expression of a selected panel of marker genes. The analyzed genes included brown fat-specific markers (*Ucp1*, *Cidea*, *Elovl3*, *Prdm16*), the brite marker *Tbx1*, genes related to mitochondrial biogenesis and functionality (*Ppargc1a*, *Cyc1*), genes expressing LD-associated proteins (*Cidec*, *Plin1*) and brain-derived neurotrophic factor (*Bdnf*), a neurotrophin whose browning activity has been investigated *in vivo* and displayed a role in regulating energy balance and insulin signaling [123, 161]. For this experiment, 3T3-L1 cells were cultured with the medium reported in Table 5.2. Concomitantly with the switch from differentiation to maintenance medium, cells were treated with different concentrations of BAIBA in a racemic mixture; selected concentrations were 1, 3 and 5 µM, as deduced from the work by Roberts and colleagues [122]. Treated cells were analyzed at 4 (4d), 8 (8d) and 10 days (10d) after the induction of differentiation, which correspond respectively to 2, 6 and 8 days of incubation with the active molecule. A negative vehicle control was established by the supplementation of H_2O to the medium.

The results on 3T3-L1 cells treated with BAIBA were published in the European Journal of Histochemistry in 2018 [162] and showed that different BAIBA doses administered to cultured cells for different times of exposure produced a variety of outcomes. In terms of LD dynamic and expression of browning markers, the 5 µM dose was the most effective during early differentiation of 3T3-L1 cells. The browning effect of the compound decreased in following days of exposure and disappeared at 10 days after

the induction of differentiation. This research highlighted the early effect of BAIBA in inducing WAT browning and brought new evidence about it lack of effectiveness after prolonged exposure.

Chapter 13

Browning effect of capsaicin

Adipose tissue browning research is currently focused in the detection of endogenous and exogenous substances that can recruit thermogenic adipocytes in both BAT and WAT. Natural compounds are an interesting target in this research, as they can be included in functional foods with therapeutic properties [109].

Capsaicin is an alkaloid found in the fruit of *Capsicum* spp. (hot pepper), which is responsible for its spicy flavor [163].

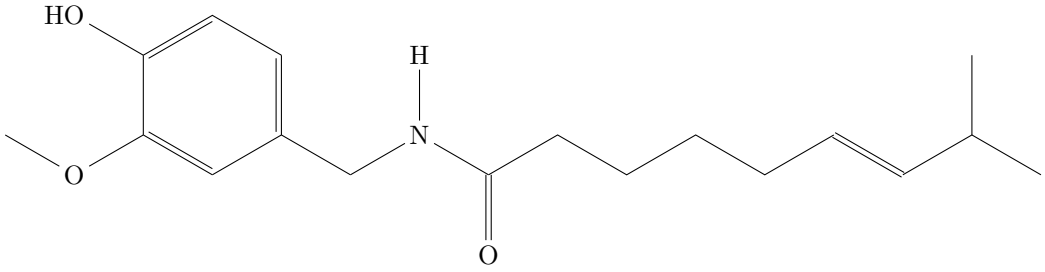

Its biological effects are due to its interaction with the transient receptor potential vanilloid 1 (TRPV1). This receptor is mainly found in peripheral sensory neurons involved in pain sensation [164] and it is also extensively distributed in the gastrointestinal tract [165] and in AT [166]. After the interaction with its ligands, adipose TRPV1 opens its ion channel, causing an intracellular influx of Ca^{2+}. The high intracellular Ca^{2+} concentration activate the Ca^{2+}/calmodulin-activated protein kinase (CaMKII), which in turn phosphorylates AMPK and, eventually, sirtuin 1 (SIRT1). Phosphorylated

SIRT1 promotes the deacetylation of PRDM16 and PPARγ. When active, these two transcription factors interact with each other and promote *Ucp1* expression [125]. Capsaicin triggers an indirect browning stimulation also when interacting with gastrointestinal TRPV1: the signal produced in the guts is transmitted through CNS to WAT depots following the activation of sympathetic adrenergic pathway [126].

The browning potential of capsaicin on white adipocytes has been recently elucidated [125, 167], but long-term effects need further investigation. Moreover, the effect of capsaicin on LD remodeling and on the expression of LD-associated proteins have not been properly studied.

This research enriches previous results on the browning effect of capsaicin by studying it on two different cell models: 3T3-L1 and X9 murine cells. These lines differ in their origin and could show different responses to browning stimulation, being X9 cells responsive to browning stimuli, as they were isolated from an inguinal depot [80]. Conversely, 3T3-L1 cells display features of multiple adipocytes lineages following appropriate stimulation [168]. The changes in LD dynamics and gene expression profile after the administration of different doses of capsaicin have been analyzed between two times of differentiation. Finally, long-term effects of capsaicin, in combination with norepinephrine, were also tested.

Cell culture was achieved with conditions reported in Table 5.3 for 3T3-L1 and in Table 5.5 for X9 cells. Treatment of both cell lines with capsaicin (CP) and norepinephrine (NE), alone or in combination, started at day 3 of differentiation, concurrently with the switch from the differentiation medium to the maintenance one and lasted until analysis either at 4 days of differentiation (4d), 1 day of treatment, or at 8 days of differentiation (8d), 5 days of treatment. Experimental groups were identified by adding to the maintenance medium different combinations of compounds. A vehicle negative control (CTRL) was established by adding to the maintenance medium absolute ethanol (1:1000 dilution). The positive control was represented by cells treated with 10 µM norepinephrine (NE). Cap-

saicin concentrations were tested at 0.1 µM (0.1CP) and 1 µM (1CP). These doses were found to be effective in triggering a brite phenotype on differentiating 3T3-L1 cells [167], but have never been tested neither on mature 3T3-L1 adipocytes nor on X9 cells. The two compounds were also combined into two additional treatments (0.1CPNE and 1CPNE) to understand if any synergies or antagonisms between the two factors could occur and to mimic the cold-independent adrenergic response that CP is able to trigger *in vivo* [124] (Figure 13.1).

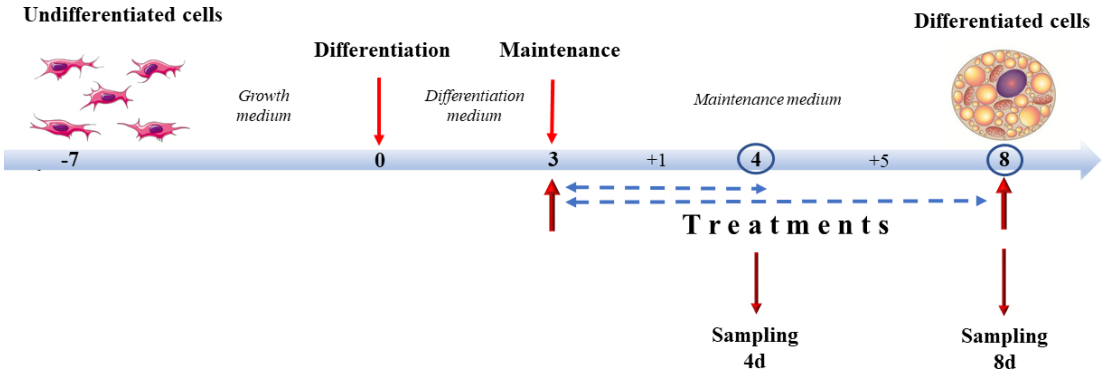

Figure 13.1: Cell culture treatment protocol. Cells were grown until 90% (X9) or 100% (3T3-L1) confluence. Differentiation lasted 3 days. From day 3, cells were incubated with maintenance medium supplemented with different treatments lasting for one (4d) or 5 days (8d).

The results of this research have been published in Frontiers in Physiology, section Lipid and Fatty Acid Research, in 2019 [169]. The study highlighted important differences in the response of the two cell models to different treatments. 3T3-L1 cells responded to 1CP treatment ad 8d with a significant up-regulation of *Ucp1* and other browning markers, while the incubation with NE, alone or in association with capsaicin, did not significantly affect gene expression. Conversely, capsaicin treatments coupled with NE significantly reduced LD area surface and size at 4d. Capsaicin treatments on X9 cells poorly affected their gene expression; browning markers were significantly over-expressed following NE exposure. Also LD measurements were significantly affected by NE alone or in combination with capsaicin doses.

The measurement of intracellular Ca^{2+} influx in 3T3-L1 cells confirmed

the activation of TRPV1 receptor following capsaicin exposure, although this result should be further stressed by treating cells with a TRPV1 inhibitor, i.e. capsazepine. Nevertheless, preliminary promising results of TRPV1 inhibition in 3T3-L1 adipocytes have been already described by Baboota and colleagues [167].

In conclusion, 3T3-L1 cells activated a brite phenotype following direct capsaicin exposure, while X9 cells were insensitive to this treatment and responded only to the incubation with NE.

Chapter 14

The browning action of myokine BDNF

14.1 Introduction

Brain-derived neurotrophic factor (BDNF) is a member of the neurotrophin family of growth factors, which have a role in nerve growth regulation and synaptic plasticity [170]. BDNF and its receptor tropomyosin-related kinase B (TrkB) are abundantly expressed in neuronal cells, including neurons in energy homeostasis centers within the hypothalamus [171]. Recently, it has been pointed out that BDNF is not only expressed in the nervous system, but also in other tissues like skeletal muscles [172] and adipose tissue [173]. Now it has been established the role of BDNF in mediating the whole body adaptive responses to variations in energy intake and expenditure [174]. For instance, BDNF directly affects cells with a role in glucose metabolism, such as β cells, hepatocytes and skeletal muscle, towards a hypoglycaemic phenotype [174].

Concerning adipose metabolism, hypothalamic BDNF up-regulates UCP1 levels in BAT, promoting energy expenditure [175], and can promote WAT browning through sympathetic neuron activation in response to environmental stimuli [123]. In addition to neuronal-mediated metabolic effects,

BDNF can regulate peripheral energy metabolism by directly affecting non-neuronal cells, like adipocytes themselves.

Being synthesized also in skeletal muscles during their contraction, BDNF has been classified as a myokine that acts as an autocrine factor to improve mitochondrial fat metabolism [176].

Clearly, BDNF has a key role in regulating metabolism of non-neuronal tissues, but the mechanisms of action and the involved pathways still deserve a deeper understanding.

3T3-L1 cells were cultured with the medium formulation reported in Table 5.4. At the 6^{th} day of supplementation of the maintenance medium, 3T3-L1 cells were fully differentiated into mature adipocytes. At this point, cells were treated with 1 ng/mL BDNF for 3 (BDNF_3h) or 24 (BDNF_24h) hours. The choice of BDNF dose was performed by analyzing freely accessible data of murine pro-B cells transfected with TkrB. The ED_{50} calculated for these non-neuronal cells was 0.2–2 ng/mL. A negative vehicle control was established by treating cells with PBS 1X and a positive control was realized by incubating cells with 1 µM NE for 3 hours.

14.2 Results

14.2.1 mRNA and protein expression

Relative fold change of tested genes is reported in Figure 14.1. The relative fold change of *Adipoq* was mostly uneffected by different treatments. The browning markers *Ucp1* ($p < 0.0001$ *vs* CTRL and NE), *Tbx1* ($p < 0.0001$ *vs* CTRL, $p < 0.01$ *vs* NE) and *Prdm16* ($p < 0.0001$ *vs* CTRL and NE) are up-regulated in BDNF_3h cells. Their expression is significantly increased also in BDNF_24h cells ($p < 0.0001$ *vs* NE; $p < 0.05$ *vs* CTRL; $p < 0.05$ *vs* CTRL, respectively) (Figure 14.1, a). The lower *Ucp1* relative fold change reported in BDNF_24h cells with respect to BDNF_3h corresponded to a significantly higher protein content ($p < 0.01$ *vs* CTRL, $p <$

0.0001 *vs* NE), as detected by ICW (Figure 14.2).

Ppargc1a expression was significantly lower *vs* NE in BDNF-treated cells at both time points ($p < 0.0001$) (Figure 14.1, a). Conversely, the PGC-1α content was significantly elevated in BDNF_24h samples ($p < 0.01$ *vs* NE) (Figure 14.2).

Mfn2 was significantly down-regulated in BDNF_24h cells ($p < 0.0001$ *vs* CTRL and NE), while *Drp1* expression did not report any significant variation (Figure 14.1, a).

The expression of brown marker and LD-associated gene *Cidea* was significantly elevated in BDNF_3h cells ($p < 0.01$ *vs* CTRL). Conversely, *Cidec* expression did not significantly vary among treatments, despite *Plin1* relative fold change showed the same trend, but significant differences were displayed by BDNF_3h and BDNF_24h ($p < 0.01$ *vs* CTRL) (Figure 14.1, b). The administration of BDNF up-regulated the adipocyte-specific *Bdnf* expression in an autocrine fashion, with significant differences at both 3 hours ($p < 0.01$ *vs* CTRL) and 24 hours ($p < 0.05$ *vs* NE) (Figure 14.1, b).

14.2.2 Mitochondrial morphology

The output of MicroP software was processed in order to depict morphological differences among samples that underwent various treatments. Mitochondrial area surface, mitochondrial number, elongation index and solidity were analyzed to classify mitochondrial subtypes detected by the software. These include small globules, large globules, simple tubules, twisted tubules, donuts and branched tubules.

Mitochondrial subtypes

Figure 14.3 presents the % of mitochondrial subtypes in controls and in BDNF-treated cells.

The relative % of total mitochondria ranged from 18.94% (CTRL) to 29.02% (BDNF_24h). Small globules significantly increased in NE ($p <$

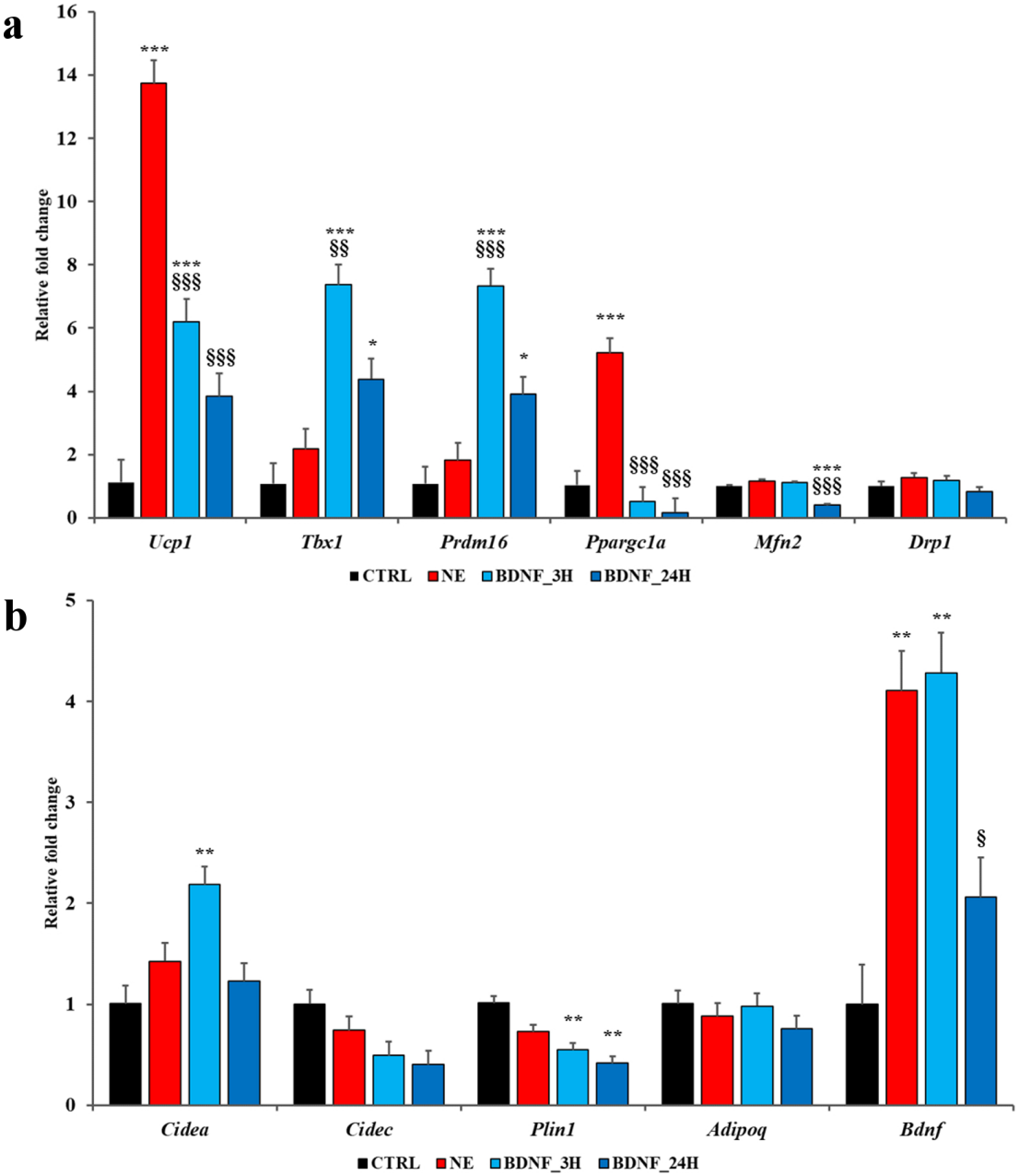

Figure 14.1: Differentially expressed genes in BDNF-treated cells and controls (CTRL and NE). **(a)** Relative fold change of brown markers and mitochondrial dynamic-related genes. **(b)** Relative fold change of LD-associated genes, *Adipoq* and *Bdnf*. Data from one-way ANOVA with *post-hoc* Tukey HSD correction are presented as LS means of relative fold change ± SEM. *** $p < 0.0001$ *vs* CTRL; ** $p < 0.01$ *vs* CTRL; * $p < 0.05$ *vs* CTRL; §§§ $p < 0.0001$ *vs* NE; §§ $p < 0.01$ *vs* NE; § $p < 0.05$ *vs* NE.

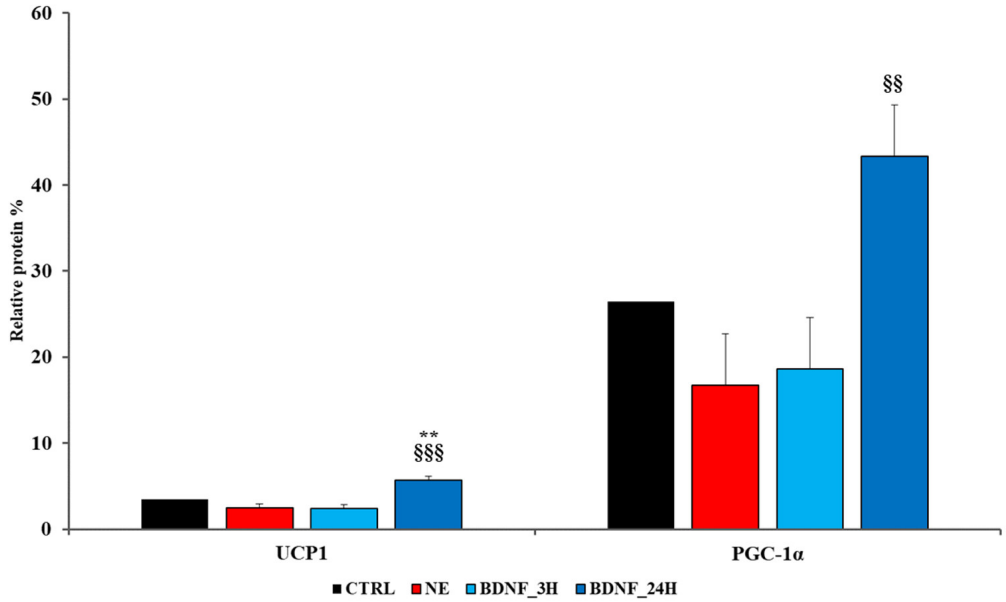

Figure 14.2: Relative percentage of proteins detected by ICW. The percentage of proteins has been normalized against the expression of α-tubulin as an internal housekeeping. Data from one-way ANOVA with *post-hoc* Tukey HSD correction are presented as LS means of relative % of protein ± SEM. ** $p < 0.01$ *vs* CTRL; §§§ $p < 0.0001$ *vs* NE; §§ $p < 0.01$ *vs* NE.

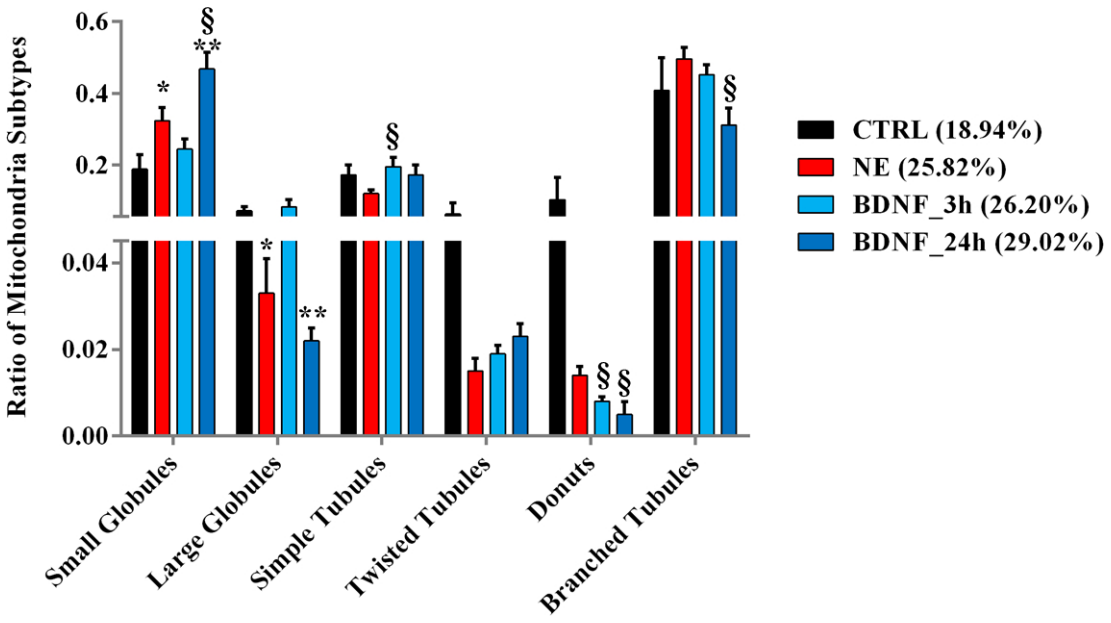

Figure 14.3: Presence of different mitochondrial subtypes in BDNF-treated and in control cells. Data are presented as the ratio of mitochondrial subtypes relative to the total number ± SEM. Statistical significance was determined through two-tailed t-test *vs* positive and negative controls. ** $p < 0.01$ *vs* CTRL; * $p < 0.05$ *vs* CTRL; § $p < 0.05$ *vs* NE.

0.05 *vs* CTRL) and in BDNF_24h cells ($p < 0.01$ *vs* CTRL and $p < 0.05$ *vs* NE). This result might account for an increased mitochondrial fission in these samples, since the presence of tubular structures was reduced. This was particularly true for branched tubules, which were significantly less present in BDNF_24h cells ($p < 0.05$ *vs* NE). Large globules decreased significantly in NE ($p < 0.05$ *vs* CTRL) and BDNF_24h ($p < 0.01$ *vs* CTRL) treatments, indicating reduced swelling phenomena. A sensitive, although not always statistically significant, decrease relative to CTRL cells has been observed for twisted tubules and donuts ($p < 0.05$ *vs* NE in BDNF-treated samples). Taken together, these results outlined a distribution of mitochondrial subtypes coherent with fission events in 3T3-L1 cells that were incubated with NE and with BDNF for 24 hours.

Mitochondrial area surface

The analysis of mitochondrial area surface per each subtype can provide useful information about the dynamic of each morphological type following the administration of a browning compound.

The distribution of mitochondrial area surface is presented in Figure 14.4. The area surface of small globules in BDNF_24h cells was significantly higher than in controls ($p < 0.01$ *vs* CTRL and $p < 0.05$ *vs* NE); by contrast, the area surface of branched tubules was the significantly lowest in the same sample ($p < 0.01$ *vs* both CTRL and NE). Simple tubules ($p < 0.05$ *vs* both CTRL and NE) and twisted tubules ($p < 0.01$ *vs* both CTRL and NE) had a significantly larger area surface in BDNF_24h, although the total area surface of twisted tubules was substantially lower compared to other mitochondrial subtypes. In the same sample, donuts displayed a significantly low area surface ($p < 0.01$ *vs* CTRL and $p < 0.05$ *vs* NE). BDNF_3h sample displayed a similar trend in mitochondrial area surface distribution, in particular in branched tubules ($p < 0.05$ *vs* CTRL), donuts ($p < 0.05$ *vs* both CTRL and NE) and simple tubules ($p < 0.05$ *vs* CTRL), while small globules were not significantly different from control cells. De-

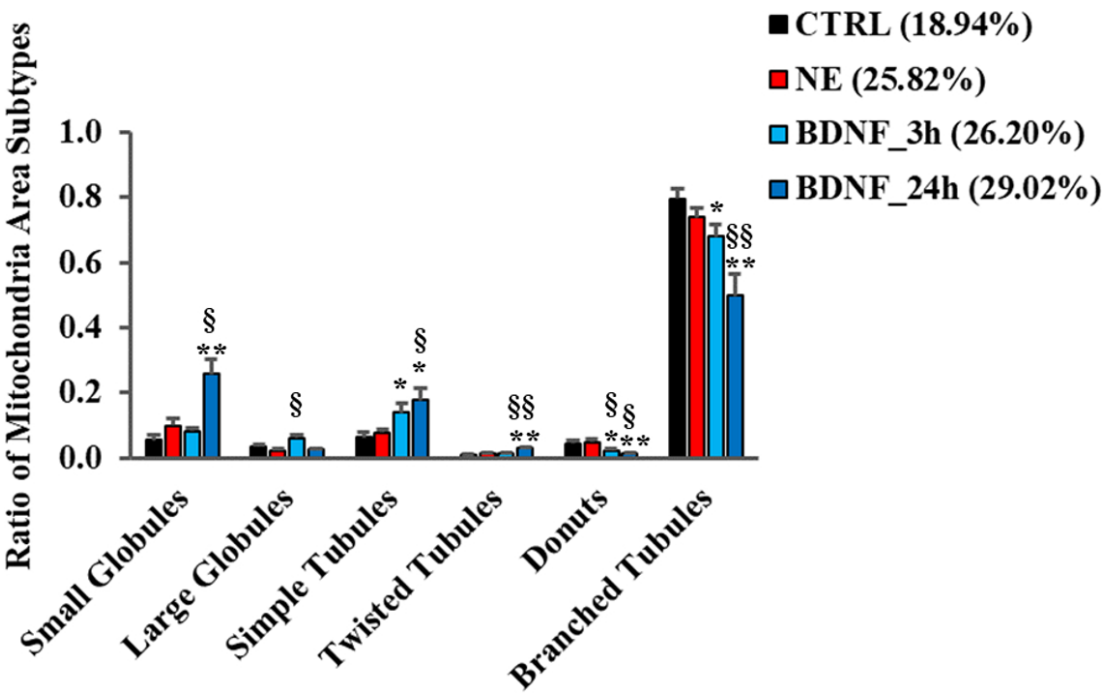

Figure 14.4: Distribution of total mitochondrial area surface among treatments and different morphological subtypes. Data are presented as the ratio of area relative to the total area ± SEM. Statistical significance was determined through two-tailed t-test *vs* negative and positive controls. ** $p < 0.01$ *vs* CTRL; * $p < 0.05$ *vs* CTRL; §§ $p < 0.01$ *vs* NE; § $p < 0.05$ *vs* NE.

spite this, the area surface of large globules in BDNF_3h was significantly higher compared to controls ($p < 0.05$ *vs* NE).

Figure 14.5 reports the cumulative frequency of morphological subtypes' area surface among different bins of area, flanked by boxplots showing the differences of medians, first-to-third quartiles and the most extreme values within the interquartile range among samples. Small globules in NE and BDNF_24h samples displayed the lowest area surface compared to other treatments ($p < 0.0001$), as their cumulative frequency was higher in low bins of area surface. A similar pattern occurred also in large globules, where their area in BDNF_24h was the significantly lowest ($p < 0.0001$). The pattern of simple and twisted tubules was quite similar to each other: the area surface of NE and BDNF_24h cells was significantly lower and showed little or no statistical difference among them. Nevertheless, the abundance of mitochondria with small area surface was higher in BDNF_24h sample.

BDNF_24h had a substantially minor area surface ($p < 0.0001$) in donuts compared to other treatments; this was also evident from the cumulative frequency curve, as this sample reached the highest frequency in small bins of area surface. A similar trend was observed also in branched tubules ($p < 0.0001$).

In summary, results about the area surface of mitochondrial subtypes showed that NE and BDNF_24h cells had the lowest area for most of morphological subtypes, especially in tubular-shaped mitochondria. This feature confirmed previous assumptions about the onset of mitochondrial fission.

Elongation index of mitochondria

The elongation index is a parameter that quantifies the degree of elongation of a mitochondrion: higher values account for elongated mitochondria. This index is calculated by MicroP as skeletal ratio, that is the ratio between the major and the minor axes of the selected mitochondrion. Fig-

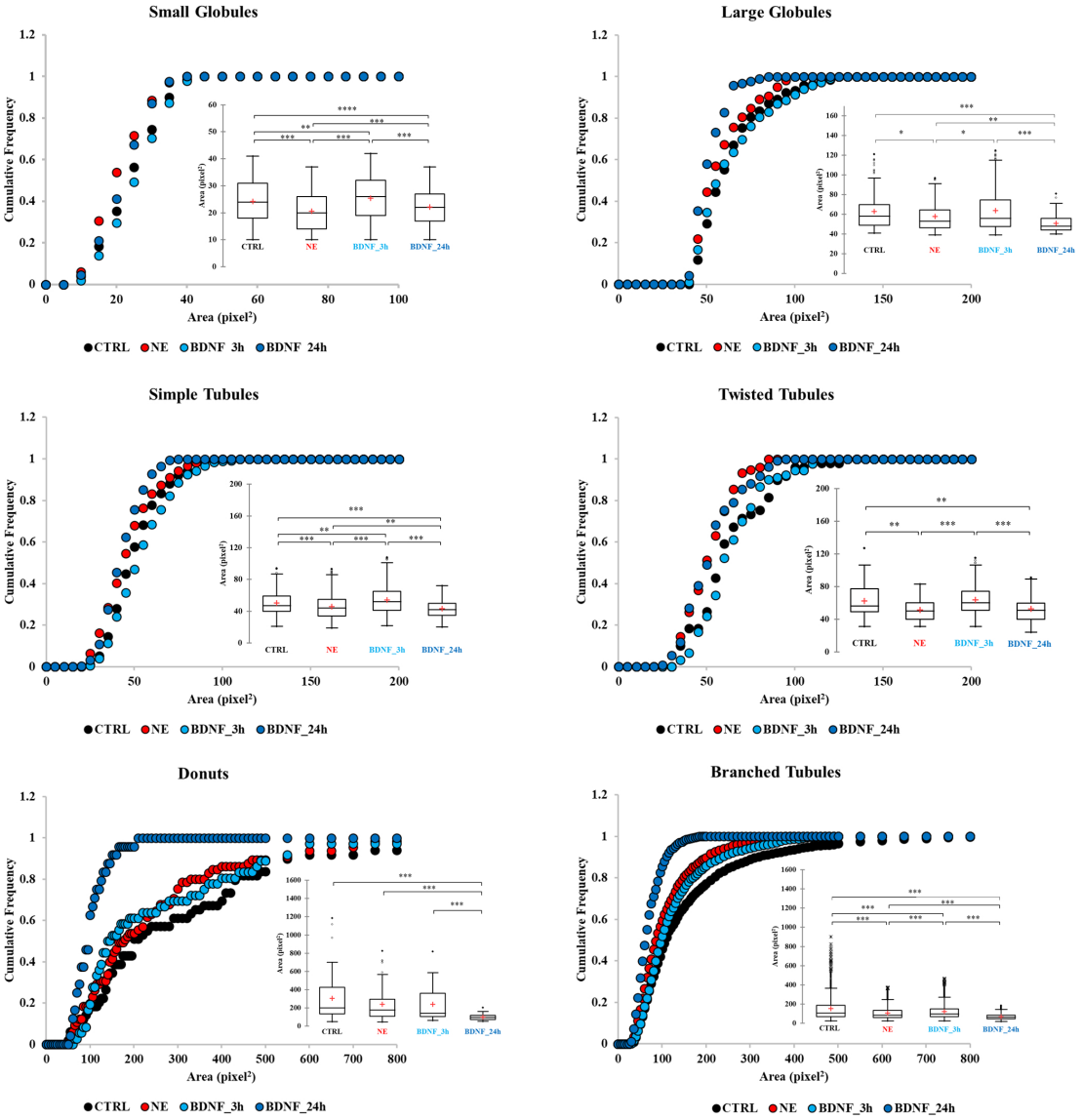

Figure 14.5: Cumulative frequency of total area surface of mitochondrial subtypes. In boxplots is showed the difference between medians, first-to-third quartiles and the most extreme values within the interquartile range among treatments. Statistical significance in boxplots was determined through Kruskal-Wallis statistical test with Bonferroni correction. *** $p < 0.0001$; ** $p < 0.01$; * $p < 0.05$.

ure 14.6 presents the cumulative frequencies of the elongation index among mitochondrial subtypes and treatments.

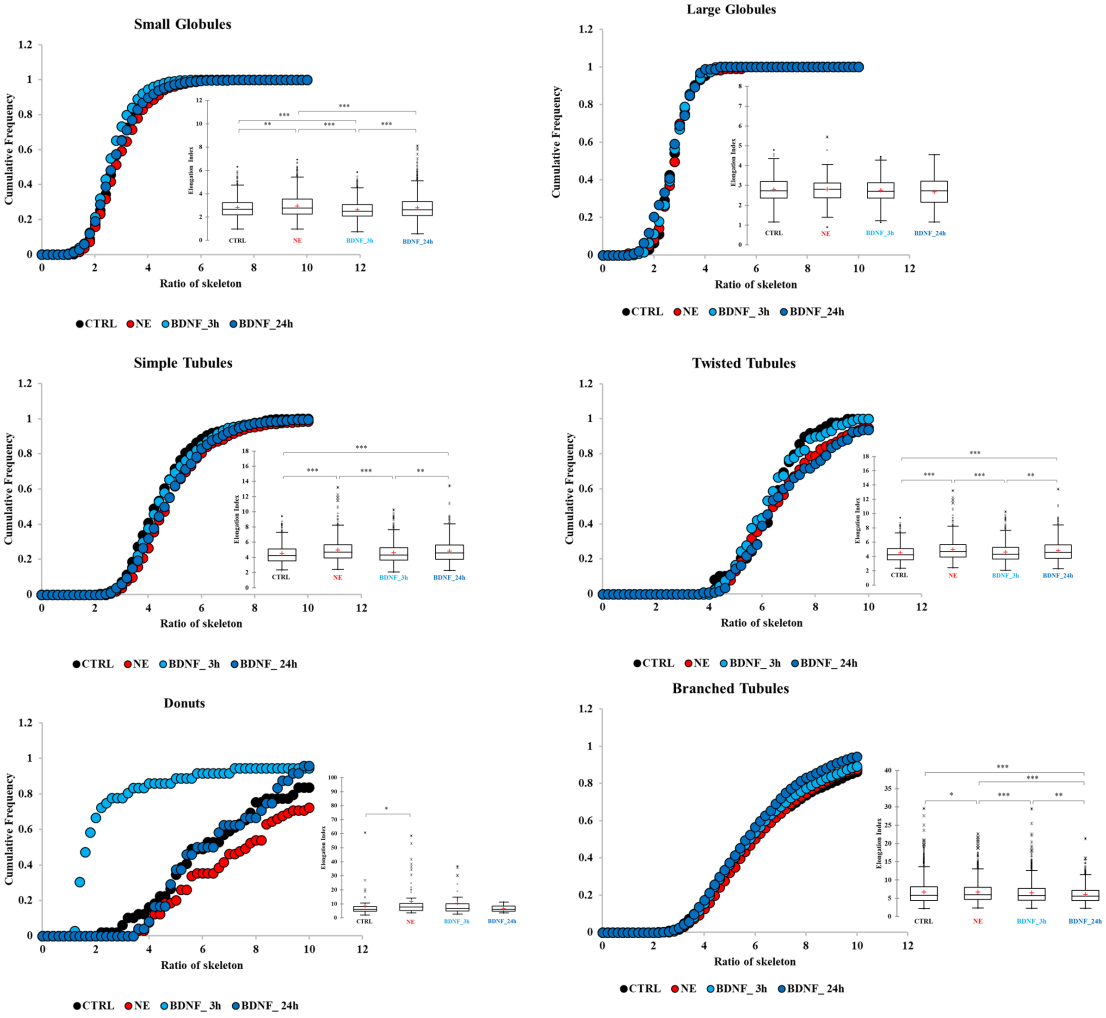

Figure 14.6: Cumulative frequency of elongation index of mitochondrial subtypes. In boxplots is showed the difference between medians, first-to-third quartiles and the most extreme values within the interquartile range among treatments. Statistical significance in boxplots was determined through Kruskal-Wallis statistical test with Bonferroni correction. *** $p < 0.0001$; ** $p < 0.01$; * $p < 0.05$.

The elongation index of small globules was the lowest in BDNF_3h sample ($p < 0.0001$), as the highest frequency of this morphological subtype was detected in low clusters of skeletal ratio. The differences of the elongation index in large globules were not significant; in fact, the cumulative frequency curves were overlapping. Simple tubules and twisted tubules displayed a trend similar to that observed for small globules: also

in this case, the lowest elongation index was displayed in BDNF_3h cells ($p < 0.0001$). No significant differences were displayed among controls and BDNF-treated cells in elongation index for donuts, even if the cumulative frequency curve of BDNF_3h cells was clearly shifted to less elongated mitochondria, indicating that the majority of donuts in this sample displayed a small elongation index. In branched tubules, the elongation index was higher in CTRL and BDNF_3h treatments and lower in BDNF_24h ($p < 0.0001$).

The results about mitochondrial elongation interestingly showed a time point-dependent reduction of skeletal ratio in BDNF-treated cells, as those incubated with BDNF for 3 hours displayed the lowest elongation.

Discriminant analysis

Key morphological features of mitochondria might significantly indicate the way 3T3-L1 cells respond to different treatments. To determine the extent of treatment-specific variations in an unbiased manner, the percentage of area surface, elongation index and solidity of each mitochondrial subtypes were integrated into a single multivariate model through discriminant analysis (DA) (Figure 14.7).

The model captured 85.53% of the total variance in the dataset and achieved a clear separation between different samples. Rank ordering of the variable importance in projection (VIP) scores for each parameter identified the most important morphological features that discriminate each sample. These data have been reported in Table 14.1.

The most impacting features were those relative to small globules and, to a lesser extent, twisted or branched tubules: the parameters with the lowest Wilk's lambda display the strongest discriminant power (Table 14.1) [177, 178].

This analysis suggested that the largest part of the variance among treatments concerning mitochondrial dynamic relied on the architecture of small globules and twisted or branched tubules.

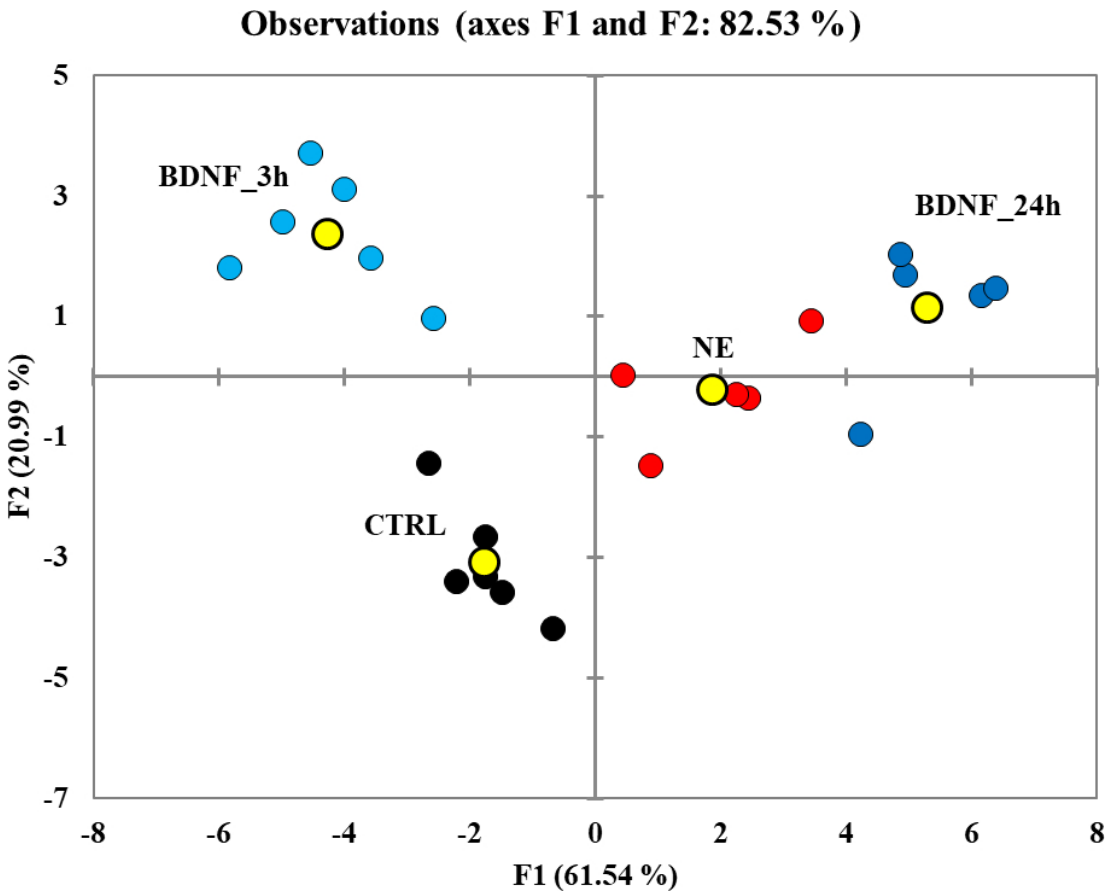

Figure 14.7: Sample clustering produced by discriminant analysis with multivariate modeling of mitochondrial subtypes and their morphological features. Centroids are reported as yellow dots.

Table 14.1: Significant VIP in discriminant analysis illustrating the contribution of different morphological features to the separation of differentially treated cells. The most discriminant parameters have a low Wilk's lambda and a high F.

Morphological variable	Mitochondrial subtype	Wilk's lambda	F	*p*-value
Area	Small globules	0.328	12.280	0.000
Area	Large globules	0.494	6.156	0.005
Area	Simple tubules	0.564	4.629	0.014
Area	Twisted tubules	0.401	8.944	0.001
Area	Branched tubules	0.395	9.188	0.001
Elongation	Small globules	0.352	11.061	0.000
Elongation	Large globules	0.552	4.868	0.012
Elongation	Simple tubules	0.596	4.075	0.023
Elongation	Twisted tubules	0.521	5.520	0.007
Solidity	Small globules	0.382	9.716	0.000
Solidity	Large globules	0.578	4.379	0.018
Solidity	Donuts	0.508	5.813	0.006
Solidity	Branched tubules	0.417	8.395	0.001

14.3 Discussion

This study provided interesting preliminary results on the browning effect of ectopic BDNF administration to cultured white adipocytes. In particular, the analysis of the expression profile of selected target genes is supported by a thorough evaluation of changes in mitochondrial structure, which showed morphological characteristics close to the typical brown ones. The expression of adiponectin has been used as a marker of differentiation: since its mRNA level has not been affected by the treatments, we can infer that cells were completely differentiated.

Results produced by gene and protein expression analyses showed interesting patterns in BDNF-treated 3T3-L1 cells. The rise of the mRNA of canonical brown markers is significantly higher after 3 hours of incubation with BDNF. Conversely, the UCP1 protein content after 3 hours of incubation is the lowest, while it increases after 24 hours of incubation. Possibly, the protein traslation happens later than mRNA transcription [179]. This also occurred with PGC-1α: the lowest mRNA expression after the 24 hours treatment is flanked by the significantly highest protein level at the same time point [180]. Hence, the high protein content of PGC-1α in BDNF-treated 3T3-L1 cells could account for an increased mitochondrial biogenesis, which is a typical feature of brite adipocytes recruitment [181]. This result is in agreement with the increased rate of mitochondrial content (29.02% in BDNF_24h and 18.94% in CTRL).

The alterations in the expression of mitochondria-related genes depict a more fissed phenotype in BDNF-treated cells. *Mfn2* expression is the significantly lowest among treatments. Since this gene encodes for a protein that participates in mitochondrial fusion [101], its down-regulation may be directly linked to a decrease in fusion events. This phenotype has been observed in thermogenic adipocytes [103], but in the present research, the expression of *Drp1*, the regulator of mitochondrial fission, has not been significantly impacted by the administration of BDNF. This is not coherent

with the results of mitochondrial dynamic analysis, but this could be related to the different time-course expression between mRNA and protein. Further investigation is needed to clarify the molecular biology of mitochondrial fission events.

CIDE proteins have a role in favoring LD fusion, but while CIDEC is necessary to obtain one large LD, typical of white adipocytes, CIDEA alone is not sufficient to induce an empowered LD fusion, hence it is associated to a multilocular phenotype [95]. CIDE protein-coding genes *Cidea* and *Cidec* show an expression pattern coherent with a multilocular phenotype, since *Cidea* is significantly up-regulated in BDNF-treated cells after 3 hours of incubation. Despite no significant differences have been recorded in *Cidec* expression among samples, its mRNA levels decrease quite linearly from CTRL to BDNF_24h. This pattern could be associated to a decline in LD fusion. It has been in fact observed an increase in *Cidea* mRNA in cold-exposed mice and NE-treated adipocytes [92]. The level of *Plin1* clearly reflects the pattern observed in *Cidec* expression. This may be because CIDEC and PLIN1 narrowly cooperate in promoting the unilocular phenotype [96], so their simultaneous down-regulation could reflect a decrease in LD fusion in favor of a multilocular phenotype. These results should be implemented and supported by LD morphological studies as performed in [99, 162].

The expression of *Bdnf* in BDNF-treated cells increased, especially after three hours of incubation. This positive feedback loop has been described to occur in microglia [182], hippocampal neurons and cortical neurons and this feedback seems to be mediated by a TrkB-C/EBPβ signaling pathway [183, 184]. This loop may occur in these cell types to prolong their activation under proper stimulation [182] and to improve their physiological outcome, such as the consolidation of memory [183]. At the best of our knowledge, this is the first time that this feedback loop has been detected in adipose cells, but further research is needed to clarify the molecular biology underneath this feedback, as the TrkB expression has not been inves-

tigated in cultured adipocytes, although its presence has been confirmed in adipocytes by Colitti *et al.* [185]. Likely, the effects of the loop detected in the present research include the persistance of the brite phenotype.

The analysis of modifications in mitochondrial dynamic show a treatment-dependent variation in their morphology: 3T3-L1 cells treated with BDNF for 24 hours show the most significant change of mitochondrial structures, being their profile quite similar to positive control cells. Indeed, the analysis of mitochondrial number, area surface and elongation confirmed the onset of mitochondrial fission after BDNF incubation. This is particularly evident after 24 hours-treatment, where cells displayed a reduction of the number of branched tubular mitochondria flanked by an increase of small globules. These features are in agreement with the onset of mitochondrial fission, considering also the increase of simple tubules, that can derive from the fragmentation of branched tubules [141]. Nevertheless, these results are produced by a snapshot of a moment in cell life. Hence, they can be corroborated by a time-lapse imaging of mitochondrial dynamic following BDNF treatment to appreciate in real time the evolving structure of mitochondria.

Taken together, these results show that BDNF has a role in elevating brown adipose markers and in significantly modulate mitochondrial morphology in a time-dependent manner.

Chapter 15

Retinoic acid as a browning agent

15.1 Introduction

Carotenoids are a class of pigments present in many dietary sources. They are precursors of retinoids, a set of bioactive molecules related to vitamin A [186]. The most abundant carotenoid in human diet is β-carotene, which can be metabolized by human tissues through the action of β-carotene-15,15'-oxygenase 1 (BCO1). This enzyme cleaves β-carotene into two molecules of retinaldehyde (Rald), which can be ultimately oxidized to RA by the action of aldehyde dehydrogenase [187].

In recent years, the involvement of carotenoids and, more importantly, their metabolic products in regulating body fat mass and energy metabolism has been confirmed [63]. The regulatory effects of retinoids in adipocytes are primarily caused by their interaction with different kinds of nuclear receptors, namely canonical retinoic acid receptors (RARs) and retinoid X receptors (RXRs) [188], together with PPAR proteins. The most active agonist ligands of these classes of receptors are the isomers of RA: *all*-trans retinoic acid (atRA) and *cis*-9 retinoic acid (c9RA). atRA binds to RARs, while c9RA binds to both RARs and RXRs. Activated RXRs form heterodimers with

RARs, PPARs and other nuclear receptors to modulate gene expression in adipocytes [189].

RA can induce *Ucp1* expression, since the receptors heterodimers activated by RA isomers can bind to *Ucp1* promoter [190]. Treatments with atRA have been demonstrated to induce WAT browning and mitochondrial biogenesis on animal models and *in vitro* cultures [191, 192]. Nevetheless, evidence of browning effect triggered by its isomer c9RA (see chemical structure below) is still lacking.

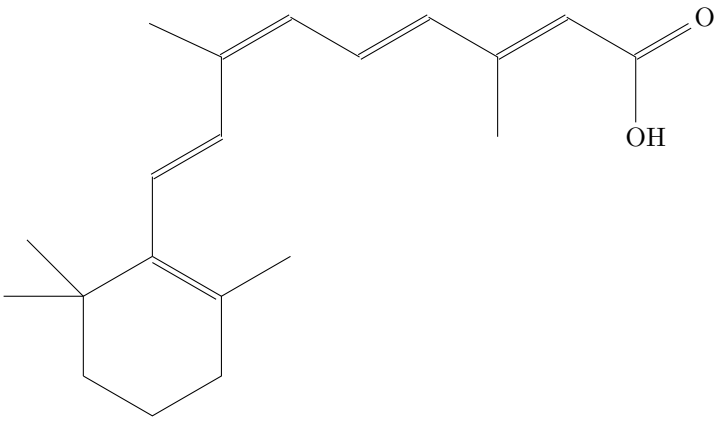

The present research aims to test the browning effect of c9RA on cultured 3T3-L1 adipocytes by producing gene expression preliminary results that will be implemented towards cytomorphological studies.

3T3-L1 culture was performed with conditions stated in Table 5.3. Concomitantly with the switch from differentiation to maintenance medium, cells were treated with different concentrations of c9RA. A positive control with 10 µM of isoproterenol, a selective β_3-adrenergic agonist, has also been established. A negative vehicle control was implemented by treating cells with DMSO. All the treatments lasted 24 hours prior to sampling.

15.2 Preliminary results

15.2.1 Cell viability

To select the optimal dosage of c9RA, a cell viability test has been performed with growing concentrations of the chemical. The tested doses were 0.5, 2, 10 and 20 µM. The viability of 3T3-L1 significantly diminished in a dose-dependent manner, from around 90% of viable cells in the 0.5 µM dose to less than 60% in the 20 µM one (Figure 15.1). According to this result, the chosen doses for the subsequent experiments were 0.5 µM and 1 µM, because the viability of 2 µM c9RA-treated cells was not acceptable.

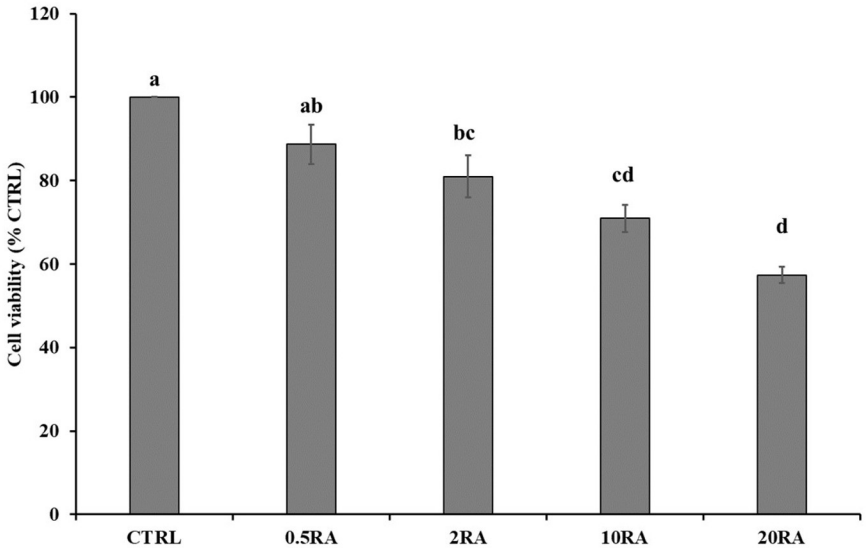

Figure 15.1: Cell viability of 3T3-L1 cells treated with 0.5 (0.5RA), 2 (2RA), 10 (10RA) and 20 (20RA) µM c9RA. Data are expressed as the mean of % viability relatively to negative control (CTRL) ± SEM. One-way ANOVA with Bonferroni correction was used to detect significant differences. Small letters indicate $p < 0.05$.

15.2.2 Gene expression analysis

All retinoid receptors increased their expression after the treatment of cells with both 0.5 and 1 µM doses of c9RA (Figure 15.2, a). In detail, *Rara*, *Rxra* ($p < 0.05$) and *Rxrb* ($p < 0.01$) were significantly up-regulated compared to the positive control, while *Rxra* and *Rxrb* expression was sig-

nificantly higher ($p < 0.05$) than the negative control in 3T3-L1 cells treated with 0.5 µM c9RA. *Rarb* was significantly up-regulated ($p < 0.05$) in cells treated with 1 µM c9RA. As expected, the expression of RA receptors in isoproterenol-treated cells was not significantly different compared to the negative control.

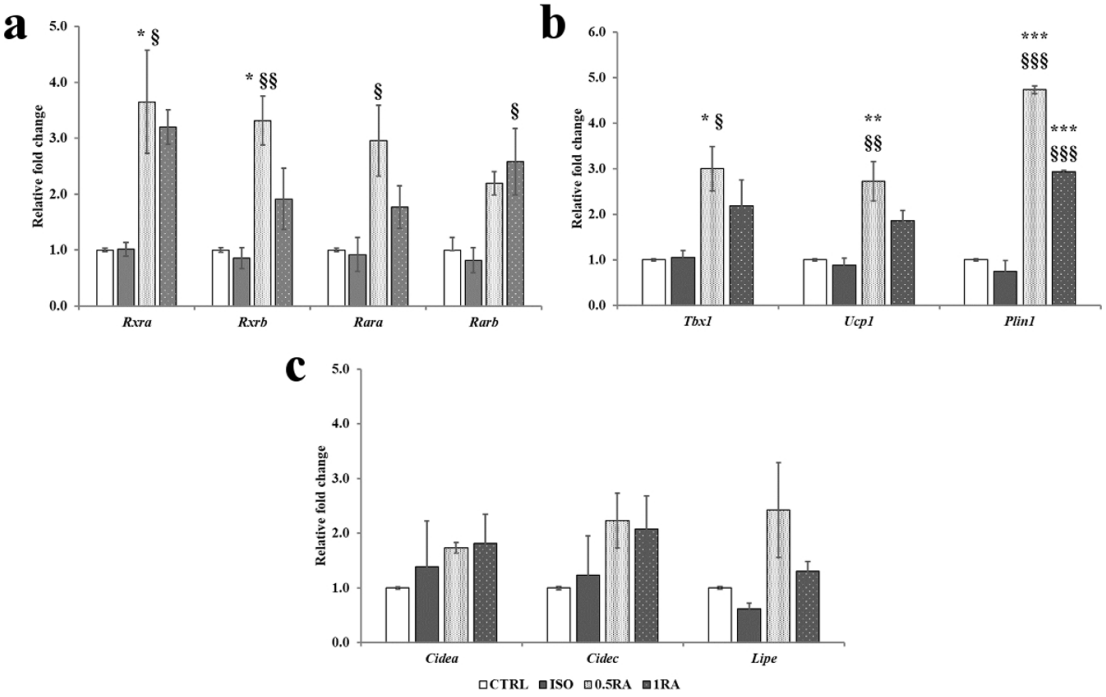

Figure 15.2: Relative fold change of retinoid receptors **(a)**, browning markers **(b)** and LD-associated genes **(c)**. Data are expressed as the mean of relative fold change ± SEM. One-way ANOVA with Bonferroni correction was used to detect significant differences. *** $p < 0.0001$ *vs* CTRL; ** $p < 0.01$ *vs* CTRL; * $p < 0.05$ *vs* CTRL; §§§ $p < 0.0001$ *vs* ISO; §§ $p < 0.01$ *vs* ISO; § $p < 0.05$ *vs* ISO.

The browning markers *Ucp1* and *Tbx1* were significantly up-regulated with the 0.5 µM dose of c9RA (Figure 15.2, b). Also *Plin1* was significantly up-regulated in c9RA-treated cells (Figure 15.2, b), but other LD-associated genes and *Lipe* did not show any significant variation (Figure 15.2, c).

Interestingly, cells treated with isoproterenol did not produce a significant upregulation of browning markers. This is probably due to the fact that cells were over-incubated with this molecule, which is known to produce effects after few hours following the administration, so the expression of the markers might have come back to a basal state.

15.2.3 In-cell Western

To gain more information about the protein level of UCP1 and of PGC-1α, a marker of mitochondrial biogenesis, ICW analysis was performed. Since the administration of 0.5 µM c9RA produced the highest up-regulation of browning markers, this analysis excluded the 1 µM dose. Figure 15.3 showed that the protein level of UCP1 was significantly low in ISO ($p < 0.01$) and in samples treated with 0.5 µM c9RA ($p < 0.05$). These data could reflect on one side the lack of effectiveness of the treatment with isoproterenol, on the other side could mean that, in cells treated with c9RA, the translation of mRNA into protein is not an immediate consequence of the transcription of *Ucp1* gene. Data about the PGC-1α show a clear up-regulation of the protein in c9RA-treated cells with respect to both negative and positive controls ($p < 0.05$). This might lead to the assumption that mitochondrial biogenesis is enhanced in c9RA-treated cells, but this result needs to be corroborated by mitochondrial dynamic analysis and by the analysis of *Ppargc1a* mRNA level.

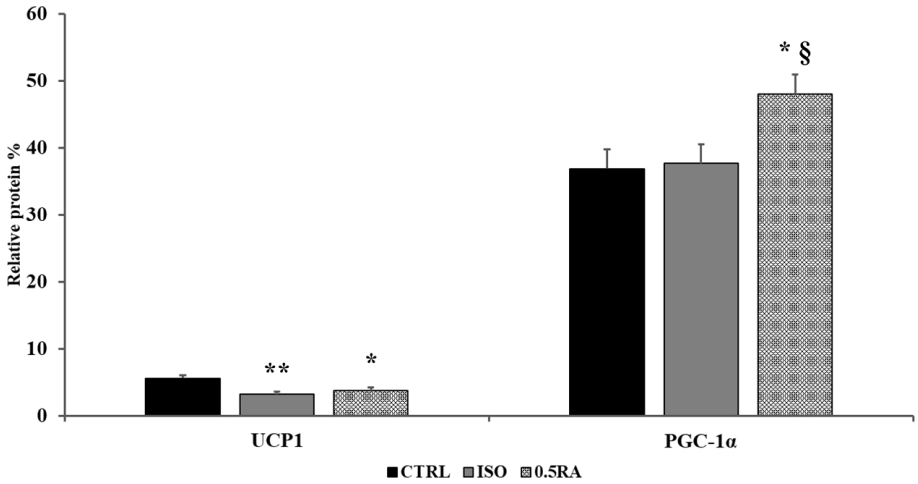

Figure 15.3: Relative protein % from ICW analysis. Raw data were normalized against the expression of α-tubulin, which served as housekeeping. Data are expressed as the mean of relative fold change ± SEM. One-way ANOVA with Tukey's range test was used to detect significant differences. ** $p < 0.01$ *vs* CTRL; * $p < 0.05$ *vs* CTRL; § $p < 0.05$ *vs* ISO.

15.3 Discussion

This preliminary study showed that the isomer of *all*-trans retinoic acid, *cis*-9 retinoic acid, has a browning effect on 3T3-L1 adipocytes. RA has been described as a factor promoting adipogenesis [193] and regulating lipid metabolism [194], so it has been inferred its involvement in regulating WAT browning. The mechanism by which both isomers regulate *Ucp1* expression involves their interaction with RAR and RXR nuclear receptors. When activated, these receptors form heterodimers with each other and also with other nuclear receptors, including PPARγ, to modulate the expression of *Ucp1* and a number of other genes [195]. Nevertheless, recent studies showed that atRA mediates mitochondrial biogenesis also through an AMPK-dependent up-regulation of *Ppargc1a* gene [195]. This seems to occur also with c9RA administration, as the protein level of PGC-1α increased following the treatment. The administration of c9RA to 3T3-L1 up-regulates the expression of its nuclear receptor, in line with previous results [196]. The up-regulation of *Ucp1* and *Tbx1* can indicate that a brite phenotype has been established on treated cells, but further analyses are needed to strengthen this observation. Recent findings highlighted the involvement of lipocalin 2, a novel adipokine, in the regulation of atRA-mediated browning [197], hence its role in mediating the cellular response to c9RA deserves further elucidation.

Among genes associated in LD remodeling, those encoding for CIDE-proteins did not show any significant variation, probably due to the high level of individual variability. Nevertheless, Figure 15.2c showed that their mRNA level is higher in cells treated with the two doses of c9RA, so this might account for a dynamic remodeling of LDs. Morphological studies on LDs are required to verify if c9RA triggers a LD remodeling towards a multilocular phenotype, which has been observed as a typical feature of browning white adipocytes [92]. The significant up-regulation of *Plin1* has a similar pattern to *Lipe*, so there might be a relation between these two

proteins. Despite PLIN1 has a role in improving CIDEC's functionality during LD fusion, some findings indicate a role of phosphorylated PLIN1 in favoring a multilocular phenotype through its interaction with key LD-remodeling proteins [198]. Moreover, it has been observed that PLIN1 can promote *Lipe* expression [199] and that an up-regulation of *Plin1* has a protective effect against diet-induced obesity [200, 201].

Taken together, these preliminary data account for an involvement of c9RA in browning of white adipocytes, but further research is necessary to validate these assumptions.

Chapter 16

Concluding remarks

The results presented in this thesis demonstrated that analyzed bioactive factors induced browning in different cellular models. This evaluation has been performed through the analysis of the expression of browning molecular markers and of structural modifications of lipid droplets and mitochondria. The tested molecules displayed different degrees of browning efficacy in function of their dose or the duration of the incubation period through multiple pathways that should be deeper investigated. The knowledge of the best combination of browning factor dose and time of exposure will be of outstanding importance in transferring the results of this research into clinical practice for the treatment of obesity and related comorbidities (i.e. type 2 diabetes mellitus), since prolonged exposure and sub-optimal doses do not produce satisfactory outcomes in terms of thermogenic activation and reduction of adiposity. Research on bioactive molecules can be translated in the realization of effective nutraceutical preparations in support of traditional obesity treatments, while the study of endogenous molecules may spread new light on the beneficial effect of physical exercise and other positive behaviors on energy expenditure.

The results of this research improved our understanding of WAT browning, bringing novel knowledge about the expression of brown and brite markers after prolonged treatments on fully differentiated adipocytes. For the first time, new approaches to study browning induced by the selected

compounds involved variations of LDs size and mitochondrial shape. Nevertheless, trials with the selected or other compounds could deeper analyze the molecular pathways that lead to the phenotypic conversion in treated cells, i.e. with gene silencing experiments, inhibition of target receptors or proteins involved in the signal transduction and transcriptomic analyses.

Moreover, morphological variations were highly descriptive and useful to outline phenotypic changes and can be improved with time-lapse experiments to exploit time-course modifications and with electron microscopy to depict ultrastructural changes. Moreover, these experiments will be repeated on immortalized murine brown adipocytes (IMBAT cells) to strengthen the results.

Most importantly, this thesis evidenced that browning of WAT is not just an increase of UCP1 content, as many other factors participate to the onset of a thermogenic response and this response varies among different types of cell. Hence, to produce significant results that could be translated into clinical practice to treat obesity, a further effort is required in multiple research lines.

Bibliography

1. KERSHAW, E. E. & FLIER, J. S. "*Adipose tissue as an endocrine organ*". The journal of clinical endocrinology & metabolism 89: 2548–2556. (2004).

2. SANCHEZ-GURMACHES, J. & GUERTIN, D. A. "*Adipocyte lineages: tracing back the origins of fat*". Biochimica et biophysica acta 1842: 340–351. (2014).

3. WANG, R. & LI, X. "*Different adipose tissue depots and metabolic syndrome in human*". Sheng li xue bao 69: 357–365. (2017).

4. WALDÉN, T. B., HANSEN, I. R., TIMMONS, J. A., *et al.* "*Recruited vs. nonrecruited molecular signatures of brown, brite, and white adipose tissues*". American journal of physiology – Endocrinology and metabolism 302: E19–E31. (2011).

5. JUNG, S. M., SANCHEZ-GURMACHES, J. & GUERTIN, D. A. in *Brown adipose tissue* 3–36 (Springer, 2018).

6. WRONSKA, A. & KMIEC, Z. "*Structural and biochemical characteristics of various white adipose tissue depots*". Acta physiologica 205: 194–208. (2012).

7. LEE, Y.-H., MOTTILLO, E. P. & GRANNEMAN, J. G. "*Adipose tissue plasticity from WAT to BAT and in between*". Biochimica et biophysica acta 1842: 358–369. (2014).

8. STRAWFORD, A., ANTELO, F., CHRISTIANSEN, M. & HELLERSTEIN, M. "*Adipose tissue triglyceride turnover, de novo lipogenesis, and cell proliferation in humans measured with ^2H_2O*". American journal of physiology – Endocrinology and metabolism 286: E577–E588. (2004).

9. SPALDING, K. L., ARNER, E., WESTERMARK, P. O., *et al.* "*Dynamics of fat cell turnover in humans*". Nature 453: 783. (2008).

10. RIGAMONTI, A., BRENNAND, K., LAU, F. & COWAN, C. A. "*Rapid cellular turnover in adipose tissue*". PloS one 6: e17637. (2011).

11. JOE, A. W., YI, L., EVEN, Y., *et al.* "*Depot-specific differences in adipogenic progenitor abundance and proliferative response to high-fat diet*". Stem cells 27: 2563–2570. (2009).

12. TCHOUKALOVA, Y. D., VOTRUBA, S. B., TCHKONIA, T., *et al.* "*Regional differences in cellular mechanisms of adipose tissue gain with overfeeding*". Proceedings of the National Academy of Sciences 107: 18226–18231. (2010).

13. OSBORN, O. & OLEFSKY, J. M. "*The cellular and signaling networks linking the immune system and metabolism in disease*". Nature medicine 18: 363–374. (2012).

14. HIRSCH, J. & BATCHELOR, B. "*Adipose tissue cellularity in human obesity*". Clinics in endocrinology and metabolism 5: 299–311. (1976).

15. CINTI, S., MITCHELL, G., BARBATELLI, G., *et al.* "*Adipocyte death defines macrophage localization and function in adipose tissue of obese mice and humans*". Journal of lipid research 46: 2347–2355. (2005).

16. SAMUEL, V. T. & SHULMAN, G. I. "*The pathogenesis of insulin resistance: integrating signaling pathways and substrate flux*". The journal of clinical investigation 126: 12–22. (2016).

17. TSENG, Y.-H., CYPESS, A. M. & KAHN, C. R. "*Cellular bioenergetics as a target for obesity therapy*". Nature reviews Drug discovery 9: 465–481. (2010).

18. LEMOS, D. R., PAYLOR, B., CHANG, C., *et al.* "*Functionally convergent white adipogenic progenitors of different lineages participate in a diffused system supporting tissue regeneration*". Stem cells 30: 1152–1162. (2012).

19. BILLON, N., IANNARELLI, P., MONTEIRO, M. C., *et al.* "*The generation of adipocytes by the neural crest*". Development 134: 2283–2292. (2007).

20. SERA, Y., LARUE, A. C., MOUSSA, O., *et al.* "*Hematopoietic stem cell origin of adipocytes*". Experimental hematology 37: 1108–1120. (2009).

21. LEE, Y.-H., PETKOVA, A. P., MOTTILLO, E. P. & GRANNEMAN, J. G. "*In vivo identification of bipotential adipocyte progenitors recruited by β_3-adrenoceptor activation and high-fat feeding*". Cell metabolism 15: 480–491. (2012).

22. BERRY, R. & RODEHEFFER, M. S. "*Characterization of the adipocyte cellular lineage in vivo*". Nature cell biology 15: 302–308. (2013).

23. GUPTA, R. K., MEPANI, R. J., KLEINER, S., *et al.* "*Zfp423 expression identifies committed preadipocytes and localizes to adipose endothelial and perivascular cells*". Cell metabolism 15: 230–239. (2012).

24. SENGENÈS, C., LOLMEDE, K., ZAKAROFF-GIRARD, A., *et al.* "*Preadipocytes in the human subcutaneous adipose tissue display distinct features from the adult mesenchymal and hematopoietic stem cells*". Journal of cellular physiology 205: 114–122. (2005).

25. TANG, W., ZEVE, D., SUH, J. M., *et al.* "*White fat progenitor cells reside in the adipose vasculature*". Science 322: 583–586. (2008).

26. VALET, P., TAVERNIER, G., CASTAN-LAURELL, I., *et al.* "*Understanding adipose tissue development from transgenic animal models*". Journal of lipid research 43: 835–860. (2002).

27. LOWE, C. E., O'RAHILLY, S. & ROCHFORD, J. J. "*Adipogenesis at a glance*". Journal of cell science 124: 2681–2686. (2011).

28. CHRISTODOULIDES, C., LAGATHU, C., SETHI, J. K. & VIDAL-PUIG, A. "*Adipogenesis and WNT signalling*". Trends in endocrinology & metabolism 20: 16–24. (2009).

29. COUSIN, W., FONTAINE, C., DANI, C. & PERALDI, P. "*Hedgehog and adipogenesis: fat and fiction*". Biochimie 89: 1447–1453. (2007).

30. ROSEN, E. D. & MACDOUGALD, O. A. "*Adipocyte differentiation from the inside out*". Nature reviews – Molecular cell biology 7: 885–896. (2006).

31. GUAN, H.-P., ISHIZUKA, T., CHUI, P. C., *et al.* "*Corepressors selectively control the transcriptional activity of PPARγ in adipocytes*". Genes & development 19: 453–461. (2005).

32. ENGIN, A. B. in *Obesity and lipotoxicity* 489–509 (Springer, 2017).

33. CANNON, B. & NEDERGAARD, J. "*Brown adipose tissue: function and physiological significance*". Physiological reviews 84: 277–359. (2004).

34. VIRTANEN, K. A., LIDELL, M. E., ORAVA, J., *et al.* "*Functional brown adipose tissue in healthy adults*". New England journal of medicine 360: 1518–1525. (2009).

35. GIFFORD, A., TOWSE, T. F., WALKER, R. C., *et al.* "*Characterizing active and inactive brown adipose tissue in adult humans using PET-CT and MR imaging*". American journal of physiology – Endocrinology and metabolism 311: E95–E104. (2016).

36. EL HADI, H., VETTOR, R. & ROSSATO, M. "*Functional imaging of brown adipose tissue in human*". Hormone molecular biology and clinical investigation 31: (2017).

37. JEREMIC, N., CHATURVEDI, P. & TYAGI, S. C. "*Browning of white fat: novel insight into factors, mechanisms, and therapeutics*". Journal of cellular physiology 232: 61–68. (2017).

38. KLINGENBERG, M. "*Uncoupling protein – A useful energy dissipator*". Journal of bioenergetics and biomembranes 31: 419–430. (1999).

39. TIMMONS, J. A., WENNMALM, K., LARSSON, O., *et al.* "*Myogenic gene expression signature establishes that brown and white adipocytes originate from distinct cell lineages*". Proceedings of the National Academy of Sciences 104: 4401–4406. (2007).

40. BRAUN, T. & GAUTEL, M. "*Transcriptional mechanisms regulating skeletal muscle differentiation, growth and homeostasis*". Nature reviews – Molecular cell biology 12: 349–361. (2011).

41. CRISTANCHO, A. G. & LAZAR, M. A. "*Forming functional fat: a growing understanding of adipocyte differentiation*". Nature reviews – Molecular cell biology 12: 722–734. (2011).

42. SANCHEZ-GURMACHES, J., HUNG, C.-M., SPARKS, C. A., *et al.* "*PTEN loss in the Myf5 lineage redistributes body fat and reveals subsets of white adipocytes that arise from Myf5 precursors*". Cell metabolism 16: 348–362. (2012).

43. KAJIMURA, S., SEALE, P. & SPIEGELMAN, B. M. "*Transcriptional control of brown fat development*". Cell metabolism 11: 257–262. (2010).

44. PUIGSERVER, P., WU, Z., PARK, C. W., *et al.* "*A cold-inducible coactivator of nuclear receptors linked to adaptive thermogenesis*". Cell 92: 829–839. (1998).

45. SEALE, P., KAJIMURA, S., YANG, W., *et al.* "*Transcriptional control of brown fat determination by PRDM16*". Cell metabolism 6: 38–54. (2007).

46. SEALE, P., BJORK, B., YANG, W., *et al.* "*PRDM16 controls a brown fat/skeletal muscle switch*". Nature 454: 961–967. (2008).

47. TSENG, Y.-H., KOKKOTOU, E., SCHULZ, T. J., *et al.* "*New role of bone morphogenetic protein 7 in brown adipogenesis and energy expenditure*". Nature 454: 1000–1004. (2008).

48. BRYCHTA, R. & CHEN, K. "*Cold-induced thermogenesis in humans*". European journal of clinical nutrition 71: 345–352. (2017).

49. MORRISON, S. F. "*2010 Carl Ludwig distinguished lectureship of the APS neural control and autonomic regulation section: central neural pathways for thermoregulatory cold defense*". Journal of applied physiology 110: 1137–1149. (2011).

50. BROEDERS, E., BOUVY, N. D. & VAN MARKEN LICHTENBELT, W. D. "*Endogenous ways to stimulate brown adipose tissue in humans*". Annals of medicine 47: 123–132. (2015).

51. COLLINS, S., YEHUDA-SHNAIDMAN, E. & WANG, H. "*Positive and negative control of Ucp1 gene transcription and the role of β-adrenergic signaling networks*". International journal of obesity 34: S28–S33. (2010).

52. THONBERG, H., FREDRIKSSON, J. M., NEDERGAARD, J. & CANNON, B. "*A novel pathway for adrenergic stimulation of cAMP-response-element-binding protein (CREB) phosphorylation: mediation via α_1-adrenoceptors and protein kinase C activation*". Biochemical journal 364: 73–79. (2002).

53. CAO, W., DANIEL, K. W., ROBIDOUX, J., *et al.* "*p38 mitogen-activated protein kinase is the central regulator of cyclic AMP-dependent transcription of the brown fat uncoupling protein 1 gene*". Molecular and cellular biology 24: 3057–3067. (2004).

54. SZTALRYD, C. & BRASAEMLE, D. L. "*The perilipin family of lipid droplet proteins: gatekeepers of intracellular lipolysis*". Biochimica et biophysica acta 1862: 1221–1232. (2017).

55. HOLM, C. *Molecular mechanisms regulating hormone-sensitive lipase and lipolysis* 2003.

56. PIDOUX, G., WITCZAK, O., JARNÆSS, E., *et al.* "*Optic atrophy 1 is an A-kinase anchoring protein on lipid droplets that mediates adrenergic control of lipolysis*". The EMBO journal 30: 4371–4386. (2011).

57. SHU, L., HOO, R. L., WU, X., *et al.* "*A-FABP mediates adaptive thermogenesis by promoting intracellular activation of thyroid hormones in brown adipocytes*". Nature communications 8: 14147. (2017).

58. VILLARROYA, F., PEYROU, M. & GIRALT, M. "*Transcriptional regulation of the uncoupling protein-1 gene*". Biochimie 134: 86–92. (2017).

59. KOZAK, U. C., KOPECKY, J., TEISINGER, J., *et al.* "*An upstream enhancer regulating brown-fat-specific expression of the mitochondrial uncoupling protein gene.*" Molecular and cellular biology 14: 59–67. (1994).

60. DEMPERSMIER, J., SAMBEAT, A., GULYAEVA, O., *et al.* "*Cold-inducible Zfp516 activates UCP1 transcription to promote browning of white fat and development of brown fat*". Molecular cell 57: 235–246. (2015).

61. YUBERO, P., MANCHADO, C., CASSARDDOULCIER, A.-M., *et al.* "*CCAAT/enhancer binding-proteins α and β are transcriptional activators of the brown fat uncoupling protein gene promoter*". Biochemical and biophysical research communications 198: 653–659. (1994).

62. VILLARROYA, F., IGLESIAS, R. & GIRALT, M. "*PPARs in the control of uncoupling proteins gene expression*". PPAR research 2007: 74364. (2007).

63. BONET, M. L., CANAS, J. A., RIBOT, J. & PALOU, A. "*Carotenoids and their conversion products in the control of adipocyte function, adiposity and obesity*". Archives of biochemistry and biophysics 572: 112–125. (2015).

64. RABELO, R., SCHIFMAN, A., RUBIO, A., *et al.* "*Delineation of thyroid hormone-responsive sequences within a critical enhancer in the rat uncoupling protein gene*". Endocrinology 136: 1003–1013. (1995).

65. DE JESUS, L. A., CARVALHO, S. D., RIBEIRO, M. O., *et al.* "*The type 2 iodothyronine deiodinase is essential for adaptive thermogenesis in brown adipose tissue*". The journal of clinical investigation 108: 1379–1385. (2001).

66. GANTNER, M. L., HAZEN, B. C., EURY, E., *et al.* "*Complementary roles of estrogen-related receptors in brown adipocyte thermogenic function*". Endocrinology 157: 4770–4781. (2016).

67. HALLBERG, M., MORGANSTEIN, D. L., KISKINIS, E., *et al.* "*A functional interaction between RIP140 and PGC-1α regulates the expression of the lipid droplet protein CIDEA*". Molecular and cellular biology 28: 6785–6795. (2008).

68. SHARMA, B. K., PATIL, M. & SATYANARAYANA, A. "*Negative regulators of brown adipose tissue (BAT)-mediated thermogenesis*". Journal of cellular physiology 229: 1901–1907. (2014).

69. WONG, K. E., KONG, J., ZHANG, W., *et al.* "*Targeted expression of human vitamin D receptor in adipocytes decreases energy expenditure and induces obesity in mice*". Journal of biological chemistry 286: 33804–33810. (2011).

70. SCIMÈ, A., GRENIER, G., HUH, M. S., *et al.* "*Rb and p107 regulate preadipocyte differentiation into white versus brown fat through repression of PGC-1*α". Cell metabolism 2: 283–295. (2005).

71. FAJAS, L., EGLER, V., REITER, R., *et al.* "*The retinoblastoma-histone deacetylase 3 complex inhibits PPAR*γ *and adipocyte differentiation*". Developmental cell 3: 903–910. (2002).

72. PAN, D., FUJIMOTO, M., LOPES, A. & WANG, Y.-X. "*Twist-1 is a PPAR*δ*-inducible, negative-feedback regulator of PGC-1*α *in brown fat metabolism*". Cell 137: 73–86. (2009).

73. PICARD, F., GÉHIN, M., ANNICOTTE, J.-S., *et al.* "*SRC-1 and TIF2 control energy balance between white and brown adipose tissues*". Cell 111: 931–941. (2002).

74. COSTE, A., LOUET, J.-F., LAGOUGE, M., *et al.* "*The genetic ablation of SRC-3 protects against obesity and improves insulin sensitivity by reducing the acetylation of PGC-1*α". Proceedings of the national academy of sciences 105: 17187–17192. (2008).

75. YE, L., KLEINER, S., WU, J., *et al.* "*TRPV4 is a regulator of adipose oxidative metabolism, inflammation, and energy homeostasis*". Cell 151: 96–110. (2012).

76. PALMIERI, F. "*Mitochondrial transporters of the SLC25 family and associated diseases: a review*". Journal of inherited metabolic disease 37: 565–575. (2014).

77. BERTHOLET, A. M. & KIRICHOK, Y. "*UCP1: A transporter for H^+ and fatty acid anions*". Biochimie 134: 28–34. (2017).

78. NICHOLLS, D. G. "*The physiological regulation of uncoupling proteins*". Biochimica et biophysica acta 1757: 459–466. (2006).

79. LAZAR, M. A. "*How now, brown fat?*" Science 321: 1048–1049. (2008).

80. WU, J., BOSTRÖM, P., SPARKS, L. M., *et al.* "*Beige adipocytes are a distinct type of thermogenic fat cell in mouse and human*". Cell 150: 366–376. (2012).

81. RO, S.-H., JANG, Y., BAE, J., *et al.* "*Autophagy in adipocyte browning: emerging drug target for intervention in obesity*". Frontiers in physiology 10: 22. (2019).

82. CAO, Q., JING, J., CUI, X., *et al.* "*Sympathetic nerve innervation is required for beigeing in white fat*". Physiological reports 7: e14031. (2019).

83. FISCHER, A. W., SCHLEIN, C., CANNON, B., *et al.* "*Intact innervation is essential for diet-induced recruitment of brown adipose tissue*". American journal of physiology – Endocrinology and metabolism 316: E487–E503. (2018).

84. USSAR, S., LEE, K. Y., DANKEL, S. N., *et al.* "*ASC-1, PAT2, and P2RX5 are cell surface markers for white, beige, and brown adipocytes*". Science translational medicine 6: 247ra103. (2014).

85. WANG, G.-X., ZHAO, X.-Y., MENG, Z.-X., *et al.* "*The brown fat–enriched secreted factor Nrg4 preserves metabolic homeostasis through attenuation of hepatic lipogenesis*". Nature medicine 20: 1436–1443. (2014).

86. COMAS, F., MARTINEZ, C., SABATER, M., *et al.* "*Neuregulin 4 is a novel marker of beige adipocyte precursor cells in human adipose tissue*". Frontiers in physiology 10: 39. (2019).

87. ROSENWALD, M., PERDIKARI, A., RÜLICKE, T. & WOLFRUM, C. "*Bi-directional interconversion of brite and white adipocytes*". Nature cell biology 15: 659–667. (2013).

88. GARCIA, R. A., ROEMMICH, J. N. & CLAYCOMBE, K. J. "*Evaluation of markers of beige adipocytes in white adipose tissue of the mouse*". Nutrition & metabolism 13: 24. (2016).

89. TU, T. H., KIM, C.-S., GOTO, T., *et al.* "*4-1BB/4-1BBL interaction promotes obesity-induced adipose inflammation by triggering bidirectional inflammatory signaling in adipocytes/macrophages*". Mediators of inflammation 2012: 972629. (2012).

90. GAO, Q. & GOODMAN, J. M. "*The lipid droplet – a well-connected organelle*". Frontiers in cell and developmental biology 3: 49. (2015).

91. BARNEDA, D. & CHRISTIAN, M. "*Lipid droplet growth: regulation of a dynamic organelle*". Current opinion in cell biology 47: 9–15. (2017).

92. BARNEDA, D., FRONTINI, A., CINTI, S. & CHRISTIAN, M. "*Dynamic changes in lipid droplet-associated proteins in the browning of white adipose tissues*". Biochimica et biophysica acta 1831: 924–933. (2013).

93. ZHOU, Z., TOH, S. Y., CHEN, Z., *et al.* "*Cidea-deficient mice have lean phenotype and are resistant to obesity*". Nature genetics 35: 49–56. (2003).

94. NISHIMOTO, Y. & TAMORI, Y. "*CIDE family-mediated unique lipid droplet morphology in white adipose tissue and brown adipose tissue*

determines the adipocyte energy metabolism". Journal of atherosclerosis and thrombosis 24: 989–998. (2017).

95. WU, L., ZHOU, L., CHEN, C., *et al.* "*Cidea controls lipid droplet fusion and lipid storage in brown and white adipose tissue*". Science China life sciences 57: 107–116. (2014).

96. GRAHN, T. H. M., ZHANG, Y., LEE, M.-J., *et al.* "*FSP27 and PLIN1 interaction promotes the formation of large lipid droplets in human adipocytes*". Biochemical and biophysical research communications 432: 296–301. (2013).

97. NISHIMOTO, Y., NAKAJIMA, S., TATEYA, S., *et al.* "*Cell death-inducing DNA fragmentation factor A-like effector A and fat-specific protein 27*β *coordinately control lipid droplet size in brown adipocytes*". Journal of biological chemistry 292: 10824–10834. (2017).

98. PURI, V., RANJIT, S., KONDA, S., *et al.* "*Cidea is associated with lipid droplets and insulin sensitivity in humans*". Proceedings of the National Academy of Sciences 105: 7833–7838. (2008).

99. MONTANARI, T. & COLITTI, M. "*Simpson–Golabi–Behmel syndrome human adipocytes reveal a changing phenotype throughout differentiation*". Histochemistry and cell biology 149: 593–605. (2018).

100. SEPA-KISHI, D. M. & CEDDIA, R. B. "*White and beige adipocytes: are they metabolically distinct?*" Hormone molecular biology and clinical investigation 33: 20180003. (2018).

101. FRIEDMAN, J. R. & NUNNARI, J. "*Mitochondrial form and function*". Nature 505: 335–343. (2014).

102. LIESA, M. & SHIRIHAI, O. S. "*Mitochondrial dynamics in the regulation of nutrient utilization and energy expenditure*". Cell metabolism 17: 491–506. (2013).

103. WIKSTROM, J. D., MAHDAVIANI, K., LIESA, M., *et al.* "*Hormone-induced mitochondrial fission is utilized by brown adipocytes as an amplification pathway for energy expenditure*". The EMBO journal 33: 418–436. (2014).

104. MEYER, J. N., LEUTHNER, T. C. & LUZ, A. L. "*Mitochondrial fusion, fission, and mitochondrial toxicity*". Toxicology 391: 42–53. (2017).

105. GUILLERY, O., MALKA, F., LANDES, T., *et al.* "*Metalloprotease-mediated OPA1 processing is modulated by the mitochondrial membrane potential*". Biology of the cell 100: 315–325. (2008).

106. GRIPARIC, L., VAN DER WEL, N. N., OROZCO, I. J., *et al.* "*Loss of the intermembrane space protein Mgm1/OPA1 induces swelling and localized constrictions along the lengths of mitochondria*". Journal of biological chemistry 279: 18792–18798. (2004).

107. IKEDA, K., MARETICH, P. & KAJIMURA, S. "*The common and distinct features of brown and beige adipocytes*". Trends in endocrinology & metabolism 29: 191–200. (2018).

108. NARENDRA, D., TANAKA, A., SUEN, D.-F. & YOULE, R. J. "*Parkin is recruited selectively to impaired mitochondria and promotes their autophagy*". The journal of cell biology 183: 795–803. (2008).

109. MONTANARI, T., POŠĆIĆ, N. & COLITTI, M. "*Factors involved in white-to-brown adipose tissue conversion and in thermogenesis: a review*". Obesity reviews 18: 495–513. (2017).

110. WAJCHENBERG, B. L. "*Subcutaneous and visceral adipose tissue: their relation to the metabolic syndrome*". Endocrine reviews 21: 697–738. (2000).

111. ASTRUP, A. & LUNDSGAARD, C. "*What do pharmacological approaches to obesity management offer? Linking pharmacological mechanisms*

of obesity management agents to clinical practice". Experimental and clinical endocrinology & diabetes 106: 29–34. (1998).

112. PENG, X.-R., GENNEMARK, P., O'MAHONY, G. & BARTESAGHI, S. "*Unlock the thermogenic potential of adipose tissue: pharmacological modulation and implications for treatment of diabetes and obesity*". Frontiers in endocrinology 6: 174. (2015).

113. WANG, Q., ZHANG, M., XU, M., *et al.* "*Brown adipose tissue activation is inversely related to central obesity and metabolic parameters in adult human*". PloS one 10: e0123795. (2015).

114. VAN MARKEN LICHTENBELT, W. D. & SCHRAUWEN, P. "*Implications of nonshivering thermogenesis for energy balance regulation in humans*". American journal of physiology – Regulatory, integrative and comparative physiology 301: R285–R296. (2011).

115. HALL, K. D., SACKS, G., CHANDRAMOHAN, D., *et al.* "*Quantification of the effect of energy imbalance on bodyweight*". The Lancet 378: 826–837. (2011).

116. GENNEMARK, P., HJORTH, S. & GABRIELSSON, J. "*Modeling energy intake by adding homeostatic feedback and drug intervention*". Journal of pharmacokinetics and pharmacodynamics 42: 79–96. (2015).

117. CANNON, B. & NEDERGAARD, J. "*Thermogenesis challenges the adipostat hypothesis for body-weight contro*". Proceedings of the Nutrition Society 68: 401–407. (2009).

118. CYPESS, A. M., WEINER, L. S., ROBERTS-TOLER, C., *et al.* "*Activation of human brown adipose tissue by a β_3-adrenergic receptor agonist*". Cell metabolism 21: 33–38. (2015).

119. FELDMANN, H. M., GOLOZOUBOVA, V., CANNON, B. & NEDERGAARD, J. "*UCP1 ablation induces obesity and abolishes diet-induced ther-*

mogenesis in mice exempt from thermal stress by living at thermoneutrality". Cell metabolism 9: 203–209. (2009).

120. KEIPERT, S. & JASTROCH, M. "*Brite / beige fat and UCP1 – is it thermogenesis?*" Biochimica et biophysica acta 1837: 1075–1082. (2014).

121. NEDERGAARD, J. & CANNON, B. "*The browning of white adipose tissue: some burning issues*". Cell metabolism 20: 396–407. (2014).

122. ROBERTS, L. D., BOSTRÖM, P., O'SULLIVAN, J. F., *et al.* "β-*aminoisobutyric acid induces browning of white fat and hepatic* β*-oxidation and is inversely correlated with cardiometabolic risk factors*". Cell metabolism 19: 96–108. (2014).

123. CAO, L., CHOI, E. Y., LIU, X., *et al.* "*White to brown fat phenotypic switch induced by genetic and environmental activation of a hypothalamic-adipocyte axis*". Cell metabolism 14: 324–338. (2011).

124. EL HADI, H., DI VINCENZO, A., VETTOR, R. & ROSSATO, M. "*Food ingredients involved in white-to-brown adipose tissue conversion and in calorie burning*". Frontiers in physiology 9: 1954. (2018).

125. BASKARAN, P., KRISHNAN, V., REN, J. & THYAGARAJAN, B. "*Capsaicin induces browning of white adipose tissue and counters obesity by activating TRPV1 channel-dependent mechanisms*". British journal of pharmacology 173: 2369–2389. (2016).

126. OHYAMA, K., NOGUSA, Y., SHINODA, K., *et al.* "*A synergistic antiobesity effect by a combination of capsinoids and cold temperature through promoting beige adipocyte biogenesis*". Diabetes 65: 1410–1423. (2016).

127. WABITSCH, M., BRENNER, R., MELZNER, I., *et al.* "*Characterization of a human preadipocyte cell strain with high capacity for adipose differentiation*". International journal of obesity 25: 8–15. (2001).

128. OTTOSSON, M., LÖNNROTH, P., BJÖRNTORP, P. & EDEN, S. "*Effects of cortisol and growth hormone on lipolysis in human adipose tissue*". The journal of clinical endocrinology & metabolism 85: 799–803. (2000).

129. MACKALL, J., STUDENT, A., POLAKIS, S. & LANE, M. "*Induction of lipogenesis during differentiation in a" preadipocyte" cell line.*" Journal of biological chemistry 251: 6462–6464. (1976).

130. YANG, Y.-H. K., OGANDO, C. R., SEE, C. W., *et al.* "*Changes in phenotype and differentiation potential of human mesenchymal stem cells aging in vitro*". Stem cell research & therapy 9: 131. (2018).

131. ASANO, H., KANAMORI, Y., HIGURASHI, S., *et al.* "*Induction of beige-like adipocytes in 3T3-L1 cells*". Journal of veterinary medical science 76: 57–64. (2013).

132. RUBIN, C., LAI, E. & ROSEN, O. "*Acquisition of increased hormone sensitivity during in vitro adipocyte development.*" Journal of biological chemistry 252: 3554–3557. (1977).

133. ZEBISCH, K., VOIGT, V., WABITSCH, M. & BRANDSCH, M. "*Protocol for effective differentiation of 3T3-L1 cells to adipocytes*". Analytical biochemistry 425: 88–90. (2012).

134. WU, L. & XU, B. in *Thermogenic fat* 203–212 (Springer, 2017).

135. TAKAGI, M., KIMURA, K., NAKASHIMA, K.-I., *et al.* "*Induction of beige adipocytes by naturally occurring β_3-adrenoceptor agonist p-synephrine*". European journal of pharmacology 836: 67–74. (2018).

136. MEHLEM, A., HAGBERG, C. E., MUHL, L., *et al.* "*Imaging of neutral lipids by oil red O for analyzing the metabolic status in health and disease*". Nature protocols 8: 1149–1154. (2013).

137. BÄCKER, V. *ImageJ macro tool sets for biological image analysis* in *Proceedings of the ImageJ user and developer conference, Luxembourg* (2012), 24–26.

138. RIZZATTI, V., BOSCHI, F., PEDROTTI, M., *et al.* "*Lipid droplets characterization in adipocyte differentiated 3T3-L1 cells: size and optical density distribution*". European journal of histochemistry 57: e24. (2013).

139. BOSCHI, F., RIZZATTI, V., ZOICO, E., *et al.* "*Relationship between lipid droplets size and integrated optical density*". European journal of histochemistry 63: 3017. (2019).

140. DAGDA, R. K., CHERRA, S. J., KULICH, S. M., *et al.* "*Loss of PINK1 function promotes mitophagy through effects on oxidative stress and mitochondrial fission*". Journal of biological chemistry 284: 13843–13855. (2009).

141. PENG, J.-Y., LIN, C.-C., CHEN, Y.-J., *et al.* "*Automatic morphological subtyping reveals new roles of caspases in mitochondrial dynamics*". PLoS computational biology 7: e1002212. (2011).

142. KUMAR, P., NAGARAJAN, A. & UCHIL, P. D. "*Analysis of cell viability by the MTT assay*". Cold Spring Harbor protocols 2018: 095505. (2018).

143. ROZEN, S. & SKALETSKY, H. in *Bioinformatics methods and protocols* 365–386 (Springer, 2000).

144. RAO, X., HUANG, X., ZHOU, Z. & LIN, X. "*An improvement of the* $2^{-\Delta\Delta Ct}$ *method for quantitative real-time polymerase chain reaction data analysis*". Biostatistics, bioinformatics and biomathematics 3: 71–85. (2013).

145. PATHAN, M., KEERTHIKUMAR, S., ANG, C.-S., *et al.* "*FunRich: an open access standalone functional enrichment and interaction network analysis tool*". Proteomics 15: 2597–2601. (2015).

146. BOOTMAN, M. D., RIETDORF, K., COLLINS, T., *et al.* "*Ca^{2+}-sensitive fluorescent dyes and intracellular Ca^{2+} imaging*". Cold Spring Harbor protocols 2013: 066050. (2013).

147. MUTO, A., OHKURA, M., ABE, G., *et al.* "*Real-time visualization of neuronal activity during perception*". Current biology 23: 307–311. (2013).

148. HUBER, R., MAZZARELLA, R., CHEN, C.-N., *et al.* "*Glypican 3 and glypican 4 are juxtaposed in Xq26. 1*". Gene 225: 9–16. (1998).

149. TERESPOLSKY, D., FARRELL, S., SIEGEL-BARTELT, J. & WEKSBERG, R. "*Infantile lethal variant of Simpson-Golabi-Behmel syndrome associated with hydrops fetalis*". American journal of medical genetics 59: 329–333. (1995).

150. LAPUNZINA, P., BADIA, I., GALOPPO, C., *et al.* "*A patient with Simpson-Golabi-Behmel syndrome and hepatocellular carcinoma.*" Journal of medical genetics 35: 153–156. (1998).

151. GRISARU, S. & ROSENBLUM, N. D. "*Glypicans and the biology of renal malformations*". Pediatric nephrology 16: 302–306. (2001).

152. CAPURRO, M. I., XU, P., SHI, W., *et al.* "*Glypican-3 inhibits Hedgehog signaling during development by competing with patched for Hedgehog binding*". Developmental cell 14: 700–711. (2008).

153. DAVOODI, J., KELLY, J., GENDRON, N. H. & MACKENZIE, A. E. "*The Simpson–Golabi–Behmel syndrome causative glypican-3, binds to and inhibits the dipeptidyl peptidase activity of CD26*". Proteomics 7: 2300–2310. (2007).

154. ALLOTT, E. H., OLIVER, E., LYSAGHT, J., *et al.* "*The SGBS cell strain as a model for the in vitro study of obesity and cancer*". Clinical and translational oncology 14: 774–782. (2012).

155. GUENNOUN, A., KAZANTZIS, M., THOMAS, R., *et al.* "*Comprehensive molecular characterization of human adipocytes reveals a transient brown phenotype*". Journal of translational medicine 13: 135. (2015).

156. YEO, C. R., AGRAWAL, M., HOON, S., *et al.* "*SGBS cells as a model of human adipocyte browning: a comprehensive comparative study with primary human white subcutaneous adipocytes*". Scientific reports 7: 4031. (2017).

157. BOSTRÖM, P., WU, J., JEDRYCHOWSKI, M. P., *et al.* "*A PGC1-α-dependent myokine that drives brown-fat-like development of white fat and thermogenesis*". Nature 481: 463–468. (2012).

158. VAN KUILENBURG, A. B., STROOMER, A. E., VAN LENTHE, H., *et al.* "*New insights in dihydropyrimidine dehydrogenase deficiency: a pivotal role for beta-aminoisobutyric acid?*" Biochemical journal 379: 119–124. (2004).

159. KITASE, Y., VALLEJO, J. A., GUTHEIL, W., *et al.* "*β-aminoisobutyric acid, l-BAIBA, is a muscle-derived osteocyte survival factor*". Cell reports 22: 1531–1544. (2018).

160. LEHNIG, A. C. & STANFORD, K. I. "*Exercise-induced adaptations to white and brown adipose tissue*". Journal of experimental biology 221: jeb161570. (2018).

161. YAMANAKA, M., TSUCHIDA, A., NAKAGAWA, T., *et al.* "*Brain-derived neurotrophic factor enhances glucose utilization in peripheral tissues of diabetic mice*". Diabetes, obesity and metabolism 9: 59–64. (2007).

162. COLITTI, M., BOSCHI, F. & MONTANARI, T. "*Dynamic of lipid droplets and gene expression in response to β-aminoisobutyric acid treatment on 3T3-L1 cells*". European journal of histochemistry 62: 2984. (2018).

163. REYES-ESCOGIDO, M., GONZALEZ-MONDRAGON, E. G. & VAZQUEZ-TZOMPANTZI, E. "*Chemical and pharmacological aspects of capsaicin*". Molecules 16: 1253–1270. (2011).

164. BEVAN, S., QUALLO, T. & ANDERSSON, D. A. in *Mammalian transient receptor potential (TRP) cation channels* 207–245 (Springer, 2014).

165. YU, X., YU, M., LIU, Y. & YU, S. *TRP channel functions in the gastrointestinal tract* in *Seminars in immunopathology* **38** (2016), 385–396.

166. BISHNOI, M., KONDEPUDI, K. K., GUPTA, A., *et al.* "*Expression of multiple Transient Receptor Potential channel genes in murine 3T3-L1 cell lines and adipose tissue*". Pharmacological reports 65: 751–755. (2013).

167. BABOOTA, R. K., SINGH, D. P., SARMA, S. M., *et al.* "*Capsaicin induces "brite" phenotype in differentiating 3T3-L1 preadipocytes*". PloS one 9: e103093. (2014).

168. MORRISON, S. & MCGEE, S. L. "*3T3-L1 adipocytes display phenotypic characteristics of multiple adipocyte lineages*". Adipocyte 4: 295–302. (2015).

169. MONTANARI, T., BOSCHI, F. & COLITTI, M. "*Comparison of the effects of browning-inducing capsaicin on two murine adipocyte models*". Frontiers in physiology 10: 1380. (2019).

170. KOWIAŃSKI, P. *et al.* "*BDNF: a key factor with multipotent impact on brain signaling and synaptic plasticity*". Cellular and molecular neurobiology 38: 579–593. (2018).

171. ROSAS-VARGAS, H., MARTÍNEZ-EZQUERRO, J. D. & BIENVENU, T. "*Brain-derived neurotrophic factor, food intake regulation, and obesity*". Archives of medical research 42: 482–494. (2011).

172. MATTHEWS, V. B., ÅSTRÖM, M.-B., CHAN, M., *et al.* "*Brain-derived neurotrophic factor is produced by skeletal muscle cells in response to contraction and enhances fat oxidation via activation of AMP-activated protein kinase*". Diabetologia 52: 1409–1418. (2009).

173. SORNELLI, F., FIORE, M., CHALDAKOV, G. N. & ALOE, L. "*Adipose tissue-derived nerve growth factor and brain-derived neurotrophic factor: results from experimental stress and diabetes*". General physiology and biophysics 28: 179–83. (2009).

174. MAROSI, K. & MATTSON, M. P. "*BDNF mediates adaptive brain and body responses to energetic challenges*". Trends in endocrinology & metabolism 25: 89–98. (2014).

175. TSUCHIDA, A., NONOMURA, T., ONO-KISHINO, M., *et al.* "*Acute effects of brain-derived neurotrophic factor on energy expenditure in obese diabetic mice*". International journal of obesity 25: 1286–1293. (2001).

176. YANG, X., BROBST, D., CHAN, W. S., *et al.* "*Muscle-generated BDNF is a sexually dimorphic myokine that controls metabolic flexibility*". Science signaling 12: eaau1468. (2019).

177. VAVOUGIOS, G. D., DOSKAS, T. & KONSTANTOPOULOS, K. "*An electroglottographical analysis-based discriminant function model differentiating multiple sclerosis patients from healthy controls*". Neurological Sciences 39: 847–850. (2018).

178. VINCENT, A. E., WHITE, K., DAVEY, T., *et al.* "*Quantitative 3D mapping of the human skeletal muscle mitochondrial network*". Cell reports 26: 996–1009. (2019).

179. NEDERGAARD, J. & CANNON, B. "*UCP1 mRNA does not produce heat*". Biochimica et biophysica acta 1831: 943–949. (2013).

180. CHANG, J. S., FERNAND, V., ZHANG, Y., *et al.* "*NT-PGC-1α protein is sufficient to link β3-adrenergic receptor activation to transcriptional and physiological components of adaptive thermogenesis*". Journal of biological chemistry 287: 9100–9111. (2012).

181. WU, Z., PUIGSERVER, P., ANDERSSON, U., *et al.* "*Mechanisms controlling mitochondrial biogenesis and respiration through the thermogenic coactivator PGC-1*". Cell 98: 115–124. (1999).

182. ZHANG, X., ZENG, L., YU, T., *et al.* "*Positive feedback loop of autocrine BDNF from microglia causes prolonged microglia activation*". Cellular physiology and biochemistry 34: 715–723. (2014).

183. BAMBAH-MUKKU, D., TRAVAGLIA, A., CHEN, D. Y., *et al.* "*A positive autoregulatory BDNF feedback loop via C/EBPβ mediates hippocampal memory consolidation*". Journal of neuroscience 34: 12547–12559. (2014).

184. TUVIKENE, J., PRUUNSILD, P., ORAV, E., *et al.* "*AP-1 transcription factors mediate BDNF-positive feedback loop in cortical neurons*". Journal of neuroscience 36: 1290–1305. (2016).

185. COLITTI, M., LOOR, J. J. & STEFANON, B. "*Expression of NGF, BDNF and their receptors in subcutaneous adipose tissue of lactating cows*". Research in veterinary science 102: 196–199. (2015).

186. GRUNE, T., LIETZ, G., PALOU, A., *et al.* "*β-carotene is an important vitamin A source for humans*". The journal of nutrition 140: 2268S–2285S. (2010).

187. VON LINTIG, J. "*Provitamin A metabolism and functions in mammalian biology*". The American journal of clinical nutrition 96: 1234S–1244S. (2012).

188. BONET, M. L., RIBOT, J. & PALOU, A. "*Lipid metabolism in mammalian tissues and its control by retinoic acid*". Biochimica et biophysica acta 1821: 177–189. (2012).

189. AL TANOURY, Z., PISKUNOV, A. & ROCHETTE-EGLY, C. "*Vitamin A and retinoid signaling: genomic and nongenomic effects thematic review series: Fat-soluble vitamins: Vitamin a*". Journal of lipid research 54: 1761–1775. (2013).

190. RABELO, R., REYES, C., SCHIFMAN, A. & SILVA, J. E. "*A complex retinoic acid response element in the uncoupling protein gene defines a novel role for retinoids in thermogenesis*". Endocrinology 137: 3488–3496. (1996).

191. MERCADER, J., PALOU, A. & BONET, M. L. "*Induction of uncoupling protein-1 in mouse embryonic fibroblast-derived adipocytes by retinoic acid*". Obesity 18: 655–662. (2010).

192. MURHOLM, M., ISIDOR, M. S., BASSE, A. L., *et al.* "*Retinoic acid has different effects on UCP1 expression in mouse and human adipocytes*". BMC cell biology 14: 41. (2013).

193. DANI, C., SMITH, A., DESSOLIN, S., *et al.* "*Differentiation of embryonic stem cells into adipocytes in vitro*". Journal of cell science 110: 1279–1285. (1997).

194. MERCADER, J., RIBOT, J., MURANO, I., *et al.* "*Remodeling of white adipose tissue after retinoic acid administration in mice*". Endocrinology 147: 5325–5332. (2006).

195. OKLA, M., KIM, J., KOEHLER, K. & CHUNG, S. "*Dietary factors promoting brown and beige fat development and thermogenesis*". Advances in nutrition 8: 473–483. (2017).

196. MARTIN, C. A., ZIEGLER, L. M. & NAPOLI, J. L. "*Retinoic acid, dibutyryl-cAMP, and differentiation affect the expression of retinoic acid receptors in F9 cells*". Proceedings of the National Academy of Sciences 87: 4804–4808. (1990).

197. GUO, H., FONCEA, R., O'BYRNE, S. M., *et al.* "*Lipocalin 2, a regulator of retinoid homeostasis and retinoid-mediated thermogenic activation in adipose tissue*". Journal of biological chemistry 291: 11216–11229. (2016).

198. BRASAEMLE, D. L., SUBRAMANIAN, V., GARCIA, A., MARCINKIEWICZ, A. & ROTHENBERG, A. "*Perilipin A and the control of triacylglycerol metabolism*". Molecular and cellular biochemistry 326: 15. (2009).

199. MIYOSHI, H., SOUZA, S. C., ZHANG, H.-H., *et al.* "*Perilipin promotes hormone-sensitive lipase-mediated adipocyte lipolysis via phosphorylation-dependent and-independent mechanisms*". Journal of biological chemistry 281: 15837–15844. (2006).

200. SAWADA, T., MIYOSHI, H., SHIMADA, K., *et al.* "*Perilipin overexpression in white adipose tissue induces a brown fat-like phenotype*". PloS one 5: e14006. (2010).

201. MIYOSHI, H., SOUZA, S. C., ENDO, M., *et al.* "*Perilipin overexpression in mice protects against diet-induced obesity*". Journal of lipid research 51: 975–982. (2010).

Acknowledgements

I wish to thank my supervisor, prof. Monica Colitti for her constant presence and support and for transmitting to me the love and the passion for scientific research. A special thank also to other members of the research group: prof. Bruno Stefanon for believing in my skills since my first laboratory experience, Dr. Sandy Sgorlon, Dr. Elisa Scarsella and Dr. Giulia Polacchini for always helping me when needed and for their honest friendship.

I wish to thank also the external supervisor prof. Luisa Dalla Valle for her feedbacks on my research work and for teaching me how to look at my results with a critical sense and to understand my limitations.

I thank Dr. Federico Boschi and his research group from University of Verona for their precious collaboration in understanding the dynamic of lipid droplets in adipocytes.

I would like to thank prof. Jeff Stuart and dr. Andrew Valente for hosting me in their laboratory at Brock University and giving me the opportunity to improve my skills in microscopy.

A final thank goes to all my friends inside and outside the university, to my fiancé and to my family for their constant support and for the strength they gave to me to face all the little and big problems that occurred in these three years of work.

doi: 10.1111/obr.12520

Physiology

Factors involved in white-to-brown adipose tissue conversion and in thermogenesis: a review

T. Montanari, N. Pošćić and M. Colitti

Department of Agricultural, Food, Environmental and Animal Sciences, University of Udine, Udine, Italy

Received 24 October 2016; revised 10 January 2017; accepted 11 January 2017

Address for correspondence: M Colitti, Department of Agricultural, Food, Environmental and Animal Sciences, University of Udine, via delle Scienze, 206, Udine 33100, Italy.
E-mail: monica.colitti@uniud.it

Summary

Obesity is the result of energy intake chronically exceeding energy expenditure. Classical treatments against obesity do not provide a satisfactory long-term outcome for the majority of patients. After the demonstration of functional brown adipose tissue in human adults, great effort is being devoted to develop therapies based on the adipose tissue itself, through the conversion of fat-accumulating white adipose tissue into energy-dissipating brown adipose tissue. Anti-obesity treatments that exploit endogenous, pharmacological and nutritional factors to drive such conversion are especially in demand. In the present review, we summarize the current knowledge about the various molecules that can be applied in promoting white-to-brown adipose tissue conversion and energy expenditure and the cellular mechanisms involved.

Keywords: Brown adipose tissue, browning, thermogenesis, white adipose tissue.

Abbreviations: 5-HT, serotonin; 5-HT1B, serotonin receptor 1B; 5-HT2C, serotonin receptor 2C; β_3-ARs, β_3-adrenergic receptors; AC, adenylyl cylcase; AMPK, cAMP-activated protein kinase; AR, adrenoreceptor; AT, adipose tissue; atRA, all-*trans* retinoic acid; BAIBA, β-aminoisobutyric acid; BAT, brown adipose tissue; BC, β-carotene; BCO1, β-carotene-15,15′-oxygenase; BCO2, β-carotene-9′,10′-oxygenase; BMP, bone morphogenetic protein; BNP, brain natriuretic peptide; cAMP, cyclic adenosine monophosphate; CLA, conjugated linoleic acid; COX, cyclooxygenase; DIO2, type II iodothyronine 5′-deiodinase; DMH, dorsomedial hypothalamus; FA, fatty acid; FGF21, fibroblast growth factor 21; FNDC5, fibronectin type III domain-containing protein 5; FX, fucoxanthin; Gs, stimulatory G protein; HFD, high fat diet; IL, interleukin; MAPK, mitogen-activated protein kinase; MT, melatonin receptor; Myf5, myogenic factor 5; NE, norepinephrine; OX, orexin; PG, prostaglandin; PGC-1α, PPARγ coactivator-1α; PKA, protein kinase A; PPAR, peroxisome proliferator-activated receptor; PRDM16, PR/SET domain 16; PUFA, polyunsaturated fatty acid; Rald, retinaldehyde; RAR, retinoic acid receptor; RXR, retinoid X receptor; SA, synephrine alkaloid; SIRT1, silent information regulator type 1; T3, triiodothyronine; T4, thyroxine; TR, thyroid hormone receptor; TRPM8, transient receptor potential cation channel subfamily M, member 8; TRPV1, transient receptor potential cation channel, subfamily V, member 1; TX, thromboxane; UCP1, uncoupling protein 1; VMH, ventromedial hypothalamus; WAT, white adipose tissue.

Introduction

Adipose tissue (AT) is the main form of storage of excess energy intake derived from food. This feature guarantees the survival of an organism even during long fasting periods. Nowadays, food availability to mankind is far greater than in past centuries; thus, dietary habits dramatically changed all over the world. This has led to the epidemic diffusion of obesity in last decades, with the highest number of cases being recorded in western countries (i.e. Europe and USA). Today, this problem has reached devastating proportions, as obese patients are growing in number also in developing countries. According to recent data published by the World Health Organization (1), 1.9 billion adults (39%) are overweight (body mass index $\geq$25 kg m^{-2}) and 600 million individuals (13%) are obese (body mass index $\geq$30 kg m^{-2}). This health issue is not gender-specific, as 38% of men and 40% of women are overweight and 11% of men and 15% of women are obese. Moreover, great concern is growing from the diffusion of child obesity, as over 41 million children are overweight before reaching puberty (1).

Obesity is a serious risk factor as it is associated with metabolic syndrome (2), a cluster of morbidities that includes type 2 diabetes mellitus (3,4), cardiovascular disease, including hypertension (5) and chronic kidney disease. Moreover, obese patients are more prone to contract several forms of cancer with reduced chances of survival (6).

In light of these facts, it is of primary importance to find more effective approaches to treat obesity. The traditional approach that involves the modification of dietary habits and the increase of physical activity often is not effective, as often the fat mass loss is only transient and the regain of body weight after a long period of diet and exercise is very common (7). On the other hand, the bariatric surgery, which could be an effective alternative, is not viable in all cases. After the discovery of functional brown adipose tissue (BAT) masses in human adults through several combined imaging techniques (8,9), there is a growing interest in finding therapies for obesity that start from the AT itself, as the conversion of fat-accumulating white adipose tissue (WAT) into energy-dissipating BAT may be an effective and potentially harmless solution.

This review has the purpose to illustrate the current findings about all factors and natural compounds that have been studied in recent years, classifying them as endogenous, pharmacological and nutritional factors. In order to explain the potential efficiency of these agents in WAT to BAT conversion, their biochemical and molecular mechanisms are also elucidated.

Conversion of white adipocytes into brown-like adipocytes

The biology and developmental origins of BAT and the differences between WAT and BAT have been clearly and deeply reviewed in the past years (10–13). BAT has become central in research on obesity because of adaptive thermogenesis, i.e. the process of regulated heat production that is in part mediated by the catabolism of energy substrates without the release of chemical energy from the breakdown of adenosine triphosphate. This process is led by uncoupling protein 1 (UCP1), a transmembrane protein present in the inner mitochondrial membrane of mitochondria in brown adipocytes. UCP1 participates in adaptive thermogenesis by uncoupling the production of adenosine triphosphate from the catabolic pathways of lipids and carbohydrates. The derived energy is released by the brown adipocytes in form of heat that diffuses in the body, thanks to the rich vascularization of BAT.

Uncoupling protein 1 is uniquely expressed in BAT; thus, an increase in BAT mass in obese patients may improve energy dissipation. One of the possible ways to increase the presence of functional UCP1-rich cells in AT is the conversion of white (pre)adipocytes into brown-like fat cells, known as WAT browning. The result is the appearance in WAT of dispersed masses of brown-like adipocytes, named beige or brite (brown-in-white) adipocytes. These cells share a number of characteristics with brown adipocytes, as they show a multilocularized accumulation of fat reserves, are rich in mitochondria and express high levels of UCP1 and factors that increase the transcription of key proteins of thermogenesis, (e.g. members of the peroxisome proliferator-activated receptor (PPAR) family, cell death-inducing DFFA-like effector A, PR domain containing 16 (PRDM16) and others reviewed in (ref. (11)). Brite adipocytes show, nevertheless, a unique gene expression profile, which is different from both white and brown adipocytes (14–16). Browning is not the only way to obtain brite adipocytes: other developmental pathways, e.g. differentiation from $Myh11^+$ smooth muscle precursor cells or from mesodermal stem cells-derived preadipocytes are involved (17).

White adipose tissue browning is mainly driven by sympathetic stimulation and by the interaction of norepinephrine (NE) with β_3-adrenergic receptors (β_3-ARs) present on the plasma membrane of white adipocytes. Such an interaction starts a signal transduction cascade that ends in the overexpression of UCP1 and other thermogenic proteins. A number of studies and observations confirmed the fact that, endogenously, the mechanisms that drive classic BAT recruitment and WAT browning are the same (18), while the administration of exogenous molecules may selectively activate BAT thermogenesis or recruit brite adipocytes.

Chronic cold exposure is the most effective sympathetic activator (18), as it induces a massive thermogenic response in WAT. Exposure to cold is quite unsuitable and uncomfortable for obese patients; hence, other so-called "browning agents" have been investigated in the last years. Here follows a description of the most relevant and promising

endogenous, pharmacological and nutritional browning factors and their cellular pathways.

Endogenous browning factors

Norepinephrine and central sympathetic activators

As previously mentioned, the expression of UCP1 is under adrenergic control: the activation of β_3-ARs by NE triggers a signal transduction cascade that involves a number of enzymes and transcription factors that, either directly or indirectly, affect the expression level of UCP1 (19). The interaction of NE with β_3-ARs causes the activation of a linked stimulatory G protein (Gs) that, in turn, activates the membrane enzyme adenylyl cylcase (AC). AC stimulates the production of cyclic adenosine monophosphate (cAMP), which is the necessary activator of protein kinase A (PKA). This is a key enzyme in NE stimulation; therefore, the sympathetic-mediated adaptive thermogenesis is known as a cAMP/PKA-dependent process. The PKA-dependent transduction pathways that lead to the overexpression of UCP1 are (i) p38 mitogen-activated protein kinase (MAPK), which stimulates the expression of the PPARγ coactivator-1α (PGC-1α) and the activating transcription factor 2, that are directly involved in the overexpression of UCP1; (ii) cAMP response element binding protein, which directly binds on UCP1 promoter in a p38 MAPK-independent manner (10,19); (iii) the Janus kinase/signal transducer and activator of transcription pathway, which mediates thermogenesis by transducing the signal of several adipose-affecting substances (20); (iv) the silent information regulator type 1 (SIRT1), which amplifies adrenergic response and stimulates PGC-1α (21). These pathways are also involved in the mitochondrial biogenesis, which is fundamental in reaching a brown-like phenotype.

The peripheral release of NE is centrally regulated by a number of proteins produced either by the central nervous system itself or by other peripheral tissues. Leptin is an adipokine whose release is proportional to AT mass, and it has a role in the regulation of food intake and regulation of metabolism (22). Receptors for leptin are centrally located mainly in the arcuate and in the ventromedial (VMH) nuclei of hypothalamus. Recently, leptin receptors involved in the stimulation of thermogenesis were also found in dorsomedial hypothalamus (DMH) (23). Sympathetic stimulation driven by leptin is mediated by the melanocortin system via the release of the α-melanocyte-stimulating hormone, which interacts with the melanocortin-4 receptor. The activation of this receptor causes a production of corticotropin-releasing hormone that finally activates the peripheral release of NE (24). In the adipocyte, leptin positively regulates the expression of β_3-ARs, and *in vitro* studies demonstrated that leptin can stimulate the expression of PGC-1α and the peroxisome proliferator-activated receptor α (PPARα) (25–27). PPARα is another key transcription factor involved in the expression of UCP1 and other genes linked to thermogenesis (28).

The neuropeptide VGF nerve growth factor inducible is engaged in energy homeostasis, and its proteolytic cleavage produces a number of bioactive polypeptides. Among these, TLQP-21 was shown to centrally activate the release of NE, and, consequently, its effects include the overexpression of UCP1 in WAT and the reduction of fat mass following a high fat diet (HFD) in rats (29). Similarly, the brain-derived neurotrophic factor modulates the sympathetic activity leading to WAT browning in response to environmental cues, such as cold exposure and enriched environments (30). Afterwards, it has been demonstrated that the central activity of brain-derived neurotrophic factor is peripherally mediated by the fat depot-specific expression of the vascular endothelial growth factor (31), which has also a role in angiogenesis of BAT and brown-like AT (32).

Myokines

Myokines are endocrine mediators produced by skeletal muscles. They are usually released during the contraction of muscle fibers and link the physical exercise to the loss of fat mass (33).

Irisin is a PGC-1α-dependent myokine that derives from a specific proteolytic cleavage of the fibronectin type III domain-containing protein 5 (FNDC5). Its anti-obesity effect is mediated through the expression of genes linked to lipid catabolism and uncoupling process (including UCP1) selectively in WAT depots, mainly subcutaneous ones (33). AT FNDC5 mRNA and irisin levels in circulation are negatively associated to type 2 diabetes mellitus, leptin and myostatin and positively related to the muscle mass (34). Irisin is recognized as a powerful myokine inducing WAT browning in many animal models. A recent study on human adipocytes showed that irisin acts via the stimulation of p38 MAPK pathway and positively autoregulates adipocyte FNDC5 expression (35).

The β-aminoisobutyric acid (BAIBA) is again a PGC-1α-mediated and exercise-triggered, non-adrenergic activator of WAT browning. This myokine, a metabolite of valine and thymine metabolism, is released during muscle contraction. In animal models, it was demonstrated that BAIBA is a strong stimulator of the mitochondrial activity and enhances the expression of BAT-related genes in white adipocytes, via a PPARα-dependent mechanism. Through the same mechanism, BAIBA improves the lipolytic catabolism in liver, by increasing the expression of specific enzymes involved in β-oxidation (36–38).

Meteorin-like protein is a myokine having an indirect action on WAT browning. Circulating meteorin-like protein can activate eosinophils in WAT to produce interleukin-4 (IL4) and IL13 with a browning effect (39).

Interleukin-6 can be also considered as a myokine because it is markedly released by skeletal muscle during exercise. Daily intramuscular injections of IL6 in mice showed to raise UCP1 expression levels in WAT (40).

Thyroid hormones

The regulation of UCP1 synthesis, mediated by thyroid hormones, is independent of adrenergic stimulation, and these two pathways cooperate in a synergistic way (41). Triiodothyronine (T3) is the hormone that actively and directly regulates UCP1 expression. It is mainly released by the thyroid gland, but the adipocyte itself is able to catalyze the conversion of thyroxine (T4) to T3 by the enzyme type II iodothyronine 5′-deiodinase (DIO2). The enzyme DIO2 is activated by adrenergic stimulation and is strongly inhibited by its own substrate, T4 (42).

The adipocyte has two nuclear receptors for T3, the thyroid hormone receptor α (TRα) and TRβ. The latter stimulates UCP1 expression (13) that is proportional to T3 concentration in AT. The distal enhancer of UCP1 contains the thyroid response element with the binding site for the T3/thyroid hormone receptor β complex. T3, as a sympathetic activator, induces UCP1 expression at central level, too (43).

Fibroblast growth factor 21

The fibroblast growth factor 21 (FGF21) is an endocrine factor involved in the regulation of hepatic lipid metabolism, glycaemia and the functionality of pancreatic β-cells, and it is mainly produced by liver (44). In adipose cells FGF21 interacts with the FGF receptor and its co-receptor β-Klotho. The activated receptor triggers the p38 MAPK pathway that in turn stimulates UCP1 expression inducing both BAT activity and WAT browning (45). Notably, thermogenic activation induces FGF21 release by brown adipocytes (but not by white ones), thus exerting an autocrine effect on the brown fat cell (46). Thus while hepatic FGF21 triggers thermogenesis in BAT and induces WAT browning with an endocrine mechanism, adipose FGF21 sustains the progression of the thermogenesis itself in brown and brite adipocytes with an autocrine mechanism.

It is important to notice that in obese patients, FGF21 signalling is impaired by the pro-inflammatory environment established in WAT masses, because increased tumour necrosis factor α develops an FGF21-resistant phenotype by interfering with the expression of β-Klotho co-receptor (47,48).

Bone morphogenetic proteins

Proteins belonging to this family are involved in normal BAT development and in WAT browning. The bone morphogenetic protein 7 (BMP7) is a key factor in brown adipocyte differentiation as it participates in programming of $Myf5^+$ precursor cells towards a BAT phenotype (49). BMP7 stimulates the expression of early BAT regulator PRDM16 and PGC-1α, thus the synthesis of UCP1. According to a recent study, BMP7 is able to recruit UCP1-rich and mitochondria-rich brite adipocytes from both human adipose-derived stem cells and white adipocytes (50).

Another member of the number 7 morphogenetic proteins family, BMP8B, is not a browning agent at a peripheral level but is crucial in maintaining the thermogenic process in BAT. It is able to improve NE response in brown adipocytes enhancing the p38 MAPK/cAMP response element binding protein pathway for UCP1 expression (51). At a central level, the thermogenic effect of BMP8B in both BAT and WAT is sexually dimorphic: it is observed only in females as it is dependent on ovarian estradiol levels (52). The thermogenic effect of BMP8B is achieved by the regulation of hypothalamic cAMP-activated protein kinase (AMPK) in VMH, with peripheral consequences on BAT activation and WAT browning (53). Moreover, central BMP8B increases orexin (OX) release in the lateral hypothalamic area through a glutamatergic signalling (53). The key role of OX in BAT activity will be discussed in the next sections.

BMP4 was believed to uniquely induce lipid accumulation and differentiation of white adipocytes (54). Several recent studies suggest a possible role of BMP4 in WAT browning, even though such role is still controversial. Xue *et al.* (55) assume that BMP4 induces PGC-1α expression in white preadipocytes and cultured stem cells, leading to the development of brite adipocytes with a strong increase of brite markers expression and biogenesis of mitochondria. This mechanism is supported by further research (56,57). A more recent study demonstrates an opposite role for BMP4 as an inducer of the switch from a brown phenotype to a white-like one (58).

Cardiac natriuretic peptides

Recently, cardiac natriuretic peptides have been recognized as metabolic hormones with a role in regulation of fat mobilization during physical exercise, in fat oxidation by skeletal muscles and browning of white adipocytes. Three peptides belong to this family: atrial natriuretic peptide, brain natriuretic peptide (BNP) and C-type natriuretic peptide (59). They are produced by the heart and target a number of organs, including WAT and BAT. Atrial natriuretic peptide and BNP achieve their biological effects through the natriuretic peptide receptor A, while C-type natriuretic peptide preferentially binds to NPRB. They are both guanylyl ciclase receptors. In WAT, natriuretic peptide (NP) signalling stimulates lipolytic pathways via activation of a cyclic guanosine monophosphate-regulated protein kinase, which in turn phosphorylates hormone-sensitive lipase and perilipin (60).

Cold exposure promotes the secretion of BNP and the synthesis of natriuretic peptide receptor A: activated cyclic guanosine monophosphate-regulated protein kinase in adipocytes stimulates the p38 MAPK pathway, increasing the synthesis of UCP1 and thus triggering the browning process. The NP-mediated browning pathway is independent from NE stimulation, and the effects are more likely additive (61).

Adipokines

Besides leptin – discussed previously – some other adipokines can participate into the browning process of WAT. Cold exposure strongly raises the production of adiponectin in subcutaneous WAT. A study on mice shows that the increased circulating adiponectin recruits beige adipocyte through the increase of resident M2 macrophages in the stromal vascular fraction of subcutaneous WAT, strongly highlighting a link between immunity and WAT browning (62).

Apelin concentration in plasma increases with obesity and hyperinsulinaemia (63). In the adipocyte, apelin triggers a brite phenotype by increasing the expression of UCP1 gene and its transcription factors affecting phosphoinositide 3-kinase/protein kinase B and AMPK pathways (64). However, it has been demonstrated that chronic intracerebroventricular infusion of apelin in mice depresses energy expenditure and BAT functionality, contributing to the development of obesity and related morbidities (65).

Lipid mediators

The role of WAT in the production of both pro-inflammatory and anti-inflammatory lipid mediators, i.e. prostaglandins, thromboxanes, and leukotrienes, was investigated by Garcia-Alonso *et al.* (66). According to the current understanding, arachidonic acid is oxygenated by the isoforms of the enzyme cyclooxygenase (COX) to release prostaglandins and thromboxanes and by lipooxygenase to synthesize leukotrienes. The coordinated activity of enzymes COX-2 and microsomal PGE synthase-1 leads to the synthesis of PGE_2, which stimulates the differentiation, towards a brown-like phenotype, of white preadipocytes. This is possibly achieved through a cAMP-dependent and PPARγ-dependent mechanism, because PGE_2 and some related compounds are agonist ligands of PPARγ isoforms (67). The evidence of a link between WAT browning and COX-2 overexpression is provided in a previous study (68). A more recent research, on the other hand, shows that an excess of PGE_2 and $PGF_{2\alpha}$, accumulated by a marked increase in dietary arachidonic acid, inhibits the white-to-brown conversion pathway by decreasing UCP1 expression in a Ca^{2+}-regulated and extracellular signal-regulated kinase pathway-dependent fashion, but without negative consequences on mitochondriogenesis (69). PGE_2 affects brown thermogenesis also by mediating the activity of CC chemokine ligand 22, a pyrogenic cytokine that binds to the CC chemokine receptor 4 in the anterior hypothalamus/pre-optic area. This area of the nervous system is functionally linked to thermogenic tissues, including BAT; hence, the hyperthermic effect of CC chemokine ligand 22 is carried out by a change in the metabolic rate of BAT (70).

A recent study highlights the browning potential of another metabolite of arachidonic acid, i.e. prostacyclin. *In vitro* treatment of human multipotent adipose-derived stem cell cultures with prostacyclin's analogue carbaprostacyclin induces the development of functional brite adipocytes through the functional coupling between membrane receptor IP-R and Gs protein, thus using the cAMP-dependent pathway in activating AC (71). This lipid mediator produces an amplified effect thanks to its ability to agonistically bind to PPARγ isoforms that are promoters of both, adipogenesis and UCP1 synthesis (66,71).

Serotonin

Serotonin (5-HT) is a monoamine with a number of functions both, at central and at peripheral level, including regulation of appetite and energy homeostasis. Central 5-HT has an anorexigenic effect because 5-HT modulates the hypothalamic feeding circuit (which involves some of the hypothalamic nuclei already mentioned) through the activation of receptors 5-HT1B and 5-HT2C (72). 5-HT can also affect BAT metabolism in the hypothalamus, because neurons of DMH are synaptically linked to the *raphe pallidus*, which modulates sympathetic activation through a serotoninergic circuit. In mice, this circuit promotes thermogenesis when cholinergic muscarinic receptors linking DMH to *raphe pallidus* are antagonized (73). Moreover, the depletion of serotoninergic neurons in mice produces severe impairments in glucose and lipid metabolisms and in brown and brite adipocyte's thermogenic capacities (74). Hence, central serotoninergic regulation is fundamental in the control of both, appetite and energy homeostasis.

At a peripheral level, the major source of 5-HT is gut, and AT represents a target, as 5-HT regulates many functions related to adipogenesis and energy metabolism. In AT itself, 5-HT was found to be an obesogenic factor that promotes lipid accumulation in WAT and inhibits WAT browning and BAT thermogenesis. A study performed on mice demonstrated that the inhibition of tryptophan hydroxylase 1, the enzyme responsible for peripheral 5-HT synthesis, induced lean phenotypes with activated BAT and recruited brite adipocytes (75).

Other endogenous factors

Adenosine plays a dual role in AT: in WAT, it inhibits lipolysis, while in BAT, it increases it. It is likely that the different adenosine receptors present in the two cell types trigger different effects. In white adipocytes, there is a high abundance of A1 receptor, while in brown adipocytes, the Gs-coupled A2a type (adenosine receptor 2a) is the most present. Adenosine released from sympathetic nerves and from the adipocyte itself, following adrenergic stimulation, increases the synthesis of UCP1 through a cAMP-dependent pathway (76,77). A proper pharmacological stimulation of adenosine receptor 2a with agonists can induce browning in WAT.

The appetite-inducing neuropeptide OX is produced in lateral hypothalamic area and has a fundamental role in mediating the differentiation of mature brown adipocytes and in promoting thermogenesis and uncoupled metabolism. OX-null mice displayed a lack of mature, thermogenically active brown adipocytes and an abundance of preadipocytes unable to accumulate lipid droplets and to perform thermogenesis (78). As previously mentioned, the presence of a sustained OX signalling is also fundamental for the mediation of BMP8B effects on BAT functionality (53). Effects of OX on BAT are achieved through its interaction with OX receptor-1 (79).

Melatonin is a hormone acting as an autocrine/paracrine factor. It is secreted by many tissues and organs, but the main melatonin source is the pineal gland. The synthesis of melatonin by the pineal gland is regulated by the hypothalamic paraventricular nucleus and is triggered by the release of NE in specific ganglia. This activation is further regulated by the suprachiasmatic nucleus of the hypothalamus (80). Physiological effects of melatonin are driven by melatonin receptors MT1, MT2 and MT3, even if receptor-independent actions of melatonin are possible, and they concern the scavenging of free radicals (80). Melatonin regulation of energy metabolism involves the circadian distribution of different metabolic processes (81), the control of insulin synthesis and effectiveness (82,83) and the regulation of AT energy metabolism. In this respect, recent findings evidence that long-term pinealectomized rats are overweight, diabetic and with impaired AT physiology, but normal conditions are restored by daily melatonin supplementation (80). In normal animals, the supplementation with melatonin is shown to reduce body weight and abdominal fat mass through activation of BAT and browning of WAT (84). Moreover, chronic administration of melatonin also reduces ageing-related loss of insulin sensitivity in rats (85). Taken together, these findings highlight the therapeutic potential of melatonin against obesity and insulin resistance.

All endogenous browning factors are summarized in Fig. 1 and Table 1.

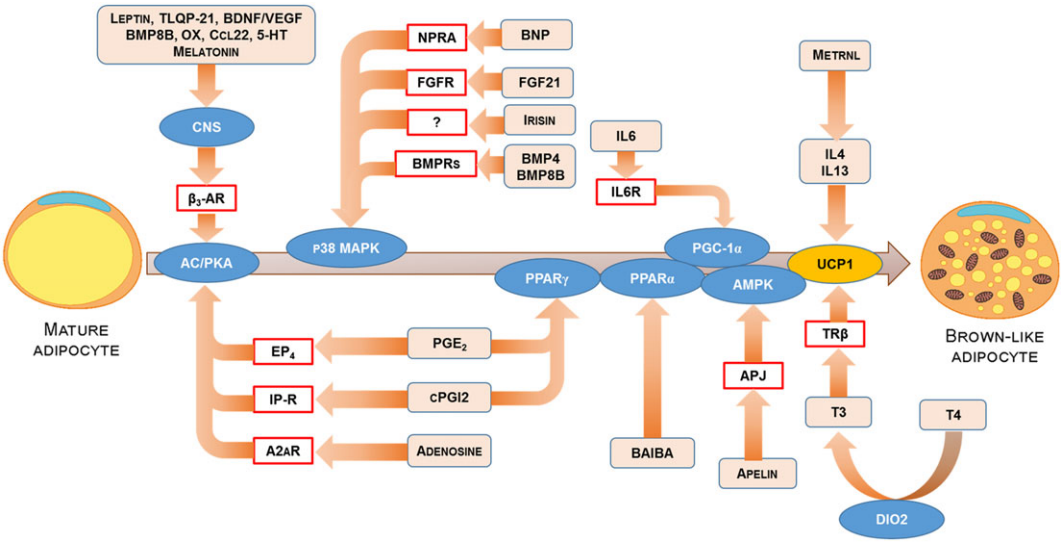

Figure 1 Endogenous factors (orange squares) involved in white adipose tissue browning and their cellular targets (blue circles). Receptors are reported in red boxes. The pathways that directly participate to upregulation of UCP1 (yellow circle) are reported along the brown arrow. All orange arrows indicate a stimulatory effect. 5-HT, serotonin; A2aR, adenosine receptor 2a; AMPK, cAMP-activated protein kinase; APJ, apelin receptor; BAIBA, β-aminoisobutyric acid; BDNF, brain-derived neurotrophic factor; BMP, bone morphogenetic protein; BNP, brain natriuretic peptide; DIO2, type II iodothyronine 5′-deiodinase; FGF21, fibroblast growth factor 21; IL, interleukin; NPRA, natriuretic peptide receptor A; OX, orexin; p38 MAPK, p38 mitogen-activated protein kinase; PGC-1α, PPARγ coactivator-1α; PKA, protein kinase A; PPAR, peroxisome proliferator-activated receptor; T3, triiodothyronine; T4, thyroxine; TRβ, thyroid hormone receptor β; UCP1, uncoupling protein 1; VEGF, vascular endothelial growth factor. [Colour figure can be viewed at wileyonlinelibrary.com]

Table 1 Endogenous factors involved in BAT development and recruitment, WAT browning and UCP1 upregulation

Browning factors	Cellular target	Mechanisms of action	Effect	Ref.
Norepinephrine	β_3-AR	Activation of cAMP/PKA-dependent signalling pathways	Upregulation of UCP1	10
Leptin	ObR	Inhibition of orexigenic NPY/AgRP neurons and stimulation of anorexigenic POMC/CART neurons	Suppression of appetite	22,23,25–27
		Stimulation of melanocortin/corticotropin system	Increase of noradrenergic stimulation of BAT and WAT Upregulation of β_3-AR, p38 MAPK and PGC-1α	
	?	Activation of JAK/STAT signalling pathway	Stimulation of WAT lipolysis. Upregulation of ACO, CPT1 and PPARα	
TLQP-21	?	Central, prostaglandin-dependent stimulation of adrenal medulla	Increase of epinephrine and upregulation of β_2-AR in BAT Upregulation of β_3-AR, PPARδ and UCP1 in WAT	29
BDNF	TrkB	Early regulation of hypothalamic activity	Increase of sympathetic output Upregulation of adipose VEGF	30,31
Irisin	?	Stimulation of p38 MAPK signalling pathway and positive autoregulation of FNDC5 expression	Upregulation of UCP1 Stimulation of lipid catabolism	33,35
BAIBA	PPARα	Regulation of gene expression	Upregulation of PPARα and UCP1 Increase of FA oxidation	37
Meteorin-like	?	Recruitment of eosinophils and alternative activation of macrophages	Indirect WAT browning through IL4 and IL13 signalling	39
Interleukin 6	IL6R	PGC-1α-dependent modulation of gene expression	Upregulation of UCP1	40
Triiodothyronine	TRβ	Bond of activated TRβ to UCP1 distal enhancer	Upregulation of UCP1	41
Thyroxine	DIO2	Intracellular conversion to triiodothyronine	Upregulation of UCP1	42
FGF21	FGFR, β-Klotho	Stimulation of p38-MAPK. Autocrine effect on brown adipocytes	Upregulation of UCP1	45,46
BMP7	BMPR1	Early brown adipocyte programming of Myf5$^+$ progenitor cells	Differentiation of brown adipocytes	49
	BMPR2	Promotion of the expression of brown and brite fat gene markers	Differentiation of brite adipocytes from not fully differentiated white fat cells	50
BMP8B	BMPR1A	Stimulation of p38 MAPK/CREB signalling pathway in brown adipocytes Central, estradiol-dependent stimulation of hypothalamic nuclei, in opposition to AMPK and increase of sympathetic tone	Maintenance of the thermogenic machinery, upregulation of orexin synthesis	51,53
BMP4	BMPR1 BMPR2	Stimulation of p38 MAPK/PGC-1α/ATF2 signalling pathway	Upregulation of glucose and lipid metabolism, expression of brite phenotype in differentiating adipocytes	56,57
ANP and BNP	NPRA	cGMP/PKG-dependent stimulation of p38 MAPK/PGC-1α signalling pathway	Upregulation of UCP1 and increase of lipolysis	59,60
Adiponectin	adipoR1 adipoR2	Promotion of polarization and maintenance of resident M2 macrophages after cold-exposure	scWAT browning	62
Apelin	APJ	Activation of PI3K/Akt and AMPK signalling pathways in brown adipocytes. Autocrine positive feedback	Brown adipogenesis, upregulation of UCP1	64
		Stimulation of AMPK signalling pathway and upregulation of PRDM16 in white adipocytes	WAT browning, inhibition of adipogenesis	
Prostaglandin E_2	EP_4	Modulation of cAMP level in the adipocyte	Increased lipolysis	66
		Stabilization of white-to-brown transcriptional regulators	Promotion of WAT browning	
	PPARγ	Interaction with PPARγ	Upregulation of UCP1	
Carbaprostacyclin	IP-R PPARγ	Activation of cAMP/PKA-dependent signalling pathway Interaction with PPARγ	Upregulation of UCP1 and WAT browning	71
Serotonin	5-HT1B	Activation of POMC neurons and inhibition of NPY/AgRP neurons	Suppression of appetite	72

(*Continues*)

Table 1 (Continued)

Browning factors	Cellular target	Mechanisms of action	Effect	Ref.
	5-HT2C	Activation of central hypothalamic serotoninergic neurons	WAT browning, regulation of glucose and lipid metabolism	74
Adenosine	A2aR	Stimulation of cAMP/PKA-dependent signalling pathway in brown adipocytes	Upregulation of UCP1	76
Orexin	OX1R	Activation of PLC/p38 MAPK signalling pathway	BAT adipogenesis	78
		BMP-dependent phosphorylation of pSmad 1/5		
Melatonin	MT1	Activation of sympathetic release of norepinephrine via the suprachiasmatic nucleus	Increase of norepinephrine turnover	80,84
	MT2	Activation of PLC/PKC signalling pathway in the adipocyte	Upregulation of UCP1	
	Cyt C	Melatonin conversion into AFMK	Enhancement of mitochondrial thermogenesis	
	DIO2	Increase of DIO2 enzymatic activity	Upregulation of UCP1	

5-HT1B, serotonin receptor 1B; 5-HT2C, serotonin receptor 2C; β_3-ARs, β_3-adrenergic receptors; A2aR, adenosine receptor 2a; ACO, acyl-CoA-oxidase; adipoR1, adipoR2, adiponectin receptors 1 and 2; AFMK, N-acetyl-N-formyl-5-methoxykynurenamine; AgRP, agouti-related peptide; Akt, protein kinase B; ANP, atrial natriuretic peptide; APJ, apelin receptor; ATF2, Activating transcription factor 2; BAIBA, β-aminoisobutyric acid; BAT, brown adipose tissue; BDNF, brain-derived neurotrophic factor; BMP, bone morphogenetic protein; cAMP, cyclic adenosine monophosphate; CART, cocaine-regulated and amphetamine-regulated transcript; cGMP, cyclic guanosine monophosphate; CREB, cAMP response element binding protei; Cyt C, cytochrome C; DIO2, type II iodothyronine 5′-deiodinase; FA, fatty acid; FGF21, fibroblast growth factor 21; FNDC5, fibronectin type III domain-containing protein 5; JAK/STAT, Janus kinase/signal transducer and activator of transcription; IL, interleukin; MT, melatonin receptor; NPRA, natriuretic peptide receptor A; NPY, neuropeptide Y; ObR, leptin receptor; OX1R, orexin receptor 1; p38, MAPK: p38 mitogen-activated protein kinase; PI3K, phosphatidylinositol-4,5-biphosphate 3-kinase; PGC-1α, PPARγ coactivator-1α; PKA, protein kinase A; PKC, protein kinase C; PKG, Protein Kinase G; PLC, phospholipase C; PPAR, peroxisome proliferator-activated receptor; POMC, proopiomelanocortin; PRDM16, PR/SET domain 16; TrkB, tyrosine kinase receptor B; TRβ, thyroid hormone receptor β; VEGF, vascular endothelial growth factor; UCP1, uncoupling protein 1; WAT, white adipose tissue.

Pharmacological browning factors

β_3-selective adrenergic agonists

The β_3-AR is an atypical adrenoreceptor found in AT (10). Hence, the selective stimulation of this receptor may drive BAT activation and WAT browning with light or absent cardiovascular side effects, which are reported for non-selective sympathomimetic drugs. A number of molecules underwent clinical trials, but the majority was rejected at the clinical phase II because of lack of efficacy in human β_3-AR (86).

L-796568 was among the first β_3 agonists with documented increased energy expenditure in humans (87). Tests on humans accounted for acute increase (8%) of energy expenditure in obese patients (88), but chronic effects were not observed (89). This drug produced no cardiovascular side effects, as the bond with β_1-AR and β_2-AR did not occur.

Mirabegron is a recently discovered β_3 agonist which produces a marked increase in resting metabolic rate (13%) in young male, suggesting a powerful activation of BAT thermogenesis (90,91). This is a promising anti-obesity drug, despite cardiovascular side effects due to its weak affinity to other β-ARs.

Drugs affecting the serotoninergic system

As previously discussed, central 5-HT is an important factor in stimulating thermogenesis and recruiting brite adipocytes; hence, drugs affecting the central serotoninergic circuit may increase the 5-HT-mediated actions on AT.

Selective serotonin re-uptake inhibitors are classically used as antidepressant drugs, but they can also find interesting applications in obesity treatment. Sibutramine is a drug that inhibits the re-uptake of both 5-HT and NE in central synapses; it is converted in two active metabolites that achieve the anti-obesity effect by reducing appetite and increasing thermogenesis (92). Chronic treatment with sibutramine also improves biochemical blood parameters associated with obesity and diabetes: glycaemia, insulinaemia, triglycerides, total cholesterol, low-density lipoprotein cholesterol, high-density lipoprotein cholesterol and glycosylated haemoglobin (92,93). Side effects include severe cardiovascular outcomes, like increase in heart rate and blood pressure and in the likelihood of non-fatal myocardial infarction or stroke. For this reason, the drug was not eligible for patients with a history of cardiovascular disease, and it has been withdrawn from the market (94).

Fluoxetine is another member of selective serotonin re-uptake inhibitor class of pharmaceuticals. A recent study performed on rats shows that chronic fluoxetine administration reduces body mass and WAT mass without affecting food intake of the animals. Rats displayed also an increase

in BAT mass, UCP1 expression and mitochondria metabolic rate, measured as O_2 consumption (95).

Fenfluramine and its d-isomer, dexfenfluramine, are serotoninergic drugs that suppress appetite by increasing the synaptic release of 5-HT. Like sibutramine, these molecules produce serious side effects, including heart valve damages and pulmonary arterial hypertension (96). The association with other drugs, like phentermine (a centrally active, noradrenergic drug) attenuates the side effects (97). Nevertheless, both fenfluramine and dexfenfluramine were withdrawn from the market (94).

Tamoxifen

The modulator of oestrogen receptor tamoxifen is currently used in the oestrogen-dependent breast cancer therapy. It has been recently tested on mice for its effect on AT metabolism and WAT browning (98). The study shows no acute effects on body weight and food intake, but chronic tamoxifen administration affected the histology of subcutaneous AT, by reducing the size of white adipocytes and increasing the presence of brite adipocytes. Also lipid and glucose metabolisms are affected (98).

Thiazolidinediones

The class of thiazolidinediones includes anti-hyperglicemic drugs (i.e. rosiglitazone and pioglitazone) that participate in BAT activation and WAT browning, acting as agonist ligands of PPARγ. Several *in vitro* studies show the ability of rosiglitazone to promote the synthesis of UCP1 and other mitochondrial proteins involved in electron transport chain in both preadipocytes and mature adipocytes (99,100). Nevertheless, the synthesis of UCP1 induced by thiazolidinediones is not sufficient to trigger thermogenesis in recruited cells, because a proper noradrenergic activation is needed (18). *In vivo* rosiglitazone treatment on mice increased UCP1 expression and lipid accumulation in brown adipocytes, but failed in triggering thermogenesis, maybe because of the downregulation of β_3-ARs and DIO2 (101,102).

Pioglitazone treatment in cultured human subcutaneous adipocytes led to a modest increase in UCP1 transcription (103).

All pharmacological browning factors are summarized in Table 2 and Fig. 2a.

Nutritional browning factors

Nutritional factors and nutraceuticals are gaining high interest in obesity research, because many natural compounds have been tested in a number of studies and show marked lipolytic and/or anti-adipogenic activity (104,105). Moreover, many molecules also have a positive effect on thermogenesis and WAT browning.

Capsaicin and capsinoids

Capsaicin is an alkaloid present in plant species belonging to the genus *Capsicum*, which includes the hot pepper. This chemical compound is responsible for the burning sensation of hot pepper, and its ability to induce WAT browning has been known for many years. The exact mechanism of capsaicin action has been recently elucidated by Baskaran *et al.* (106). The authors showed that in mice fed with a HFD, capsaicin suppressed weight gain without affecting food

Table 2 Pharmacological factors involved in BAT development and recruitment, WAT browning and UCP1 upregulation. Side effects of drugs are reported in italic

Browning factors	Cellular target	Mechanisms of action	Effect	Ref.
L-796568	β_3-AR	Selective β_3-sympathomimetic	Acute increase of thermogenesis	87–89
Mirabegron	β_3-AR	Selective β_3-sympathomimetic, weak affinity to other β-adrenoreceptors	Upregulation of UCP1. *Cardiovascular side effects.*	90,91
Sibutramine	5-HT and NE synapses	Inhibition of the reuptake of serotonin and norepinephrine	Appetite reduction, increase of thermogenesis, improvement of blood parameters. *Increased heart rate, increased blood pressure, myocardial infarction, stroke.*	92–94
Fluoxetine	5-HT synapses	Inhibition of the reuptake of serotonin	Upregulation of UCP1, increase in BAT mass	95
Fenfluramine Dexfenfluramine	5-HT synapses	Increase of the synaptic release of serotonin	Appetite suppression. *Heart valve damage, pulmonary arterial hypertension*	94,96
Tamoxifen	ER	Agonist of oestrogen receptor	Chronic scWAT browning. Modification of lipid and glucose metabolism	98
Rosiglitazone	PPARγ	Agonist ligand of PPARγ	Upregulation of UCP1 in preadipocytes and mature adipocytes Downregulation of β_3-AR and DIO2	99,100 101,102
Pioglitazone	PPARγ	Agonist ligand of PPARγ	Modest upregulation of UCP1	103

5-HT, serotonin; β_3-ARs, β_3-adrenergic receptors; BAT, brown adipose tissue; DIO2, type II iodothyronine 5′-deiodinase; ER, oestrogen receptor; NE, norepinephrine; PPARγ, peroxisome proliferator-activated γ; scWAT, subcutaneous WAT; UCP1, uncoupling protein 1; WAT, white adipose tissue.

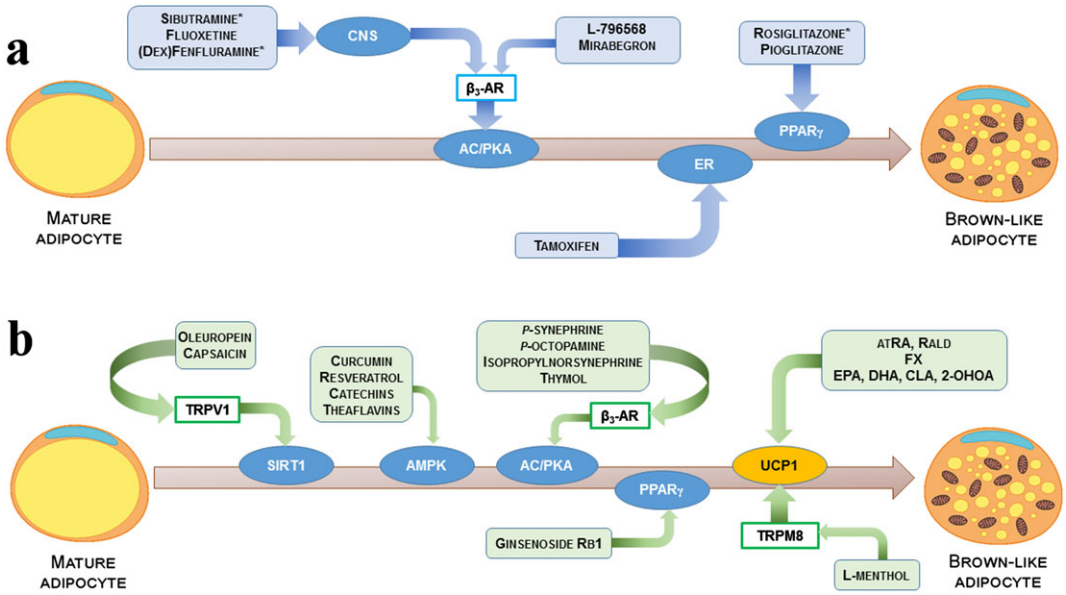

Figure 2 (a) Pharmacological factors (light blue squares) involved in white adipose tissue browning and their cellular targets (blue circles). Receptors are reported in cyan boxes. All blue arrows indicate a stimulatory effect. *The drug has been withdrawn from the market. (b) Nutritional factors (light green squares) involved in white adipose tissue browning and their cellular targets (blue circles). Receptors are reported in green boxes. The pathways that directly participate to upregulation of UCP1 (yellow circle) are reported along the brown arrow. All green arrows indicate a stimulatory effect. β_3-ARs, β_3-adrenergic receptors; AMPK, cAMP-activated protein kinase; DHA, docosahexaenoic acid; EPA, eicosapentaenoic acid; FX, fucoxanthin; PKA, protein kinase A; PPAR, peroxisome proliferator-activated receptor; TRPM8, transient receptor potential cation channel subfamily M, member 8; TRPV1, transient receptor potential cation channel, subfamily V, member 1; Rald, retinaldehyde; SIRT1, silent information regulator type 1; UCP1, uncoupling protein 1. [Colour figure can be viewed at wileyonlinelibrary.com]

intake, by overexpressing the transient receptor potential cation channel, subfamily V, member 1 (TRPV1), which is usually downregulated by HFD (106,107). The *in vitro* analyses showed that capsaicin stimulates Ca^{2+} influx in subcutaneous cultured adipocytes that express TRPV1. The Ca^{2+} influx activates the Ca^{2+}/calmodulin-dependent protein kinase II, which in turn activates AMPK. This enzyme phosphorylates SIRT1, which deacetylates both PPARγ and PRDM16. The interaction of these two transcription factors increases their own stability. The final step is the stimulation of the synthesis of UCP1 and BMP8B in white adipocytes, with the consequent stimulation of browning and thermogenesis. Capsaicin is also active at a transcriptional level, because it increases the expression of PPARα, PPARγ, SIRT1 and PGC-1α. The increased expression of PPARα is associated with an increased lipolytic activity of the adipocyte (106).

Capsinoids, i.e. capsiate, dihydrocapsiate and nordihydrocapsiate, are non-pungent analogues of capsaicin found in some *Capsicum* species (108,109). Despite their structural affinity with capsaicin, these molecules show some different behaviours in the organism. They are unstable in aqueous environment and rapidly hydrolyzed in the gastrointestinal tract (110). Capsinoids are not detectable in plasma after oral administration of a capsinoid-supplemented diet to mice (111). The capsinoids binding affinity to TRPV1 is similar to that of capsaicin, but the influx of Ca^{2+} is almost 10 times lower (112). According to these findings, Ohyama *et al.* (111) proposed a capsinoid's central-mediated signalling. This pathway involves the interaction of capsinoids to gastrointestinal TRPV1 receptors which in turn activate the vagal afferent nerves, which are able to stimulate VMH. This stimulation triggers a β_2-adrenergical sympathetic response in WAT depots that increase the stability and half-life of PRDM16 and that is independent from cold-induced, β_3-adrenergic stimulation. So the two adrenergic pathways act on WAT browning in a synergistic way.

Protoalkaloids of bitter orange

Synephrine alkaloids (SAs) are molecules that can be found in fruits of bitter orange (*Citrus aurantium* L.). These molecules are *p*-synephrine, often referred to as synephrine or oxedrine, and *m*-synephrine, i.e. phenylephrine. The presence of both SAs in bitter orange fruit is subject to variations, i.e. *m*-synephrine is not always detected (113).

Synephrine alkaloids are sympathomimetics with non-specific affinity for AR, as their structure is very similar to that of NE and ephedrine. In detail, *p*-synephrine with α-AR, β_1-AR and β_2-AR presents little binding affinity, being

the β_3-ARs the most likely preferential target (114). On the contrary, *m*-synephrine evidences affinity with the α-AR, β_1-AR and β_2-AR. However, *m*-synephrine and *p*-synephrine are, respectively, 100-fold and 40,000-fold less potent than NE in binding β_1-AR and β_2-AR (114).

Studies report the lipolytic effect of *p*-synephrine in both rat and human adipocytes, with stronger outcome in rat cells (115). Moreover, this alkaloid is also active on rat hepatic carbohydrate metabolism, as shown by liver perfusion with bitter orange extract (116) and with pure *p*-synephrine (115). SAs stimulate glycogenolysis, glycolysis, gluconeogenesis and oxygen uptake in hepatocytes through α-adrenergic and β-adrenergic stimulation, with higher extent of α-ARs stimulation.

The fluctuating binding capacity of SAs to different isoforms of ARs raised high concern about the safety of these molecules from a cardiovascular point of view. In this regard, Haaz *et al.* (117) extensively reviewed clinical studies and case reports showing a lack of significant data due to suboptimal planning of administrations and trials.

The alkaloid *p*-octopamine is also present in bitter orange fruit in lower concentration than *p*-synephrine. It is preferentially a β_3-adrenergic agonist, and it induces lipolysis and browning in white rat adipocytes but not in human cells (118). A comparative study between rat and human adipocytes highlights the lipolytic effect of several *C. aurantium* alkaloids, the most active being *p*-synephrine thanks to its higher concentration in the bitter orange extract (119).

A synthetic derivative of SAs, isopropylnorsynephrine, has a more powerful lipolytic effect compared to natural-occurring compounds. The study conducted by Mercader *et al.* (119) infers a specific β_3-adrenergic agonism for this molecule; hence theoretically, cardiovascular side effects should be negligible compared to non-selective sympathomimetic alkaloids. Therefore, isopropylnorsynephrine could be an interesting anti-obesity molecule candidate, pending further testing (119).

Fucoxanthin

Fucoxanthin (FX) is an isoprenoid molecule found in many edible seaweeds, with the highest levels found in the diatom *Phaeodactylum tricornutum* (120). It has a manifold beneficial role in the control of adiposity and carbohydrate metabolism; hence, it is used as a protective functional ingredient against weight gain and metabolic disorders.

Administration of FX significantly downregulates the expression and activity of lipogenic enzymes, while upregulates oxidative pathways of fatty acids (FAs) and the expression of β_3-ARs in adipocytes (120). This induces an increase of UCP1 expression in both, WAT and BAT (121,122).

Fucoxanthin effects may be potentiated through the combination with other lipophilic substances such as medium-chain triglycerides (123), conjugated linoleic acid (124), fucoxanthinol (which is a deacetylated FX-derivative) (125) and fish oil (126). Xanthigen is a dietary product that includes fucoxanthin and pomegranate seed oil, which is rich in ω5 punicic acid (127). A recent pilot study, using ^{18}F-fluorodeoxyglucose positron emission tomography, demonstrates that chronic administration of Xanthigen in a premenopausal, obese woman activates BAT in cervical, supraclavicular and paravertebral areas (128).

Fucoxanthin is accumulated in form of different metabolites: in heart and liver as fucoxanthinol and in AT as amarouciaxanthin A. These metabolites are very effective in inhibiting the differentiation of white preadipocytes into mature white adipocytes (129,130).

Fucoxanthin also improves blood parameters and hepatic accumulation of lipids (131,132).

Carotenoids and related compounds and metabolites

Carotenoids include a broad spectrum of C_{40} isoprenoid compounds which affect AT biology either directly or through their metabolic products, i.e. retinoids. The most important carotenoid is pro-vitamin A β-carotene (BC), which can be metabolized in adipocytes by the enzymes β-carotene-15,15′-oxygenase (BCO1) and β-carotene-9′,10′-oxygenase (BCO2) (which are differentially expressed in subcutaneous and visceral AT) (133) to generate several cleavage products, including retinoic acid (RA) and relative isomers, retinaldehyde (Rald) and several β-apocarotenals and β-apocarotenones (134). The effects of carotenoids and retinoids on AT mostly rely on their ability to bind to specific nuclear receptors, namely RA receptors (RARs) and retinoid X receptors (RXRs), in order to modulate gene expression in the adipocyte. All-*trans* RA (atRA) is a ligand of RARs, while 9-*cis* RA binds both RARs and RXRs. Activated RARs achieve their effect on gene expression by forming a heterocomplex with RXRs. In turn, RXRs may interact also with other nuclear receptors, including TRs and PPARs (134). Besides retinoid receptors, other receptors represent potential targets for retinoids and carotenoids: atRA, Rald, several apocarotenoids and astaxanthin act as enhancers or inhibitors of PPAR isoforms (134). Also extranuclear, non-genomic effects are achieved by these compounds through Janus kinase 2 signalling pathway (135).

Effects of carotenoids and retinoids in counteracting lipid accumulation and preadipocyte differentiation have been studied in both, *in vitro* and *in vivo* models and have been extensively reviewed by Bonet *et al.* (134). A number of studies report also an effect of carotenoid-related compounds in increasing energy expenditure and thermogenesis

in both WAT and BAT. The participation of BC in the modulation of UCP1 expression was early established by *in vitro* studies (136), and it is due to the conversion of BC and other pro-vitamin A carotenoids into atRA, whose interaction with RARs strongly triggers UCP1 synthesis. The non-metabolized form of BC is not active on UCP1 expression and WAT browning (19).

All-*trans* RA treatment of murine white fat cells induced the overexpression of thermogenic and catabolic proteins and the increase in mitochondrial biogenesis. These effects seem to be promoted by lipocalin 2, a recently discovered adipokine which is involved in the regulation of the cellular uptake and metabolism of retinoids (137). The same molecule was tested on human SGBS cell line, multipotent adipose-derived stem cells and primary preadipocyte cell culture; the experiment shows no effect of atRA in inducing UCP1 synthesis and WAT browning in any of these cell culture models (138).

A role in WAT browning has been attributed also to Rald, independently of its conversion to atRA (134).

Long chain (poly)unsaturated fatty acids

As previously highlighted in this review, an excess in dietary arachidonic acid leads to an increased WAT adipogenesis, flanked by a reduction in BAT functionality and WAT browning (69). This is true for other ω6 polyunsaturated fatty acids (PUFAs) as well. Nowadays, food habits privilege the intake of ω6 PUFAs rather than ω3 ones, and the prevalence of dietary ω6 PUFAs has been proposed to be detrimental because of its adverse effects on lipid metabolism and obesity development. Several studies have investigated the role of PUFAs on AT from metabolic and genomic point of view, and these findings have been comprehensively reviewed by Simopoulos (139).

Eicosapentaenoic acid and docosahexaenoic acid are ω3 PUFAs abundantly present in fish oil. They are known to reduce and prevent weight gain through their positive action on PPAR members expression in BAT, which leads to an increase in metabolism of glucose and FAs (140). A study on mice reveals that ω3 PUFAs activate thermogenesis, as the reduction of body weight is not accompanied by a diminished food intake (141). Dietary eicosapentaenoic acid and docosahexaenoic acid (administered in daily doses ranging from 119 to 238 g kg^{-1}) increase the expression of UCP1, PPARs and β_3-AR genes, which are directly involved in thermogenesis, and of other genes involved in the uptake and metabolism of glucose and FAs (i.e. *GLUT4*, *CD36* and *CPT1*) (141). These observations were confirmed by *in vitro* studies on human adipose-derived stem cells (142).

Conjugated linoleic acid (CLA) is a mixture of linoleic acid isomers which are naturally present in cow milk. CLA effects on lipid metabolism, AT inflammation and thermogenesis are reviewed in detail by Shen and McIntosh (143). A number of studies reveal that CLA has a great potential to reduce adiposity and trigger browning especially in visceral WAT, through G protein-coupled receptors and noradrenergic stimulation of AT. However, the long-term effects of CLA-induced WAT browning may harm the defence of body temperature (143).

Chemical modification of dietary FAs has shown beneficial effects on health in several cases (144,145). 2-hydroxyoleic acid is formed by addition of hydroxylic group in α position of oleic acid and possesses an ability to induce thermogenesis by upregulating UCP1 expression. Normal oleic acid also causes body weight reduction in rats but does not affect UCP1 expression (146).

Polyphenolic and non-aromatic alcoholic compounds

Polyphenols are aromatic molecules found in plants characterized by the presence of multiples of phenol structural units. Thymol, although having a single aromatic group, is included in this category. Thymol, found in thyme species (*Thymus* spp.) has recently been tested as an anti-obesity compound (147) and as activator of thermogenesis (148). A recent study on 3T3-L1 murine adipocytes shows that thymol, acting as a β_3-adrenergic agonist, promotes lipolysis, FA oxidation, expression of UCP1 and mitochondrial biogenesis (148). Interestingly, its isomer carvacrol, also found in thyme, has anti-obesity properties as well but cannot stimulate thermogenesis (149).

Resveratrol is a polyphenol present in the skin of grapes (*Vitis vinifera* L.) and in other fruit species with known beneficial effects on adiposity and metabolic disorders (150,151). The effect of resveratrol in AT biology is due to its ability to activate AMPK (152). In murine primary stromal vascular cells separated from inguinal WAT, resveratrol induces browning of WAT through AMPK-dependent pathway that leads to the increase of UCP1 mRNA and protein content in white adipocytes and enhances the expression of a number of brite-specific gene markers (153).

Oleuropein is a polyphenolic glycoside present in extra virgin olive oil. It is present also as an aglycone and gives a pungent taste to olive oil. It has been recognized as a powerful antioxidant compound and also has anti-obesity properties, like many other molecules detected in olive oil, including hydroxytyrosol (154–156). Studies on rats confirmed that anti-obesity effect of oleuropein and oleuropein aglycone is achieved through the activation of thermogenesis in BAT and an increased release of both epinephrine and NE, which in turn activates lipolytic pathways in AT. Interestingly, these molecules, and in particular oleuropein aglycone, are agonists of the capsaicin receptor TRPV1;

hence, their anti-obesity effect could be comparable to that of capsaicin (157).

Curcumin is a polyphenolic compound extracted from *Curcuma longa* L. with well documented beneficial effects for a wide spectrum of diseases (158–160). In 3T3-L1 cells and rat primary inguinal white adipocytes, curcumin stimulates lipolysis and induces a brite phenotype through an AMPK-dependent mechanism that influences the expression of UCP1 and brite gene markers (161). The role of curcumin in WAT browning was previously reported by Wang *et al.* (162) in mice. They inferred an NE-dependent pathway because, after curcumin administration, plasma NE levels and the expression of β_3-ARs in WAT increase in mice.

Other polyphenolic compounds can be found in tea (*Camellia sinensis* (L.) Kuntze). The positive effect of tea on energy expenditure and thermogenesis has been known,

Table 3 Nutritional factors involved in BAT development and recruitment, WAT browning and UCP1 upregulation. Side effects of natural compounds are reported in italic

Browning factors	Source	Cellular target	Mechanisms of action	Effect	Ref
Capsaicin	*Capsicum* spp.	TRPV1	CaMKII/AMPK/SIRT1-dependent deacetylation of PPARγ and PRDM16	Upregulation of UCP1 and BMP8B	106
Capsiate Dihydricapsiatee Nordihydrocapsiat	*Capsicum annuum*	TRPV1	TRPV1/VMH-mediated increase of β_2-adrenergic stimulation	Increase of stability and half-life of PRDM16	111
p-synephrine *m*-synephrine	*Citrus aurantium*	α-ARs β-ARs	Non-selective sympathomimetics	Activation of adipose tissue lipolysis. *Cardiovascular side effects*	114–117
p-octopamine		β_3-AR	Selective β_3-sympathomimetic, weak affinity to other β-adrenoreceptors	Induction of lipolysis and browning in non-human WAT	118,119
Isopropylnorsynephrine	Synthetic		Selective β_3-sympathomimetic	High lipolytic power	119
Fucoxanthin	Several edible seaweeds	Genomic DNA	Downregulation of lipogenic enzymes Upregulation of β_3-AR and oxidative enzymes	Inhibition of adipogenesis Upregulation of UCP1	120–122
β-carotene Astaxanthin	Red-coloured fruits and vegetables	BCO1 BCO2	Conversion into retinoids and apocarotenoids	Indirect WAT browning	134,136–138
All-*trans* retinoic acid 9-*cis* retinoic acid Retinaldehyde	Carotenoid metabolism	RAR RXR RAR Aldh1a1	Lipocalin 2-driven regulation of gene transcription Conversion into all-*trans* retinoic acid	Upregulation of UCP1	
Eicosapentaenoic acid Docosahexaenoic acid	Fish oil	PPARα PPARγ	Agonists of PPARα and PPARγ	Increase in glucose and lipid metabolism. Upregulation of UCP1, PPARs and β_3-AR	140,141
Conjugated linoleic acid	Cow milk	GPCR	NE-dependent activation of adipocyte	Selective browning of omWAT	143
2-hydroxyoleic acid	Synthetic	?	Upregulation of UCP1	Induction of WAT browning	146
Thymol	*Thymus* spp.	β_3-AR	Selective β_3-sympathomimetic	Promotion of lipolysis and lipid oxidation Upregulation of UCP1 Mitochondrial biogenesis	147,148
Resveratrol	*Vitis vinifera*	AMPK	Activation of AMPK-dependent signal pathways	Upregulation of UCP1 and of brite-specific markers	152,153
Oleuropein Oleuropein aglycone	*Olea europaea*	TRPV1	Not described	Upregulation of UCP1 Increase of epinephrine and NE release	157
Curcumin	*Curcuma longa*	AMPK	Activation of AMPK-dependent signal pathways	Upregulation of UCP1 and of brite-specific markers	161
Catechins Theaflavins	*Camellia sinensis*	AMPK	Activation of AMPK-dependent signal pathways	Upregulation of UCP1 and of brite-specific markers	163–168
L-menthol	*Mentha* spp.	TRPM8 TRPA1	Ca^{2+}-dependent phosphorylation of PKA and activation of downstream pathways	Upregulation of UCP1 Mitochondrial biogenesis	169,171
Ginsenoside Rb1	*Panax* spp.	PPARγ	Agonist of PPARγ	Upregulation of UCP1	172

α-ARs, α-adrenergic receptors; β_3-adrenergic receptors; Aldh1a1, aldehyde dehydrogenase 1A1; AMPK, cAMP-activated protein kinase; BAT, brown adipose tissue; BCO1, β-carotene-15,15′-oxygenase; BCO2, β-carotene-9′,10′-oxygenase; BMP, bone morphogenetic protein; GPRC, G protein–coupled receptors; NE, norepinephrine; omWAT, omental WAT; PPARγ, peroxisome proliferator-activated γ; PKA, protein kinase A; PRDM16, PR/SET domain 16; RAR, retinoic acid receptor; RXR, retinoid X receptor; SIRT1, silent information regulator type 1; TRPM8, transient receptor potential cation channel subfamily M, member 8;TPRV1, transient receptor potential cation channel, subfamily V, member 1; UCP1, uncoupling protein 1; VMH, ventromedial hypothalamus; WAT, white adipose tissue.

and it has been attributed to its caffeine content. In 2000, Dulloo *et al.* (163) showed that the thermogenic potential of green tea extract cannot be explained by the sole presence of caffeine, as also catechins participate in BAT activation. Among these, epigallocatechin 3-gallate is the most abundant in green tea leaves (163,164). The oral administration of encapsulated green tea and Guaraná extracts to humans showed a synergistic role of caffeine and epigallocatechin 3-gallate in acutely activating thermogenesis and energy expenditure (165).

A recent study conducted on mice demonstrated that decaffeinated green tea has also anti-obesity properties, so the presence of caffeine would not be mandatory to achieve thermogenic activation (166). However, in this study, the administration of decaffeinated green tea was combined also with physical exercise; therefore, the observed thermogenic activation could be due to the effect of myokines secreted by muscle rather than to the only decaffeinated green tea.

Depending on the level of oxidation and fermentation, teas contain caffeine and different amounts of polyphenolic molecules, as catechins and theaflavins. While green tea is rich in catechins, black tea has a higher content of theaflavins that were responsible to the AMPK activation in obese mice fed with black tea (167). Phytochemicals of teas exert their anti-obesity effect through the activation of AMPK, which in turn triggers the overexpression of different anti-adipogenic genes, including those promoting the development of a brown-like phenotype in white adipocytes, especially UCP1 and the other uncoupling proteins (168).

L-menthol is an alcoholic cooling chemical present in mint oils (*Mentha* spp.), which is an agonist of the transient receptor potential cation channel subfamily M, member 8 (TRPM8). This is a cold receptor recently found on plasma membrane of both brown and white adipocytes (169,170). Preliminary *in vitro* and *in vivo* studies showed that the stimulation of adipose TRPM8 with L-menthol triggers an overexpression of UCP1 and an increase in mitochondrial biogenesis and electrochemical potential, which results in an increase of thermogenesis and WAT browning (171). The cellular mechanism is NE-independent, as the activation of TRPM8 induces the phosphorylation of PKA via a Ca^{2+} influx (169). L-menthol can bind also to another plasma membrane receptor, the transient receptor potential cation channel subfamily A, member 1, but its role in the thermogenic response is still controversial (171). Hence, L-menthol is a potential candidate for the anti-obesity therapy, but further research is needed.

Ginsenoside Rb1 is a sterol-like-structured molecule extracted from plants belonging to the genus *Panax* that includes several ginseng species. In 3T3-L1 adipocytes, ginsenoside Rb1 induces WAT browning through an increased PPARγ-mediated UCP1 expression (172).

All nutritional browning factors are summarized in Table 3 and Fig. 2b.

Conclusions

The activation of BAT and the recruitment of brite adipocytes in adult humans have gained outstanding interest in obesity research, as nowadays the role of BAT in counteracting the accumulation of excess energy and promoting energy expenditure is well established (173) Indeed, in the last years, the involvement of brown and brite adipocytes in stimulating energy expenditure through the activation of both cold-induced and diet-induced thermogenesis has been confirmed (173–176). Using positron emission tomography, it was demonstrated that in adult humans, the acute cold exposure effectively triggers BAT oxidative metabolism with an increase in total energy expenditure (177). Nevertheless, as highlighted in the present review, also many endogenous and exogenous factors could effectively trigger WAT browning, through the activation of different cellular pathways, producing a significant outcome in BAT activation and brite cell recruitment. However, as reported by Chechi *et al.* (175), it should be considered that BAT activation could activate important metabolic adaptations that counteract the weight loss. Moreover, in mice subjected to chronic cold exposure and adrenergic stimulation, inguinal WAT depot shows a lower increase of oxidative metabolism and energy expenditure than iBAT (178). These features open questions about the significance of the increase in energy expenditure and thermogenesis generated by brite adipocytes or by BAT activation.

Conflict of interest statement

The authors declare that there is no conflict of interest.

Acknowledgements

We are grateful to Prof. Bruno Stefanon who provided feedback on earlier drafts of this manuscript.

References

1. World Health Organization. Obesity and overweight. [WWW document] 2016; URL http://www.who.int/mediacentre/factsheets/fs311/en/.
2. Canale MP, Manca di Villahermosa S, Martino G *et al.* Obesity-related metabolic syndrome: mechanisms of sympathetic overactivity. *Int J Endocrinol* 2013; **2013**: 865965.
3. Kohlgruber A, Lynch L. Adipose tissue inflammation in the pathogenesis of type 2 diabetes. *Curr Diab Rep* 2015; **15**: 92.
4. Khodabandehloo H, Gorgani-Firuzjaee S, Panahi G, Meshkani R. Molecular and cellular mechanisms linking inflammation to insulin resistance and β-cell dysfunction. *Transl Res* 2016; **167**: 228–256.

5. Kotsis V, Stabouli S, Papakatsika S, Rizos Z, Parati G. Mechanisms of obesity-induced hypertension. *Hypertens Res* 2010; **33**: 386–393.
6. Basen-Engquist K, Chang M. Obesity and cancer risk: recent review and evidence. *Curr Oncol Rep* 2011; **13**: 71–76.
7. Astrup A, Lundsgaard C. What do pharmacological approaches to obesity management offer? Linking pharmacological mechanisms of obesity management agents to clinical practice. *Exp Clin Endocrinol Diabetes* 1998; **106**: 29–34.
8. Virtanen KA, Lidell ME, Orava J *et al.* Functional brown adipose tissue in healthy humans. *N Engl J Med* 2009; **360**: 1518–1525.
9. Gifford A, Towse TF, Walker RC, Avison MJ, Welch EB. Characterizing active and inactive brown adipose tissue in adult humans using PET-CT and MR imaging. *Am J Physiol Endocrinol Metab* 2016; **311**: E95–E104.
10. Cannon B, Nedergaard J. Brown adipose tissue: function and physiological significance. *Physiol Rev* 2004; **84**: 277–359.
11. Kajimura S, Seale P, Spiegelman BM. Transcriptional control of brown fat development. *Cell Metab* 2010; **11**: 257–262.
12. Virtanen KA, van Marken Lichtenbelt WD, Nuutila P. Brown adipose tissue functions in humans. *Biochim Biophys Acta* 2013; **1831**: 1004–1008.
13. Bargut TCL, Aguila MB, Mandarim-de-Lacerda CA. Brown adipose tissue: updates in cellular and molecular biology. *Tissue Cell* 2016; **48**: 452–460.
14. Wu J, Boström P, Sparks LM *et al.* Beige adipocytes are a distinct type of thermogenic fat cells in mouse and human. *Cell* 2012; **150**: 366–376.
15. Harms M, Seale P. Brown and beige fat: development, function and therapeutic potential. *Nat Med* 2013; **19**: 1252–1263.
16. Garcia RA, Roemmich JE, Claycombe KJ. Evaluation of markers of beige adipocytes in white adipose tissue of the mouse. *Nutr Metab* 2016; **13**: 24.
17. Long JZ, Svensson KJ, Tsai L *et al.* A smooth muscle-like origin for beige adipocytes. *Cell Metab* 2014; **19**: 810–820.
18. Nedergaard J, Cannon B. The browning of white adipose tissue: some burning issues. *Cell Metab* 2014; **20**: 396–407.
19. Bonet ML, Oliver P, Palou A. Pharmacological and nutritional agents promoting browning of white adipose tissue. *Biochim Biophys Acta* 1831; **2013**: 969–985.
20. Shi SY, Zhang W, Luk CT *et al.* JAK2 promotes brown adipose tissue function and is required for diet- and cold-induced thermogenesis in mice. *Diabetologia* 2016; **59**: 187–196.
21. Boutant M, Joffraud M, Kulkarni SS *et al.* SIRT1 enhances glucose tolerance by potentiating brown adipose tissue function. *Mol Metab* 2015; **4**: 118–131.
22. Wynne K, Stanley S, McGowan B, Bloom S. Appetite control. *J Endocrinol* 2005; **184**: 291–318.
23. Rezai-Zadeh K, Yu S, Jiang Y *et al.* Leptin receptor neurons in the dorsomedial hypothalamus are key regulators of energy expenditure and body weight, but not food intake. *Mol Metab* 2014; **3**: 681–693.
24. Smith SM, Vale WW. The role of hypothalamic–pituitary-adrenal axis in neuroendocrine responses to stress. *Dialogues Clin Neurosci* 2006; **8**: 383–395.
25. Kakuma T, Wang ZW, Pan W, Unger RH, Zhou YT. Role of leptin in peroxisome proliferator-activated receptor gamma coactivator-1 expression. *Endocrinology* 2000; **141**: 4576–4582.
26. Wendel AA, Purushotham A, Liu LF, Belury MA. Conjugated linoleic acid induces uncoupling protein 1 in white adipose tissue of ob/ob mice. *Lipids* 2009; **44**: 975–982.
27. Dodd GT, Decherf S, Loh K *et al.* Leptin and insulin act on POMC neurons to promote the browning of white fat. *Cell* 2015; **160**: 88–104.
28. Rachid TL, Penna-de-Carvalho A, Bringhenti I, Aguila MB, Mandarim-de-Lacerda CA, Souza-Mello V. PPAR-alpha agonists elicit metabolically active brown adipocytes and weight loss in diet-induced obese mice. *Cell Biochem Funct* 2015; **33**: 249–256.
29. Bartolomucci A, La Corte G, Possenti R *et al.* TLQP-21, a VGF-derived peptide, increases energy expenditure and prevents the early phase of diet-induced obesity. *Proc Natl Acad Sci U S A* 2006; **103**: 14584–14589.
30. Cao L, Choi EY, Liu X *et al.* White to brown fat phenotypic switch induced by genetic and environmental activation of a hypothalamic-adipocyte axis. *Cell Metab* 2011; **14**: 324–338.
31. During MJ, Liu X, Huang W *et al.* Adipose VEGF links the white-to-brown switch with environmental, genetic and pharmacological stimuli in male mice. *Endocrinology* 2015; **156**: 2059–2073.
32. Garcia-Martin R, Alexaki VI, Qin N *et al.* Adipocyte-specific hypoxia-inducible factor 2α deficiency exacerbates obesity-induced brown adipose tissue dysfunction and metabolic dysregulation. *Mol Cell Biol* 2016; **36**: 376–393.
33. Boström P, Wu J, Jedrychowski MP *et al.* A PGC-1α-dependent myokine that drives brown-fat-like development of white fat and thermogenesis. *Nature* 2012; **481**: 463–468.
34. Jeremic N, Chaturvedi P, Tyagi SC. Browning of white fat: novel insights into factors, mechanisms and therapeutics. *J Cell Physiol* 2016; **232**: 61–68.
35. Zhang Y, Xie C, Wang H *et al.* Irisin exerts dual effects on browning and adipogenesis of human white adipocytes. *Am J Physiol Endocrinol Metab* 2016; **311**: E530–E541.
36. Kammoun HL, Febbraio MA. Come on BAIBA light my fire. *Cell Metab* 2014; **19**: 1–2.
37. Roberts LD, Boström P, O'Sullivan JF *et al.* β-aminoisobutyric acid induces browning of white fat and hepatic β-oxidation and is inversely correlated with cardiometabolic risk factors. *Cell Metab* 2014; **19**: 96–108.
38. Forest C, Joffin N, Jaubert AM, Noirez P. What induces watts in WAT? *Adipocyte* 2016; **5**: 136–152.
39. Rao RR, Long JZ, White JP *et al.* Meteorin-like is a hormone that regulates immune-adipose interactions to increase beige fat thermogenesis. *Cell* 2014; **157**: 1279–1291.
40. Knudsen JG, Murholm M, Carey AL *et al.* Role of IL-6 in exercise training- and cold-induced UCP1 expression in subcutaneous white adipose tissue. *PLoS One* 2014; **9**: e84910.
41. Solmonson A, Mills EM. Uncoupling proteins and the molecular mechanism of thyroid thermogenesis. *Endocrinology* 2016; **157**: 455–462.
42. Christoffolete MA, Linardi CC, de Jesus L *et al.* Mice with targeted disruption of the Dio2 gene have cold-induced overexpression of the uncoupling protein 1 gene but fail to increase brown adipose tissue lipogenesis and adaptive thermogenesis. *Diabetes* 2004; **53**: 577–584.
43. Lopez M, Varela L, Vazquez MJ *et al.* Hypothalamic AMPK and fatty acid metabolism mediate thyroid regulation of energy balance. *Nat Med* 2010; **16**: 1001–1008.
44. Cereijo R, Villarroya J, Villarroya F. Non-sympathetic control of brown adipose tissue. *Int J Obes (Lond)* 2015; **5/1**(Suppl): S40–S44.
45. Fisher FM, Kleiner S, Douris N *et al.* FGF21 regulates PGC-1α and browning of white adipose tissues in adaptive thermogenesis. *Genes Dev* 2012; **26**: 271–281.
46. Hondares E, Iglesias R, Giralt A *et al.* Thermogenic activation induces FGF21 expression and release in brown adipose tissue. *J Biol Chem* 2011; **286**: 12983–12990.
47. Fisher FM, Chui PC, Antonellis PJ *et al.* Obesity is a fibroblast growth factor 21 (FGF21)-resistant state. *Diabetes* 2010; **59**: 2781–2789.

48. Diaz-Delfin J, Hondares E, Iglesias R, Giralt M, Caelles C, Villarroya F. TNF-α represses β-Klotho expression and impairs FGF21 action in adipose cells: involvement of JNK1 in the FGF21 pathway. *Endocrinology* 2012; **153**: 4238–4245.
49. Seale P. Transcriptional regulatory circuits controlling brown fat development and activation. *Diabetes* 2015; **64**: 2369–2375.
50. Okla M, Ha JH, Temei RE, Chung S. BMP7 drives human adipogenic stem cells into metabolically active beige adipocytes. *Lipids* 2015; **50**: 111–120.
51. Whittle AJ, Carobbio S, Martins L *et al.* BMP8B increases brown adipose tissue thermogenesis through both central and peripheral actions. *Cell* 2014; **149**: 871–885.
52. Martinez de Morentin PB, Gonzalez-Garcia I, Martins L *et al.* Estradiol regulates brown adipose tissue thermogenesis via hypothalamic AMPK. *Cell Metab* 2014; **20**: 41–53.
53. Martins L, Seoane-Collazo P, Contreras C *et al.* A functional link between AMPK and orexin mediates the effect of BMP8B on energy balance. *Cell Rep* 2016; **16**: 2231–2242.
54. Suenaga M, Kurosawa N, Asano H *et al.* BMP4 expressed in preadipocytes is required for the onset of adipocyte differentiation. *Cytokine* 2013; **64**: 138–145.
55. Xue R, Wan Y, Zhang S, Zhang Q, Ye H, Li Y. Role of bone morphogenetic protein 4 in the differentiation of brown fat-like adipocytes. *Am J Physiol Endocrinol Metab* 2014; **306**: E363–E372.
56. Elsen M, Raschke S, Tennagels N *et al.* BMP4 and BMP7 induce the white-to-brown transition of primary human adipose stem cells. *Am J Physiol Cell Physiol* 2014; **306**: C431–C440.
57. Gustafson B, Hammarstedt A, Hedjazifar S *et al.* BMP4 and BMP antagonists regulate human white and beige adipogenesis. *Diabetes* 2015; **64**: 1670–1681.
58. Modica S, Straub LG, Balaz M *et al.* BMP4 promotes a brown to white-like adipocyte switch. *Cell Rep* 2016; **16**: 2243–2258.
59. Coue M, Moro C. Natriuretic peptide control of energy balance and glucose homeostasis. *Biochimie* 2016; **124**: 84–91.
60. Moro C, Lafontan M. Natriuretic peptides and cGMP signaling control of energy homeostasis. *Am J Physiol Heart Circ Physiol* 2013; **304**: H358–H368.
61. Bordicchia M, Liu D, Amri EZ *et al.* Cardiac natriuretic peptides act via p38 MAPK to induce the brown fat thermogenic program in mouse and human adipocytes. *J Clin Invest* 2012; **122**: 1022–1036.
62. Hui X, Gu P, Zhang J *et al.* Adiponectin enhances cold-induced browning of subcutaneous adipose tissue via promoting M2 macrophage proliferation. *Cell Metab* 2015; **22**: 279–290.
63. Boucher J, Masri B, Daviaud D *et al.* Apelin, a newly identified adipokine up-regulated by insulin and obesity. *Endocrinology* 2005; **146**: 1764–1771.
64. Than A, He HL, Chua SH *et al.* Apelin enhances brown adipogenesis and browning of white adipocytes. *J Biol Chem* 2015; **290**: 14679–14691.
65. Drougard A, Fournel A, Marlin A *et al.* Central chronic apelin infusion decreases energy expenditure and thermogenesis in mice. *Sci Rep* 2016; **6**: 31849.
66. Garcia-Alonso V, Titos E, Alcaraz-Quiles J *et al.* Prostaglandin E2 exerts multiple regulatory actions on human obese adipose tissue remodeling, inflammation, adaptive thermogenesis and lipolysis. *PLoS One* 2016; **11**: e0153751.
67. Garcia-Alonso V, Lopez-Vicario C, Titos E *et al.* Coordinate functional regulation between microsomal prostaglandin E synthase-1 (mPGES-1) and peroxisome proliferator-activated receptor γ (PPARγ) in the conversion of white-to-brown adipocytes. *J Biol Chem* 2013; **288**: 28230–28242.
68. Vegiopoulos A, Müller-Decker K, Strzoda D *et al.* Cyclooxygenase-2 controls energy homeostasis in mice by *de novo* recruitment of brown adipocytes. *Science* 2010; **328**: 1158–1161.
69. Pisani DF, Ghandour RA, Beranger GE *et al.* The ω6-fatty acid, arachidonic acid, regulates the conversion of white to brite adipocyte through a prostaglandin/calcium mediated pathway. *Mol Metab* 2014; **3**: 834–847.
70. Osborn O, Sanchez-Alavez M, Dubins JS *et al.* Ccl22/MDC, is a prostaglandin dependent pyrogen, acting in the anterior hypothalamus to induce hyperthermia via activation of brown adipose tissue. *Cytokine* 2011; **53**: 311–319.
71. Ghandour RA, Giroud M, Vegiopoulos A *et al.* IP-receptor and PPARs trigger the conversion of human white to brite adipocyte induced by carbaprostacyclin. *Biochim Biophys Acta* 1861; **2016**: 285–293.
72. Oh CM, Park S, Kim H. Serotonin as a new therapeutic target for diabetes mellitus and obesity. *Diabetes Metab J* 2016; **40**: 89–98.
73. Jeong JH, Lee DK, Blouet C *et al.* Cholinergic neurons in the dorsomedial hypothalamus regulate mouse brown adipose tissue metabolism. *Mol Metab* 2015; **4**: 483–492.
74. McGlashon JM, Gorecki MC, Kozlowski AE *et al.* Central serotoninergic neurons activate and recruit thermogenic brown and beige fat and regulate glucose and lipid homeostasis. *Cell Metab* 2015; **21**: 692–705.
75. Oh CM, Namkung J, Go Y *et al.* Regulation of systemic energy homeostasis by serotonin in adipose tissues. *Nat Commun* 2015; **6**: 6794.
76. Gnad T, Scheibler S, von Kügelgen I *et al.* Adenosine activates brown adipose tissue and recruits beige adipocytes via A2A receptors. *Nature* 2014; **516**: 395–399.
77. Dempersmier J, Sul HS. Shades of brown: a model for thermogenic fat. *Front Endocrinol* 2015; **6**: 71.
78. Sellayah D, Bharaj P, Sikder D. Orexin is required for brown adipose tissue development, differentiation, and function. *Cell Metab* 2011; **14**: 478–490.
79. Sellayah D, Sikder D. Orexin receptor-1 mediates brown fat developmental differentiation. *Adipocyte* 2012; **1**: 58–63.
80. Cipolla-Neto J, Amaral FG, Afeche SC, Tan DX, Reiter RJ. Melatonin, energy metabolism, and obesity: a review. *J Pineal Res* 2014; **56**: 371–381.
81. Saarela S, Reiter RJ. Function of melatonin in thermoregulatory processes. *Life Sci* 1994; **54**: 295–311.
82. Mellado C, Rodriguez V, de Diego JG, Alvarez E, Blazquez E. Effect of pinealectomy and of diabetes on liver insulin and glucagon receptor concentration in the rat. *J Pineal Res* 1989; **6**: 295–306.
83. Nogueira TC, Lellis-Santos C, Jesus DS *et al.* Absence of melatonin induces night-time hepatic insulin resistance and increased gluconeogenesis due to stimulation of nocturnal unfolded protein response. *Endocrinology* 2011; **152**: 1253–1263.
84. Tan DX, Manchester LC, Fuentes-Broto L, Paredes SD, Reiter RJ. Significance and application of melatonin in the regulation of brown adipose tissue metabolism: relation to human obesity. *Obes Rev* 2011; **12**: 167–188.
85. Zanuto R, Siqueira-Filho MA, Caperuto LC *et al.* Melatonin improves insulin sensitivity independently of weight loss in old obese rats. *J Pineal Res* 2013; **55**: 156–165.
86. Peng XR, Gennemark P, O'Mahony G, Bartesaghi S. Unlock the thermogenic potential of adipose tissue: pharmacological modulation and implications for treatment of diabetes and obesity. *Front Endocrinol* 2015; **6**: 174.
87. Mathvink RJ, Tolman JS, Chitty D *et al.* Discovery of a potent, orally bioavailable β_3-adrenergic receptor agonist, (R)-N-[4-[2-[[2-hydroxy-2-(3-pyridinyl)ethyl]amino]ethyl]phenyl]-4-[4-[4-

(trifluoromethyl)phenyl]thiazol-2-yl]benzenesulfonamide. *J Med Chem* 2000; **43**: 3832–3836.
88. van Baak MA, Hul GB, Toubro S *et al.* Acute effect of L-796568, a novel β_3-adrenergic receptor agonist, on energy expenditure in obese men. *Clin Pharmacol Ther* 2002; **71**: 272–279.
89. Larsen TM, Toubro S, van Baak MA *et al.* Effect of a 28-d treatment with L-796568, a novel β_3-adrenergic receptor agonist, on energy expenditure and body composition in obese men. *Am J Clin Nutr* 2002; **76**: 780–788.
90. Cypess AM, Weiner LS, Roberts-Toler C *et al.* Activation of human brown adipose tissue by a β_3-adrenergic receptor agonist. *Cell Metab* 2015; **21**: 33–38.
91. Hainer V. β_3-adrenoreceptor agonist mirabegron – a potential antiobesity drug? *Expert Opin Pharmacother* 2016; **17**: 2125–2127.
92. Arterburn DE, Crane PK, Veenstra DL. The efficacy and safety of sibutramine, an anti-obesity drug with a novel mechanism of action. *Obes Rev* 2004; **1**: 127–139.
93. McNulty SJ, Ur E, Williams G. A randomized trial of sibutramine in the management of obese type 2 diabetic patients treated with metformin. *Diabetes Care* 2003; **26**: 125–131.
94. Li MF, Cheung BMY. Rise and fall of anti-obesity drugs. *World J Diabetes* 2011; **2**: 19–23.
95. da Silva AI, Braz GRF, Pedroza AA *et al.* Fluoxetine induces lean phenotype in rat by increasing the brown/white adipose tissue ration and UCP1 expression. *J Bioenerg Biomembr* 2015; **47**: 309–318.
96. Connolly HM, Cray JL, McGoon MD *et al.* Valvular heart disease associated with fenfluramine-phentermine. *N Engl J Med* 1997; **337**: 581–588.
97. Weintraub M, Hasday JD, Mushlin AI, Lockwood DH. A double-blind clinical trial in weight control. Use of fenfluramine and phentermine alone and in combination. *Arch Intern Med* 1984; **144**: 1143–1148.
98. Hesselbarth N, Pettinelli C, Gericke M *et al.* Tamoxifen affects glucose and lipid metabolism parameters, causes browning of subcutaneous adipose tissue and transient body composition changes in C57BL/6NTac mice. *Biochem Biophys Res Commun* 2015; **464**: 724–729.
99. Petrovic N, Shabalina IG, Timmons JA, Cannon B, Nedergaard J. Thermogenically competent noradrenergic recruitment in brown preadipocytes by a PPARγ agonist. *Am J Physiol Endocrinol Metab* 2008; **295**: E287–E296.
100. Ohno H, Shinoda K, Spiegelman BM, Kajimura S. PPARγ agonists induce a white-to-brown fat conversion through stabilization of PRDM16 protein. *Cell Metab* 2012; **15**: 395–404.
101. Festuccia WT, Oztezcan S, Laplante M *et al.* Peroxisome proliferator-activated receptor-gamma-mediated positive energy balance in the rat is associated with reduced sympathetic drive to adipose tissue and thyroid status. *Endocrinology* 2008; **149**: 2121–2130.
102. Festuccia WT, Blanchard PG, Turcotte V *et al.* The PPARγ agonist rosiglitazone enhances rat brown adipose tissue lipogenesis from glucose without altering glucose uptake. *Am J Physiol Regul Integr Comp Physiol* 2009; **296**: R1327–R1335.
103. Bogacka I, Ukropcova B, McNeil M, Gimble JM, Smith SR. Structural and functional consequences of mitochondrial biogenesis in human adipocytes *in vitro*. *J Clin Endocrinol Metab* 2005; **90**: 6650–6656.
104. Colitti M, Grasso S. Nutraceuticals and regulation of adipocyte life: premises or promises. *Biofactors* 2014; **40**: 398–418.
105. Colitti M, Stefanon B. Different anti-adipogenic effects of biocompounds on primary visceral pre-adipocytes and adipocytes. *EXCLI J* 2016; **15**: 362–377.
106. Baskaran P, Krishnan V, Ren J, Thyagarajan B. Capsaicin induces browning of white adipose tissue and counters obesity by activating TRPV1 channel-dependent mechanisms. *Br J Pharmacol* 2016; **173**: 2369–2389.
107. Zhang LL, Yan Liu D, Ma LQ *et al.* Activation of transient receptor potential vanilloid type-1 channel prevents adipogenesis and obesity. *Circ Res* 2007; **100**: 1063–1070.
108. Kobata K, Yazawa S, Iwai K, Watanabe T. Novel capsaicinoid-like substances, capsiate and dihydrocapsiate, from the fruits of a nonpungent cultivar, CH-19 Sweet, of pepper (*Capsicum annuum* L.). *J Agric Food Chem* 1998; **46**: 1695–1697.
109. Kobata K, Sutoh K, Todo T, Yazawa S, Iwai K, Watanabe T. Nordihydrocapsiate, a new capsinoid from the fruits of a nonpungent pepper, *Capsicum annuum*. *J Nat Prod* 1999; **62**: 335–336.
110. Shirai Y, Ueno S, Nakayama A *et al.* Studies of the toxicological potential of capsinoids, XII: pharmacokinetic study of capsinoid-containing CH-19 Sweet extract in rats. *Int J Toxicol* 2010; **29**: 15S–21S.
111. Ohyama K, Nogusa Y, Shinoda K, Suzuki K, Bannai M, Kajimura S. A synergistic anti-obesity effect by a combination of capsinoids and cold temperature through promoting beige adipocyte biogenesis. *Diabetes* 2016; **65**: 1410–1423.
112. Sasahara I, Furuhata Y, Iwasaki Y *et al.* Assessment of the biological similarity of three capsaicin analogs (capsinoids) found in non-pungent chili pepper (CH-19 Sweet) fruits. *Biosci Biotechnol Biochem* 2010; **74**: 274–278.
113. Allison DB, Cutter G, Poehlman ET, Moore DR, Barnes S. Exactly which synephrine alkaloids does *Citrus aurantium* (bitter orange) contain? *Int J Obes Relat Metab Disord* 2005; **29**: 443–446.
114. Stohs SJ, Preuss HJ, Shara M. The safety of *Citrus aurantium* (bitter orange) and its primary protoalkaloid *p*-synephrine. *Phytother Res* 2011; **25**: 1421–1428.
115. de Oliveira AL, Comar JF, de Sa-Nakanishi AB, Peralta RM, Bracht A. The action of *p*-synephrine on hepatic carbohydrate metabolism and respiration occurs via both Ca^{2+}-mobilization and cAMP production. *Mol Cell Biochem* 2014; **388**: 135–147.
116. Peixoto JS, Comar JF, Moreira CT *et al.* Effects of *Citrus aurantium* (bitter orange) fruit extract and *p*-synephrine on metabolic fluxes in the rat liver. *Molecules* 2012; **17**: 5854–5869.
117. Haaz S, Fontaine KR, Cutter G, Limdi N, Perumean-Chaney S, Allison DB. *Citrus aurantium* and synephrine alkaloids in the treatment of overweight and obesity: an update. *Obes Rev* 2006; **7**: 79–88.
118. Carpéné C, Galitzky J, Fontana E, Atgié C, Lafontan M, Berlan M. Selective activation of β_3-adrenoreceptors by octopamine: comparative studies in mammalian fat cells. *Naunyn Schmiedebergs Arch Pharmacol* 1999; **359**: 310–321.
119. Mercader J, Wanecq E, Chen J, Carpéné C. Isopropylnorepinephrine is a stronger lipolytic agent in human adipocytes than synephrine and other amines present in *Citrus aurantium*. *J Physiol Biochem* 2011; **67**: 443–452.
120. Kim SM, Jung YJ, Kwon ON *et al.* A potential commercial source of fucoxanthin extracted from the microalga *Phaeodactylum tricornutum*. *Appl Biochem Biotechnol* 2012; **166**: 1843–1855.
121. Maeda H, Hosokawa M, Sashima T, Funayama K, Miyashita K. Fucoxanthin from edible seaweed, *Undaria pinnatifida*, shows antiobesity effect through UCP1 expression in white adipose tissues. *Biochem Biophys Res Commun* 2005; **332**: 392–397.
122. Woo MN, Jeon SM, Shin YC, Lee MK, Kang MA, Choi MS. Anti-obese property of fucoxanthin is partly mediated by altering lipid-regulating enzymes and uncoupling proteins of visceral adipose tissue in mice. *Mol Nutr Food Res* 2009; **53**: 1603–1611.
123. Maeda H, Hosokawa M, Sashima T, Funayama K, Miyashita K. Effect of medium-chain triacylglycerols on anti-obesity effect of fucoxanthin. *J Oleo Sci* 2007a; **56**: 615–621.

124. Hu X, Li Y, Li C *et al.* Combination of fucoxanthin and conjugated linoleic acid attenuates body weight gain and improves lipid metabolism in high-fat diet-induced obese rats. *Arch Biochem Biophys* 2012; **519**: 59–65.
125. Tsukui T, Konno K, Hosokawa M, Maeda H, Sashima T, Miyashita K. Fucoxanthin and fucoxanthinol enhance the amount of docosahexaenoic acid in the liver of KKA^{y} obese/diabetic mice. *J Agric Food Chem* 2007; **55**: 5025–5029.
126. Maeda H, Hosokawa M, Sashima T, Miyashita K. Dietary combination of fucoxanthin and fish oil attenuates the weight gain of white adipose tissue and decreases blood glucose in obese/diabetic KK-A^{y} mice. *J Agric Food Chem* 2007b; **55**: 7701–7706.
127. Abidov M, Ramazanov Z, Seifulla R, Grachev S. The effects of Xanthigen in the weight management of obese premenopausal women with non-alcoholic fatty liver disease and normal liver fat. *Diabetes Obes Metab* 2010; **12**: 72–81.
128. Kim KM, Kim SM, Cho DY, Park SJ, Joo NS. The effect of Xanthigen on the expression of brown adipose tissue assessed by ^{18}F-FDG PET. *Yonsei Med J* 2016; **57**: 1038–1041.
129. Hashimoto T, Ozaki Y, Taminato M *et al.* The distribution and accumulation of fucoxanthin and its metabolites after oral administration in mice. *Br J Nutr* 2009; **102**: 242–248.
130. Sangeetha RK, Bhaskar N, Divakar S, Baskaran V. Bioavailability and metabolism of fucoxanthin in rats: structural characterization of metabolites by LC–MS (APCI). *Mol Cell Biochem* 2012; **333**: 299–310.
131. Woo MN, Jeon SM, Kim HJ *et al.* Fucoxanthin supplementation improves plasma and hepatic lipid metabolism and blood glucose concentration in high-fat fed C57BL/6 N mice. *Chem Biol Interact* 2010; **186**: 316–322.
132. Kang SI, Shin HS, Kim HM *et al. Petalonia binghamiae* extract and its constituent fucoxanthin ameliorate high-fat diet-induced obesity by activating AMP-activated protein kinase. *J Agric Food Chem* 2012; **60**: 3389–3395.
133. Gerhard GS, Styer AM, Strodel WE *et al.* Gene expression profiling in subcutaneous, visceral and epigastric adipose tissues of patients with extreme obesity. *Int J Obes (Lond)* 2014; **38**: 371–378.
134. Bonet ML, Canas JA, Ribot J, Palou A. Carotenoids and their conversion products in the control of adipocyte function, adiposity and obesity. *Arch Biochem Biophys* 2015; **572**: 112–125.
135. Al Tanoury Z, Piskunov A, Rochette-Egly C. Vitamin A and retinoid signaling: genomic and nongenomic effects. *J Lipid Res* 2013; **54**: 1761–1775.
136. Serra F, Bonet ML, Puigserver P, Oliver J, Palou A. Stimulation of uncoupling protein 1 expression in brown adipocytes by naturally occurring carotenoids. *Int J Obes Relat Metab Disord* 1999; **23**: 650–655.
137. Guo H, Foncea R, O'Byrne SM *et al.* Lipocalin 2, a regulator of retinoid homeostasis and retinoid-mediated thermogenic activation in adipose tissue. *J Biol Chem* 2016; **291**: 11216–11229.
138. Murholm M, Isidor MS, Basse AL *et al.* Retinoic acid has different effects on UCP1 expression in mouse and human adipocytes. *BMC Cell Biol* 2013; **14**: 41.
139. Simopoulos AP. An increase in the Omega-6/Omega-3 fatty acid ratio increases the risk for obesity. *Nutrients* 2016; **8**: 128.
140. Calder PC. Mechanism of action of (n-3) fatty acids. *J Nutr* 2012; **142**: 592S–599S.
141. Bargut TCL, Silva-e-Silva ACAG, Souza-Mello V, Mandarim-de-Lacerda CA, Aguila MB. Mice fed fish oil diet and upregulation of brown adipose tissue thermogenic markers. *Eur J Nutr* 2015; **55**: 159–169.
142. Fleckenstein-Elsen M, Dinnies D, Jelenik T, Roden M, Romacho T, Eckel J. Eicosapentaenoic acid and arachidonic acid differentially regulate adipogenesis, acquisition of a brite phenotype and mitochondrial function in primary human adipocytes. *Mol Nutr Food Res* 2016; **60**: 2065–2075.
143. Shen W, McIntosh MK. Nutrient regulation: conjugated linoleic acid's inflammatory and browning properties in adipose tissue. *Annu Rev Nutr* 2016; **36**: 183–210.
144. Madsen L, Guerre-Millo M, Flindt EN *et al.* Tetradecylthioacetic acid prevents high fat diet induced adiposity and insulin resistance. *J Lipid Res* 2002; **43**: 742–750.
145. Larsen LN, Granlund L, Holmeide AK, Skattebøl L, Nebb HI, Bremer J. Sulfur-substituted and α-methylated fatty acids as peroxisome proliferator-activated receptor activators. *Lipids* 2005; **40**: 49–57.
146. Vögler O, Lopez-Bellan A, Alemany R *et al.* Structure-effect relation of C18 long-chain fatty acids in the reduction of body weight in rats. *Int J Obes (Lond)* 2008; **32**: 464–473.
147. Haque MR, Ansari SH, Najmi AK, Ahmad MA. Monoterpene phenolic compound thymol prevents high fat diet induced obesity in murine model. *Toxicol Mech Methods* 2014; **24**: 116–123.
148. Choi JH, Kim SW, Yu R, Yun JW. Monoterpene phenolic compound thymol promotes browning of 3 T3-L1 adipocytes. *Eur J Nutr* 2016. DOI: 10.1007/s00394-016-1273-2.
149. Cho S, Choi Y, Park S, Park T. Carvacrol prevents diet-induced obesity by modulating gene expression involved in adipogenesis and inflammation in mice fed with high-fat diet. *J Nutr Biochem* 2012; **23**: 192–201.
150. Szkudelska K, Szkudelski T. Resveratrol, obesity and diabetes. *Eur J Pharmacol* 2010; **635**: 1–8.
151. Lam YY, Peterson CM, Ravussin E. Resveratrol vs. calorie restriction: data from rodents to humans. *Exp Gerontol* 2013; **48**: 1018–1024.
152. Um JH, Park SJ, Kang H *et al.* AMP-activated protein kinase-deficient mice are resistant to the metabolic effects of resveratrol. *Diabetes* 2010; **59**: 554–563.
153. Wang S, Liang X, Yang Q *et al.* Resveratrol induces brown-like adipocyte formation in white fat through activation of AMP-activated protein kinase (AMPK) α1. *Int J Obes (Lond)* 2015a; **39**: 967–976.
154. Stark AH, Mader Z. Olive oil as a functional food: epidemiology and nutritional approaches. *Nutr Rev* 2002; **60**: 170–176.
155. Visioli F, Galli C. Biological properties of olive oil phytochemicals. *Crit Rev Food Sci Nutr* 2002; **42**: 209–221.
156. Stefanon B, Colitti M. Original research: hydroxytyrosol, an ingredient of olive oil, reduces triglyceride accumulation and promotes lipolysis in human primary visceral adipocytes during differentiation. *Exp Biol Med* 2016; **241**: 1796–1802.
157. Oi-Kano Y, Kawada T, Watanabe T *et al.* Oleuropein, a phenolic compound in extra virgin olive oil, increases uncoupling protein 1 content in brown adipose tissue and enhances noradrenaline and adrenaline secretions in rats. *J Nutr Sci Vitaminol* 2008; **54**: 363–370.
158. Jurenka JS. Anti-inflammatory properties of curcumin, a major constituent of *Curcuma longa*: a review of preclinical and clinical research. *Altern Med Rev* 2009; **14**: 141–153.
159. Hishikawa N, Takahashi Y, Amakusa Y *et al.* Effects of tumeric on Alzheimer's disease with behavioral and psychological symptoms of dementia. *Ayu* 2012; **33**: 499–504.
160. Chen QY, Zheng Y, Jiao DM *et al.* Curcumin inhibits lung cancer cell migration and invasion through Rac1-dependent signaling pathway. *J Nutr Biochem* 2014; **25**: 177–185.
161. Lone J, Choi JH, Kim SW, Yun JW. Curcumin induces brown fat-like phenotype in 3T3-L1 and primary white adipocytes. *J Nutr Biochem* 2016; **27**: 193–202.

162. Wang S, Wang X, Ye Z *et al.* Curcumin promotes browning of white adipose tissue in a norepinephrine-dependent way. *Biochem Biophys Res Commun* 2015b; **466**: 247–253.
163. Dulloo A, Seydoux J, Girardier L, Chantre P, Vandermander J. Green tea and thermogenesis: interactions between catechin-polyphenols, caffeine and sympathetic activity. *Int J Obes Relat Metab Disord* 2000; **24**: 252–258.
164. Rains TM, Agarwal S, Maki KC. Antiobesity effects of green tea catechins: a mechanistic review. *J Nutr Biochem* 2011; **22**: 1–7.
165. Bérubé-Parent S, Pelletier C, Doré J, Tremblay A. Effects of encapsulated green tea and Guarana extracts containing a mixture of epigallocatechin-3-gallate and caffeine on 24 h energy expenditure and fat oxidation in men. *Br J Nutr* 2005; **94**: 432–436.
166. Sae-Tan S, Rogers CJ, Lambert JD. Decaffeinated green tea and voluntary exercise induce gene changes related to beige adipocyte formation in high fat-fed obese mice. *J Funct Foods* 2015; **14**: 210–214.
167. Yamashita Y, Wang L, Wang L, Tanaka Y, Zhang T, Ashida H. Oolong, black and pu-erh tea suppresses adiposity in mice *via* activation of AMP-activated protein kinase. *Food Funct* 2014; **5**: 2420–2429.
168. Murase T, Misawa K, Haramizu S, Hase T. Catechin-induced activation of the LKB1/AMP-activated protein kinase pathway. *Biochem Pharmacol* 2009; **78**: 78–84.
169. Ma S, Yu H, Zhao Z *et al.* Activation of the cold-sensing TRPM8 channel triggers UCP1-dependent thermogenesis and prevents obesity. *J Mol Cell Biol* 2012; **4**: 88–96.
170. Rossato M, Granzotto M, Macchi V *et al.* Human white adipocytes express the cold receptor TRPM8 which activation induces UCP1 expression, mitochondrial activation and heat production. *Mol Cell Endocrinol* 2014; **382**: 137–146.
171. Sakellariou P, Valente A, Carillo AE *et al.* Chronic L-menthol-induced browning of white adipose tissue hypothesis: a putative therapeutic regime for combating obesity and improving metabolic health. *Med Hypotheses* 2016; **93**: 21–26.
172. Mu Q, Fang X, Li X *et al.* Ginsenoside Rb1 promotes browning through regulation of PPARγ in 3 T3-L1 adipocytes. *Biochem Biophys Res Commun* 2015; **466**: 530–535.
173. Saito M, Yoneshiro T, Matsushita M. Activation of brown adipose tissue by cold exposure and food ingredients in humans. *Best Pract Res Clin Endocrinol Metab* 2016; **30**: 537–547.
174. van der Lans AA, Wierts R, Vosselman MJ, Schrauwen P, Brans B, van Marken Lichtenbelt WD. Cold-activated brown adipose tissue in human adults: methodological issues. *Am J Physiol Regul Integr Comp Physiol* 2014; **307**: R103–R113.
175. Chechi K, Nedergaard J, Richard D. Brown adipose tissue as an anti-obesity tissue in humans. *Obes Rev* 2014; **15**: 92–106.
176. Hanssen MJ, van der Lans AA, Brans B *et al.* Short-term cold acclimation recruits brown adipose tissue in obese humans. *Diabetes* 2016; **65**: 1179–1189.
177. Ouellet V, Labbé SM, Blondin DP *et al.* Brown adipose tissue oxidative metabolism contributes to energy expenditure during acute cold exposure in humans. *J Clin Invest* 2012; **122**: 545–552.
178. Labbé SM, Caron A, Chechi K, Laplante M, Lecomte R, Richard D. Metabolic activity of brown, "beige" and white adipose tissues in response to chronic adrenergic stimulation in male mice. *Am J Physiol Endocrinol Metab* 2016; **311**: E260–E268.

Histochemistry and Cell Biology (2018) 149:593–605
https://doi.org/10.1007/s00418-018-1663-z

ORIGINAL PAPER

Simpson–Golabi–Behmel syndrome human adipocytes reveal a changing phenotype throughout differentiation

T. Montanari[1] · M. Colitti[1]

Accepted: 20 March 2018 / Published online: 24 March 2018

Abstract

The Simpson–Golabi–Behmel syndrome (SGBS) cell strain is widely considered to be a representative in vitro model of human subcutaneous white pre-adipocytes. These cells achieve a transient expression of classical brown markers, such as uncoupling protein 1, peaking at day 14 of differentiation and decreasing thereafter. Adipocyte browning process involves dynamic changes in lipid droplet (LD) dimension, in mitochondria morphology, and in the expression of brown-specific marker genes. This study analyzes SGBS transient phenotypic transformation by quantifying the heterogeneity of LDs, mitochondrial dynamics, and a panel of genes involved in adipocyte differentiation and browning. LDs at 21 days of differentiation were larger than in the previous stages, without any change in the number per cell. The expression of genes such as peroxisome peroxisome proliferator-activated receptor γ, leptin, and lipase E significantly raised from 0 to 21 days. Adiponectin was significantly upregulated at 14 days of differentiation. Brown-specific marker PR domain containing 16 was highly expressed at D0. The variability of mitochondrial shape and interconnectivity reflects differences in the relative rates of fusion and fission, resulting in a significant shift from a networked shape at D7 to a fragmented and swollen one at D14 and D21. The transient phenotype experienced by this cellular model should be considered whether used in studies involving the stimulation of adipocyte browning and could be an interesting human model to further elucidate the browning process in the absence of any stimulation.

Keywords SGBS adipocytes · UCP1 expression · Lipid droplets · Mito-Morphology

Introduction

The Simpson–Golabi–Behmel Syndrome (SGBS) cell strain is widely considered to be a representative in vitro model of human white pre-adipocytes. These cells were first described in 2001 and have been originally isolated from the subcutaneous adipose tissue of an infant with Simpson–Golabi–Behmel syndrome (Wabitsch et al. 2001). This syndrome is X-linked and characterized by pre- and postnatal overgrowth (gigantism), developmental delay, macrocephaly, abnormal facial appearance with prominent eyes, polydactyly, and many other malformations (DeBaun et al. 2001). The syndrome arises from either deletions or point mutations within the glypican-3 (*GPC3*) gene at Xq26. Sometimes, these rearrangements also include the glypican-4 gene (*GPC4*). Glypicans are heparan sulfate proteoglycans which have a role in the control of cell growth and cell division (Tenorio et al. 2014).

SGBS cells are neither immortalized nor transformed and retain their ability to differentiate into adipocytes for more than 50 generations, so they can be considered an appropriate model for the study of various aspects of white adipocyte differentiation in humans (Chen et al. 2016).

However, these cells were recently shown to present a changeful phenotype (Guennon et al. 2015). In fact, SGBS adipocyte achieves a transient expression of classical brown markers, such as uncoupling protein 1 (*UCP1*), at day 14 that decrease after day 28 of differentiation, when a progression to a white adipocyte phenotype appeared (Guennoun et al. 2015). SGBS cells have also been demonstrated to display a greater induction of adipogenic gene expression during differentiation, although metabolically distinct from subcutaneous white adipocytes (Yeo et al. 2017). The genes involved in adipocyte differentiation such as peroxisome

✉ M. Colitti
monica.colitti@uniud.it

[1] Department of Agricultural, Food, Environmental and Animal Sciences, University of Udine, via delle Scienze, 206, 33100 Udine, Italy

proliferator-activated receptor γ (*PPARG*), CCAAT/enhancer binding protein α (*CEBPA*), adiponectin (*ADIPOQ*), and leptin (*LEP*) were 10–15 folds higher in SGBS in comparison with primary human white subcutaneous adipocytes (Yeo et al. 2017).

During the differentiation process, SGBS cells increase the synthesis of triglycerides which accumulated in lipid droplets (LDs) in the cytoplasm. On the other hand, extracellular signals, such as β_3-adrenergic stimulation, can promote the release of lipid species packed within neutral LDs, as demonstrated in 3T3-L1 cells (Barneda et al. 2013). A dynamic change in proteins associated with LDs and in LD dimension has been demonstrated after the stimulation of adipocyte browning, which induced the formation of microLDs in response to lipolytic release of fatty acids (Barneda et al. 2013). Thus, considering the changeful phenotype of SGBS cells, the investigation of features involving lipid metabolism may require the assessment of cellular neutral lipid content. Mitochondria, primarily involved in energy expenditure in brown adipose tissue, showed as well a dynamic morphological change (Gao and Houtkooper 2014). Cold exposure and adrenergic stimulation have been demonstrated to induce rapid mitochondrial fragmentation before heat production (Wikstrom et al. 2014).

The goal of the present study is to gather features of the transient phenotypic transformation experienced by SGBS cells during differentiation by quantifying the heterogeneity of LDs, mitochondrial morphology, and a panel of genes involved in adipocytes differentiation and browning. This study stresses some characteristics of these cells, since a deeper understanding of this transient phenotype could be useful to further elucidate the browning process in the absence of any stimulation.

Materials and methods

Chemicals and culture media

Dulbecco's modified Eagle medium (DMEM)/F-12 medium (1:1) enriched with L-glutamine and 15 mM 4-(2-hydroxyethyl)-1-piperazineethanesulfonic acid (HEPES), fetal bovine serum (FBS) and penicillin streptomycin solution were purchased from Gibco by Life Technologies (Thermo Fisher Scientific Inc., Waltham, Massachusetts). Dipyrromethene boron difluoride (BODIPY) 493/503 and MitoTracker Orange (CMTMRos) fluorescent dyes, TRIzol reagent, PureLink™ RNA Mini Kit and SuperScript™ III one-step RT-PCR system with Platinum™ *Taq* DNA polymerase were purchased from Invitrogen (Thermo Fisher Scientific Inc., Waltham, Massachusetts). Rosiglitazone was purchased from Cayman Chemical (Ann Arbor, Michigan). 4′,6-diamidin-2-phenylindole (DAPI)-containing mounting medium was purchased from Abcam (Cambridge, Massachusetts). Normal goat (NG) serum was purchased from Vector Laboratories (Burlingame, California). GelRed 10,000X was purchased from Biotinum (Hayward, California).

All other chemicals used in the experiment and not listed above were purchased from Sigma-Aldrich (Darmstadt, Germany).

Cell culture

Human SGBS cells were kindly provided by prof. M. Wabitsch (University of Ulm, Germany). Cells were grown in DMEM/F-12 supplemented with 10% FBS, 3.3 mM biotin, 1.7 mM panthotenat, and 1% penicillin/streptomycin solution, at 37 °C with 5% CO_2 and 95% relative humidity. Differentiation was induced on confluent cells with serum-free growth medium supplemented with 10 µg/ml transferrin, 0.2 nM triiodothyronine (T_3), 250 nM hydroxycortisone, 20 nM human insulin, 25 nM dexamethasone, 250 µM 3-isobutyl-1-methylxanthine (IBMX), and 2 µM rosiglitazone (day 0 of differentiation). After 4 days, the differentiation medium was replaced with a maintenance medium composed by serum-free growth medium supplemented with 10 µg/ml transferrin, 0.2 nM T_3, 250 nM hydroxycortisone, and 20 nM human insulin. Fresh maintenance medium was added every 4 days.

Cells were analyzed before differentiation at day 0 (D0) and during differentiation at day 7 (D7), at day 14 (D14), and at day 21 (D21).

Cytomorphology

MitoTracker and BODIPY staining

Prior to cell fixation for immunofluorescence protocols, some ibiTreat 8-well µ-Slides (ibidi GmbH, Planegg/Martinsried, Germany) were stained with 100 nM MitoTracker Orange in growth medium to detect mitochondria. To proceed, culture medium was removed and replaced with MitoTracker solution 100 nM in growth medium. Incubation was carried out at 37 °C and 5% CO_2 for 30 min.

After cell fixation in a 2% formalin solution diluted in phosphate saline buffer (PBS) 1× at room temperature (RT) for 15 min, the slides were washed three times in PBS 1× and then incubated in a solution of BODIPY493/503 in PBS 1× to fluorescently label lipid droplets. The incubation was carried at RT in dark for 45 min. After the incubation, the slides were washed in PBS 1× three times and then mounted with mounting medium with DAPI. Images were acquired with the fluorescence microscope Axio Observer Z1 equipped with D-PLAN Neofluar objective lenses with N.A. 0.75 and Infinity Color Corrected System

(ICS) and with AxioCam and Zen blue software (Carl Zeiss, Jena, Germany). The filters used for MitoTracker were 550/605 nm, for BODIPY were 470/525 nm, and 390/460 nm for DAPI.

Morphology of LDs

MRI_Lipid Droplets tool (http://dev.mri.cnrs.fr/projects/imagej-macros/wiki/Lipid_Droplets_Tool), a macro of ImageJ1.50b software (http://rsb.info.nih.gov/ij/), was used to measure LD area (Bäcker 2012). The scale was settled for magnification and the global checkbox on the set scale dialog was chosen. The option-dialog 's' by right-clicking on the s-button was used to settle the objects size; then, the measurements were checked by the ROI manager. Total area occupied by LDs in each field at different days of differentiation was calculated by summing up the area of each LD. The count of cells in each field was used to calculate the area and the number of LDs per cell. The average area of a single LD was calculated by dividing the area of LDs/cells by the number of LDs/cell. The area (μm^2) and number of LDs were measured and counted on 15 fields for each day of differentiation.

Mitochondrial morphology analysis

Mito-Morphology is a useful macro that calculates different parameters to quantify and compare mitochondrial morphology (http://imagejdocu.tudor.lu/doku.php?id=plugin:morphology:mitochondrial_morphology_macro_plug-in:start) (Dagda et al. 2009), even if it has some limitations, since it is strictly for two dimensional analysis and the measurements are based on elliptical approximation (Valente et al. 2017). Mito-Morphology was used to measure mitochondrial morphology from the fluorescence micrographs of D0, D7, D14, and D21 cells stained with MitoTracker (10 fields for each). The scale was settled for magnification and the global checkbox on the set scale dialog was chosen. The images were extracted to grayscale and inverted to show mitochondria-specific fluorescence as black pixels. Then, contrast-limited adaptive histogram equalization (CLAHE) was used to adjust pixel intensities and the images were thresholded to optimally resolve individual mitochondria. The following measurements were considered: mitochondrial content, calculated as percentage of cytosol occupied by mitochondria; the area/perimeter ratio, as an index of mitochondrial interconnectivity and area/perimeter normalized to minor axis employed as a measure of mitochondrial swelling. Morphological phenotypes (shapes) comprised networks, rod-like, puncta and large and round in agreement with Leonard et al. (2015).

Immunofluorescence analysis of cultured SGBS cells

Medium was removed from cells grown on ibiTreat 8-well µ-Slides (Giemme Snc, Milan, Italy) and washed with pre-heated PBS 1× pH 7.4. Then, cells were fixed with 2% formalin solution at RT for 15 min. Formalin solution was removed and cells were washed twice with PBS 1× and then with PBS 1× containing 0.05% Tween 20 (PBST) at pH 7.4. Permeabilization of plasma membrane was achieved by incubating cells in a Triton X-100 0.1% solution in PBS 1× for 10 min at RT. Fixative-induced autofluorescence was quenched with 0.3 M glycine solution in PBS 1×. Background labeling was prevented by incubating cells in blocking solution containing 10% FBS and 5% NG serum in PBST 1× for 1 h at RT. The slides were then incubated overnight at 4 °C in a moist chamber with the primary antibody diluted in blocking solution.

The polyclonal anti-peroxisome proliferator-activated receptor γ (PPARγ) antibody (PAA886Bo01, Cloud-Clone Corp., Wuhan Korea) was reactive against the epitope corresponding to amino acids 311–500 of bovine sequence at C-terminal of protein, where it recognizes both protein isoforms. To find out if the antibody could be useful also in human, bovine, and human amino acids, homology sequences were checked, showing 100% identities between those amino acids.

The anti-perlipin 1 (PLIN1) was a rabbit polyclonal antibody (sc-67,164, Santa Cruz Biotechnology Inc. Heidelberg, Germany) raised against amino acids 1-300 mapping at the N-terminus of perilipin of human origin.

The anti-uncoupling protein 1 (UCP1) polyclonal antibody (ab10983, Abcam, Cambridge, Massachusetts) raised against a peptide mapping to amino acids 145–159 of human UCP1 protein. The following day, after three washes in PBST 1×, cells were treated with goat anti-rabbit IgG (H + L) Alexa Fluor® 555 labeled antibody (ab150078, 1:1000 Abcam, Massachusetts) in blocking solution at RT for 45′ in the dark. Cells were then washed three times in PBST 1× and mounted with DAPI-containing mounting medium. The filters were 550/605 nm for Alexa Fluor® 555 antibody conjugate and 390/460 nm for DAPI.

RNA extraction and RT-PCR

After culture medium removal from Petri dishes (3 technical replicates for 4 different cell days of differentiation), 1 ml/10 cm^2 of TRIzol reagent was added in each plate and repeatedly pipetted to induce a severe breakdown of cell structures. These samples were immediately proceeded with the PureLink™ RNA Mini Kit following the manufacturer's instructions.

The concentration of the extracted total RNA was quantified using a spectrophotometer (NanoDrop 1000

Spectrophotometer, ThermoScientific, Wilmington, Delaware) and the purity of RNA samples ranged between 1.8 and 1.9. RNA integrity was evaluated through the observation of 18S and 28S ribosomal bands after electrophoresis on 1% agarose gel, in the presence of GelRed. β-actin expression was used as internal control, confirming thorough integrity of the RNA. RT-PCR reactions were performed using the one-step RT-PCR kit. A Primer3 Input software (Rozen and Skaletsky 2000) was used to design primers. GenBank accession, primer sequences, product lengths and relative annealing temperatures for each gene are listed in Table 1, according to the HUGO Gene Nomenclature Committee.

Total RNA (500 ng) from each sample was reverse-transcribed and amplified using an MJ thermal cycler (PT-100; MJ Research, Inc., Waltham, MA, USA). RT-PCR cycle conditions were as follows: cDNA synthesis: 50 °C, 30 min; SuperScript III RT inactivation: 94 °C, 2 min; cDNA amplification: [94 °C (30 s), primers annealing at different temperatures according to Table 1 (30 s), 72 °C (30 s) 40 cycles]; ending of reaction: 72 °C (5 min). PCR reactions carried out without reverse transcription of the RNA samples, using the same sets of primers, did not give any amplification product, ruling out the possibility that the observed bands may be due to the presence of contaminant genomic DNA.

Transcription data analysis

Agarose bands were quantified using NIH image analysis software (ImageJ version 1.50e, National Institutes of Health, Bethesda, Maryland). Gel analysis method is outlined in the ImageJ documentation (http://rsb.info.nih.gov/ij/docs/menus/analyze.html#gels). The results 'Area' and 'Percent' returned by ImageJ were expressed as density values, based only on the peaks highlighted on the gel. The relative density values were calculated for each loading band, dividing the percent value for each lane of gene of interest by the percent value of the control gene (*ACTB*) (http://lukemiller.org/index.php/2010/11/analyzing-gels-and-western-blots-with-image-j/).

Statistical analysis

The measurements of area of LDs/cell, number of LDs/cell, and the area of a single LD and all the parameters obtained by Mito-Morphology macro were analyzed between days of differentiation using boxplots generated by SPSS version 20.0 software. The results were compared through Kruskal–Wallis statistical test followed by pairwise comparisons using the Dunn–Bonferroni approach.

All the relative densities recorded (12 biological replicates per developmental stage, for each gene) and the percentage of PPARγ nuclear positivity were submitted to the

Table 1 Oligonucleotide primer sequences for RT-PCR (*ACTB* actin beta; *PPARG1* peroxisome proliferator-activated receptor gamma, variant 1; *PPARG2*, peroxisome proliferator-activated receptor gamma, variant 2; *PPARA*, peroxisome proliferator-activated receptor alpha; *PRDM16*, PR domain containing 16; *PPARGC1A*, PPARG coactivator 1 alpha; *UCP1*, uncoupling protein 1; *LEP*, leptin; *ADIPOQ*, adiponectin; *LIPE*, lipase E, hormone-sensitive type)

Gene	GenBank accession	Primer sets	Product length (bp)	T_m (°C)
ACTB	JN038572.1	Forward: 5′-CTCTTCCAGCCTTCCTTCCT-3′ Reverse: 5′-AGCACTGTGTTGGCGTACAG-3′	116	59.4
PPARG1	NM_138712.3	Forward: 5′-GCCGCAGATTTGAAAGAAGC-3′ Reverse: 5′-TGGCATCTCTGTGTCAACCA-3′	110	57.3
PPARG2	NM_015869.4	Forward: 5′-TACAGCAAACCCCTATTCCA-3′ Reverse: 5′-GAGAAGTCAACAGTAGTGAAG-3′	240	55.6
PPARA	NM_005036.4	Forward: 5′-TCTGTCGGGATGTCACACAA-3′ Reverse: 5′-CGGGCTTTGACCTTGTTCAT-3′	191	57.3
PRDM16	AF294278.1	Forward: 5′-GAGGAGGACGATGAGGACAG-3′ Reverse: 5′-GCTCCTCATCCTCCTCATCC-3′	103	61.4
PPARGC1A	NM_001330751	Forward: 5′-GCCCAGGTACAGTGAGTCTT-3′ Reverse: 5′-GTGAGGACTGAGGACTTGCT-3′	105	59.4
UCP1	NM_021833.4	Forward: 5′-GCGGATGAAACTCTACAGCG-3′ Reverse: 5′-GTTTCTTTCCCTGCGGTGAG-3′	117	59.4
LEP	D63519.2	Forward: 5′-ACCAAGGTCTTCAGCCATCA-3′ Reverse: 5′-CCCTCTGCCCTCTCTGAAAT-3′	108	58.4
ADIPOQ	EU420013.1	Forward: 5′-CCTAAGGGAGACATCGGTGA-3′ Reverse: 5′-GTAAAGCGAATGGGCATGTT-3′	173	57.4
LIPE	NM_005357.3	Forward: 5′-CTCTGGTCTACTACGCCCAG-3′ Reverse: 5′-CATCCCTTATGCAGCGTGAC-3′	121	60.4

analysis of variance (one-way ANOVA) followed by Bonferroni's test to compare the means. Values are shown as means ± standard error of the mean (SEM).

Results

Cytomorphology

BODIPY 493/503 is a lipophilic fluorescent dye that emits bright green fluorescence and has been frequently used to label LDs, and has thus been convenient for adipocytes (Ohsaki et al. 2010; Xu et al. 2017). To avoid any technical or biological variance due to cell number among slides, the total LD area was normalized to the number of cells.

Figure 1 illustrates LD formation during SGBS cells differentiation at D7, D14, and D21. Figure 2 evidences statistically significant differences of area of LDs/cells, the number of LDs/cell, and the area of a single LD/cell according to different days of differentiation. The area of LDs/cell was significantly different at D21 in comparison with D7 ($p < 0.001$) and D14 ($p < 0.05$) and also between D7 and D14 ($p < 0.01$) (Fig. 2a). The area of a single LD/cell was significantly different between D21 and D7 ($p < 0.001$) and between D21 and D14 ($p < 0.01$). Moreover, the area of a single LD/cell was higher at D14 in comparison with D7 ($p < 0.05$) (Fig. 2c). Since the number of LDs/cell did not significantly change between groups (Fig. 2b), the increase of the area was accounted for the lipid accumulation rather than a droplet generation from a lipolytic release of fatty acids.

Mitochondrial morphology

Figure 3 shows fluorescence micrographs of cells stained for mitochondria at 0 (a), 7 (b), 14 (c), and 21 (d) days of differentiation. Dispersed network-like shape of mitochondria is displayed in SGBS cells at D0 (Fig. 3a). They appeared elongated and interconnected (Fig. 3a, insert). At D7, mitochondria seemed to follow the rim of LDs (Fig. 3b) and were less interconnected, with a pearl necklace shape (Fig. 3b, insert). Interestingly, punctate intense staining was evident in mitochondria at D14 (Fig. 3c): they appeared rounded and

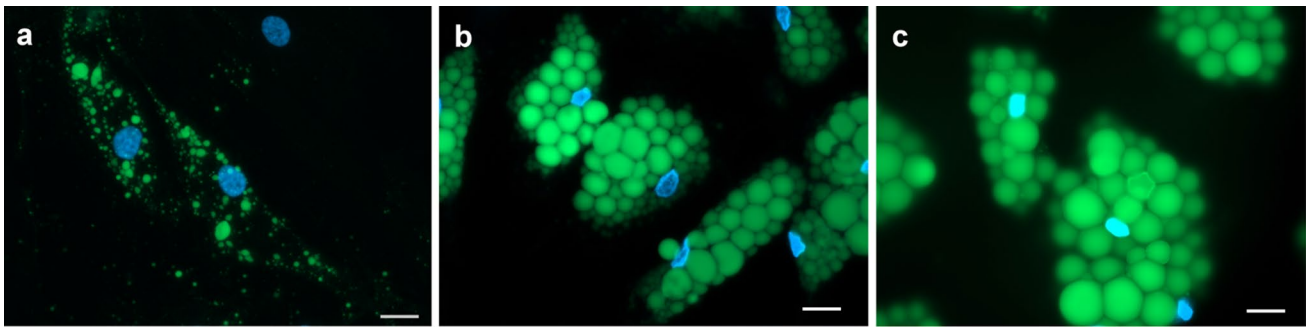

Fig. 1 Lipid droplets formation (stained with BODIPY 493/503) in fixed SGBS cells at D7 (**a**), D14 (**b**), and D21 (**c**). Nuclear staining DAPI. Images are representative of n. 4 biological replicates. *Scale bars* indicate 20 µm

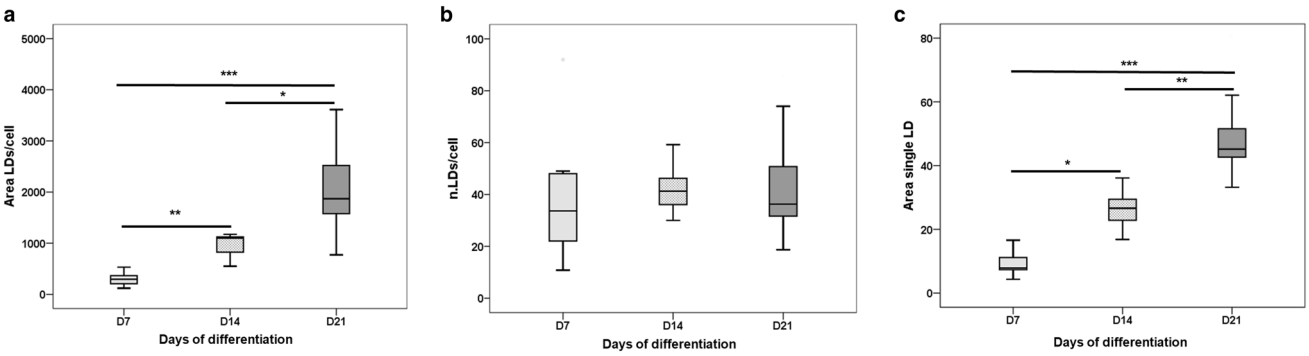

Fig. 2 Lipid droplets box plots show median (horizontal lines), first-to-third quartile (box), and the most extreme values with the interquartile range (vertical lines). Pairwise comparisons using the Dunn–Bonferroni approach were automatically produced for any dependent variables for which the Kruskal–Wallis test was significant between days of differentiation of SGBS cells. The area measures are expressed in μm^2 and are the average of 15 fields of each developmental stage. $^{***}p < 0.001$, $^{**}p < 0.01$, $^{*}p < 0.05$

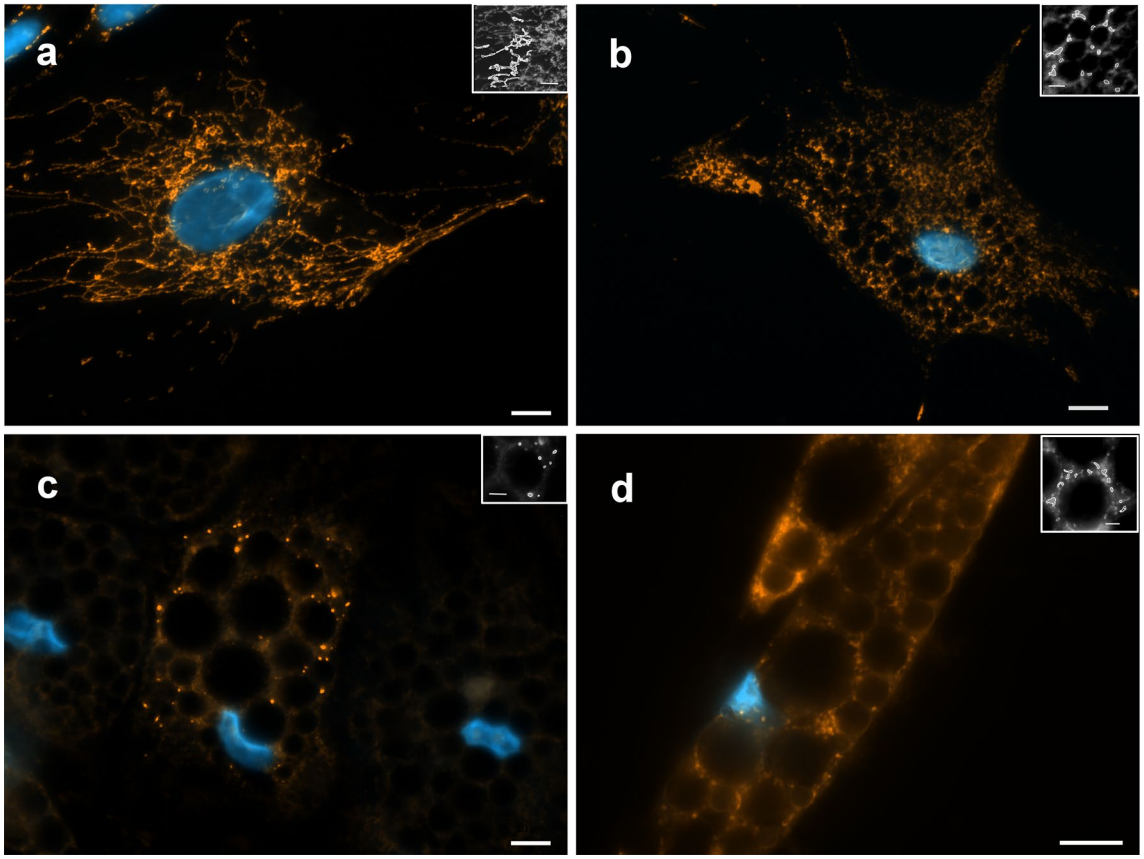

Fig. 3 MitoTracker Orange staining in SGBS cells at D0 (**a**), D7 (**b**), D14 (**c**), and D21 (**d**). **a** At D0, mitochondria displayed their normal tubular morphology, with numerous interconnections (insert, particular of networked mitochondria). **b** At D7 (insert, a magnified portion of cells showing pearl necklace shape mitochondria). **c** At D14, mitochondria appear mostly punctate (insert, particular of punctate mitochondria). **d** At D21, mitochondria showed round larger and rod-like shape (insert, rod shape mitochondria, as intermediate phenotype between puncta and network). Nuclear staining DAPI. Images are representative of n. 10 biological replicates. *Scale bars* indicate 20 µm. *Scale bars* in inserts indicate 2 µm

fragmented (Fig. 3c, insert). At D21 mitochondria appeared larger, with either a round or a rod shape (Fig. 3d, insert).

Mitochondrial content was significantly higher at D7 in comparison with D14 ($p < 0.01$) and D21 ($p < 0.001$). No statistical differences were observed between D7 and D0 (Fig. 4a). Mitochondrial interconnectivity (Fig. 4b) was significantly higher ($p < 0.05$) at D7 in comparison with D14 and D21 and this score was consistent with the degree of mitochondrial branching at the first two stages of development. Surprisingly, no significative difference was found between D0, D14, and D21. This is probably due to the high interquartile range at D0. The area/perimeter ratio normalized to minor axis (Fig. 4c) significantly decreased between D0 and D14 ($p < 0.001$), and also between D7 and D14 ($p < 0.01$). No statistical differences were observed between D0, D7, and D21, but the increased score value at D21 significantly differed ($p < 0.05$) from D14. Although the interconnectivity score at D21 did not differ from D14 (Fig. 4b), the area/perimeter ratio normalized to minor axis accounted for mitochondrial swelling and larger, rod-like shape, which is a transitional phenotype between puncta and networks (Fig. 4c).

Immunofluorescence analysis of PPARγ, PLIN1 and UCP1

The immunofluorescence of PPARγ, PLIN1, and UCP1 in SGBS cells at D0, D7, D14, and D21 is shown in Figs. 5, 6, and 7. No reaction was observed in controls performed for each developmental stage by substituting the primary antibodies with PBST blocking solution (data not shown).

Localization of PPARγ was strong in nuclei at D0 (Fig. 5). At D7, moderate immunoreactivity was detected in cytoplasm of cells but mostly was again in nuclei (Fig. 5). Positive cytoplasmatic staining was observed in cells at 14 days of differentiation (Fig. 5). At D21, PPARγ fluorescence was evident in cytoplasm, but some nuclei showed a positive reaction (Fig. 5 arrows). The percentage of nuclear PPARγ

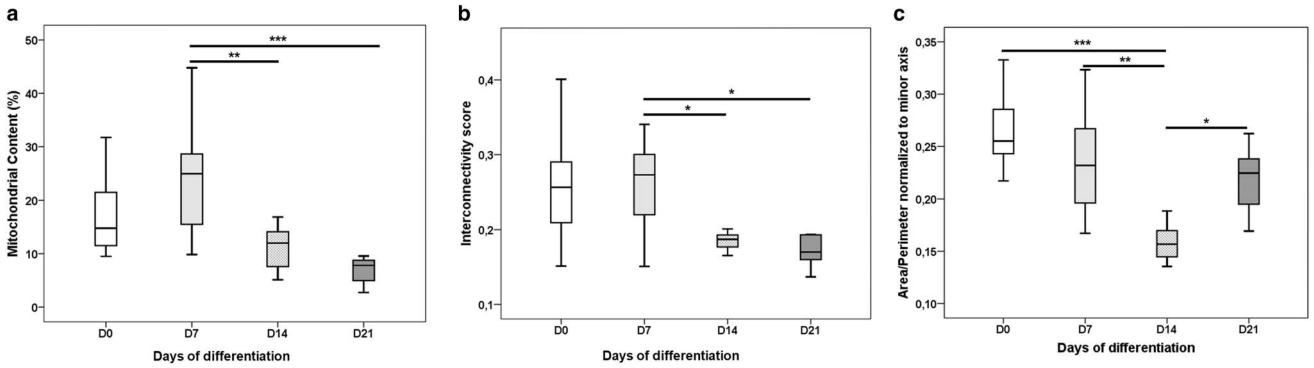

Fig. 4 Results from Mito-morphology analysis, as summary statistics for all measured cells. Box plots show median (horizontal lines), first-to-third quartile (box), and the most extreme values times the interquartile range (vertical lines). Pairwise comparisons using the Dunn–Bonferroni approach were automatically produced for any dependent variables for which the Kruskal–Wallis test was significant between days of differentiation of SGBS cells. The measurements are the average of ten fields of each developmental stage. ***$p < 0.001$, **$p < 0.01$, *$p < 0.05$

positivity ranged from 94.1 ± 0.55 at D0, 69.6 ± 0.68 at D7, 6.9 ± 0.21 at D14, and 29.3 ± 0.25 at D21. Nuclear positive percentages at D0 and D7 significantly differed ($p < 0.001$) from those at D14 and D21. The nuclear positivity percentage at D21 was also different ($p < 0.05$) from D14.

Localization of PLIN1 showed positive staining in D7 cells in close proximity to small lipid droplets (Fig. 6a). The reaction became more evident in adipocytes at D14 (Fig. 6b) and D21 (Fig. 6c) as long the cells accumulated fat, as evidenced also by BODIPY staining (Fig. 1).

Very weakly, punctate and disperse cellular staining identified UCP1 expression at D7 (Fig. 7a). At D14, the growing adipocytes showed UCP1 positive reaction in the cytoplasm (Fig. 7b). Clear positive reaction was observed in the cytoplasm of cells after 21 days of differentiation along the circular cytoplasmic rim may be juxtaposed to lipid droplets (Fig. 7c).

Gene expression analysis

The expression of genes involved in adipogenesis, browning process, and the markers of mature adipocytes was assessed in SGBS cells at different developmental stages (from D0 to D21) by means of RT-PCR assay (Fig. 8). *ACTB* mRNA expression was quantified in all samples and resulted in constant expression levels. No significant differences between the stages could be shown in the investigated adipocytes (data not shown); therefore, *ACTB* was chosen as internal control to quantify relative densities of genes.

Changes in the cellular differentiation and phenotype were confirmed by the expression of a set of genes involved in adipogenesis and browning. All genes involved in adipogenesis and gene markers of mature adipocytes shown an increased expression from D0 to D21 except *ADIPOQ*, which had the highest relative expression at D14 (Fig. 8a, c). While the expression of *PPARG1, PPARG2, LEP* and *LIPE* genes was significantly higher in later stages of adipogenesis, *ADIPOQ* expression level was reduced by at least 0.42 fold at D21 in comparison with D14 (Fig. 8c).

The ratio between the relative density of *PPARG1* and *PPARG2* was significantly higher at D0 in comparison with all other stages (3.07 ± 0.055 vs 0.85 ± 0.012 at D7, 0.73 ± 0.036 at D14, 0.91 ± 0.016 at D21). The expression of *PPARG1* and *PPARG2* at D21 differed from D0 by 1.00 and 5.67 fold, respectively (Fig. 8a).

Among the genes involved in browning process (Fig. 8b), relative expression of *PPARA* and *UCP1* was higher at D0 in comparison with D7 and increased thereafter. At D0, the expression of *PRDM16* was 0.85 fold higher in comparison with D7, 0.55 and 0.22 fold higher in comparison with D14 and D21, respectively. *PPARGC1A* had the highest expression on D14 in comparison with all other days of differentiation.

Discussion

Obesity and diabetes have widely boosted the interest in brown fat researches. Several studies have been involved in the possible white-to-brown cells conversion to produce heat instead of storing chemical energy (Lone et al. 2016; Matsukawa et al. 2017, as reviewed by Montanari et al. 2017). The key protein able to induce this uncoupled respiration and to dissipate chemical energy as heat is UCP1, expressed in brown fat. The main effectors that induce UCP1 expression are identified in prolonged cold exposure or in pathways that elevate intracellular cyclic AMP (cAMP), such as β-adrenergic signaling (Cypess et al. 2015). However, secreted protein factors, pharmacological molecules, and nutraceuticals have been employed to elucidate the adaptive

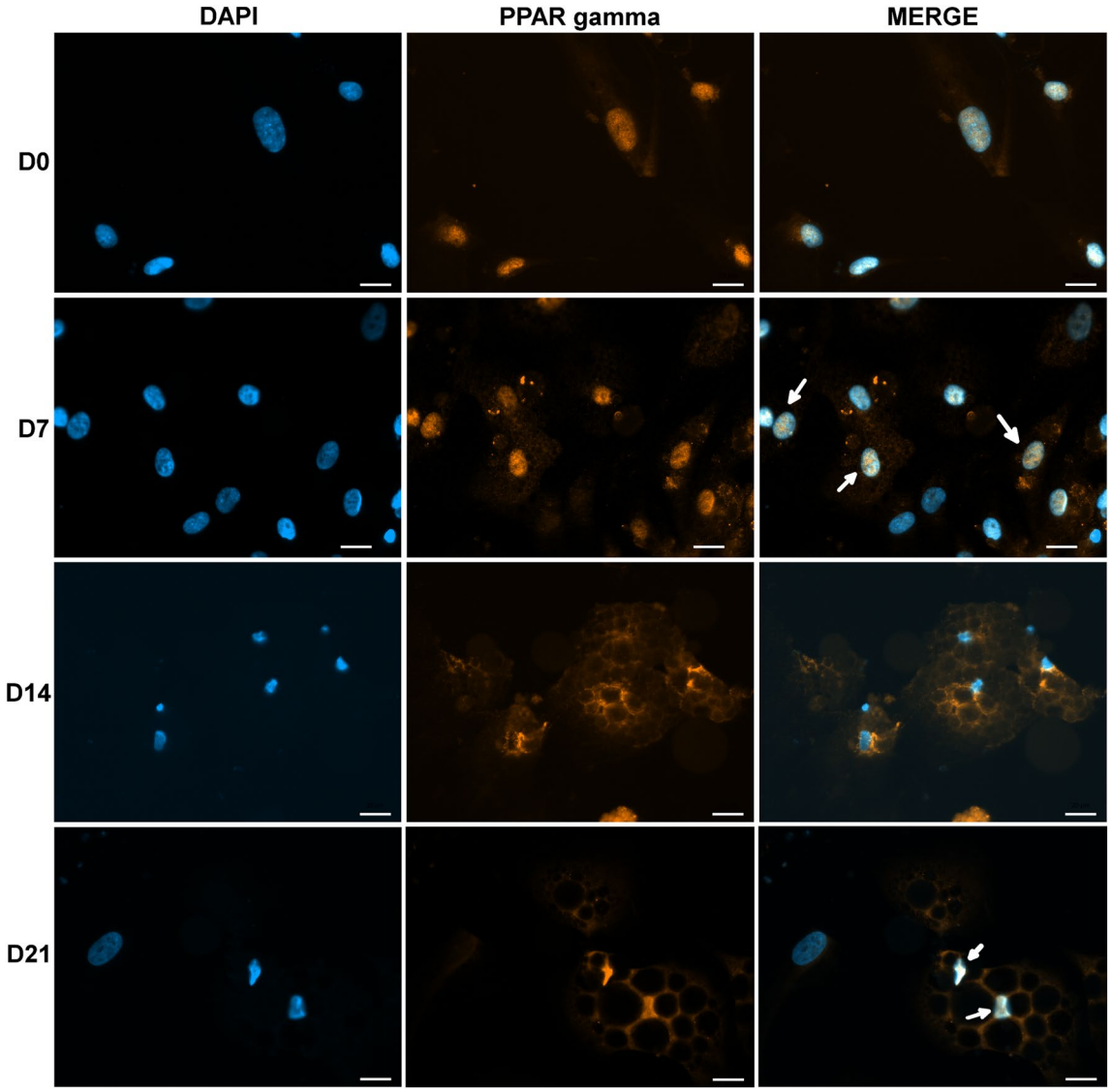

Fig. 5 PPARγ immunoreactivity in SGBS cells at D0, at D7, at D14, and at D21. Interestingly, PPARγ was expressed in nuclei before differentiation at D0 (**a**) and at D7 (**b**), was cytoplasmic at D14 (**c**), and moved to the nuclei (arrows) at D21 (**d**). Images are representative of n. 3 biological replicates. Scale bars indicate 20 µm

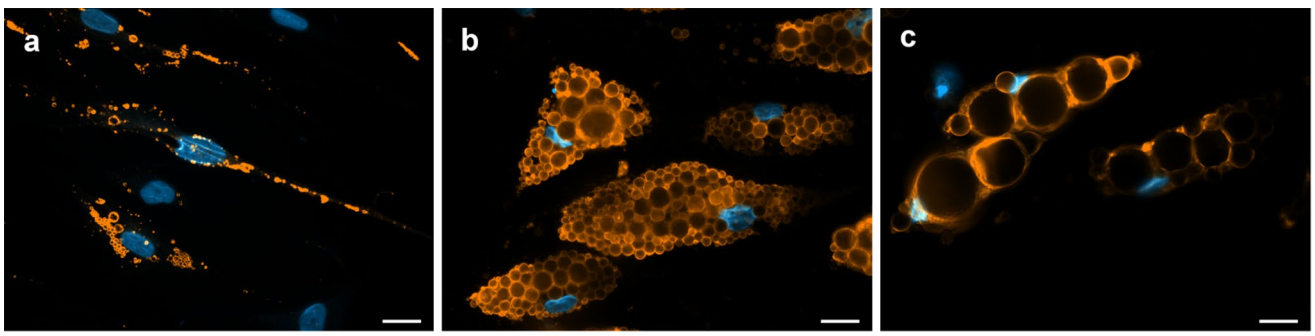

Fig. 6 Perilipin 1 immunoreactivity in SGBS cells at 7 days (D7, **a**), 14 days (D14, **b**), and 21 days (D21, **c**) of differentiation. D0 is not included in the analysis, because any lipid droplets take shape yet. Nuclear staining DAPI. Images are representative of n. 3 biological replicates. *Scale bars* indicate 20 µm

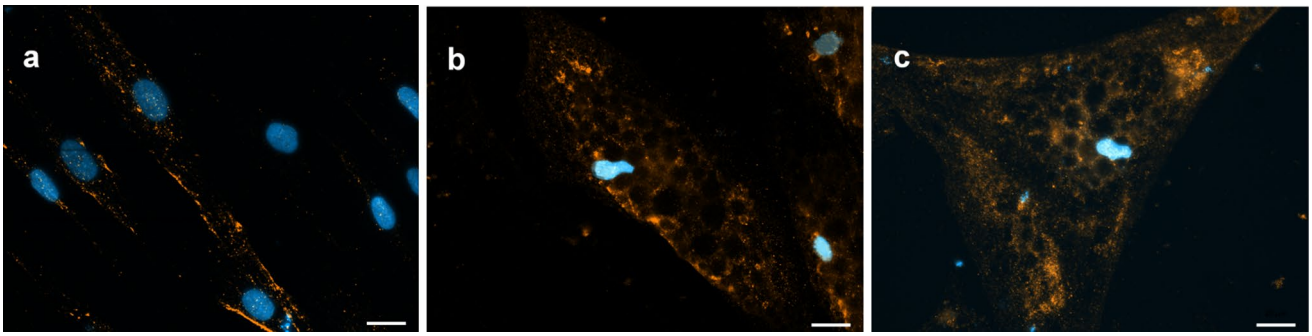

Fig. 7 UCP1 immunoreactivity in SGBS cells at 7 days (D7, **a**), 14 days (D14, **b**), and 21 days (D21, **c**) of differentiation. Nuclear staining DAPI. Images are representative of n. 3 biological replicates. *Scale bars* indicate 20 µm

thermogenesis (Montanari et al. 2017). Different cellular models from various animal species, particularly rodents, have been used over the years. They included mouse cell lines such as 3T3-L1, 3T3-F442A, C3H10T1/2 stromal cells, OP9, murine embryonic fibroblasts (MEF) obtained from different sources (Ruiz-Ojeda et al. 2016). However, since results from human cells can be more reliable in the utility towards human diseases than those obtained from animal models, human cellular models have also been developed (Shanks et al. 2009). The stromal vascular fraction (SVF), which comprehends mix of cells including pre-adipocytes and adipose stem cells, is the main source.

SGBS pre-adipocyte cell strain, isolated from the SVF of subcutaneous adipose tissue of an infant with Simpson–Golabi–Behemil syndrome, is the only fully inducible pre-adipocyte human cell line (Ruiz-Ojeda et al. 2016). It is an useful model for studying adipocyte differentiation in humans, but recently a transient feature of brown adipocytes at day 14 has been reported (Guennoun et al. 2015; Yeo et al. 2017). At the best of our knowledge, only the cited studies demonstrated that SGBS cells displayed an upregulation of several genes relating to brown/beige lineage that declined towards day 28. To specify the characteristics of these cells around the day 14 of differentiation, in the present paper, the morphological dynamics of LDs and mitochondria was investigated together with a panel of genes involved in differentiation, maturation and browning.

Mature white adipocytes are known to have a single or a few large LDs, whereas the brown adipocytes contain multiple small lipid droplets to facilitate efficient intracellular lipolysis from the LD surface and the subsequent promotion of free fatty acids transport to mitochondria for β-oxidation in BAT (Nishimoto and Tamori 2017). In fact, mitochondria are known to be in close physical association to LDs in brown adipocytes to promote the activity of UCP1 (Yu et al. 2015). Cold exposure triggers a high rate of lipolysis followed by a resynthesis of triglycerides, as demonstrated in murine BAT (Yu et al. 2015). Statistical analysis demonstrated that total and single surface of LDs in SGBS cells at 21 days of development were significantly larger than in the previous stages, but since the number of LDs per cell did not change, the enlargement was considered as an increase in lipids depots, naturally induced by development. Genes involved in adipocyte differentiation such as *LEP* and *ADIPOQ* were significantly upregulated, respectively, at D21 and D14 as already reported by Yeo et al. (2017) when also *LIPE* expression significantly raised from D0 to D21 in our results. Recent studies highlighted that adiponectin suppresses energy expenditure and thermogenesis, inhibiting lipolysis without binding its receptors (Qiao et al. 2014). Considering that *ADIPOQ* was downregulated at D21, the highest expression of *LIPE* and *UCP1* at the same time suggested that the lower expression of *ADIPOQ* released the transcription of genes associated with phenotypic transformation.

The human *PPARG* gene produces several transcripts that encode for two proteins: PPARγ1, localized in several tissues, and PPARγ2, which is adipose tissue-specific and possesses a more powerful adipogenic activity (Aprile et al. 2014). According to Yeo et al. (2017), in SGBS cells, the expression of *PPARG* transcripts increased from the first day of differentiation trough D7 and D21. PPARγ is known to enhance the activation of UCP1, but only in brown adipocytes and not in white adipocytes (Tapia et al. 2017), probably because other transcriptional regulators are mandatory to promote the UCP1 expression in brown adipocytes.

Immunofluorescence showed that the PPARγ proteins were mainly localized in the nucleus in early stages of differentiation, but at D14 and D21, their positive localization gradually moved to the cytoplasm and significantly reappeared in the nuclei at D21. In thermogenic adipocytes, the PPARγ translocation from nucleus to cytoplasm was related to a reduced transcriptional activity when the thermogenic machinery is not stimulated, while proper stimulation, i.e., cold exposure, induces a translocation back into the nucleus (Rim et al. 2004). However, PPARγ genomic signal can be

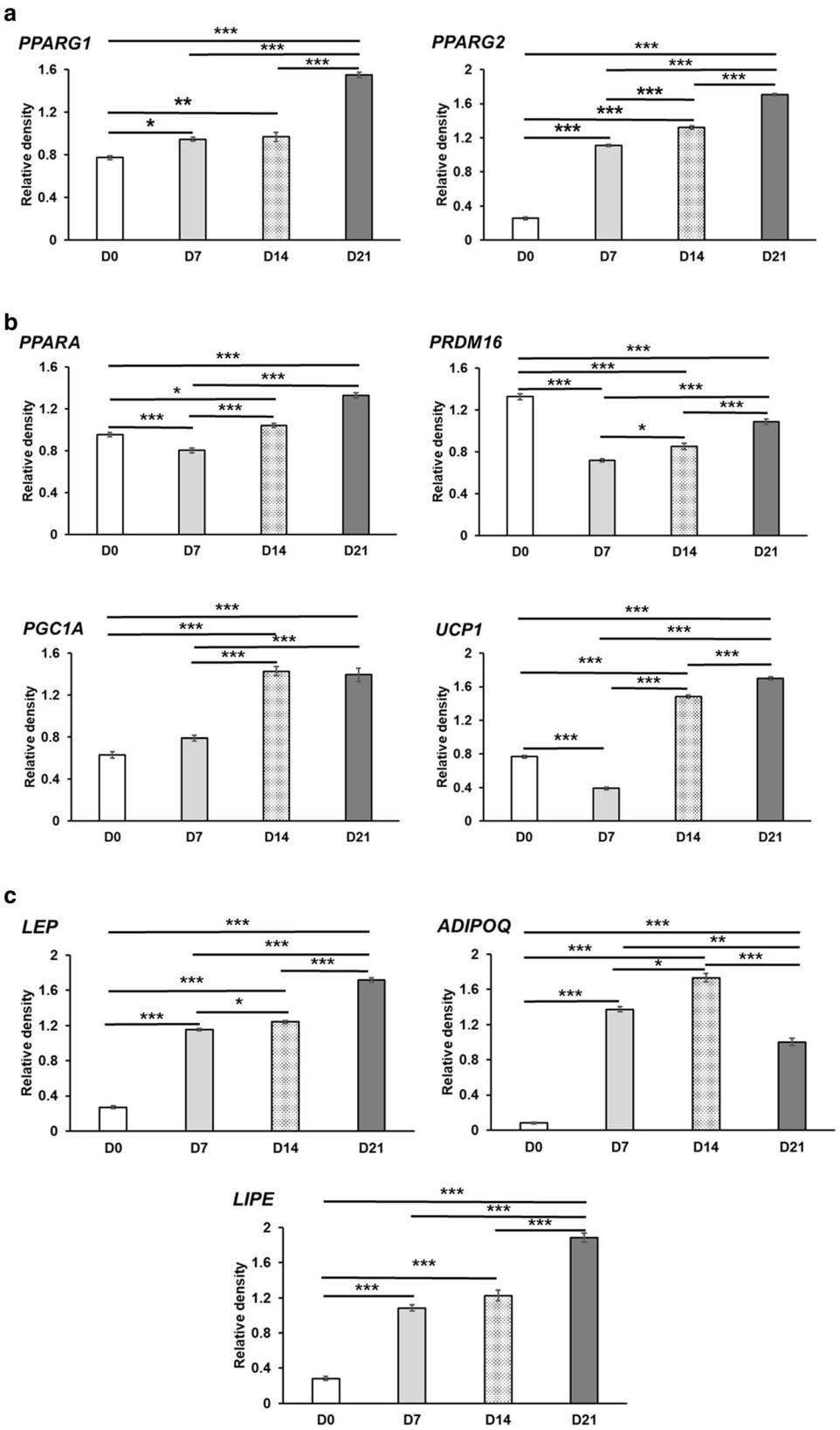

Fig. 8 Relative density profiles of undifferentiated and differentiated SGBS cells. **a** Adipogenesis transcription factor genes at D0 and D7, D14, and D21 days of differentiation (three biological replicates per stage). *PPARG1*, peroxisome proliferator-activated receptor gamma, variant 1; *PPARG2*, peroxisome proliferator-activated receptor gamma, variant 2. **b** Genes involved in browning at different developmental stage (three biological replicates per stage). *PPARA*, peroxisome proliferator-activated receptor alpha; *PRDM16*, PR domain containing 16; *PGC1A*, peroxisome proliferator-activated receptor gamma coactivator 1-alpha; *UCP1*, uncoupling protein 1. **c** Marker genes of mature cells at different developmental stage (three biological replicates per stage). *LEP*, lepin; *ADIPOQ*, adiponectin; *LIPE*, hormone-sensitive lipase. Bars represent the mean plus/minus standard error of the mean (SEM). One-way ANOVA was used to test for statistical significance adjusting values with Bonferroni correction. ***$p < 0.001$, **$p < 0.01$, *$p < 0.05$

abrogated by its removal out of the nucleus by ERK cascade (Burgermeister et al. 2007) and cytosolic PPARγ can then trigger nongenomic signaling pathways (Burgermeister and Seger 2007). The highest expression of cytosolic PPARγ in SGBS at D14 could be associated with other proteins or transcriptional coactivators that are involved in the change of phenotype.

It should be considered that SGBS cells derived from patients with mutations in the glypican-3 gene (*GPC3*) (Veugelers et al. 2000). These mutations prevent glypican 3 from inhibiting the hedgehog signaling pathway, resulting in an increase of cell proliferation and development of tissues, including mesenchyme cells and progenitors of adipose tissue. Moreover, hedgehog signaling has an antiadipogenic effect which has also been demonstrated in 3T3-L1, although the molecular basis of this inhibition remains controversial (Cousin et al. 2007). Interestingly, in vitro and in vivo hedgehog activation resulted in a virtually complete block of white adipocytes development, leaving the differentiation process of brown adipocytes completely intact (Pospisilik et al. 2010). Notably, in hepatocellular carcinoma, *GPC3* gene modulates other growth factors involved in brown adipocyte phenotype, such as BMP7 and FGF-2 (Midorikawa et al. 2003).

Among the brown-specific markers, *PPARA* was highly expressed in D21 SGBS cells. This gene is involved in the molecular mechanism that leads to the differentiation of mature brown adipocytes and to the expression of *UCP1* itself. *PPARA*, along with *PPARG*, directly affects *UCP1* expression by binding the distal enhancer region of the gene and participates in increasing the lipid oxidation capacity of the cell (Pradhan et al. 2017). *PPARGC1A* and *PRDM16* have been shown to serve as important molecular determinants of the brown fat cell phenotype (Kajimura et al. 2010). *PPARGC1A* is a transcriptional coactivator that interacts with nuclear receptor PPARγ and stimulates mitochondrial biogenesis in brown adipocytes and in white adipocytes undergoing browning, after a proper activation (Park et al. 2017). The higher expression level of this gene at D14 is coherent with the followed higher transcription of *UCP1* at D21. *PRDM16* was highly expressed in undifferentiated SGBS cells. The early expression of *PRDM16* in SGBS cells is in agreement with its activity observed in undifferentiated MEF. It has been demonstrated that PRDM16 alters the enhancer–promoter proximity by binding to and recruiting MED1 to the *UCP1* and *PPARGC1A* gene loci, for a full or partial transcriptional activation of this gene (Iida et al. 2014).

The changeful expression of brown markers genes was consistent with the results obtained by mitochondrial morphology analysis. It is known that mitochondrial reorganization and free fatty acid release facilitate uncoupling and thereby heat production (Wikstrom et al. 2014). The mitochondrial content, usually related to mitochondria biogenesis, was significantly different ($p < 0.001$) at D7 suggesting that this adaptative mechanism serves to sustain the subsequent metabolic change observed at D14. The decrease in mitochondrial content at D21 could be explain by their enlargement due to an increase of swelling, as indicated by their morphology and by the A/P normalized to minor axis score. Indeed, from D0 to D14, the mitochondrial analysis demonstrated a decrease in interconnectivity and, therefore, more fission, as evidenced from the significant decrease of area/perimeter ratio normalized to minor axis at D14. This is in agreement with Liesa and Shirihai (2013), who extensively reviewed the mitochondrial dynamics in the regulation of nutrient utilization and energy expenditure. Using uncouplers that mimic physiological conditions of nutrient excess and the subsequent increase nutrient oxidation, they suggested that fragmentation is associated with both maximal respiratory rates and increased proton conductance. In other words, mitochondrial fragmentation could be consider as a mechanism to enhance the capacity of free fatty acid to induce thermogenesis, even in the absence of adrenergic stimulation. On the other hand, in white fat mitochondria, represent the main source of ATP and fusion engages the entire mitochondrial compartment in respiration to maximize ATP synthesis (Westermann 2012). After 21 days of differentiation, large, round and rod-shaped mitochondria, the significantly lower score of interconnection and higher A/P normalized to minor axis parameter indicated that mitochondria were fragmented and possibly swelled to support uncoupled fatty acid oxidation. In this regards, the mitochondrial swelling, generally considered a sign of apoptosis, represents a physiological or at least controlled response to adrenergic activation in brown adipocytes. The mitochondrial spherical shape due to swelling may favor uncoupled respiration (Wikstrom et al. 2014).

The present study investigated, during development, the intrinsic features of human SGBS cells that display a transient brown phenotype. The dynamics of lipid droplets and mitochondrial morphology together with the change in gene expression, in the absence of any stimulation, could be of interest in understanding patterns and pathways involved in the conversion from white to brown adipocytes. Furthermore, the transient phenotype experienced by this cellular model should be considered when used in studies of adipocyte browning.

Acknowledgements We thank Dr. Martin Wabitsch (Division of Pediatric Endocrinology, Department of Pediatrics and Adolescent Medicine, University of Ulm, Ulm, Germany) for providing the SGBS cells.

Compliance with ethical standards

Conflict of interest The authors declare that they have no conflict of interest.

References

Ahfeldt T, Schinzel RT, Lee YK et al (2012) Programming human pluripotent stem cells into white and brown adipocytes. Nat Cell Biol 14(2):209–219. https://doi.org/10.1038/ncb2411

Allott EH, Oliver E, Lysaght J, Gray SG, Reynolds JV, Roche HM, Pidgeon GP (2012) The SGBS cell strain as a model for the in vitro study of obesity and cancer. Clin Transl Oncol 14(10):774–782. https://doi.org/10.1007/s12094-012-0863-6

Aprile M, Ambrosio MR, D'Esposito V, Beguinot F, Formisano P, Costa V, Ciccodicola A (2014) *PPARG* in human adipogenesis: differential contribution of canonical transcripts and dominant negative isoforms. PPAR Res 2014:537865. https://doi.org/10.1155/2014/537865

Bäcker V (2012) ImageJ macro tool sets for biological image analysis. In: ImageJ User and Developer Conference

Barneda D, Frontini A, Cinti S, Christian M (2013) Dynamic changes in lipid droplet-associated proteins in the "browning" of white adipose tissues. Biochim Biophys Acta 1831(5):924–33. https://doi.org/10.1016/j.bbalip.2013.01.015

Burgermeister E, Seger R (2007) MAPK kinases as nucleo-cytoplasmic shuttles for PPARgamma. Cell Cycle 6(13):1539–1548

Burgermeister E, Chuderland D, Hanoch T, Meyer M, Liscovitch M, Seger R (2007) Interaction with MEK causes nuclear export and downregulation of peroxisome proliferator-activated receptor gamma. Mol Cell Biol 27(3):803–817

Cannon B, Nedergaard J (2004) Brown adipose tissue: function and physiological significance. Physiol Rev 84(1):277–359

Chen Y, Buyel JJ, Hanssen MJ et al (2016) Exosomal microRNA miR-92a concentration in serum reflects human brown fat activity. Nat Commun 7:11420. https://doi.org/10.1038/ncomms11420

Colitti M, Grasso S (2014) Nutraceuticals and regulation of adipocyte life: premises or promises. Biofactors 40(4):398–418. https://doi.org/10.1002/biof.1164

Cousin W, Fontaine C, Dani C, Peraldi P (2007) Hedgehog and adipogenesis: fat and fiction. Biochimie 89(12):1447–1453

Cypess AM, Weiner LS, Roberts-Toler C et al (2015) Activation of human brown adipose tissue by a β_3-adrenergic receptor agonist. Cell Metab 21(1):33–38. https://doi.org/10.1016/j.cmet.2014.12.009

Dagda RK, Cherra SJ III, Kulich SM, Tandon A, Park D, Chu CT (2009) Loss of PINK1 function promotes mitophagy through effects on oxidative stress and mitochondrial fission. J Biol Chem 284(20):13843–13855

DeBaun MR, Ess J, Saunders S (2001) Simpson Golabi Behmel syndrome: progress toward understanding the molecular basis for overgrowth, malformation, and cancer predisposition. Mol Genet Metab 72(4):279–286

Farmer SR (2005) Regulation of PPARγ activity during adipogenesis. Int J Obes (Lond) 29:S13-S16

Fischer-Posovszky P, Newell FS, Wabitsch M, Tornqvist HE (2008) Human SGBS cells—a unique tool for studies of human fat cell biology. Obes Facts 1(4):184–189. https://doi.org/10.1159/000145784

Gao AW, Houtkooper RH (2014) Mitochondrial fission: firing up mitochondria in brown adipose tissue. EMBO J 33(5):401–402. https://doi.org/10.1002/embj.201487798

Guennoun A, Kazantzis M, Thomas R, Wabitsch M, Tews D, Seetharama Sastry K, Abdelkarim M, Zilberfarb V, Strosberg AD, Chouchane L (2015) Comprehensive molecular characterization of human adipocytes reveals a transient brown phenotype. J Transl Med 13:135. https://doi.org/10.1186/s12967-015-0480-6

Harms MJ, Ishibashi J, Wang W, Lim HW, Goyama S, Sato T, Kurokawa M, Won KJ, Seale P (2014) Prdm16 is required for the maintenance of brown adipocyte identity and function in adult mice. Cell Metab 19(4):593–604. https://doi.org/10.1016/j.cmet.2014.03.007

Iida S, Chen W, Nakadai T, Ohkuma Y, Roeder RG (2014) PRDM16 enhances nuclear receptor-dependent transcription of the brown fat-specific *Ucp1* gene through interactions with Mediator subunit MED1. Genes Dev 29(3):308–321. https://doi.org/10.1101/gad.252809.114

Kadowaki T, Yamauchi T (2005) Adiponectin and adiponectin receptors. Endocr Rev 26(3):439–451

Kajimura S, Seale P, Spiegelman BM (2010) Transcriptional control of brown fat development. Cell Metab 11(4):257–262. https://doi.org/10.1016/j.cmet.2010.03.005

Lefterova MI, Haakonsson AK, Lazar MA, Mandrup S (2014) PPARγ and the global map of adipogenesis and beyond. Trends Endocrinol Metab 25(6):293–302. https://doi.org/10.1016/j.tem.2014.04.001

Leonard AP, Cameron RB, Speiser JL, Wolf BJ, Peterson YK, Schnellmann RG, Beeson CC, Rohrer B (2015) Quantitative analysis of mitochondrial morphology and membrane potential in living cells using high-content imaging, machine learning, and morphological binning. Biochim Biophys Acta 1853(2):348–360. https://doi.org/10.1016/j.bbamcr.2014.11.002

Liesa M, Shirihai OS (2013) Mitochondrial dynamics in the regulation of nutrient utilization and energy expenditure. Cell Metab 17(4):491–506. https://doi.org/10.1016/j.cmet.2013.03.002

Lone J, Choi JH, Kim SW, Yun JW (2016) Curcumin induces brown fat-like phenotype in 3T3-L1 and primary white adipocytes. J Nutr Biochem 27:193–202. https://doi.org/10.1016/j.jnutbio.2015.09.006

Matsukawa T, Villareal MO, Motojima H, Isoda H (2017) Increasing cAMP levels of preadipocytes by cyanidin-3-glucoside treatment induces the formation of beige phenotypes in 3T3-L1 adipocytes. J Nutr Biochem 40:77–85. https://doi.org/10.1016/j.jnutbio

Midorikawa Y, Ishikawa S, Iwanari H, Imamura T, Sakamoto H, Miyazono K, Kodama T, Makuuchi M, Aburatani H (2003) Glypican-3, overexpressed in hepatocellular carcinoma, modulates FGF2 and BMP-7 signaling. Int J Cancer 103(4):455–465

Montanari T, Pošćić N, Colitti M (2017) Factors involved in white-to-brown adipose tissue conversion and thermogenesis: a review. Obes Rev 18(5):495–513. https://doi.org/10.1111/obr.12520

Nedergaard J, Petrovic N, Lindgren EM, Jacobsson A, Cannon B (2005) PPARγ in the control of brown adipocyte differentiation. Biochim Biophys Acta 1740(2):293–304

Nishimoto Y, Tamori Y (2017) CIDE family-mediated unique lipid droplet morphology in white adipose tissue and brown adipose tissue determines the adipocyte energy metabolism. J Atheroscler Thromb 24(10):989–998. https://doi.org/10.5551/jat.RV17011

Ohsaki Y, Shinohara Y, Suzuki M, Fujimoto T (2010) A pitfall in using BODIPY dyes to label lipid droplets for fluorescence microscopy. Histochem Cell Biol 133(4):477–480. https://doi.org/10.1007/s00418-010-0678-x

Park G, Horie T, Kanayama T, Fukasawa K, Iezaki T, Onishi Y, Ozaki K, Nakamura Y, Yoneda Y, Takarada T, Hinoi E (2017) The transcriptional modulator Irfd1 controls PGC-1α expression under short-term adrenergic stimulation in brown adipocytes. FEBS J 284(5):784–795. https://doi.org/10.1111/febs.14019

Pospisilik JA, Schramek D, Schnidar H et al (2010) Drosophila genome-wide obesity screen reveals hedgehog as a determinant of brown versus white adipose cell fate. Cell 140(1):148–160. https://doi.org/10.1016/j.cell.2009.12.027

Pradhan RN, Zachara M, Deplancke B (2017) A systemic perspective on brown adipogenesis and metabolic activation. Obes Rev 18(Suppl 1):65–81. https://doi.org/10.1111/obr.12512

Qiao L, Yoo HS, Bosco C, Lee B, Feng GS, Schaack J, Chi NW, Shao J (2014) Adiponectin reduces thermogenesis by inhibiting brown

adipose tissue activation in mice. Diabetologia 57(5):1027–1036. https://doi.org/10.1007/s00125-014-3180-5

Rim JS, Xue B, Gawronska-Kozak B, Kozak LP (2004) Sequestration of thermogenic transcription factors in the cytoplasm during development of brown adipose tissue. J Biol Chem 279(24):25916–25926

Rozen S, Skaletsky HJ (2000) Primer3 on the WWW for general users and for biologist programmers. Methods Mol Biol 132:365–386

Ruiz-Ojeda FJ, Rupérez AI, Gomez-Llorente C, Gil A, Aguilera CM (2016) Cell models and their application for studying adipogenic differentiation in relation to obesity: a review. Int J Mol Sci 17(7):E1040. https://doi.org/10.3390/ijms17071040

Shanks N, Greek R, Greek J (2009) Are animal models predictive for humans? Philos Ethics Humanit Med 4:2. https://doi.org/10.1186/1747-5341-4-2

Tapia P, Fernández-Galilea M, Robledo F, Mardones P, Galgani JE, Cortés VA (2017) Biology and pathological implications of brown adipose tissue: promises and caveats for the control of obesity and its associated complications. Biol Rev Camb Philos Soc. https://doi.org/10.1111/brv.12389

Tenorio J, Arias P, Martínez-Glez V, Santos F, García-Miñaur S, Nevado J, Lapunzina P (2014) Simpson–Golabi–Behmel syndrome types I and II. Orphanet J Rare Dis 9:138. https://doi.org/10.1186/s13023-014-0138-0

Valente AJ, Maddalena LA, Robb WL, Moradi F, Stuart JA (2017) A simple ImageJ macro tool for analyzing mitochondrial network morphology in mammalian cell culture. Acta Histochem 119(3):315–326. https://doi.org/10.1016/j.acthis.2017.03.001

Veugelers M, Cat BD, Muyldermans SY et al (2000) Mutational analysis of the GPC3/GPC4 glypican gene cluster on Xq26 in patients with Simpson–Golabi–Behmel syndrome: identification of loss-of-function mutations in the GPC3 gene. Hum Mol Genet 9(9):1321–1328

Wabitsch M, Brenner RE, Melzner I, Braun M, Möller P, Heinze E, Debatin KM, Hauner H (2001) Characterization of a human preadipocyte cell strain with high capacity for adipose differentiation. Int J Obes Metab Disord 25(1):8–15

Westermann B (2012) Bioenergetic role of mitochondrial fusion and fission. Biochim Biophys Acta 1817(10):1833–1838. https://doi.org/10.1016/j.bbabio.2012.02.033

Wikstrom JD, Mahdaviani K, Liesa M et al (2014) Hormone-induced mitochondrial fission is utilized by brown adipocytes as an amplification pathway for energy expenditure. EMBO J 33(5):418–436. https://doi.org/10.1002/embj.201385014

Xu P, Li J, Liu J, Wang J, Wu Z, Zhang X, Zhai Y (2017) Mature adipocytes observed to undergo reproliferation and polyploidy. FEBS Open Bio 7(5):652–658. https://doi.org/10.1002/2211-5463.12207

Yeo CR, Agrawal M, Hoon S et al (2017) SGBS cells as a model of human adipocyte browning: a comprehensive comparative study with primary human white subcutaneous adipocytes. Sci Rep 7(1):4031. https://doi.org/10.1038/s41598-017-04369-2

Yu J, Zhang S, Cui L et al (2015) Lipid droplet remodeling and interaction with mitochondria in mouse brown adipose tissue during cold treatment. Biochim Biophys Acta 1853(5):918–928. https://doi.org/10.1016/j.bbamcr.2015.01.020

Dynamic of lipid droplets and gene expression in response to β-aminoisobutyric acid treatment on 3T3-L1 cells

Monica Colitti,[1] Federico Boschi,[2] Tommaso Montanari[1]

[1]Department of Agricultural, Food, Environmental and Animal Sciences, University of Udine
[2]Department of Computer Science, University of Verona, Italy

Abstract

Research on adipobiology has recognized the browning process of white adipocytes as a potential therapeutic strategy for the treatment of obesity and related morbidities. Physical exercise stimulates the secretion of myokines, such as β-aminoisobutyric acid (BAIBA), which in turn promotes adaptive thermogenesis. White adipocyte conversion to brown cells involves dynamic changes in lipid droplet (LD) dimension and in the transcription of brown-specific marker genes. This study analyzes the effect of different doses of BAIBA and at different days of development on 3T3-L1 cells by evaluating morphological changes in LDs and the expression of browning gene markers. Results suggested that the highest concentration of BAIBA after 4 days of differentiation produced the most significant effects. The number of LDs per cell increased in comparison to control cells, whereas the surface area significantly decreased. Brown adipocyte markers were up-regulated, but the effect of treatment was lost at 10 days of differentiation.

The thermogenic program induced by BAIBA may reflect a rapid adaptation of adipose tissue to physical exercise. This connection stresses the beneficial impact of physical exercise on metabolic health.

Introduction

Regular exercise has been shown to have many health benefits, both physically and mentally. Indeed, it increases metabolic rate, helping in weight loss, improves whole-body glucose homeostasis and increases insulin sensitivity. Recently, endocrine factors called myokines, produced by skeletal muscles and released during the contraction of muscle fibers, have been detected and linked to the loss of fat mass through the activation of thermogenesis in adipose tissue.[1,2] Thermogenesis is a physiological process typical of uncoupling protein 1 (UCP1)-expressing mature brown adipocytes and recruitable brown-like adipocytes, the so-called beige or brite adipocytes.[3] In these cells, UCP1 uncouples the mitochondrial respiration from the production of adenosine triphosphate (ATP) and the energy produced by the catabolic pathways is released in form of heat.[4,5] Brown and beige adipocytes are morphologically distinct from white ones for having multiple small lipid droplets (LDs) instead of a unique fat depot that occupies the vast majority of the cytoplasm,[6] and for having a high number of mitochondria intimately associated to them.[7] It was also demonstrated that the gene expression pattern of the three cell types is very different; despite beige adipocytes may be seen as "intermediate" between white and brown adipocytes, they present a unique gene expression pattern with highly specific molecular markers.[8-11]

This unique feature of UCP1-expressing cells has raised in recent years a great effort in brown adipobiology and obesity research, as the induction of browning by cold exposure, exercise and dietary/pharmacological factors may represent an effective way to counteract obesity and its related comorbidities.[12] In fact, many studies performed on both *in vitro* and *in vivo* models, which have been recently reviewed,[2] showed that the treatment with browning-inducing factors increases energy expenditure by enhancing the expression of *Ucp1* gene and other brown adipose tissue (BAT) markers. Canonical BAT gene markers include the elongation of very long chain fatty acids protein 3 (*Elovl3*), cell death-inducing DNA fragmentation factor A (DFFA)-like effector A (*Cidea*), PR domain-containing protein 16 (*Prdm16*) and peroxisome proliferator-activating receptor (PPAR) γ coactivator 1α (*Ppargc1a*). These last two genes are deeply involved in mitochondrial biogenesis and in early BAT differentiation.[8]

The exercise-induced adaptive thermogenesis would not make sense in white adipose tissue (WAT), since exercise *per se* increases heat production.[13] Therefore, myokines, such as irisin, myostatin, meteorin-like 1 (Metrnl) and β-aminoisobutyric acid (BAIBA), which are released during muscle contraction in physical activity, are claimed as browning-promoting factors in WAT.

BAIBA is a non-protein amino acid originating from the catabolism of thymine and valine that plays a critical role in browning and in insulin resistance.[14,15] Recently, BAIBA has been shown to protect osteocytes against reactive oxygen species and related apoptosis.[16] Despite the role of myokines in WAT browning has been extensively reviewed,[2,13] the cellular pathways through which they exert their action are mostly unknown. Roberts and colleagues hypothesized a PPARα-mediated mechanism through which BAIBA positively affects lipid metabolism in both adipocytes and hepatocytes.[15] However, the exact molecular pathway of browning, as well as the remodelling of LDs induced by BAIBA needs further investigation.

This paper aims to show the effects of BAIBA treatment on murine 3T3-L1 preadipocytes during their differentiation to mature adipocytes on morphological and numerical changes of LDs and on the expression of a selected gene pattern. The expression of a core set of brown fat-specific genes and mitochondrial biogenesis (*Ucp1*, *Cidea*, *Elovl3*, *Ppargc1a*, *Prdm16* and *Cyc1*) and a beige marker (*Tbx1*) was analyzed. Markers of LD formation and dynamics such as perilipin 1 (*Plin1*) and cell death-inducing DFFA-like effector C (*Cidec*) were investigated. Finally, the expression of brain-derived neurotrophic factor (*Bdnf*), a neurotrophin, which has a role in browning on *in vivo* models and in regulating energy balance and insulin signaling,[17,18] was also assessed.

Correspondence: Monica Colitti, Department of Agricultural, Food, Environmental and Animal Sciences, University of Udine, Via delle Scienze 206, 33100 Udine, Italy.
Tel. +39.0432.558583 -Fax: +39.0432.558603.
E-mail: monica.colitti@uniud.it

Key words: Lipid droplets; 3T3-L1; adipocytes; BAIBA.

Contributions: MC, concept, lipid droplets data acquisition, analysis and interpretation of expression data, draft of the article; FB, analysis and interpretation of data, revision of article for important intellectual content; TM, experiments on cells, interpretation of data, contribution to draft of the article.

Conflict of interest: the authors declare no conflict of interest.

Received for publication: 1 October 2018.
Accepted for publication: 20 November 2018.

European Journal of Histochemistry 2018; 62:2984
doi:10.4081/ejh.2018.2984

Materials and Methods

Chemicals and culture media

Dulbecco's modified Eagle medium (DMEM) enriched with 4.5 g/L D-glucose, 110 mg/L sodium pyruvate and 862 mg/L L-alanyl-L-glutamine (GlutaMAX™), DMEM/F-12 (1:1) medium enriched with GlutaMAX™ and 15 µM 4-(2-hydroxyethyl)-1-piperazineethanesulfonic acid (HEPES), fetal bovine serum (FBS), penicillin/streptomycin solution and amphotericin B solution were purchased from Gibco by Life Technologies (Thermo Fisher Scientific Inc., Waltham, MA, USA). Rosiglitazone was purchased from Cayman Chemical (Ann Arbor, MI, USA). BAIBA was purchased in a racemic mixture from AdipoGen SA (AdipoGen Life Science Inc., San Diego, CA, USA). Dipyrromethene boron difluoride (BODIPY) 493/503 dye, TRIzol reagent, PureLink™ RNA Mini Kit and Platinum™ SYBR™ Green qPCR SuperMix-UDG kit for real time PCR were purchased from Invitrogen (Thermo Fisher Scientific Inc.). ImProm-II™ Reverse Transcription System was purchased from Promega (Madison, WI, USA). 4,6-diamidino-2-phenylindole (DAPI)-containing mounting medium was purchased from Abcam (Cambridge, MA, USA). All other chemicals used in the experiment and not listed above were purchased from Sigma-Aldrich (Darmstadt, Germany).

Cell culture and treatment

3T3-L1 cells were chosen in the present study for their extensive use in evaluating the effects of compounds or nutrients on adipogenesis and in the potential application of various compounds and nutrients in the treatment of obesity. Moreover, at the best of our knowledge, the browning effect of BAIBA on 3T3-L1 cell model was never investigated. The murine 3T3-L1 preadipocytes (ZenBio Inc., Durham, NC, USA) were grown in high glucose DMEM supplemented with 10% FBS, 1% amphotericin B solution and 1% penicillin/streptomycin solution, at 37°C with 5% CO_2 and 95% relative humidity. Differentiation was induced 48 h after cells reached full confluence with DMEM/F-12 medium supplemented with 10% FBS, 1% amphotericin B solution, 1% penicillin/streptomycin solution, 0.5 µg/mL human insulin, 5 µM dexamethasone, 0.5 mM 3-isobutyl-1-methylxanthine (IBMX), 1 nM triiodothyronine (T_3) and 1 µM rosiglitazone. After 3 days, the differentiation medium was switched to a maintenance medium to which 0.5 µg/mL human insulin and 1 nM T_3 were added. Maintenance medium was refreshed every 2 days. After the switch from differentiation to maintenance medium, cells were treated with 1, 3 and 5 µM BAIBA until analysis. Cells were analyzed during differentiation at day 4 (4d) and at day 8 (8d), at day 10 (10d); these time points correspond to 2, 6 and 8 days of BAIBA treatment, respectively. A negative vehicle control (CTRL) was established treating cells with sterile milliQ water.

Cell viability assay

Cell viability was determined by 3-(4,5-dimethylthiazol-2-yl)-2,5-diphenyltetrazolium bromide (MTT) assay. Medium was removed from cells plated on a 96-well plate and treated with different concentrations of BAIBA. Prior to incubation with 5 mg/mL MTT solution in Hank's balanced salt solution (HBSS), cells were rinsed with phosphate buffer saline (PBS) 1x. Incubation with MTT solution was performed at 37°C for 4 h. Accumulated formazan was dissolved in dimethyl sulfoxide (DMSO) and incubated overnight at 37°C. The optical density was used as an indicator of cell viability and was measured at 550 nm.

BODIPY staining

After cell fixation in a 2% formalin solution diluted in PBS 1x at room temperature (RT) for 15 min, the slides were washed three times in PBS 1x and then incubated in a solution of BODIPY493/503 in PBS 1x to fluorescently label lipid droplets. The incubation was performed at RT in dark for 45 min. After the incubation, the slides were washed in PBS 1x three times and then mounted with mounting medium with DAPI. Images were acquired with the fluorescence microscope Axio Observer Z1 equipped with D-PLAN Neofluar objective lenses with N.A. 0.75 and Infinity Color Corrected System (ICS) and with AxioCam and Zen blue software (Carl Zeiss, Jena, Germany). The filters used for BODIPY were 470/525 nm, and 390/460 nm for DAPI.

Morphology of LDs

MRI_Lipid Droplets tool (http://dev.mri.cnrs.fr/projects/imagej-macros/wiki/Lipid Droplets_Tool), a macro of ImageJ1.50b software (http://rsb.info.nih.gov/ij/), was used to measure LD area.[19] The images were analyzed as already described.[20] For each LD area, perimeter, maximum Feret diameter (MFD) and integrated optical density (IOD) were measured. MFD is defined as the maximum distance between the two parallel planes restricting the object perpendicular to that direction and is a measure of an object size along a specified direction. It is generally used in optical microscopy to measure the size of particles.[21,22] The IOD reports the average intensity/density of each object and increases linearly with the triglycerides content in 3T3-L1 adipocytes.[23]

Total area occupied by LDs in each field at different days of differentiation was calculated by summing up the area of each LD. The count of cells in each field was used to calculate the area and the number of LDs per cell. The average area of a single LD was calculated by dividing the area of LDs/cells by the number of LDs/cells. The area (µm^2) and number of LDs were measured and counted on 15 fields for each time point.

A nonparametric representation of the LDs size probability density function (kernel) was chosen to avoid making assumptions about the distribution of the data; the kernel size distribution was evaluated with a routine written in Matlab 7.1 (Mathworks, MA, USA).

Of note, 2D examination of the LDs, which are 3D objects, leads to an underestimation of the size of bigger LDs with respect to smaller LDs, increasing the probability to detect the first ones. Despite this approach could affect the absolute kernel density distribution of the LDs size, it is used here in order to obtain a relative comparison only between different populations.

RNA extraction and RT-PCR

After culture medium removal from 6-well plates, 1 mL/10 cm^2 of TRIzol reagent was added in each well and repeatedly pipetted to induce a severe breakdown of cell structures. These samples were immediately processed with the PureLink™ RNA Mini Kit following the manufacturer's instructions.

The concentration of the extracted total RNA was quantified using a spectrophotometer (NanoDrop 1000 Spectropho-tometer; ThermoScientific, Wilmington, DE, USA) and the purity of RNA samples ranged between 1.8 and 1.9. RNA integrity was evaluated through the observation of 18S and 28S ribosomal bands after electrophoresis on 1% agarose gel, in the presence of GelRed. Primer3 Input software was used to design primers.[24] GenBank accession, primer sequences, product lengths and relative annealing temperatures for each gene are listed in Table 1, according to the HUGO Gene Nomenclature Committee.

Total RNA (500 ng) from each sample was reverse-transcribed and amplified using an MJ thermal cycler (PT-100; MJ Research, Inc., Waltham, MA, USA). For each gene, an aliquot of cDNA samples were pooled and standard curves with serial dilution of pool were used to optimize PCR conditions and to calculate the efficiency,

fluorescence baseline and threshold. Real time PCRs were performed for each sample in triplicate form using Platinum® SYBR® Green qPCR SuperMix-UDG. cDNA concentrations and primers molarities were different for each gene and determined with standard curves analyses. PCR amplification was conduced applying 45 cycles (1 s at 95ºC, 30 s at the specific annealing temperature, 30 s at 72ºC) in a 96-well spectrofluorometric thermal cycler (CFX, Biorad, Milan Italy). The melting curve analysis of amplification products was performed at the end of each PCR reaction to confirm that a single PCR product was detected.

The expression of target genes was normalized using the TATA box-binding protein (*Tbp*) mRNA levels or geometric means between *Tbp* and glyceraldehyde 3-phosphate dehydrogenase (*Gapdh*) genes and analyzed using ΔΔCt method.[25] For all the cell culture experiments, the results are generated from biological triplicates and represent similar results from at least three independent experiments.

Statistical analysis

Results are presented as relative values (means ± SEM). All experiments were performed at least three times. Two-way ANOVA was used for statistical analysis for MTT test by SPSS ver. 20.0 software. The measurements of the area of LDs/cell, number of LDs/cell and the area of a single LD were analyzed by SPSS ver. 20.0 software. The results, obtained from ten biological replicates, were compared using Kruskal-Wallis statistical test followed by pairwise comparisons using the Mann-Whitney approach.

Results

Cell viability

The percentage of cell viability after exposure of BAIBA at 4d, 8d and 10d was always around 100% (*data not shown*). No significant differences were observed for time point and for concentration x time point interaction.

Lipid droplet distribution and analysis

Figure 1 illustrated LDs formation in 3T3-L1 cells at 4d, 8d and 10d in presence of different BAIBA doses. Interestingly, at 4d with 3 and 5 μM of BAIBA, cells showed very small LDs (Figure 1, panels g and l, respectively) in comparison to CTRL cells (Figure 1a).

Indeed, kernel densiy distribution suggested an high number of cells with a small Feret diameter when incubated with 5 μM of BAIBA after 4 and 10 days of differentiation (Figure 2a). The kernel distributions of MFD at 4d, 8d and 10d are shown in Figure 2a. For all the three time points, LD size distribution of the treated cells is similar to that of control cells. In particular, using the least squares method evaluated on 100 equally spaced Feret dimensions, the differences at 4d between control and the treatments (1 μM, 3 μM and 5 μM) are respectively 0.0045, 0.0047 and 0.0538; at 8d are 0.0106, 0.0075 and 0.0062; at 10d are 0.0367, 0.0807 and 0.0736. Figure 2b evidenced statistically significant differences of IOD, number of LDs/cell and area

Table 1. Oligonucleotide primer sequences for RT-PCR.

Gene	GenBank accession	Primer sets	Product length (bp)	Tm (°C)
Tbp	NM_013684.3	Forward: 5'-CCAATGACTCCTATGACCCCTA-3' Reverse: 5'-CAGCCAAGATTCACGGTAGAT-3'	104	58.5
Gapdh	NM_008084	Forward: 5'-AATGTGTCCGTCGTGGATCTGA-3' Reverse: 5'-AGTGTAGCCCAAGATGCCCTTC-3'	117	60
Ucp1	NM_009463.3	Forward: 5'-CTTTGCCTCACTCAGGATTGG-3' Reverse: 5'-ACTGCCACACCTCCAGTCATT-3'	123	59.8
Ppargc1a	NM_008904.2	Forward: 5'-TATGGAGTGACATAGAGTGTGCT-3' Reverse: 5'-CTGGGCAAAGAGGCTGGTC-3'	191	60.0
Cidea	NM_007702.2	Forward: 5-ATCACAACTGGCCTGGTTACG-3' Reverse: 5'-TACTACCCGGTGTCCATTTCT-3'	136	58.9
Cidec	NM_178373.4	Forward: 5'-ACCTTCGACCTGTACAAGCT-3' Reverse: 5'-GTGCAGGTCATAGGAAAGCG-3'	99	58.4
Elovl3	NM_007703.2	Forward: 5'-TTCTCACGCGGGTTAAAAATGG-3' Reverse: 5'-GGCCAACAACGATGAGCAAC-3'	139	58.9
Cyc1	NM_025567.3	Forward: 5'-GGCATCAGAACCAGAGCATG-3' Reverse: 5'-CTGACCACTTATGCCGCTTC-3'	110	59.4
Plin1	NM_175640.2	Forward: 5'-TGGACCACCTGGAGGAAAAG-3' Reverse: 5'-CTTCGAAGGCGGGTAGAGATG-3'	94	60.6
Prdm16	NM_027504.3	Forward: 5'-CCACCAGCGAGGACTTCAC-3' Reverse: 5'-GGAGGACTCTCGTAGCTCGAA-3'	107	61.4
Ppara	NM_011144.6	Forward: 5 -TCTGTCGGGATGTCACACAA-3 Reverse: 5 -CGGGCTTTGACCTTGTTCAT-3	191	57.3
Bdnf	NM_007540.4	Forward: 5'-ATTACCTGGATGCCGCAAAC-3' Reverse: 5'-CCTTCCTTGGTGTAACCCAT-3'	241	58.5
Tbx1	NM_011532.2	Forward: 5'-AGGCGGAAGGAAGTGGTATT-3' Reverse: 5'-TACCAGTATCTACACCGCCC-3'	118	58.4

T_m, annealing temperature; *Tbp*; TATA box binding protein; *Gapdh*, glyceraldehyde-3-phosphate dehydrogenase; *Ucp1*, uncoupling protein 1; *Ppargc1a,* peroxisome proliferator-activated receptor coactivator 1 α; *Cidea,* cell death-inducing DFFA-like effector A; *Cidec*, cell death inducing DFFA like effector C; *Elovl3*, elongation of very long chain fatty acids protein 3; *Cyc1*, cytochrome C1; *Plin1*, perilipin 1; *Prdm16*, proline rich domain containing 16; *Ppara*, peroxisome proliferator-activated receptor α; *Bdnf,* brain derived neurotrophic factor; *Tbx1*, T-box 1.

of a single LD/cell at 4d in presence of different BAIBA doses. To avoid any technical or biological variance due to cell number among slides, the total LD area was normalized to the number of cells.

The IOD significantly ($P<0.05$) decreased between 3 μM and 5 μM, the number of LDs/cell increased between CTRL and 1 μM ($P<0.05$) and between CTRL and 5 μM ($P<0.01$). The area of a single LD/cell was significantly different between CTRL and 5 μM ($P<0.001$). Figure 2b evidenced statistically significant differences in the area of LDs at 10d. In particular, the area was higher ($P<0.05$) in CTRL and 3 μM in comparison to 5 μM. No statistical differences were found at 8d.

The decrease in IOD, which is inversely related with the amount of triglycerides in LDs, the lowest area of a single LD and the increase of the number of LDs/cell observed with 5 μM BAIBA at 4d can account for a LD generation through the lipolytic release of fatty acids.

Transcription data analysis

Figure 3 indicated the relationship between the different concentrations of BAIBA and the significant differentially expressed genes at 4d and 8d, respectively. At 10d, gene expression did not display any significant variation. Only significant differentially expressed genes were showed. At 4d

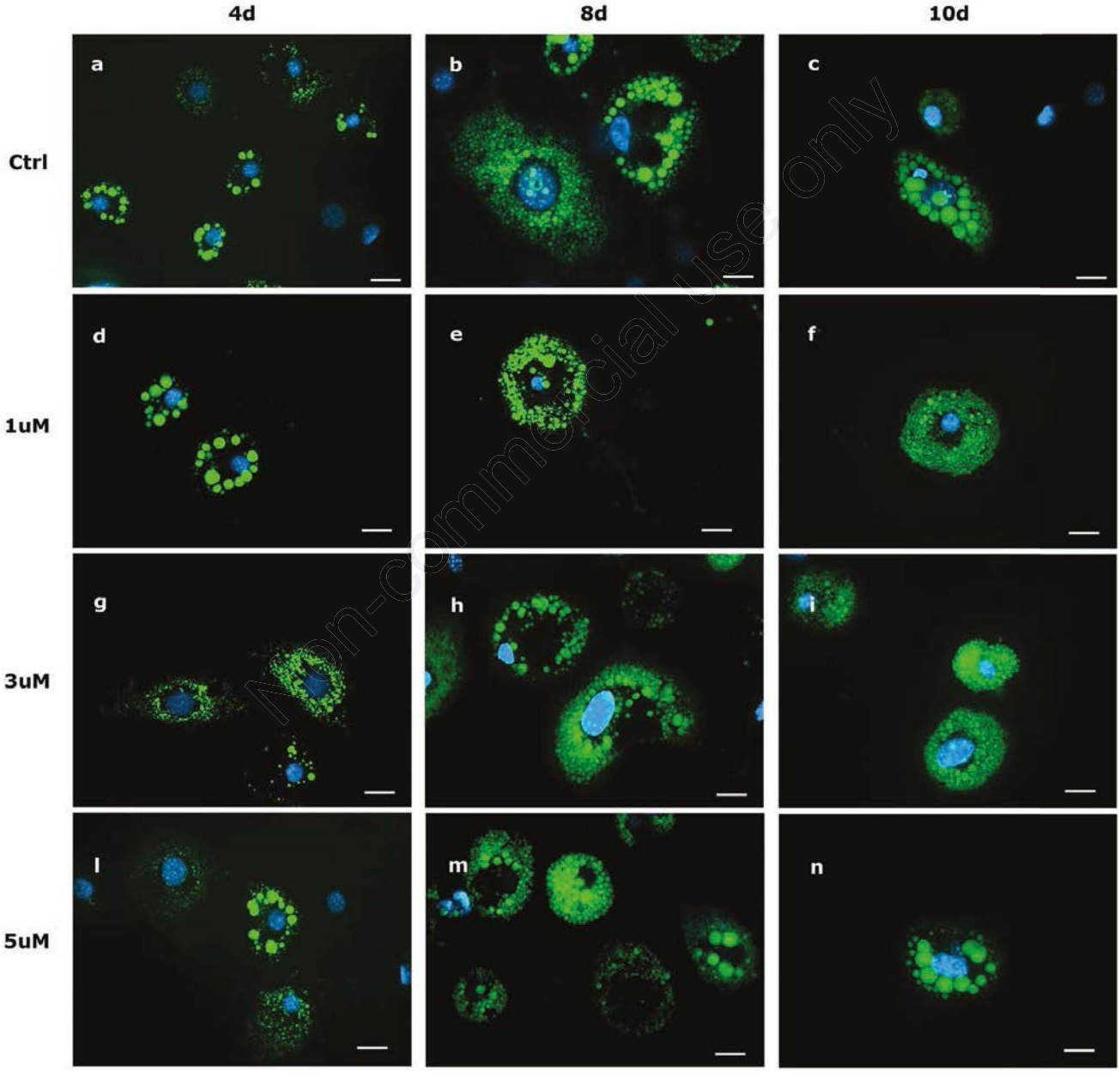

Figure 1. Lipid droplet pattern (stained with BODIPY 493/503) in fixed 3T3-L1 cells at 4d (a,d,g,l), 8d (b,e,h,m), and 10d (c,f,i,n). Control cells (a,b,c) and cells treated with 1 μM (d,e,f), 3 μM (g,h,i) and 5 μM (l,m,n) of BAIBA are shown. Nuclear staining DAPI. Images are representative of n. 5 biological replicates. Scale bars: 20 μm.

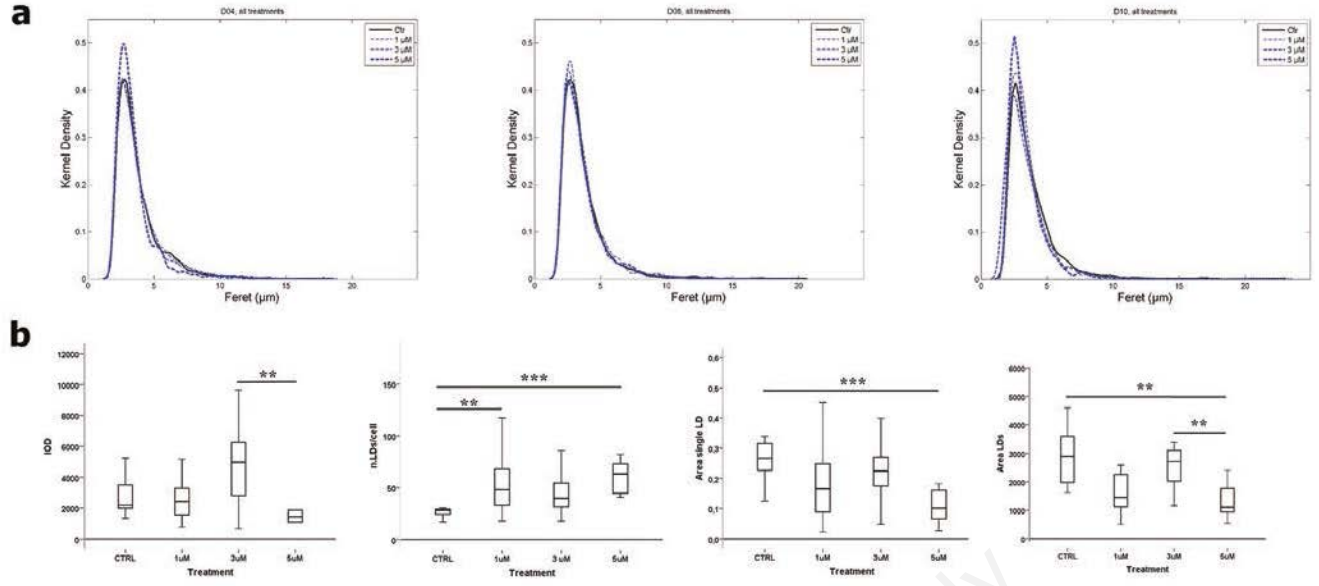

Figure 2 a) Kernel distribution of the Feret of the lipid droplets at 4, 8 and 10 days of differentiation in control and BAIBA-treated cells. b) Lipid droplet measurements on 3T3-L1 in presence of different BAIBA doses: Integrated optical density (IOD), number of LDs per cell, area of single LD after 4 days of differentiation and total area of LD and after 10 days of differentiation. Box plots show median (horizontal lines), first-to-third quartile (box), and the extreme values with the interquartile range (vertical lines). The area measures are expressed in µm² and are the average of 10 fields of each concentration. ***P<0.001, **P<0.05.

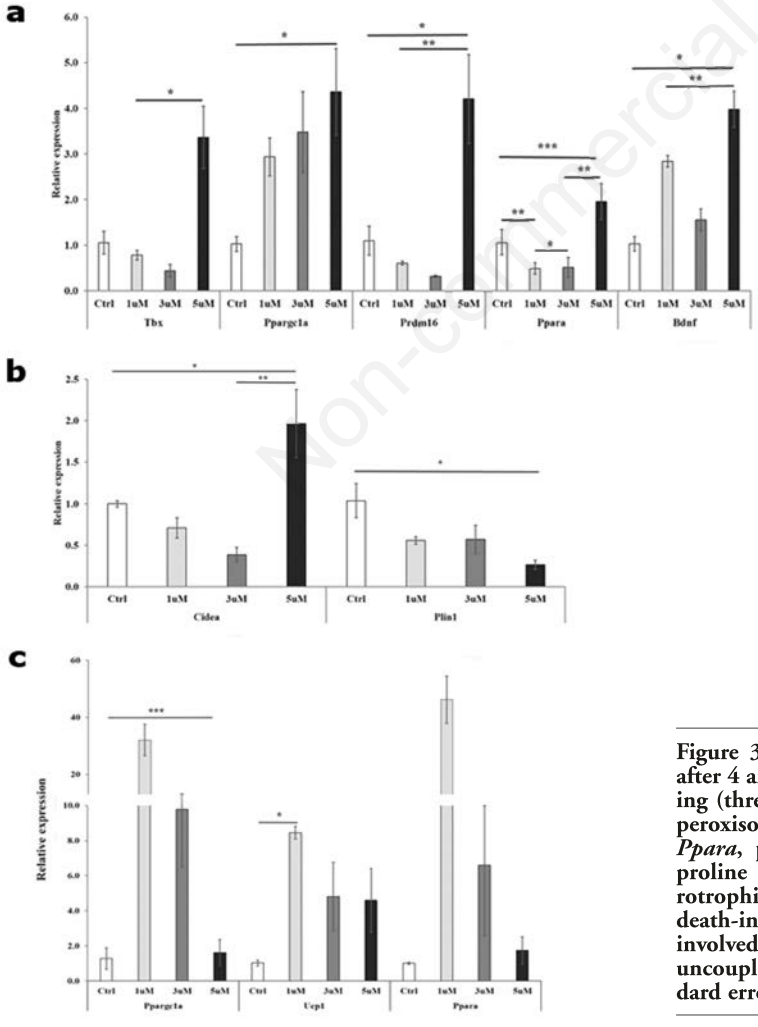

Figure 3. Differentially expressed genes between BAIBA doses after 4 and 8 days of differentiation. a) Genes involved in browning (three biological replicates) at 4d. *Tbx1*, T-box 1; *Ppargc1a*, peroxisome proliferator-activated receptor γ coactivator 1 α; *Ppara*, peroxisome proliferator-activated receptor α; *Prdm16*, proline rich domain containing 16; *Bdnf,* brain derived neurotrophic factor. b) Lipid droplets related genes at 4d. *Cidea*, cell death-inducing DFFA-like effector A; *Plin1*, perilipin 1. c) Genes involved in browning (three biological replicates) at 8d. *Ucp1*, uncoupling protein 1. Bars represent the mean plus/minus standard error of the mean (SEM). *P<0.05; **P<0.01; ***P<0.001.

the expression of *Tbx1* was significantly (P<0.05) different between 5 μM and lower doses. No significant differences were found with CTRL, maybe due to the high variability at the 5 μM dose. *Ppargc1a* (P<0.05) *Prdm16*, and *Bdnf* were up-regulated (P<0.002) at the same dose, while *Ppara* displayed significant differences for 1 μM and 5 μM in comparison to CTRL and 3 μM (Figure 3a). *Cidea* was significantly upregulated (P<0.05) at 5 μM, whereas *Plin1* showed the significantly (P<0.05) lowest expression at 5 μM in comparison to CTRL (Figure 3b).The expression of *Ppargc1a*, *Ucp1* and *Ppara* (P<0.001) was at its highest with 1 and 3 μM BAIBA doses in comparison to CTRL and 5 μM (Figure 3c).

Discussion

The present study reports the browning effect of BAIBA at different concentrations on 3T3-L1 cells at 4, 8 and 10 days of differentiation. It provides evidence showing the dynamics of LD morphology together with the expression of a panel of genes related to adaptive thermogenesis and LD formation. Although it is well established that this molecule, secreted by myocytes during exercise and circulating in blood, triggers the browning of WAT, no studies were conducted after its description by Roberts *et al*. in 2014.[15] This study tested for the first time on 3T3-L1 cells known as reliable cellular model used in obesity researches, the browning effect of BAIBA by measuring variations in morphology of LDs that have recently attracted great interest as dynamic structures at the hub of lipid and energy metabolism.

It is largely known that brown adipocytes are occupied by multilocular LDs to facilitate the efficiency of lipases and subsequent uncoupling in response to cold or other stimuli.[26] Recently, changes in LD dimension and in their associated proteins, such as CIDEC, CIDEA and PLIN1, have been demonstrated after the stimulation of browning.[6] In the present study, statistical analysis evidenced that at 4 days of differentiation and at the highest BAIBA concentration, the number of LDs per cell increased in comparison to control cells, whereas the surface area of a single LD significantly decreased. The decrease of IOD observed at the same time and concentration suggested a smaller triglyceride accumulation compared to controls. Interestingly these results occurred at 4 days of differentiation, that correspond to the peak of lipogenesis.[27] The results on LD morphology at 4d were corroborated by gene expression analysis. The browning adaptation included the up-regulation of *Ppargc1a*, *Tbx1*, *Ucp1*, *Cidea*, *Elovl3* and *Prdm16*. In particular, 5 μM BAIBA at 4d influenced the expression of *Tbx1* (Figure 3a), while the expression of *Ucp1* was induced after 8 days of differentiation (Figure 3c). This is in agreement with the results obtained on human primary subcutaneous adipocytes treated with irisin, a myokine with dubious potential role in inducing browning of white adipose tissue.[28,29] Moreover, a significant increase of *Cidea* with 5 μM BAIBA treatment (Figure 3b), but not of *Cidec*, was observed, as reported in cells obtained by primary stromal vascular fraction of inguinal WAT of mice.[15] *Cidea* is known as a brown adipocyte specific gene, related to multilocular phenotype,[8] and it is induced in WAT following cold exposure or β-adrenergic signaling.[6,30] In fact, the highest surface/volume ratio of smaller LDs increases the contact area of the LD with lipases and the subsequent facilitation of free fatty acids transport to mitochondria. CIDEA and CIDEC proteins are involved together in the fusion and enlargement of LDs, but while CIDEC is crucial in the formation of large LD in WAT, CIDEA alone is not sufficient.[27] Recently, Nishimoto *et al.* demonstrated that, in BAT, an isoform of CIDEC inhibits the homo dimerization of CIDEA and suppresses the formation of large LDs.[31] As further evidence of browning effect induced by BAIBA at 4d, *Plin1* gene was significantly down-regulated by all treatments in comparison to control (Figure 3b). In fact, perilipin 1 cooperates with CIDEC, but not with CIDEA, in inducing a super-sized, unilocular LD.[32]

After 4 days of differentiation, the expression of *Ppargc1a* and *Prdm16* was also significantly increased by 5 μM BAIBA. This is in line with *in vivo* experiments that showed that exercise training has marked effects on mitochondrial gene expression and activity in subcutaneous WAT in mice and human.[33] *Ppargc1a* controls mitochondrial biogenesis and heat production through induction of expression of *Ucp1* and other respiratory factors.[34] The higher expression level of this gene and *Prdm16*, a classic marker of brown fat, at 4d and later at 8d is coherent with the followed higher transcription of *Ucp1* (Figure 3c).

PPARα, a nuclear receptor, stimulates genes involved in mitochondrial fatty acid oxidation and increases the expression of *Ucp1* by directly interacting with *Ppargc1a* in primary murine brown adipocytes.[35] Roberts *et al*. demonstrated that browning process induced by BAIBA involved a specific *Ppara*-dependent mechanism,[15] without clarifying the upstream mechanism of action. Very recently, it has been shown that the loss of *Ppara* affected mature brown adipocytes by reducing the expression of brown markers *in vitro* but not *in vivo*, suggesting as well an important role of glycerol kinase in maintaining the activity of PPAR proteins.[36] Moreover, it should be considered that PPARα regulates *Cidea* in mouse liver without altering the expression of *Ucp1*.[37] In the present paper, the expression of *Ppara* is induced by 5 μM BAIBA at 4d and its expression was further increased at 8d with the lowest BAIBA concentration, as well as the expression of *Ppargc1a* and *Ucp1* (Figure 3c). However, at 8d no significant variations in LD morphology and number were appreciated, as observed in PPARγ2-programmed cells treated with BAIBA.[15] At 10d, BAIBA treatments did not significantly affect gene expression, although a decrease in the area of LDs was detected at the highest dose (Figure 3d).

BDNF is a neurotrophin expressed in brain, which regulates neuronal development and plasticity. However, it was also found in non-neuronal tissues, such as WAT and BAT in rodents and cows,[38,39] where it could be involved in fat metabolism and in the activation of the sympathetic response.[39,40] Moreover, mRNA and protein BDNF expression increases in human skeletal muscle after exercise, suggesting a role, as a myokine, on skeletal muscle metabolism,[41] by enhancing local and peripheral fatty acid oxidation.[42] The action of BAIBA at 4d on 3T3-L1 cells increased the *Bdnf* expression (Figure 3a), which in turn activates AMPK,[43] thus facilitating the browning conversion.

This paper demonstrated that BAIBA promotes browning phenotype on 3T3-L1 cells during first 4-8 days of differentiation. In agreement with Roberts *et al*.[15] the highest concentration during the early days of differentiation produced the strongest effect on cells in terms of LD dynamics and expression of beiging gene markers. After 8 days of differentiation, no changes were identified on LD morphology, although a browning effect was achieved as observed by brown gene marker expression. This browning effect appeared to be lost in cells after 10 days of differentiation.

The action of BAIBA significantly affects the early stage of adipocyte differentiation and can reflect a rapid adaptation of adipose tissue to physical exercise. This connection stresses the beneficial impact of physical exercise on metabolic health, providing more evidence of the preventive and therapeutic role of physical activity against obesity.

References

1. Boström P, Wu J, Jedrychowski MP, Korde A, Ye L, Lo JC et al. A PGC-1α-dependent myokine that drives brown-fat-like development of white fat and thermogenesis. Nature 2012;481:463-8.
2. Montanari T, Pošćić N, Colitti M. Factors involved in white-to-brown adipose tissue conversion and in thermogenesis: a review. Obes Rev 2017;18:495-513.
3. Wu J, Boström P, Sparks LM, Ye L, Choi JH, Giang AH, et al. Beige adipocytes are a distinct type of thermogenic fat cell in mouse and human. Cell 2012;150:366-76.
4. Shabalina IG, Petrovic N, de Jong JMA, Kalinovich AV, Cannon B, Nedergaard J. UCP1 in brite/beige adipose tissue mitochondria is functionally thermogenic. Cell Rep 2013;5:1196-203.
5. Ricquier D. UCP1, the mitochondrial uncoupling protein of brown adipocyte: a personal contribution and a historical perspective. Biochimie 2017;134:3-8.
6. Barneda D, Frontini A, Cinti S, Christian M. Dynamic changes in lipid droplet-associated proteins in the "browning" of white adipose tissues. Biochim Biophys Acta 2013;1831:924-33.
7. Yu J, Zhang S, Cui L, Wang W, Na H, Xhu X, et al. Lipid droplet remodeling and interaction with mitochondria in mouse brown adipose tissue during cold treatment. Biochim Biophys Acta 2015;1853:918-28.
8. Harms M, Seale P. Brown and beige fat: development, function and therapeutic potential. Nat Med 2013;19:1252-63.
9. Rosenwald M, Wolfrum C. The origin and definition of brite versus white and classical brown adipocytes. Adipocyte 2014;3:4-9.
10. Garcia RA, Roemmich JN, Claycombe KJ. Evaluation of markers of beige adipocytes in white adipose tissue of the mouse. Nutr Metab 2016;13:24.
11. Ikeda K, Maretich P, Kajimura S. The common and distinct features of brown and beige adipocytes. Trends Endocrinol Metab 2018;29:191-200.
12. Ruiz JR, Martinez-Tellez B, Sanchez-Delgado G, Osuna-Prieto FJ, Rensen PCN, Boon MR. Role of human brown fat in obesity, metabolism and cardiovascular disease: strategies to turn up the heat. Prog Cardiovasc Dis 2018;61:232-45.
13. Lehnig AC, Stanford KI. Exercise-induced adaptations to white and brown adipose tissue. J Exp Biol 2018; 221:jeb161570.
14. van Kuilenburg ABP, Stroomer AEM, van Lenthe H, Abeling NG, Van Gennip AH. New insights in dihydropyrimidine dehydrogenase deficiency: a pivotal role for beta-aminoisobutyric acid? Biochem J 2004;379:119-24.
15. Roberts LD, Boström P, O'Sullivan JF, Schinzel RT, Lewis GD, Dejam A, et al. β-aminoisobutyric acid induces browning of white fat and hepatic β-oxidation and is inversely correlated with cardiometabolic risk factors. Cell Metab 2014;19:96-108.
16. Kitase Y, Vallejo JA, Gutheil W, Vemula H, Jähn K, Yi J, et al. β-aminoisobutyric acid, l -BAIBA, is a muscle-derived osteocyte survival factor. Cell Rep 2018;22:1531-44.
17. Cao L, Choi EY, Liu X, Martin A, Wang C, Xu X, et al. White to brown fat phenotypic switch induced by genetic and environmental activation of a hypothalamic-adipocyte axis. Cell Metab 2011;14:324-38.
18. Yamanaka M, Tsuchida A, Nakagawa T, Nonomura T, Ono-Kishino M, Sugaru E, et al. Brain-derived neurotrophic factor enhances glucose utilization in peripheral tissues of diabetic mice. Diabetes Obes Metab 2007;9:59-64.
19. Bäcker V. ImageJ macro tool sets for biological image analysis. In: ImageJ user and developer conference. 2012.
20. Montanari T, Colitti M. Simpson-Golabi-Behmel syndrome human adipocytes reveal a changing phenotype throughout differentiation. Histochem Cell Biol 2018;149:593-605.
21. Rizzatti V, Boschi F, Pedrotti M, et al. Lipid droplets characterization in adipocyte differentiated 3T3-L1 cells: size and optical density distribution. Eur J Histochem 2013;57:24.
22. Costanzo M, Boschi F, Carton F, Conti G, Covi V, Tabaracci G, et al. Low ozone concentrations promote adipogenesis in human adipose-derived adult stem cells. Eur J Histochem 2018; 62:2969.
23. Ramírez-Zacarías JL, Castro-Muñozledo F, Kuri-Harcuch W. Quantitation of adipose conversion and triglycerides by staining intracytoplasmic lipids with Oil red O. Histochemistry 1992;97:493-7.
24. Rozen S, Skaletsky H. Primer3 on the WWW for general users and for biologist programmers. Methods Mol Biol 2000;132:365-86.
25. Rao X, Huang X, Zhou Z, Lin X. An improvement of the 2ˆ(-delta delta CT) method for quantitative real-time polymerase chain reaction data analysis. Biostat Bioinforma Biomath 2013;3:71-85.
26. Cinti S. The adipose organ at a glance. Dis Model Mech 2012;5:588-94.
27. Barneda D, Christian M. Lipid droplet growth: regulation of a dynamic organelle. Curr Opin Cell Biol 2017;47: 9-15.
28. Kristóf E, Doan-Xuan Q-M, Bai P, Bacso Z, Fésüs L. Laser-scanning cytometry can quantify human adipocyte browning and proves effectiveness of irisin. Sci Rep 2015;5: 12540.
29. Hofmann T, Elbelt U, Stengel A. Irisin as a muscle-derived hormone stimulating thermogenesis - a critical update. Peptides 2014;54:89-100.
30. Rosell M, Kaforou M, Frontini A, Okolo A, Chan YW, Nikolopoulou E, et al. Brown and white adipose tissues: intrinsic differences in gene expression and response to cold exposure in mice. Am J Physiol Endocrinol Metab 2014;306:E945-64.
31. Nishimoto Y, Nakajima S, Tateya S, Saito M, Ogawa W, Tamori Y. Cell death-inducing DNA fragmentation factor A-like effector A and fat-specific protein 27β coordinately control lipid droplet size in brown adipocytes. J Biol Chem 2017;292:10824-34.
32. Grahn THM, Zhang Y, Lee M-J, Sommer AG, Mostoslavsky G, Fried SK, et al. FSP27 and PLIN1 interaction promotes the formation of large lipid droplets in human adipocytes. Biochem Biophys Res Commun 2013;432:296-301.
33. Dewal RS, Stanford KI. Effects of exercise on brown and beige adipocytes. Biochim Biophys Acta Mol Cell Biol Lipids 2019;1864:71-8.
34. Wu Z, Puigserver P, Andersson U, Zhang C, Adelmant G, Mootha V, et al. Mechanisms controlling mitochondrial biogenesis and respiration through the thermogenic coactivator PGC-1. Cell 1999;98:115-24.
35. Barbera MJ, Schluter A, Pedraza N, Iglesias R, Villarroya F, Giralt M. Peroxisome proliferator-activated receptor alpha activates transcription of the brown fat uncoupling protein-1 gene. A link between regulation of the thermogenic and lipid oxidation pathways in the brown fat cell. J Biol Chem 2001;276:1486-93.
36. Lasar D, Rosenwald M, Kiehlmann E, Balaz M, Tall B, Opitz L, et al. Peroxisome proliferator activated receptor gamma controls mature brown adipocyte inducibility through glycerol kinase. Cell Rep 2018;22:760-73.
37. Viswakarma N, Yu S, Naik S, Kashireddy P, Matsumoto K, Sarkar J, et al. Transcriptional regulation of

Cidea, mitochondrial cell death-inducing DNA fragmentation factor alpha-like effector A, in mouse liver by peroxisome proliferator-activated receptor alpha and gamma. J Biol Chem 2007;282:18613-24.
38. Sornelli F, Fiore M, Chaldakov GN, Aloe L. Adipose tissue-derived nerve growth factor and brain-derived neurotrophic factor: results from experimental stress and diabetes. Gen Physiol Biophys 2009;28:179-83.
39. Colitti M, Loor JJ, Stefanon B. Expression of NGF, BDNF and their receptors in subcutaneous adipose tissue of lactating cows. Res Vet Sci 2015;102:196-9.
40. Chaldakov GN, Fiore M, Tonchev AB, Aloe L. Neuroadipology: a novel component of neuroendocrinology. Cell Biol Int 2010;34:1051-3.
41. Matthews VB, Aström M-B, Chan MHS, Bruce CR, Krabbe KS, Prelovsek O, et al. Brain-derived neurotrophic factor is produced by skeletal muscle cells in response to contraction and enhances fat oxidation via activation of AMP-activated protein kinase. Diabetologia 2009;52:1409-18.
42. Pedersen BK, Pedersen M, Krabbe KS, Bruunsgaard H, Matthews VB, Febbraio MA. Role of exercise-induced brain-derived neurotrophic factor production in the regulation of energy homeostasis in mammals. Exp Physiol 2009;94:1153-60.
43. Pedersen BK, Febbraio MA. Muscles, exercise and obesity: skeletal muscle as a secretory organ. Nat Rev Endocrinol 2012;8:457-65.

Relationship between lipid droplets size and integrated optical density

Federico Boschi,[1] Vanni Rizzatti,[2] Elena Zoico,[2] Tommaso Montanari,[3] Mauro Zamboni,[2] Andrea Sbarbati,[4] Monica Colitti[3]

[1]Department of Computer Science, University of Verona
[2]Department of Medicine, Geriatric Section, University of Verona
[3]Department of Agricultural, Food, Environmental and Animal Sciences, University of Udine
[4]Department of Neuroscience, Biomedicine and Movement Sciences, University of Verona, Italy

Abstract

Lipid accumulation is largely investigated due to its role in many human diseases. The attention is mainly focused on the lipid droplets (LDs), spherical cytoplasmic organelles which are devoted to the storage of the lipids. The amount of lipid content is often evaluated by measuring LDs size and/or the integrated optical density (IOD) in cultured cells. Both evaluations are directly associated to the lipid content and therefore they are correlated to each other, but a lack of theoretical relationship between size and IOD was observed in literature. Here we investigated the size-IOD relationship of LDs observed in microscopical images of cultured cells. The experimental data were obtained from immature and differentiated 3T3-L1 murine cells, which have been extensively used in studies on adipogenesis. A simple model based on the spherical shape of the LDs and the Lambert-Beer law, which describes the light absorption by an optical thick material, leads to a mathematical relationship. Despite only light rays' absorption was considered in the model, neglecting their scattering, a very good agreement between the theoretical curve and the experimental data was found. Moreover, a computational simulation corroborates the model indicating the validity of the mathematically theoretical relationship between size and IOD. The theoretical model could be used to calculate the absorption coefficient in the LDs population and it could be applied to seek for morphologically and functionally LDs subpopulations. The identification of LDs dynamic by measuring size and IOD could be related to different pathophysiological conditions and useful for understand cellular lipid-associated diseases.

Introduction

Many widespread diseases in humans, like type 2 diabetes mellitus, cardiovascular dysfunction, hypertension, metabolic syndromes, and some type of cancers are related to excessive accumulation of triglycerides,[1,2] which are stored in cells cytoplasm in form of lipid droplets (LDs).[3,4] The evaluation of the lipid content plays also a key role in the assessment of the effects of drugs and nutraceuticals acting on fat accumulation.[5-7] This evaluation is often obtained by measuring the size of the LDs or the integrated optical density (IOD) of the LDs, usually reporting their mean values in a cell. The last evaluation is based on staining the LDs with neutral lipid specific markers, such as Oil red O, and acquiring images with light microscope equipped with specific optical filters. IOD considers the absorption of the light incident on the entire LD registered on the images.

Recently, different groups suggested to use the size distribution of the LDs instead the mean size because the distribution is more informative with respect to the single mean value.[8-13] Moreover, regarding the LDs size, the Feret diameter is often used being a measure unbiased by the investigator and automatically reported by many software programs for image analysis. Finally, the kernel distribution of the LDs Feret, which is independent of the bin size of the histograms, is suggested.[8] However, the IOD of the LDs is assumed to quantify the fat accumulation. Many different studies were conducted by using the Oil red O staining and it was found that, *i.e.*, in muscle fibers IOD significantly increased in obesity and is reduced with weight loss.[14-16] IOD is also related with the triglycerides content of 3T3-L1 adipocytes.[14] 3T3-L1 is a cell line widely used as an *in vitro* model of white adipocytes and has extensively contributed to understand adipogenesis and lipid metabolism.[17,18]

In adipocytes, as the lipid content increases, an expansion of the size of the LDs is observed, leading to an increment in the IOD, thus volume and IOD measurements must be correlated. Nevertheless, at the best of our knowledge, a mathematical relationship is not reported in literature. The aim of this study was to investigate the size-IOD relationship on the experimental data obtained in cultured 3T3-L1 cells, adopting a simple theoretical model and a computational model.

Correspondence: Federico Boschi, Department of Computer Science, University of Verona, Strada Le Grazie 15, 37134 Verona, Italy.
E-mail: federico.boschi@univr.it

Key words: Lipid droplet; 3T3-L1; adipocyte; triglyceride accumulation; integrated optical density; Feret diameter.

Acknowledgments: The authors would like to acknowledge Dr. Marco Gerosa for helpful discussion and critical reading of the manuscript.

Received for publication: 18 January 2019.
Accepted for publication: 9 March 2019.

European Journal of Histochemistry 2019; 63:3017
doi:10.4081/ejh.2019.3017

Materials and Methods

Cell culture and Oil Red O staining

3T3-L1 cells (ECACC Sigma-Aldrich) were cultured at 37°C in a 5% CO_2 atmosphere in 250 mL polystyrene sterilized flasks with 0.2 µm vented plug seal cap (Becton Dickinson, Franklin Lakes, NJ, USA); as a culture medium, DMEM/GlutaMAX was used containing 10% of fetal bovine serum (FBS) and 1% of antibiotic antimycotic solution. After reaching a concentration of 2.5-3.0x10^6 cells (confluence 85-90%), 3T3-L1 cells were detached by trypsin-EDTA and seeded in 4-wells Bio Coat™ Culture Slides (Becton Dickinson). Two days after confluence in wells, cells were washed three times with PBS and differentiation was induced in DMEM/F12 containing 10% FBS, 1% antibiotic antimycotic solution, 0.2 mM IBMX, 10 µM rosiglitazone, 1 µM dexamethasone, 10 µg/mL insulin for three days. After 72 h, the cells were washed three times with PBS, and the medium was replaced with the adipocytes maintaining medium (AMM: DMEM/F12 enriched with 10% FBS, 1% antibiotic antimycotic solution, 10 µg/mL insulin) in which the cells were cultured for 2 days. The cell cultures were washed with 0.1 M PBS pH 7.4 and fixed for 20 min with 4% formalin in 0.05 M PBS; after washing with sterile double distilled water and 60% isopropanol for 2 min, the cells were stained with 0.35% Oil Red O solution in 60% isopropanol for 10 min at room temperature. Then the cells

were washed with sterile double distilled water and stained with Mayer's Hematoxylin (Bio-Optica, Milan, Italy) for 1 min at room temperature, washed with sterile double distilled water, and finally mounted in Dako faramount aqueous mounting medium (Agilent, Carpinteria, CA, USA).

Imaging

Cells were observed in an Olympus BX51 photomicroscope equipped with a KY-F58 CCD camera (JVC) using the software Image-ProPlus. Around 1400 LDs in fibroblast-like (FBL-LDs) and 800 LDs in mature adipocyte (MA-LDs) after 5 days of differentiation were measured. The time-point was selected to include a large variety of sized LDs in the analysis.

For each LD the maximum Feret's diameter (MFD) and the IOD were measured by using ImageJ software (National Institutes of Health, Bethesda, MD, USA). The MFD is the maximum distance of the object measurable with a caliper and is widely used in optical microscopy and named briefly "Feret".[19] The measures were analyzed with routines written in Matlab 7.0 (Mathworks, Nathick, MA, USA).

Theoretical model

Assuming that the light incident on a LD is composed of parallel rays passing through the LD without any change in the travelling direction (*i.e.*, scattering is neglected) and the absorption coefficient is homogeneous on the entire LDs volume, a very simple relationship between size and IOD of the LDs can be obtained.

The optical density (OD) is defined as the logarithm with base 10 of the ratio between intensity of incident light and intensity of transmitted light,[20] *i.e.*:

$$OD = log_{10} \frac{I_{incident}}{I_{transmitted}} \quad \text{(eq. 1)}$$

For a monochromatic ray incident on a slab of material, the relationship between intensity of the transmitted light (I) and the intensity of the incident light (I_0) is expressed by the Lambert-Beer law:[21]

$$I = I_0 \, e^{-\mu t} \quad \text{(eq. 2)}$$

where μ is the attenuation (absorption, cm^{-1}) coefficient and t (cm) the thickness of the slab.

The incident light on the entire LD is the sum of the intensity of each ray incident on the LD surface, *i.e.*, $I_{incident} = I_o \pi R^2$. The transmitted light, exiting from the entire LD, is the sum of the intensity of each light ray which individually follows the Lambert-Beer law (eq. 2). So, the intensity of the transmitted light can be expressed as $I_{transmitted} = Io\ A$, where A is a parameter which takes into account the total absorption contribution. Thus, the OD of the entire LD, named integrated optical density (IOD), can be written as:

$$IOD = log_{10} \frac{I_0 \, \pi \, R^2}{I_0 \, A} = log_{10} \frac{\pi \, R^2}{A} \quad \text{(eq. 3)}$$

where R is the radius of the LD, supposed to be a spherical droplet.[8] The parameter A can be calculated as follows: considering a circumference of radius r in the equatorial plane of the LD (perpendicular to the light rays), all its points are reached by the light through paths of the same length x from the surface of the LD (Figure 1C), thus the total absorption contribution can be calculated multiplying by the length $2\pi r$ and integrating, which gives:

$$A = \int_0^R 2\pi r \, e^{-2\mu x} dr \quad \text{(eq. 4)}$$

where the contribution of the entire sphere (over and below the equatorial plane) was evaluated, so that eq. 2 is applied with $t=2x$.

Since r and x are related by the Pythagorean law

$$r^2 + x^2 = R^2 \quad \text{(eq. 5)}$$

and consequently $2rdr = -2xdx$, it follows that

$$A = -2\pi \int_R^0 x \, e^{-2\mu x} dx = 2\pi \int_0^R x \, e^{-2\mu x} dx \quad \text{(eq. 6)}$$

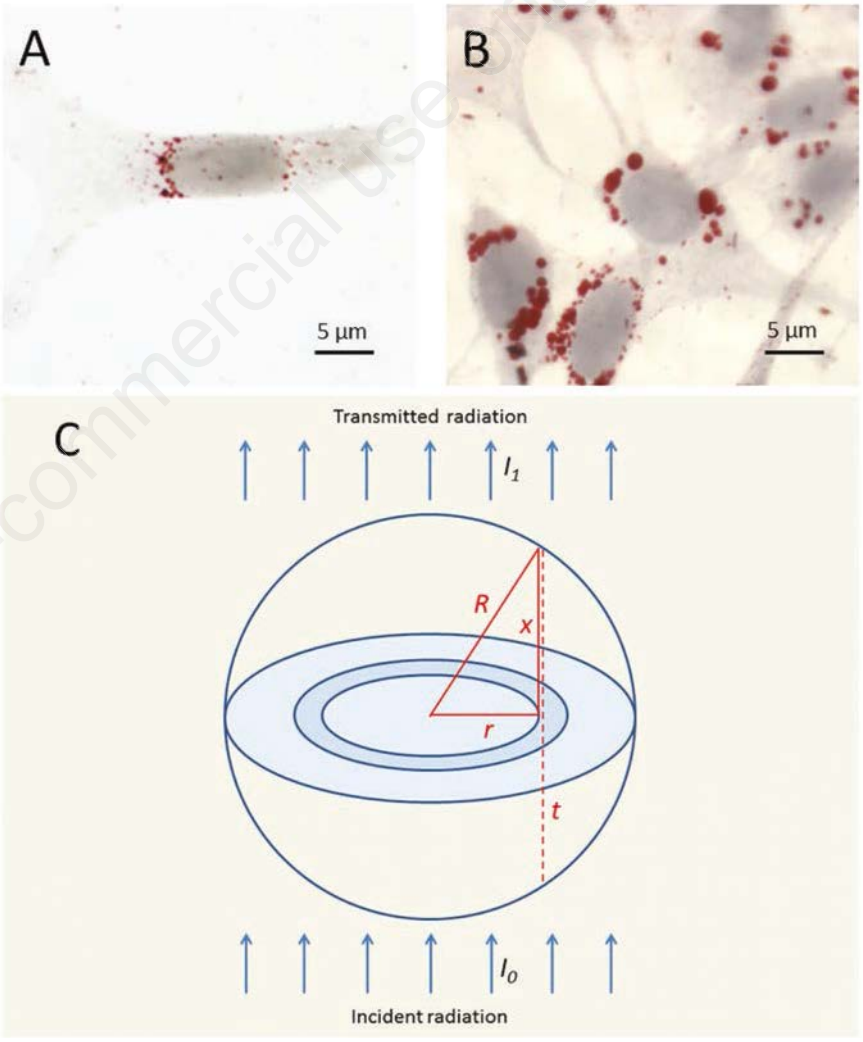

Figure 1. 373-L1 immature cells show many LDs in the cytoplasm characterized by small dimensions (A); inducing lipid accumulation, 3T3-L1 cells differentiate in adipocytes showing LDs with bigger size (B). A graphical representation of a LD, which absorbs the light rays of the incident radiation coming from the bottom (C). In light blue the LD's equatorial plane perpendicular to the light rays and in darker color the annulus for the absorption evaluation.

taking into account that, when $r = 0$ $x = R$ and when $r = R$ $x = 0$.
Integrating by parts with $f(x) = x$ and $dg(x)/dx = e^{-2\mu x}$, A results:

$$A = 2\pi\left\{\left[x\,\frac{e^{-2\mu x}}{-2\mu}\right]_0^R - \int_0^R \frac{e^{-2\mu x}}{-2\mu}\,dx\right\} \quad \text{(eq. 7)}$$

then

$$A = 2\pi\left\{-\frac{Re^{-2\mu R}}{2\mu} + \frac{1}{2\mu}\left[\frac{e^{-2\mu x}}{-2\mu}\right]_0^R\right\} \quad \text{(eq. 8)}$$

and finally

$$A = \frac{\pi}{2\mu^2}[1 - (1 + 2\mu R)e^{-2\mu R}] \quad \text{(eq. 9)}$$

Consequently, it follows that:

$$IOD = log_{10}\frac{\pi R^2}{A} = log_{10}\frac{2\mu^2 R^2}{1-(1+2\mu R)e^{-2\mu R}} \quad \text{(eq. 10)}$$

which expresses the dependence of IOD by the radius and the optical properties of the LD.

Computational model

A computational model was written in Matlab. The simulated light source is a square composed by 100x100 light rays. As assumed in the theoretical model, the LD is considered as a spherical object with radius R, with homogeneous distribution of the absorption coefficient μ. For each light ray passing at a distance r from the center of the sphere the Lambert-Beer law is applied and the intensity of the emerging light rays is calculated, taking into account the height of the LD at distance r. Again, the rays are supposed to travel straightforward without change in the direction at the surface of sphere and inside the sphere. The limits of this assumption are discussed in the last section.

The parameter A is evaluated for LDs with radius R increasing from 0 to half sides of the light square. The IOD is calculated as reported in eq. 10.

Results

Theoretical model and experimental data

Figure 2A shows the experimental data obtained measuring the Feret and the IOD of the LDs in both not differentiated (FBL) and differentiated adipocytes (MA) in order to obtain a large spread in size and IOD values. As expected, increasing the LDs' size, the IOD increases. The curves representing the best fit of the experimental data overlaid on the experimental data themselves are shown. The curves represent the size-IOD relationship based on eq. 10. The best fits are obtained with $\mu = 9.4486$ cm^{-1} for FBL-LDs and with $\mu = 8.5357$ cm^{-1} MA-LDs.

Computational model

The output of the computational model is shown in Figure 2B. It represents the size-IOD relationship obtained increasing the radius of the simulated LDs. Again, as in the theoretical model, increasing R the IOD increases. In the evaluation of the parameter A the value of $\mu = 8.5357$ cm^{-1}, obtained by the fit of the experimental data for the MA-LDs, was inserted. It is noteworthy that the results simulate very well the experimental data. The dispersion in the simulated data is due to the discontinuities in the number of light rays intercepted by the LD increasing the radius x.

Discussion

The theoretical model assumed in this study is based on the regular geometry of the LDs,[8] the homogeneous distribution of the absorption coefficient of the marker (Oil Red O) and the negligibility of the light scattering. The model leads to very simple relationship between size and IOD. In order to evaluate the absorption of the entire LD, the real direction of the light rays is less important than the absorption of each ray and the hypothesis that scattering is negligible is supported by the very good agreement between theoretical and experimental data. The computational model also predicts the size-IOD relationship found theoretically.

A very important aspect for the size-IOD relationship is the contrast of the images both in the acquisition procedure as in the post-processing steps. An example of

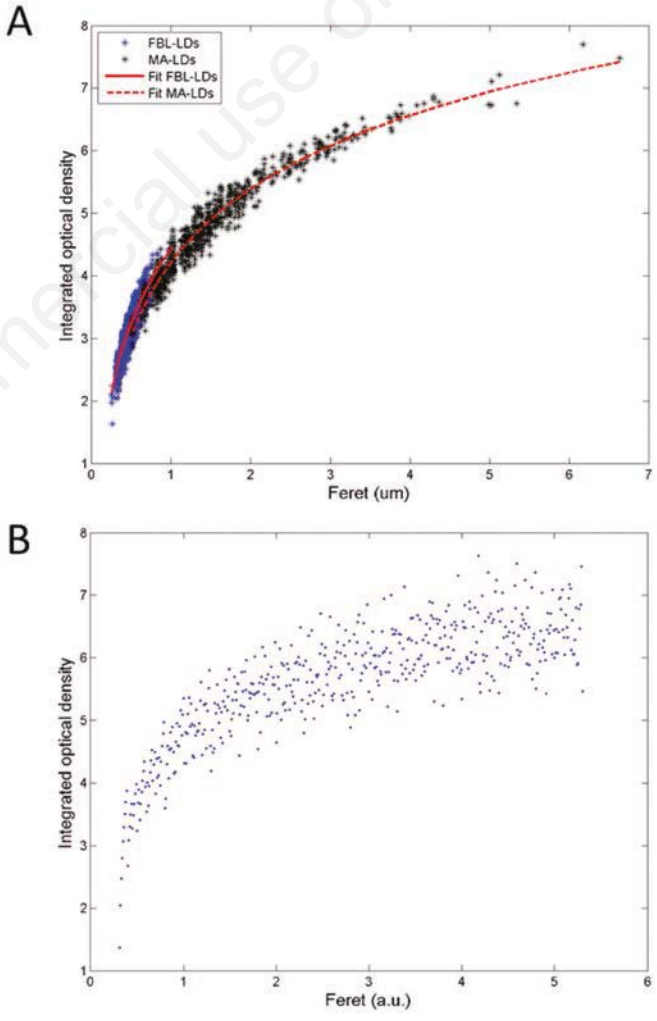

Figure 2. Experimental data (Feret *vs* IOD) of the LDs in both not differentiated (FBL, blue stars) and differentiated adipocytes (MA, black stars); the curves represent the best fit (based on eq. 10) of the experimental data (A). Computational results obtained simulating the interaction between light rays and a homogeneous absorbing sphere with increasing radius (B).

the effects of the post processing contrast variation on the relationship is shown in Figure 3C, where IOD measures were done on the images contrasted differently in order to increase the definition of the LDs' borders. In this case, the plot leads to a misleading interpretation of the data showing the presence of two or more LDs subpopulations, characterized by different optical properties and consequently different staining, which could indicate different chemical composition.

Slight variations during the staining process (temperature, duration) can affect the IOD measurements and they have to be considered in order to reduce the scattering of experimental data around the theoretical curve. The imaging process should be also carefully managed, in fact, microscopical observations must be done in one day after Oil red O staining to avoid the effects due to the marker instability, or to store them at -20 degrees.

Without changing light contrast modifications of the images, the theoretical model can be used to calculate the absorption coefficient in the LDs population and it could be really useful to seeking for morphologically and functionally LDs subpopulations, as recent studies suggested.[22] The identification of LDs dynamic by measuring Feret and IOD could be related to different pathophysiological conditions and to better understand cellular lipid-associated diseases.

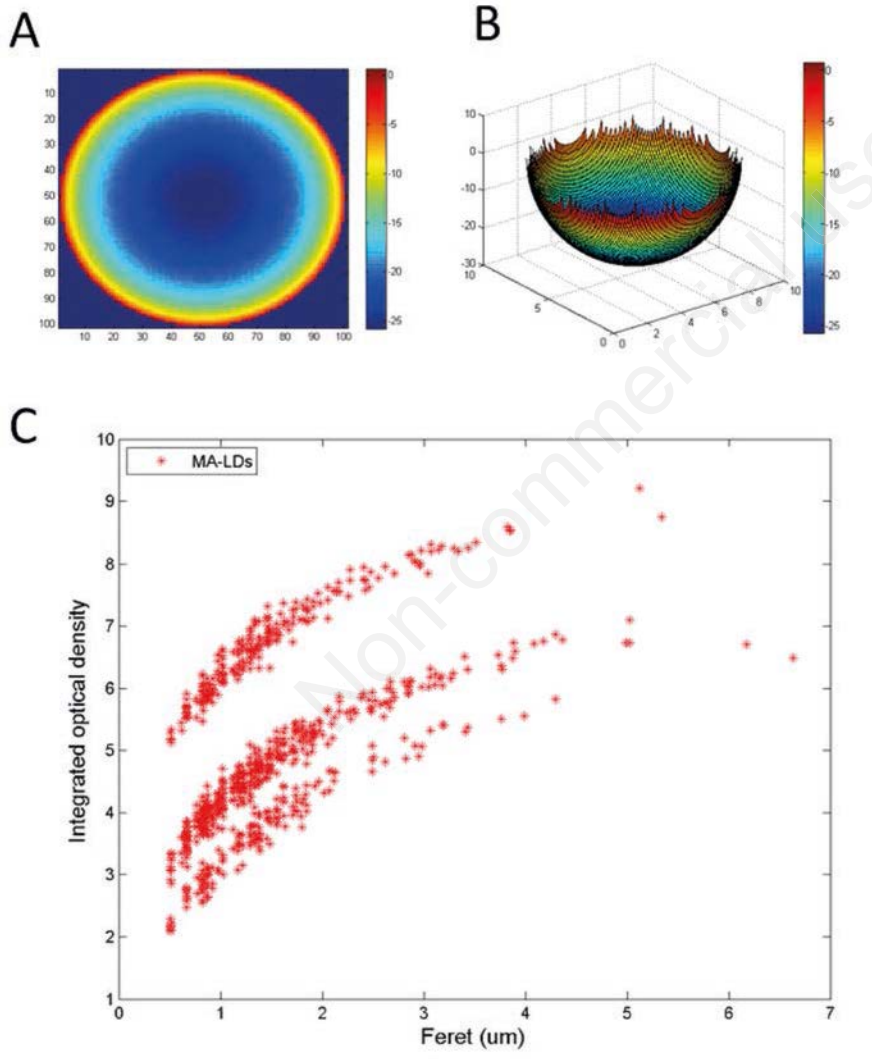

Figure 3. Evaluation of the logarithm of the parameter A (eq. 9) for each light ray passing thought the LD following the computational model; a squared light source of 100 x100 rays is considered below the LD and a LD with increasing radius from 0 to half of the size of the light source is evaluated (A). The same as (A) in a 3D visualization (B). Effects of the image contrast modification during the IOD evaluation can lead to a separation between the LDs, which can be interpreted as the presence of LDs subpopulations with different optical properties (C).

References

1. Grundy SM. Obesity, metabolic syndrome, and cardiovascular disease. J Clin Endocrinol Metab 2004;89:2595-600.
2. Haslam DW, James WP. Obesity. Lancet 2005;366:1197-209.
3. Thiele C, Spandl J. Cell biology of lipid droplets. Curr Opin Cell Biol 2008;20: 378-85.
4. 4.Guo Y, Cordes KR, Farese RV Jr, Walther TC. Lipid droplets at a glance. J Cell Sci 2009;122:749-52.
5. Stringer DM, Zahradka P, Declercq VC, Ryz NR, Diakiw R, Burr LL, et al. Modulation of lipid droplet size and lipid droplet proteins by trans-10,cis-12 conjugated linoleic acid parallels improvements in hepatic steatosis in obese, insulin-resistant rats. Biochim Biophys Acta 2010;1801:1375-85.
6. Costanzo M, Boschi F, Carton F, Conti G, Covi V, Tabaracci G, et al. Low ozone concentrations promote adipogenesis in human adipose-derived adult stem cells. Eur J Histochem 2018; 62:2969.
7. Colitti M, Boschi F, Montanari M. Dynamic of lipid droplets and gene expression in response to β-aminoisobutyric acid treatment on 3T3-L1 cells. Eur J Histochem 2018;62:2984.
8. Rizzatti V, Boschi F, Pedrotti M, Zoico E, Sbarbati A, Zamboni M. Lipid droplets characterization in adipocyte differentiated 3T3-L1 cells: size and optical density distribution. Eur J Histochem 2013;57:e24.
9. Boschi F, Rizzatti V, Zamboni M, Sbarbati. A Lipid droplets fusion in adipocyte differentiated 3T3-L1 cells: a Monte Carlo simulation. Exp Cell Res 2014;321:201-8.
10. Boschi F, Rizzatti V, Zamboni M, Sbarbati A. Models of lipid droplets growth and fission in adipocyte cells. Exp Cell Res 2015;336:253-62.
11. Moisan A, Lee YK, Zhang JD, Hudak CS, Meyer CA, Prummer M, et al. White-to-brown metabolic conversion of human adipocytes by JAK inhibition. Nat Cell Biol 2015;17:57-67.
12. Boschi F, Rizzatti V, Zamboni M, Sbarbati A. Simulating the dynamics of lipid droplets in adipocyte differentiation. Comput Methods Programs Biomed 2017;138:65-71.
13. Shoham N, Gefen A. Stochastic modeling of adipogenesis in 3T3-L1 cultures to determine probabilities of events in the cell's life cycle. Ann Biomed Eng 2011;39:2637-53.
14. Ramírez-Zacarías JL, Castro-Muñozledo F, Kuri-Harcuch W.

Quantitation of adipose conversion and triglycerides by staining intracytoplasmic lipids with Oil red O. Histochemistry 1992;97:493-7.
15. Goodpaster BH, Theriault R, Watkins SC, Kelley DE. Intramuscular lipid content is increased in obesity and decreased by weight loss. Metabolism 2000;49:467-72.
16. Porzionato A, Sfriso MM, Macchi V, Rambaldo A, Lago G, Lancerotto L, et al. Decellularized omentum as novel biologic scaffold for reconstructive surgery and regenerative medicine. Eur J Histochem 2013;57:e4.
17. Li P, Carter G, Romero J, Gower KM, Watson J, Patel NA, et al. Clk/STY (cdc2-like kinase 1) and Akt regulate alternative splicing and adipogenesis in 3T3-L1 pre-adipocytes. PLoS One 2013;8:e53268.
18. Ruiz-Ojeda FJ, Rupérez AI, Gomez-Llorente C, Gil A Aguilera CM. Cell models and their application for studying adipogenic differentiation in relation to obesity: A review. Int J Mol Sci 2016;17:pii: E1040.
19. Walton WH. Feret's statistical diameter as a measure of particle size. Nature 1948;162:329-30.
20. McNaught AD, Wilkinson A. Compendium of chemical terminology, 2nd ed. Research Triangle Park, IUPAC: 1997.
21. Beer A. Bestimmung der Absorption des rothen Lichts in farbigen Flüssigkeiten. Ann Physik Chemie 1852;86:78-88.
22. Zhang S, Wang Y, Cui L, Deng Y, Xu S, Yu J, et al. Morphologically and functionally distinct lipid droplet subpopulations. Sci Rep 2016;6:29539.

frontiers in Physiology

ORIGINAL RESEARCH
published: 05 November 2019
doi: 10.3389/fphys.2019.01380

Comparison of the Effects of Browning-Inducing Capsaicin on Two Murine Adipocyte Models

Tommaso Montanari[1], *Federico Boschi*[2] *and Monica Colitti*[1]*

[1] *Department of Agricultural, Food, Environmental and Animal Sciences, University of Udine, Udine, Italy,* [2] *Department of Computer Science, University of Verona, Verona, Italy*

The increasing prevalence of obesity and its associated comorbidities has gained attention in developing effective treatments and strategies that promote energy expenditure and the conversion of fat from a white to a brite phenotype. Capsaicin, bioactive component of chili peppers and a transient receptor potential channel vanilloid 1 (TRPV1) agonist, has been known to stimulate the process of thermogenesis. In this study, the effects of capsaicin were assessed on two murine cellular models by quantifying the dynamic of lipid droplets (LDs) and the expression of genes involved in adipocyte browning. Present findings demonstrated that treatment with norepinephrine or capsaicin combined with norepinephrine on 3T3-L1 cells and X9 cells significantly promoted the reduction of LDs area surface and size. The transcription of browning related genes such as uncoupling protein 1 (*Ucp1*), T-box transcription factor 1 (*Tbx1*), PR domain containing 16 (*Prdm16*), peroxisome proliferator-activated receptor γ coactivator 1α (*Ppargc1a*) and cell death-inducing DNA fragmentation factor A-like effector A (*Cidea*) was up-regulated by chronic capsaicin treatment on differentiated 3T3-L1 cells. Instead, X9 cells were significantly responsive only to the treatment with norepinephrine, used as positive control.

Keywords: lipid droplets, 3T3-L1, X9, adipocytes, capsaicin, thermogenesis

OPEN ACCESS

Edited by:
Anna Maria Giudetti,
University of Salento, Italy

Reviewed by:
Daniele Vergara,
University of Salento, Italy
Patrick Tso,
University of Cincinnati, United States
Rai Ajit K. Srivastava,
Gemphire Therapeutics, United States

***Correspondence:**
Monica Colitti
monica.colitti@uniud.it

Specialty section:
This article was submitted to Lipid and Fatty Acid Research, a section of the journal Frontiers in Physiology

Received: *06 August 2019*
Accepted: *21 October 2019*
Published: *05 November 2019*

Citation:
Montanari T, Boschi F and Colitti M (2019) Comparison of the Effects of Browning-Inducing Capsaicin on Two Murine Adipocyte Models. Front. Physiol. 10:1380. doi: 10.3389/fphys.2019.01380

INTRODUCTION

In recent years, research on adipose tissue biology and obesity has recognized in browning of white adipose tissue (WAT) a potential therapeutic strategy for the treatment of obesity and related morbidities (Peschechera and Eckel, 2013; Bartelt and Heeren, 2014). Unlike fat-accumulating WAT, brown adipose tissue (BAT) promotes the dissipation of energy deriving from the catabolism of fatty acids in form of heat. This process is known as thermogenesis and is driven by mitochondrial proton pump uncoupling protein 1 (UCP1) (Cannon and Nedergaard, 2004). The discovery of physiologically active BAT in adult humans (Cypess et al., 2009; Gifford et al., 2016) opened the investigation on therapeutic strategies for obesity based not only on the reduction of energy intake, but also on the increase of energy expenditure through the conversion of white adipocytes into brown-like ones, named beige or brite (brown-in-white) adipocytes (Wu et al., 2012).

The activation of BAT and the recruitment of brite adipocytes in WAT depots is mainly driven by cold exposure, which triggers a sympathetic response that induces the release of norepinephrine (NE) from sympathetic neurons and the activation of β_3 adrenoreceptors on the membrane of adipocytes. This produces a signaling cascade involving protein kinase A (PKA) and p38

mitogen activated protein kinase (MAPK), which results in the expression of *Ucp1* and other key transcription factors involved in the activation of thermogenesis (Cannon and Nedergaard, 2004). Thermogenically active adipocytes show a different architecture of organelles than white fat cells. Brown and brite adipocytes accumulate triglycerides in a multilocular depot, hence their cytoplasm shows a high number of small lipid droplets (LDs) (Montanari and Colitti, 2018). This organization optimizes the process of lipolysis, in order to provide fatty acids promptly driven to fuel thermogenesis (Gao and Houtkooper, 2014). The dynamic of LDs in adipocytes is regulated by LD-linked proteins, with a role in LD enlargement and fusion. In murine BAT, members of cell death-inducing DNA fragmentation factor A (DFFA)-like effector (CIDE) protein family CIDEA and CIDEC are the main effectors of LD fusion. While CIDEC is expressed in both WAT and BAT and is crucial in generating the unilocular fat depot in white adipocytes (Nishimoto and Tamori, 2017), CIDEA is restricted to BAT, at least in mice, and it is not sufficient to induce the formation of supersized, white-like LDs by itself (Barneda and Christian, 2017).

Research on browning is currently focused in the individuation of both endogenous and exogenous molecules that could trigger the recruitment of thermogenically active brite adipocytes in WAT depots; up to date, a plethora of such molecules has been characterized, as largely reviewed (Montanari et al., 2017). Among these chemicals, natural compounds have gained a great interest, as they can be used as nutraceuticals to prepare functional foods with therapeutic properties.

Capsaicin belongs to a class of alkaloids, named capsaicinoids, found in the fruit of *Capsicum* spp. (hot pepper), which is responsible for the spicy flavor (Reyes-Escogido Mde et al., 2011). Its biological effects derive from the interaction with the transient receptor potential vanilloid 1 (TRPV1), a transmembrane receptor expressed mainly in peripheral sensory neurons involved in pain sensation (Bevan et al., 2014), widely distributed in the gastrointestinal tract (Yu et al., 2016), but also in adipose tissue (Bishnoi et al., 2013). The activation of TRPV1 by capsaicin opens the receptor's ion channel, which allows the accumulation of intracellular Ca^{2+}. Growing levels of Ca^{2+} activate the Ca^{2+}/calmodulin-activated protein kinase (CaMKII), which in turn phosphorylates the cAMP-activated protein kinase (AMPK) and, finally, sirtuin 1 (SIRT1). The activated SIRT1 deacetylases the positive regulatory domain containing 16 (PRDM16) and peroxisome proliferator-activated receptor γ (PPARγ), which are key transcriptional factors actively involved in the positive regulation of *Ucp1* expression (Baskaran et al., 2016). In this regard, Ohyama et al. (2016) proposed that capsainoids signal, originating in the gut, is transmitted through central nervous system (CNS) to inguinal WAT by the β_2-adrenoceptor.

Recent findings described the browning potential of capsaicin on white adipocytes (Baboota et al., 2014; Baskaran et al., 2016), but long-term effects on adipocytes still need further investigation. Moreover, the effect of capsaicin on LD size and number and on LD-associated proteins are still unclear and deserve deeper studies.

The present study enriches previous results on the browning potential of capsaicin with an investigation of the role of this nutraceutical on two different murine cellular models. These lines differ to their origin and could show different responses to browning stimulation, being X9 cells usually more prone to display a brite phenotype, since they were isolated from an inguinal fat pad depot (Wu et al., 2012). However, 3T3-L1 cells, widely used to evaluate the potential application of various compounds and nutrients in the treatment of obesity (Ruiz-Ojeda et al., 2016), were described to display features of multiple adipocytes lineages following appropriate stimulation (Morrison and McGee, 2015). The characteristic features of these models may lead to some unexpected variation, since 3T3-L1 cells act as a model of visceral adipocytes and X9 are subcutaneous. The changes in LD dynamics and gene expression profile after the administration of different doses of capsaicin have been analyzed between two times of differentiation. Finally, long-term effects of capsaicin, in combination with NE, are also tested.

MATERIALS AND METHODS

Chemicals and Culture Media

Dulbecco's modified Eagle medium (DMEM) enriched with 4.5 g/L D-glucose, 110 mg/L sodium pyruvate and 862 mg/L L-alanyl-L-glutamine (GlutaMAX™), DMEM/F-12 (1:1) medium enriched with GlutaMAX™, fetal bovine serum (FBS), penicillin/streptomycin solution and amphotericin B solution were purchased from Gibco by Life Technologies (Thermo Fisher Scientific, Inc., Waltham, MA, United States). Capsaicin and rosiglitazone were purchased from Cayman Chemical (Ann Arbor, MI, United States). Dipyrromethene boron difluoride (BODIPY) 493/503 dye, TRIzol reagent, PureLink™ RNA Mini Kit and Platinum™ SYBR™ Green qPCR SuperMix-UDG kit for real time PCR were purchased from Invitrogen (Thermo Fisher Scientific, Inc., Waltham, MA, United States). ImProm-II™ Reverse Transcription System was purchased from Promega (Madison, WI, United States). Normal goat (NG) serum was purchased by Vector Laboratories (Burlingame, CA, United States). 4,6-diamidin-2-phenylindole (DAPI)-containing mounting medium and Fluo-8 AM were purchased from Abcam (Cambridge, MA, United States). Hank's balanced salt solution (HBSS) and 4-(2-hydroxyethyl)-1-piperazineethanesulfonic acid (HEPES) were purchased from Euroclone S.p.A. (Pero, Italy). All other chemicals used in the experiment and not listed above were purchased from Sigma-Aldrich (Darmstadt, Germany).

Cell Culture and Treatment

Murine 3T3-L1 preadipocytes (ZenBio, Inc., Durham, NC, United States) and X9 preadipocytes (LGC Standards Srl, Sesto San Giovanni, Italy) were chosen for this comparative experiment.

Before starting the experiments, the growth of 3T3-L1 and X9 cells with media differently formulated was tested. On 3T3-L1 cells, the differentiation medium currently in use in our laboratory and inferred from literature was adopted. The insulin-IBMX-dexamethasone cocktail was so far the best solution to

achieve excellent differentiation rates and white fat phenotype in 3T3-L1 cells. A growth protocol on X9 cells with the same growth conditions resulted in a poor differentiation rate, since quite 85% cells remained undifferentiated. The protocol suggested by Wu and Xu (2017) was then applied. Next, this medium for X9 was administered on 3T3-L1 cells, but the presence of rosiglitazone and triiodothyronine in the differentiation cocktail increased the *Ucp1* expression even if 3T3-L1 cells were not incubated with any browning factor (Chu et al., 2014). Since the administration of X9 medium could bias the results of *Ucp1* expression, different induction cocktails on two cellular models were applied as follows.

3T3-L1 preadipocytes were cultured in high-glucose DMEM supplemented with 10% FBS, 1% penicillin/streptomycin solution and 1% amphotericin B solution until 100% confluence. The differentiation was induced 48 h post-confluence by feeding cells with DMEM/F-12 supplemented with 10% FBS, 1% penicillin/streptomycin solution and 1% amphotericin B solution and enriched with 1 μg/mL insulin solution, 0.5 μM dexamethasone, and 0.5 mM isobutylmethylxanthine (IBMX) for 3 days. At day 3, maintenance was guaranteed by feeding cells with the differentiation basal medium supplemented with 1 μg/mL insulin solution; this medium was refreshed every 2 days.

X9 preadipocytes were grown in DMEM/F-12 supplemented with 15% FBS, 1% penicillin/streptomycin solution and 1% amphotericin B solution until 90% confluence. Differentiation was induced using the same differentiation basal medium formulated for 3T3-L1 cell culture enriched with 1 μg/mL insulin, 5 μM dexamethasone, 0.5 mM IBMX, 1 nM triiodothyronine (T_3), and 1 μM rosiglitazone for 3 days. At day 3, cells were switched to the maintenance medium supplemented with 1 μg/mL insulin and 1 nM T_3; the medium was refreshed every 2 days.

Treatment of 3T3-L1 cells and X9 cells with capsaicin and NE, alone or in association, started at day 3 of differentiation, concurrently with the switch from the differentiation medium to the maintenance medium, and lasted until analysis either at 4 days of differentiation (4d), 1 day of treatment, or at 8 days of differentiation (8d), 5 days of treatment. Experimental groups were identified by adding to the maintenance medium different combinations of compounds. A vehicle negative control (CTRL) was established by adding to the maintenance medium absolute ethanol (1:1000 dilution). The positive control was represented by cells treated with 10 μM norepinephrine, the main endogenous browning molecule (NE). Capsaicin concentrations were tested at 0.1 μM (0.1CP) and 1 μM (1CP). To determine if any synergies/antagonisms between NE and capsaicin occurred and to mimic cold-independent adrenergic response that occurs *in vivo* after capsaicin stimulation (El Hadi et al., 2019), samples were also treated with both 10 μM norepinephrine and 0.1 μM capsaicin (0.1CPNE) or 1 μM of capsaicin (1CPNE) (**Figure 1**).

Cell Viability Assay

Cell viability was determined by 3-(4,5-dimethylthiazol-2-yl)-2,5-diphenyltetrazolium bromide (MTT) assay. Cells were plated in a 96-well plate and treated with different concentrations of capsaicin and norepinephrine. Prior to incubation with 5 mg/mL MTT in HBSS, cells were rinsed with phosphate buffer saline (PBS) 1X. Incubation with MTT solution was performed at 37°C for 4 h and the resulting formazan was dissolved in dimethyl sulfoxide (DMSO) and incubated overnight (O/N) at 37°C. The optical density was used as an indicator of cell viability and was measured at 550 nm.

BODIPY Staining and Confocal Imaging

Cells for BODIPY staining and subsequent confocal imaging were cultured on ibiTreat 8-well μ-Slides (Ibidi GmbH, Planegg/Martinsried, Germany). Cells were fixed in a 2% formalin solution diluted in PBS 1X at room temperature (RT) for 15 min. Subsequently, after three washes in PBS 1X, cells were incubated in a solution of BODIPY 493/503 in PBS 1X to fluorescently label lipid droplets. The incubation was performed at RT in dark for 45 min. After the incubation, the slides were washed in PBS 1X three times and then mounted with a DAPI-containing mounting medium. Fluorescent images were obtained

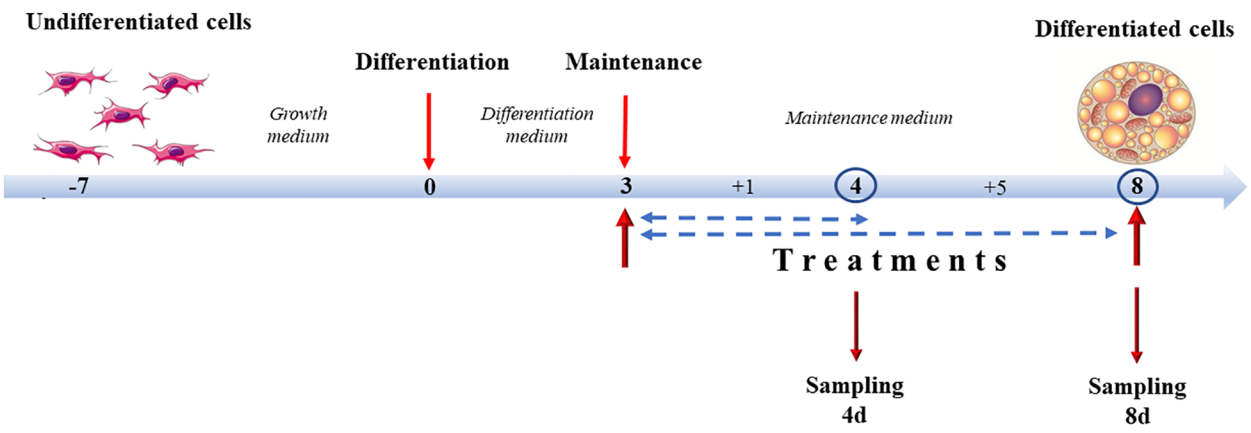

FIGURE 1 | Cell culture treatment protocol. Cells were grown until 90% (X9) or 100% (3T3-L1) confluence. Differentiation lasted 3 days. From day 3, cells were incubated with maintenance medium supplemented with different treatments lasting for 1 (4d) or 5 days (8d) (sampling times).

using a Leica SP8 confocal microscope (Leica Microsystems Srl, Milan, Italy) equipped with LAS X 3.1.5.16308 software. Slides were observed with HC PL APO CS2 40X/1.10 WATER or HCX PL APO lambda blue 63X/1.40 OIL objective lenses. DAPI fluorescence was detected by diode 405 laser (410/480 nm), while the fluorescence of BODIPY was detected by white light laser (503/588 nm). The images were acquired by a photomultiplier tube (PMT), which allowed point-by-point scanning of the region of interest (ROI) with the selected laser and produced 1024 × 1024 px images.

Morphology of LDs

MRI_Lipid Droplets tool[1], a macro of ImageJ 1.50b software[2], was used to measure LD area (Bäcker, 2012). The images were analyzed as already described (Colitti et al., 2018). For each LD, the area surface (in μm^2), the maximum Feret diameter (MFD, in μm), and integrated optical density (IOD, dimensionless), were measured. The MDF is used as a measure of the diameter of irregularly shaped objects, while IOD is related to both triglyceride accumulation and LDs size (Boschi et al., 2019).

RNA Extraction and RT-PCR

RNA extraction was performed by adding 1 mL/10 cm^2 TRIzol reagent on the culture plate. The reagent was repeatedly pipetted to induce a severe breakdown of cells. The lysates in TRIzol were immediately processed with the PureLink™ RNA Mini Kit following the manufacturer's instructions. The concentration of the isolated total RNA was quantified using a Spark multimode microplate reader (Tecan Trading AG, Switzerland) and the purity of RNA samples was over 1.9. RNA integrity was evaluated through the observation of 18 and 28S ribosomal bands after electrophoresis on 1% agarose gel with GelRed. Primer3 Input software (Rozen and Skaletsky, 2000) was used to design primers. GenBank accession, primer sequences, product lengths, and relative annealing temperatures for each gene are listed in **Table 1**, according to the HUGO Gene Nomenclature Committee.

Total RNA (500 ng) from each sample was reverse-transcribed with the ImProm-II™ Reverse Transcription System in a MJ thermal cycler PT-100 (MJ Research, Inc., Waltham, MA, United States). For each gene, an aliquot of cDNA samples was pooled and standard curves with serial dilution of the pool were used to optimize real time PCR conditions in terms of cDNA and primers concentration and to calculate the efficiency, fluorescence baseline, and threshold.

Real time PCRs were performed for each sample in triplicate using Platinum™ SYBR™ Green qPCR SuperMix-UDG. PCR amplification was achieved applying 40 cycles (10 s at 95°C, 30 s at the specific annealing temperature, 30 s at 72°C) in a 96-well spectrofluorometric thermal cycler CFX (Bio-Rad, Milan, Italy). The melting curve analysis of amplification products was performed at the end of each PCR reaction to confirm that a single PCR product was detected.

The expression of target genes was normalized using the geometric means between RPLP0 ribosomal protein (*36b4*) and glyceraldehyde 3-phosphate dehydrogenase (*Gapdh*) mRNAs and

[1]http://dev.mri.cnrs.fr/projects/imagej-macros/wiki/LipidDroplets_Tool

[2]http://rsb.info.nih.gov/ij/

TABLE 1 | Oligonucleotide primer sequences for Real-time PCR (*36b4*; RPLP0 ribosomal protein; *Gapdh*, glyceraldehyde-3-phosphate dehydrogenase; *Adrb3*, adrenoceptor beta 3; *Ucp1*, uncoupling protein 1; *Tbx1*, T-box 1; *Trpv1*, transient receptor potential vanilloid 1; *Prdm16*, proline rich domain containing 16; *Ppargc1a*, peroxisome proliferator-activated receptor γ coactivator 1 α; *Cidea,* cell death-inducing DFFA-like effector A; *Cidec,* cell death inducing DFFA like effector C; *Plin1,* perilipin 1).

Gene	GenBank accession	Primer sets	Product length (bp)	T_m (°C)
36b4	BC099384.1	Forward: 5′-GAAACTGCTGCCTCACATCC-3′ Reverse: 5′-AGGTCTTCTCGGGTCCTAGA-3′	179	59.0
Gapdh	NM_008084	Forward: 5′-AATGTGTCCGTCGTGGATCTGA-3′ Reverse: 5′-AGTGTAGCCCAAGATGCCCTTC-3′	117	60.0
Adrb3	NM_013462.3	Forward: 5′-CCAATGACTCCTATGACC-3′ Reverse: 5′-TTCTGGAGCGTTGGAGAGTT-3′	89	57.3
Ucp1	NM_009463.3	Forward: 5′-CCCTGCCATTTACTGTCAGC-3′ Reverse: 5′-TCGGTCCTTCCTTGGGTGTAC-3′	157	59.0
Tbx1	NM_011532.2	Forward: 5′-AGGCGGAAGGAAGTGGTATT-3′ Reverse: 5′-TACCAGTATCTACACCGCCC-3′	118	58.4
Trpv1	AY445519.1	Forward: 5′-CGAGATAGGCATAGCACCCA-3′ Reverse: 5′-TGCTTCATGGTGTCCCTCAT-3′	130	58.4
Prdm16	NM_027504.3	Forward: 5′-CCACCAGCGAGGACTTCAC-3′ Reverse: 5′-GGAGGACTCTCGTAGCTCGAA-3′	107	61.4
Ppargc1a	NM_008904.2	Forward: 5′-TATGGAGTGACATAGAGTGTGCT-3′ Reverse: 5′-CTGGGCAAAGAGGCTGGTC-3′	191	60.0
Cidea	NM_007702.2	Forward: 5-ATCACAACTGGCCTGGTTACG-3′ Reverse: 5′-TACTACCCGGTGTCCATTTCT-3′	136	58.9
Cidec	NM_178373.4	Forward: 5′-ACCTTCGACCTGTACAAGCT-3′ Reverse: 5′-GTGCAGGTCATAGGAAAGCG-3′	99	58.4
Plin1	NM_175640.2	Forward: 5′-TGGACCACCTGGAGGAAAAG-3′ Reverse: 5′-CTTCGAAGGCGGGTAGAGATG-3′	94	60.6

Tm = annealing temperature.

analyzed using $\Delta\Delta$Ct method (Livak and Schmittgen, 2001). For all the cell culture experiments, the results are generated from biological triplicates and replicated similar results from at least three independent experiments.

Immunofluorescence Analysis on 3T3-L1 Cells

Formalin-fixed cells were washed twice with PBS 1X containing 0.05% Tween-20 (PBST) at pH 7.4. Permeabilization of plasma membrane was performed by Triton X-100 0.1% incubation at RT. Fixative-induced autofluorescence was quenched with 50 mM ammonium chloride. Background labeling was prevented by incubating cells in a blocking solution containing 10% FBS and 5% NG serum in PBST 1X for 1 h at RT. The slides were then incubated overnight at 4°C in a moist chamber with the primary antibody diluted in blocking solution.

The anti-UCP1 polyclonal antibody (ab10983, Abcam, Cambridge, MA, United States) was raised against a peptide mapping to amino acids 145–159 of human UCP1 protein. The anti-PLIN1 was a rabbit polyclonal antibody (sc-67164, Santa Cruz Biotechnology, Inc., Heidelberg, Germany) raised against amino acids 1–300 mapping at the N-terminus of perilipin of human origin. Monoclonal anti-TRPV1 (sc-398417) was generated versus N-terminal amino acids 1–130 of rat TRPV1.

The following day, cells were incubated with 1:1000 AlexaFluor®555 goat anti-rabbit IgG (ab150078, Abcam, Cambridge, MA, United States), 1:200 fluorescein goat anti-rabbit IgG (FI-1000, Vector Laboratories, Burlingame, CA, United States) or 1:200 fluorescein goat anti-mouse IgM (FI-2020, Vector Laboratories, Burlingame, CA, United States) in blocking solution at RT for 45' in the dark. Cells were then mounted with DAPI-containing mounting medium. Images were acquired with the fluorescence microscope Axio Observer Z1 equipped with D-PLAN Neofluar objective lenses with N.A. 0.75 and Infinity Color Corrected System (ICS) and with AxioCam and Zen blue software (Carl Zeiss, Jena, Germany). The filters were 550/605 nm for Alexa Fluor®555 antibody conjugate, 470/525 nm for fluorescein antibodies and 390/460 nm for DAPI.

Intracellular Calcium Analysis on 3T3-L1 Cells

Differentiated cells at 4 and 8 days cultured on ibiTreat 8-well μ-Slides were incubated, after culture medium removal, with a 4 μM Fluo-8 AM working solution in HBSS supplemented with 15 mM HEPES for 1 h at 37°C. Stained cells were then rinsed with HEPES-HBSS and immediately imaged at Axio Observer Z1 fluorescence microscope with the 470/525 nm filter. The administration of 1 μM capsaicin was performed directly on the slide during the movie acquisition, 12–14 s after the beginning of the movie. Each acquisition lasted 180 s.

Analysis intensity over time was analyzed within selected ROIs with ImageJ[3] and the influx of Ca^{2+} was quantified, after background subtraction, as the ratio between the maximum fluorescence intensity emitted after the addition of the compound (F) and the average of baseline fluorescence (F0), recorded before the treatment. To quantify the ON-OFF response of 3T3-L1 adipocytes, standard deviation of the fluorescence intensity was calculated using ImageJ (Muto et al., 2013).

[3]http://imagej.nih.gov/ij/

Statistical Analysis

Results are presented as relative values (means ± SD). All experiments were performed at least three times. One-way ANOVA was used for statistical analysis for MTT test by SPSS version 20.0 software.

The measurements of total cell area surface, MFD and IOD were analyzed by XLSTAT (Addinsoft, 2017). Results, obtained from 10 biological replicates, were compared using through Kruskal–Wallis statistical test followed by pairwise comparisons using the Mann–Whitney approach with Bonferroni correction.

Gene expression data (relative fold change values) were analyzed within the same cell line by one-way ANOVA analysis using XLSTAT with Bonferroni correction ($p = 0.003$) and reported as least squares means (LS) ± standard error of the mean (SEM).

The relative fold change values were subjected to enrichement analysis of biological process (BP), performed by Funrich tool 3.1.3 against mouse UniProt database. Bonferroni test was applied to correct for multiple testing (Pathan et al., 2015).

Principal component analysis (PCA) was used to perform multivariate analysis of correlated variables between the percentage of protein annotation obtained by relative fold change uploaded on Funrich and the significant ($p < 0.05$) BP, at 4 and 8 days, respectively. PCA simplifies the data complexity while retaining trends and patterns. Biplots were drawn to have simultaneous representation of variables and observations in the PCA space.

RESULTS

Cell Viability

The percentage of cell viability after treatment with NE, 0.1CP, 0.1CPNE, 1CP, 1CPNE at 4 and 8 days was always around 100% (**Supplementary Figure S1**). No significant differences were observed for time point and for concentration × time point interaction.

Lipid Droplet Measurements and Analysis in 3T3-L1 Cells

Figure 2 illustrates LDs dynamic in 3T3-L1 cells at 4 and 8 days treated with different doses of compound. Tables showing mean values ± SD and *p*-values of total area surface, MFD and IOD among treatments at 4 and 8 days are reported in **Supplementary Tables S1**, **S2**.

Interestingly, at 4 days, 3T3-L1 cells treated with NE, 0.1CPNE and 1CP showed significantly ($p < 0.0001$) different total LDs area surface in comparison to CTRL cells and all other treatments (**Figure 2A**). 1CP showed the largest LD area surface and NE the smallest.

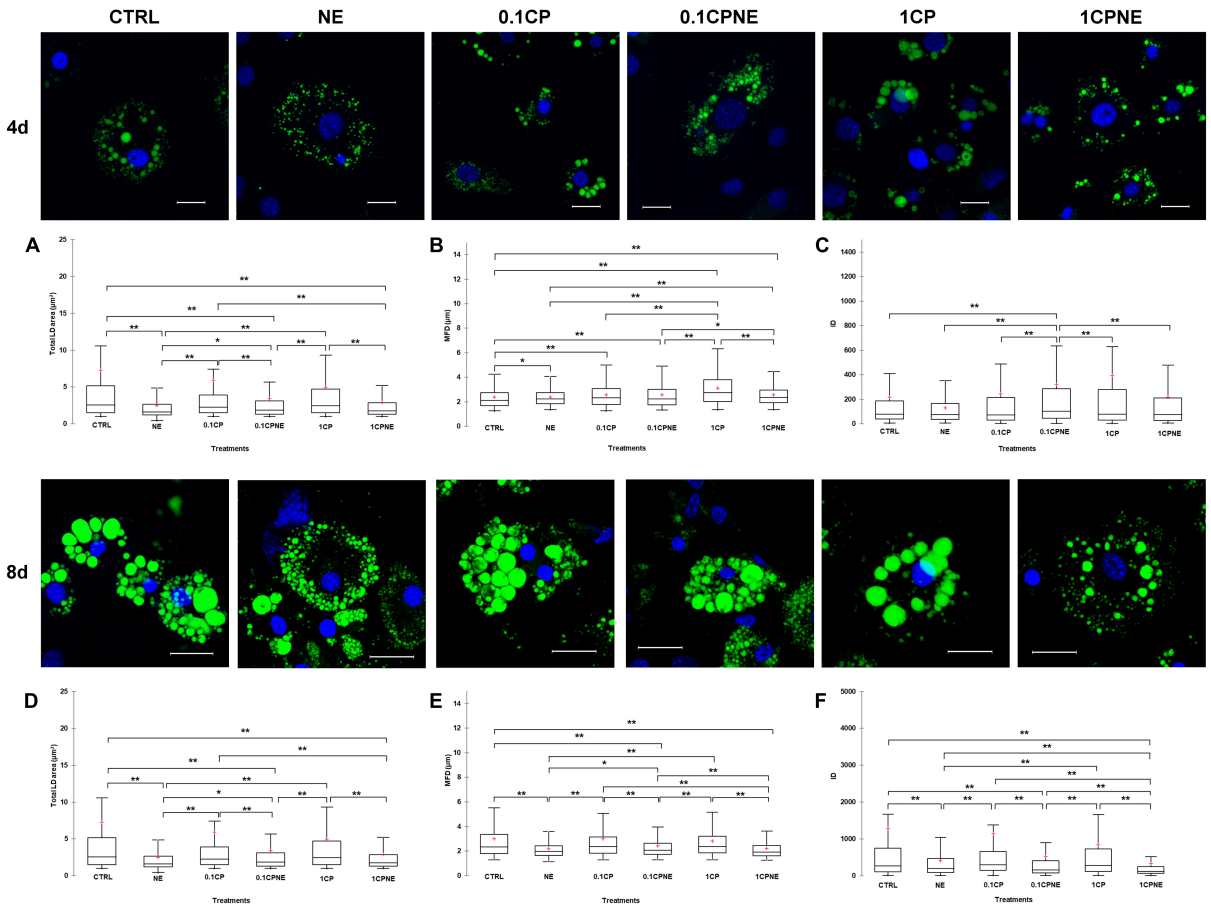

FIGURE 2 | Lipid droplets formation stained with BODIPY 493/503 in fixed 3T3-L1 cells at 4 and 8 days of differentiation. Nuclear staining DAPI. Images are representative of n. 5 biological replicates. **(A–F)** Lipid droplets box plots show median (horizontal lines), first to third quartile (box), and the most extreme values with the interquartile range (vertical lines). For all comparison, differences between treatments on 3T3-L1 cells were statistically significant, using Kruskal–Wallis test. **(A)** Total LD area surface at 4 days; **(B)** Maximum Feret diameter (MFD) at 4 days; **(C)** Intensity optical density (IOD) at 4 days. **(D)** Total LD area surface at 8 days; **(E)** Maximum Feret diameter (MFD) at 8 days; **(F)** Intensity optical density (IOD) at 8 days. The area surface measures are expressed in μm^2 and MFD μm. Measures are the average of 1224 and 853 observations at 4 at 8 days, respectively. $^{**}p < 0.0001$; $^{*}p < 0.05$. Scale bars: 20 μm. CTRL = vehicle negative control; NE = 10 μM norepinephrine; 0.1CP = 0.1 μM capsaicin; 0.1CPNE = 0.1 μM capsaicin plus 10 μM norepinephrine; 1CP = 1 μM capsaicin; 1CPNE = 1 μM capsaicin plus 10 μM norepinephrine.

The MFD of 1CP-treated cells was significantly ($p < 0.0001$) higher with respect to all other treatments. Conversely, MFD of CTRL cells was the significantly smallest compared to other treatments (**Figure 2B**). MFD of NE cells differed significantly from CTRL ones ($p < 0.05$) and it is significantly ($p < 0.0001$) lower compared to 1CP and 1CPNE treatments (**Figure 2B**).

Figure 2C evidences statistically significant differences of IOD at 4 days. For all the treatments, the IOD of 0.1CPNE-treated cells was significantly different ($p < 0.0001$) to all treatments.

At 8 days a significant decrease in total area surface of LDs was observed in NE, which was significantly different from all treatments with the exception of 1CPNE (**Figure 2D**).

Maximum Feret diameter of 0.1CPNE-treated cells was significantly different among samples (**Figure 2E**).

The strongest ($p < 0.0001$) decrease in IOD value was observed in 1CPNE-treated cells followed by NE and 0.1CPNE (**Figure 2F**).

Taken together, the results obtained at 4 and 8 days with NE and 1CPNE treatments on 3T3-L1 cells showed a strongest effect in reducing LDs area surface and IOD, whereas 0.1CP and 1CP treatments were less active and similar to CTRL at 8 days.

Lipid Droplet Measurements and Analysis in X9 Cells

Figure 3 illustrates LDs dynamic in X9 cells at 4 and 8 days treated with different doses of compound. Tables showing mean values ± SD and p-values of total area surface, MFD and IOD among treatments at 4 and 8 days are reported in **Supplementary Tables S3**, **S4**.

After 4 days of development 0.1CPNE treatment showed the strongest effect on the measure of total area surface, particularly in comparison to CTRL, 0.1CP and 1CPNE ($p < 0.0001$). NE-treated cells were different ($p < 0.05$) to 0.1CP (**Figure 3A**).

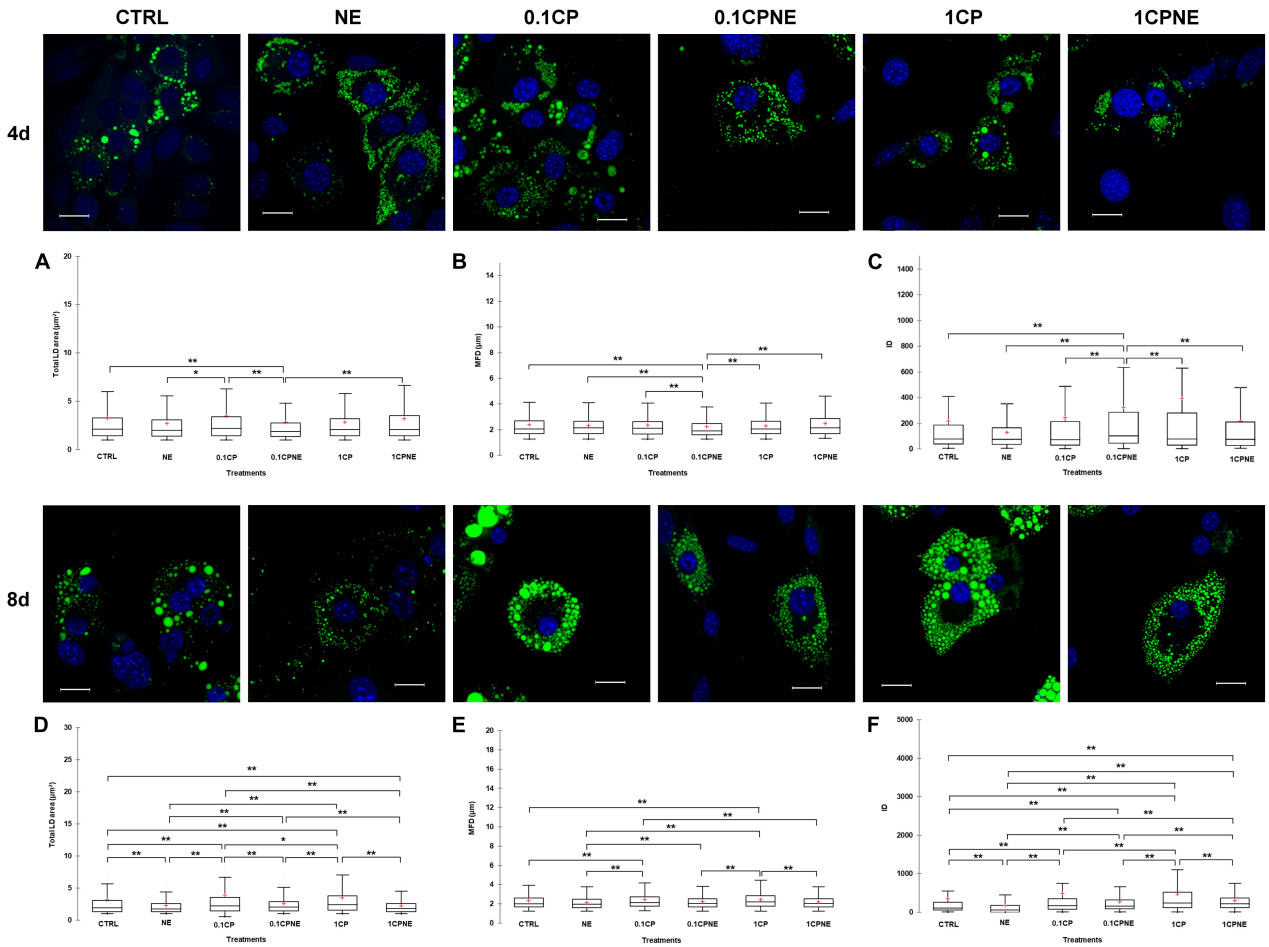

FIGURE 3 | Lipid droplets formation stained with BODIPY 493/503 in fixed X9 cells at 4 and 8 days of differentiation. Nuclear staining DAPI. Images are representative of n. 5 biological replicates. **(A–F)** Lipid droplets box plots show median (horizontal lines), first to third quartile (box), and the most extreme values with the interquartile range (vertical lines). For all comparison, differences between treatments on X9 cells were statistically significant, using Kruskal–Wallis test. **(A)** Total LD area surface at 4 days; **(B)** Maximum Feret diameter (MFD) at 4 days; **(C)** Intensity optical density (IOD) at 4 days. **(D)** Total LD area surface at 8 days; **(E)** Maximum Feret diameter (MFD) at 8 days; **(F)** Intensity optical density (IOD) at 8 days. The area surface measures are expressed in μm^2 and MFD μm. Measures are the average of 1824 and 1778 observations at 4 at 8 days, respectively. $^{**}p < 0.0001$; $^{*}p < 0.05$. Scale bars: 20 μm. CTRL = vehicle negative control; NE = 10 μM norepinephrine; 0.1CP = 0.1 μM capsaicin; 0.1CPNE = 0.1 μM capsaicin plus 10 μM norepinephrine; 1CP = 1 μM capsaicin; 1CPNE = 1 μM capsaicin plus 10 μM norepinephrine.

Maximum Feret diameter values reflected the same trend, as 0.1CPNE showed the significant lowest value in analogy to total area surface (**Figure 3B**).

Integrated optical density value in cells treated with NE alone, 0.1CP and 1CP was significantly lower in comparison to other dosages, but again 0.1CPNE-treated cells were significantly ($p < 0.0001$) different to all other treated cells (**Figure 3C**).

At 8 days, all treatments significantly affected total LDs area surface, with 0.1CP and 1CP producing the largest surface and NE and 1CPNE the smallest one. No differences were observed between CTRL and 0.1CPNE cells (**Figure 3D**).

Maximum Feret diameter significantly increased in X9 cell treated with the two capsaicin concentrations (0.1CP and 1CP, $p < 0.0001$), whereas treatments coupled with NE negatively ($p < 0.0001$) affected the MFD size (**Figure 3E**).

Integrated optical density values were significantly different among all treatments and NE-treated cells showed the lowest value ($p < 0.0001$) (**Figure 3F**).

Results obtained on X9 cells at 4 and 8 days with NE and NE in combination with 0.1CP or 1CP treatments showed the strongest effect in reducing LDs area surface, MFD and IOD, whereas 0.1CP treatment was the least effective at both differentiation times.

Comparison of LD Measurements Between Treatments at 4 and 8 Days in 3T3-L1 and in X9 Cells

Figure 4 illustrates the pairwise comparison of total area surface, MFD and IOD between the same treatment after 4 and 8 days of differentiation within 3T3-L1 cells and X9 cells.

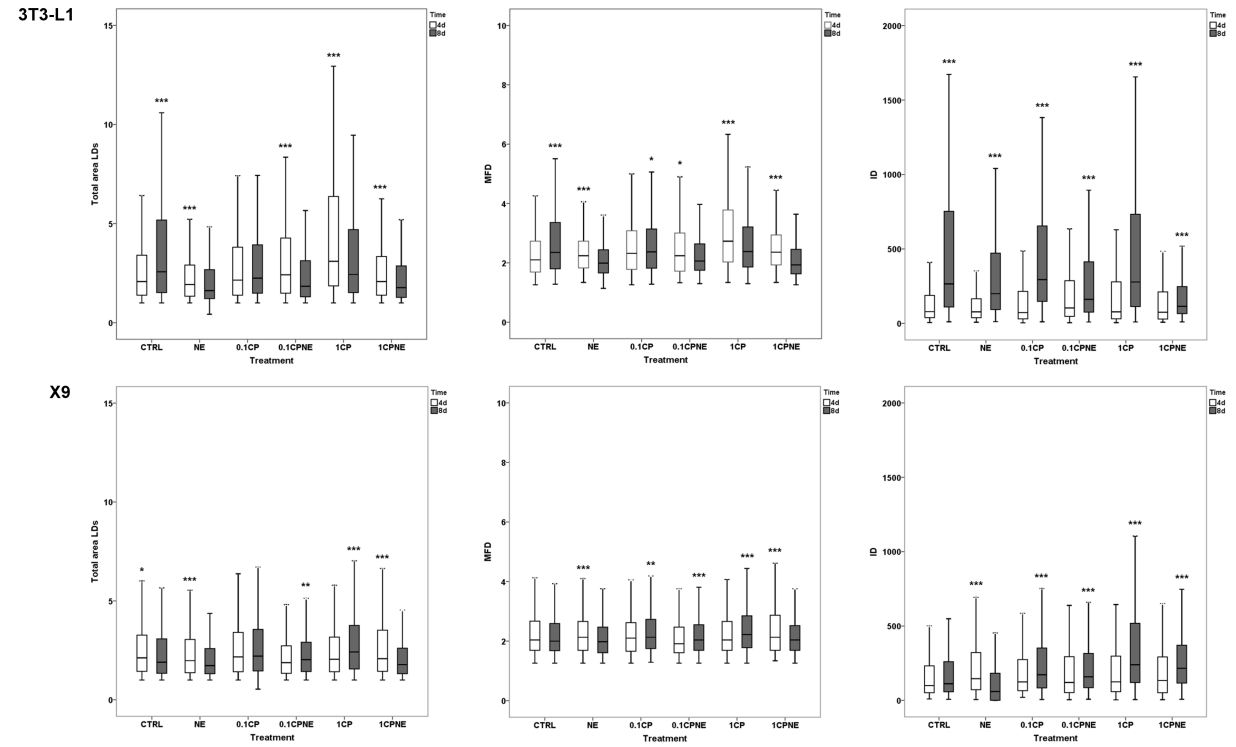

FIGURE 4 | Pairwise comparison of total area surface, MFD and IOD between the same treatment after 4 (4d) and 8 days (8d) of differentiation within 3T3-L1 cells and X9 cells. Box plots show median (horizontal lines), first to third quartile (box), and the most extreme values with the interquartile range (vertical lines). For all comparison, differences between days of differentiation of 3T3-L1 and X9 cells were statistically significant using Kruskal–Wallis test. The measurements are the average of 10 fields of each developmental stage. ***$p < 0.0001$, **$p < 0.01$, *$p < 0.05$. CTRL = vehicle negative control; NE = 10 μM norepinephrine; 0.1CP = 0.1 μM capsaicin; 0.1CPNE = 0.1 μM capsaicin plus 10 μM norepinephrine; 1CP = 1 μM capsaicin; 1CPNE = 1 μM capsaicin plus 10 μM norepinephrine.

Total LDs area surface in 3T3-L1 exhibited significant differences between CTRL cells being higher ($p < 0.0001$) at 8 days in comparison to 4 days. However, cells treated with NE, 0.1CPNE, 1CP, and 1CPNE showed the highest ($p < 0.0001$) area surface at 4 days.

Maximum Feret diameter was at its highest at 8 days in control cells ($p < 0.0001$) and in 0.1CP ($p < 0.05$), but significantly ($p < 0.0001$) decreased in NE, 1CP, 1CPNE-treated cells and in 0.1CPNE ($p < 0.05$).

Interestingly, IOD value was significantly ($p < 0.0001$) higher at 8 days in 3T3-L1 CTRL cells and in all treated cells.

Total LDs area surface in X9 cells was significantly higher at 4 days in CTRL cells ($p < 0.05$), NE and 1CPNE-treated cells ($p < 0.0001$), but significantly increased at 8 days in comparison to 4 days in 0.1CPNE ($p < 0.01$) and 1CP ($p < 0.0001$) treated cells.

Maximum Feret diameter size was significantly higher ($p < 0.0001$) in NE and 0.1CPNE X9 cells at 8 days, while 0.1CP ($p < 0.05$), 0.1CPNE and 1CPNE treatments ($p < 0.0001$) increased the value of MFD at 4 days in comparison to 8 days.

Control cells did not show any significant difference of IOD value between 4 and 8 days, only NE-treated cells decreased significantly ($p < 0.0001$) at 8 days, while other treatments showed an increase ($p < 0.0001$) at 8 days.

Transcription Data Analysis

Table 2 showed the LS means of relative fold change values ± SEM of 3T3-L1 at 4 and 8 days.

The treatment of 0.1CPNE significantly affected the expression of *Prdm16* and *Cidea* at 4 days. In particular, the expression of *Prdm16* induced by 0.1CPNE treatment significantly differed from 1CP ($p = 0.00038$), NE ($p = 0.001$), and 0.1CP ($p = 0.003$). *Cidea* expression was affected by 0.1CPNE and significantly differed from 0.1CP treatment ($p = 0.003$) and negative CTRL ($p = 0.003$). Bonferroni's corrected significance level ($p = 0.003$) produced by the analysis penalized the significance ($p = 0.042$) of *Ppargc1a* expression among treatments. 1CPNE treatment most affected the gene expression and the effect of NE was the lowest on 3T3-L1 at 4 days.

The treatment of 1CP at 8 days in 3T3-L1 significantly ($p < 0.0001$) up-regulated the expression of all genes.

NE treatment did not produce any significant modulation of genes related to browning even at 8 days.

The LS means of relative fold change values ± SEM of X9 cells is presented for all the treatments at 4 and 8 days in **Table 3**.

Adrb3, *Ucp1*, *Cidec* expression was significantly modulated in X9 cells treated with NE at 4 days. Bonferroni's corrected significance level ($p = 0.003$) produced by the analysis penalized the significance ($p = 0.039$) of *Cidec* expression among treatments. Notably, treatments coupled with NE

TABLE 2 | Differentially expressed genes in 3T3-L1 cells at 4 and 8 days.

Treatment 4d	*Adrb3*	SEM	*Ucp1*	SEM	*Tbx1*	SEM	*Trpv1*	SEM	*Prdm16*	SEM	*Ppargc1a*	SEM	*Cidec*	SEM	*Cidea*	SEM	*Plin1*	SEM
1CPNE	0.50 ± 0.16		1.83 ± 0.26		1.14 ± 0.26		1.54 ± 0.26		0.81^{AB} ± 0.18		0.60 ± 0.14		1.91 ± 0.30		1.39^{AB} ± 0.34		1.29 ± 0.17	
0.1CPNE	0.48 ± 0.16		1.66 ± 0.26		0.92 ± 0.26		1.12 ± 0.26		1.67^{A} ± 0.18		0.38 ± 0.14		0.66 ± 0.30		2.94^{A} ± 0.34		1.07 ± 0.17	
CTRL	1.04 ± 0.16		0.90 ± 0.26		1.00 ± 0.26		1.00 ± 0.26		1.01^{AB} ± 0.18		1.01 ± 0.14		0.79 ± 0.30		0.89^{B} ± 0.34		1.00 ± 0.17	
0.1CP	1.02 ± 0.16		0.85 ± 0.26		0.67 ± 0.26		0.95 ± 0.26		0.72^{B} ± 0.18		0.82 ± 0.14		1.36 ± 0.30		0.89^{B} ± 0.34		1.27 ± 0.17	
1CP	0.59 ± 0.16		1.36 ± 0.26		0.62 ± 0.26		1.28 ± 0.26		0.41^{B} ± 0.18		0.67 ± 0.14		0.84 ± 0.30		1.14^{AB} ± 0.34		1.05 ± 0.17	
NE	0.42 ± 0.16		0.93 ± 0.26		0.60 ± 0.26		0.70 ± 0.25		0.49^{B} ± 0.18		0.34 ± 0.14		0.72 ± 0.29		1.27^{AB} ± 0.34		0.78 ± 0.17	
Pr > F (Model)	0.060		0.091		0.105		0.343		0.004		0.042		0.090		0.023		0.367	
Treatment 8d	***Adrb3***	**SEM**	***Ucp1***	**SEM**	***Tbx1***	**SEM**	***Trpv1***	**SEM**	***Prdm16***	**SEM**	***Ppargc1a***	**SEM**	***Cidec***	**SEM**	***Cidea***	**SEM**	***Plin1***	**SEM**
1CP	2.71^{A} ± 0.19		13.98^{A} ± 0.63		21.47^{A} ± 1.07		12.74^{A} ± 0.67		16.45^{A} ± 1.40		4.46^{A} ± 0.47		4.37^{A} ± 0.33		14.67^{A} ± 0.71		3.20^{A} ± 0.17	
0.1CP	1.25^{B} ± 0.16		1.96^{B} ± 0.51		2.30^{B} ± 0.87		2.47^{B} ± 0.54		2.23^{B} ± 1.14		1.43^{B} ± 0.39		1.01^{B} ± 0.27		3.25^{B} ± 0.58		1.18^{B} ± 0.14	
0.1CPNE	0.45^{BC} ± 0.16		2.92^{B} ± 0.51		3.54^{B} ± 0.87		2.80^{B} ± 0.54		3.51^{B} ± 1.14		0.68^{B} ± 0.39		1.02^{B} ± 0.27		1.52^{B} ± 0.58		0.75^{B} ± 0.14	
1CPNE	0.34^{C} ± 0.16		1.64^{B} ± 0.51		1.61^{B} ± 0.87		1.43^{B} ± 0.54		1.47^{B} ± 1.14		0.62^{B} ± 0.39		0.98^{B} ± 0.27		1.45^{B} ± 0.58		0.61^{B} ± 0.14	
CTRL	0.99^{BC} ± 0.16		0.85^{B} ± 0.51		0.83^{B} ± 0.87		0.89^{B} ± 0.54		0.76^{B} ± 1.14		1.02^{B} ± 0.39		1.00^{B} ± 0.27		0.82^{B} ± 0.58		1.04^{B} ± 0.14	
NE	0.23^{C} ± 0.19		1.15^{B} ± 0.61		1.28^{B} ± 1.05		0.94^{B} ± 0.65		0.97^{B} ± 1.36		0.41^{B} ± 0.46		0.59^{B} ± 0.32		0.79^{B} ± 0.70		0.71^{B} ± 0.17	
Pr > F (Model)	<0.0001		< 0.0001		<0.0001		< 0.0001		0.001		0.001		<0.0001		< 0.0001		<0.0001	

CTRL = vehicle negative control; NE = 10 μM norepinephrine; 0.1CP = 0.1 μM capsaicin; 0.1CPNE = 0.1 μM capsaicin plus 10 μM norepinephrine; 1CP = 1 μM capsaicin; 1CPNE = 1 μM capsaicin plus 10 μM norepinephrine. Adrb3, adrenoceptor beta 3; Ucp1, uncoupling protein 1; Tbx1, T-box 1; Trpv1, transient receptor potential vanilloid 1; Prdm16, proline rich domain containing 16; Ppargc1a, peroxisome proliferator-activated receptor γ coactivator 1 α; Cidec, cell death inducing DFFA like effector C; Cidea, cell death-inducing DFFA-like effector A; Plin1, perilipin 1. 4d = at 4 days of differentiation; 8d = at 8 days of differentiation. The data are shown as Least squares (LS) means ± standard error of the mean (SEM). Pr > F (Model) = p-value for the effect of the model on the response. Capital letters indicate a significant Bonferroni-corrected difference (p < 0.003).

TABLE 3 | Differentially expressed genes in X9 cells at 4 and 8 days.

Treatment 4d	*Adrb3*	SEM	*Ucp1*	SEM	*Tbx1*	SEM	*Trpv1*	SEM	*Prdm16*	SEM	*Ppargc1a*	SEM	*Cidec*	SEM	*Cidea*	SEM	*Plin1*	SEM
NE	8.70^{A} ± 1.24		3.34^{A} ± 0.45		2.10 ± 0.33		1.57 ± 0.39		3.04 ± 0.64		2.16^{AB} ± 0.50		1.90 ± 0.28		1.34 ± 0.22		1.64 ± 0.35	
1CP	0.66^{B} ± 1.25		0.94^{AB} ± 0.45		0.92 ± 0.33		1.16 ± 0.40		0.95 ± 0.65		4.07^{A} ± 0.51		1.38 ± 0.28		1.12 ± 0.23		0.22 ± 0.36	
0.1CPNE	3.04^{AB} ± 1.53		2.12^{AB} ± 0.55		0.81 ± 0.41		1.28 ± 0.49		1.66 ± 0.79		1.86^{AB} ± 0.62		0.56 ± 0.35		0.87 ± 0.28		0.08 ± 0.44	
CTRL	0.96^{B} ± 1.25		0.95^{AB} ± 0.45		1.03 ± 0.33		1.15 ± 0.40		1.04 ± 0.65		1.18^{B} ± 0.51		1.00 ± 0.28		1.13 ± 0.23		1.15 ± 0.36	
0.1CP	0.64^{B} ± 1.25		0.52^{B} ± 0.45		0.71 ± 0.33		0.73 ± 0.40		0.84 ± 0.65		2.79^{AB} ± 0.51		1.25 ± 0.28		1.37 ± 0.23		0.42 ± 0.36	
1CPNE	2.44^{AB} ± 1.25		0.93^{AB} ± 0.45		0.69 ± 0.33		1.12 ± 0.40		2.69 ± 0.65		1.68^{AB} ± 0.51		0.44 ± 0.28		0.74 ± 0.23		0.09 ± 0.36	
Pr > F (Model)	0.007		0.018		0.088		0.790		0.136		0.029		0.039		0.383		0.064	
Treatment 8d	***Adrb3***	**SEM**	***Ucp1***	**SEM**	***Tbx1***	**SEM**	***Trpv1***	**SEM**	***Prdm16***	**SEM**	***Ppargc1a***	**SEM**	***Cidec***	**SEM**	***Cidea***	**SEM**	***Plin1***	**SEM**
CTRL	1.00^{A} ± 0.07		0.66^{B} ± 0.52		1.05 ± 0.12		1.06 ± 0.26		0.78^{B} ± 0.33		1.02 ± 0.14		1.02^{ABC} ± 0.17		1.03^{AB} ± 0.18		0.92^{A} ± 0.13	
NE	0.16^{B} ± 0.07		3.59^{A} ± 0.50		0.92 ± 0.12		1.62 ± 0.26		2.83^{A} ± 0.33		0.95 ± 0.14		0.60^{BC} ± 0.17		0.50^{B} ± 0.18		0.35^{AB} ± 0.12	
1CP	0.78^{A} ± 0.07		1.11^{AB} ± 0.52		0.72 ± 0.12		0.99 ± 0.26		0.82^{B} ± 0.33		0.76 ± 0.14		1.32^{AB} ± 0.17		0.57^{B} ± 0.18		0.66^{AB} ± 0.13	
0.1CP	0.96^{A} ± 0.07		0.66^{B} ± 0.52		0.58 ± 0.12		0.74 ± 0.26		0.56^{B} ± 0.33		0.90 ± 0.14		1.87^{A} ± 0.17		1.89^{A} ± 0.18		0.85^{A} ± 0.13	
0.1CPNE	0.14^{B} ± 0.07		1.60^{AB} ± 0.52		0.60 ± 0.12		0.74 ± 0.26		0.84^{B} ± 0.33		0.44 ± 0.14		1.04^{ABC} ± 0.17		0.27^{B} ± 0.18		0.37^{AB} ± 0.13	
1CPNE	0.09^{B} ± 0.07		2.15^{AB} ± 0.52		0.58 ± 0.12		1.52 ± 0.26		2.09^{AB} ± 0.33		0.58 ± 0.14		0.24^{C} ± 0.17		0.12^{B} ± 0.18		0.10^{B} ± 0.13	
Pr > F (Model)	<0.0001		0.015		0.072		0.125		0.002		0.088		0.000		0.000		0.005	

CTRL = vehicle negative control; NE = 10 μM norepinephrine; 0.1CP = 0.1 μM capsaicin; 0.1CPNE = 0.1 μM capsaicin plus 10 μM norepinephrine; 1CP = 1 μM capsaicin; 1CPNE = 1 μM capsaicin plus 10 μM norepinephrine. Adrb3, adrenoceptor beta 3; Ucp1, uncoupling protein 1; Tbx1, T-box 1;Trpv1, transient receptor potential vanilloid 1; Prdm16, proline rich domain containing 16; Ppargc1a, peroxisome proliferator-activated receptor γ coactivator 1 α; Cidec, cell death inducing DFFA like effector C; Cidea, cell death-inducing DFFA-like effector A; Plin1, perilipin 1. 4d = at 4 days of differentiation; 8d = at 8 days of differentiation. The data are shown as Least squares (LS) means ± standard error of the mean (SEM). Pr > F (Model) = p-value for the effect of the model on the response. Capital letters indicate a significant Bonferroni-corrected difference (p < 0.003).

significantly modulated gene expression in comparison to capsaicin treatments. *Ucp1* and *Prdm16* expression were significantly induced at 8 days by NE. Interestingly, no treatments induced a significant regulation of *Trpv1*.

Biological Process Enrichment Analysis

The comparison of the relative fold change values among treatments and times were enriched in biological process (BP) using Funrich 3.1.3 finding tool. *p*-Values, after Bonferroni correction, were calculated based on the comparison within samples of 3T3-L1 cells at 4 and 8 days and of X9 at the same times. Funrich tool returned results as percentage of annotated proteins and the analysis produced 233 BPs. Among these, 29 were significant for $p < 0.05$. Within the significant BPs, the eight most enriched were chosen due to their relation with the study. All selected significant BPs showing the percentage of expression in 3T3-L1 and X9 cell, according to treatments and times, are reported in **Supplementary Table S5**. The most significant BP were "diet induced thermogenesis" ($p < 2.7 \times 10^{-10}$) and "brown fat cell differentiation" ($p < 7.3 \times 10^{-9}$) followed by "response to cold" ($p < 1.8 \times 10^{-7}$), "positive regulation of cold-induced thermogenesis" ($p < 2.0 \times 10^{-7}$), "response to capsazepine" ($p < 3.4 \times 10^{-6}$), "adaptive thermogenesis" ($p < 3.4 \times 10^{-6}$ "lipid metabolic process" ($p < 1.4 \times 10^{-4}$) and "calcium ion import across plasma membrane" ($p < 2.3 \times 10^{-3}$). Interestingly, in 3T3-L1 cells 1CP at 8 days, 1CP and 1CPNE at 4 days accounted for the highest percentage of annotated proteins in "brown fat cell differentiation," "response to cold," "positive regulation of cold-induced thermogenesis," and "adaptive thermogenesis." The highest percentage of annotated proteins of "response to capsazepine" and "calcium ion import across plasma membrane" was recorded by 1CP at 4 days.

In X9 cells, about 70% of annotated proteins involved "brown fat cell differentiation," "positive regulation of cold-induced thermogenesis" in cells treated with 1CPNE, 0.1CPNE and NE at 4 days, followed by NE at 8 days. The BPs "calcium ion import across plasma membrane" and "response to capsazepine" displayed the lowest protein percentage in all treatments especially in NE-treated cells.

Principal Component Analysis

To better understand the relation between BPs (active variables) and treatments (active observations) in 3T3-L1 cells and in X9 cells at 4 and 8 days, PCA analysis was performed and distance biplots were displayed (**Figure 5**).

Figure 5A plotted the result of PCA for 3T3-L1 cells. The first two principal components (D1, D2) explained 51.4 and 27.8%, respectively (total variability 79.23%) of the total observed variances of BPs and the individual data were clustered according to treatments and times of differentiation on the first principal component (D1). In this cell line a positive correlation was observed between "calcium ion import across plasma membrane," "response to capsazepine," "positive regulation of cold-induced thermogenesis," and "brown fat cell differentiation." These BPs were not correlated with "response to cold," "adaptive thermogenesis," and "diet induced thermogenesis." Capsaicin-treated samples 1CPNE at 4 days and 1CP at 8 days were closely related to these BPs and were negatively correlated to "lipid metabolic process." It is highly significant the position of these active observations which stand completely by themselves and separate from the rest of the fields. This is due to the high values of their percentage of annotated proteins included in active variables (**Supplementary Table S5**).

Figure 5B plotted the PCA results for X9 cell samples. The first two principal components (D1, D2) explained 56.0% and 29.1%, respectively (total variance 85.17%), of the total observed variances and they clustered treatments between the times of differentiation. Active observations (treatments) at 4 and 8 days were clearly distinguishable in the biplot, grouping with respect to the first principal component (D1) except 0.1CP at 8 days. The BPs "response to cold," "positive regulation of cold-induced thermogenesis," and "brown fat cell differentiation" were positively correlated and close to NE, 1CPNE and 0.1CPNE at 4 days observations, which displayed the highest upregulation of browning markers (**Table 3**) and the highest percentage of protein annotation (**Supplementary Table S5**). These BPs and the active observations were not correlated with "adaptive thermogenesis" and "diet induced thermogenesis." BPs showed a negative correlation with "response to capsazepine," "calcium ion import across plasma membrane" and "lipid metabolic process," and with the active observations at 8 days.

Immunofluorescence Analysis of PLIN1, UCP1, and TRPV1 on 3T3-L1 Cells

In order to deeper investigate the effect of 1CP treatment in 3T3-L1 on protein expression, the immunofluorescence of PLIN1, UCP1, and TRPV1 at 8 days is shown in **Figure 6**. No reaction was observed in controls performed for each developmental stage by substituting the primary antibodies with PBST blocking solution (data not shown).

PLIN1 showed positive staining in cells, being localized around large LDs and smaller ones in close proximity to them (**Figure 6a**).

Punctate and disperse cellular staining identified UCP1 expression at 8 days along the circular cytoplasmic rim surrounding nuclei and individual LDs (**Figure 6b**). TRPV1 was evident along the membranes, although a weak staining was also observed in cytoplasm (**Figure 6c**).

Flow of Intracellular Calcium in 3T3-L1 Cells

To confirm that the physiological effect in 1CP-treated 3T3-L1 cells was achieved by TRPV1 channel activation, the levels of intracellular Ca^{2+} were measured before and after 1CP treatment (**Figure 7**). *In vivo* imaging of Fluo-8 AM-treated cells showed a ubiquitous localization of internalized Ca^{2+} in adipocytes. The baseline green fluorescence produced bright pulses after capsaicin administration during imaging, strenghtening the observation that capsaicin treatment on 3T3-L1 cells activates TRPV1 receptors, producing an acute Ca^{2+} influx (**Figure 7A**). Interestingly, maximum fluorescence pulses were produced early after capsaicin addition, within 20 and 42 s, and ended approximately within 120 s as shown by **Figure 7B**

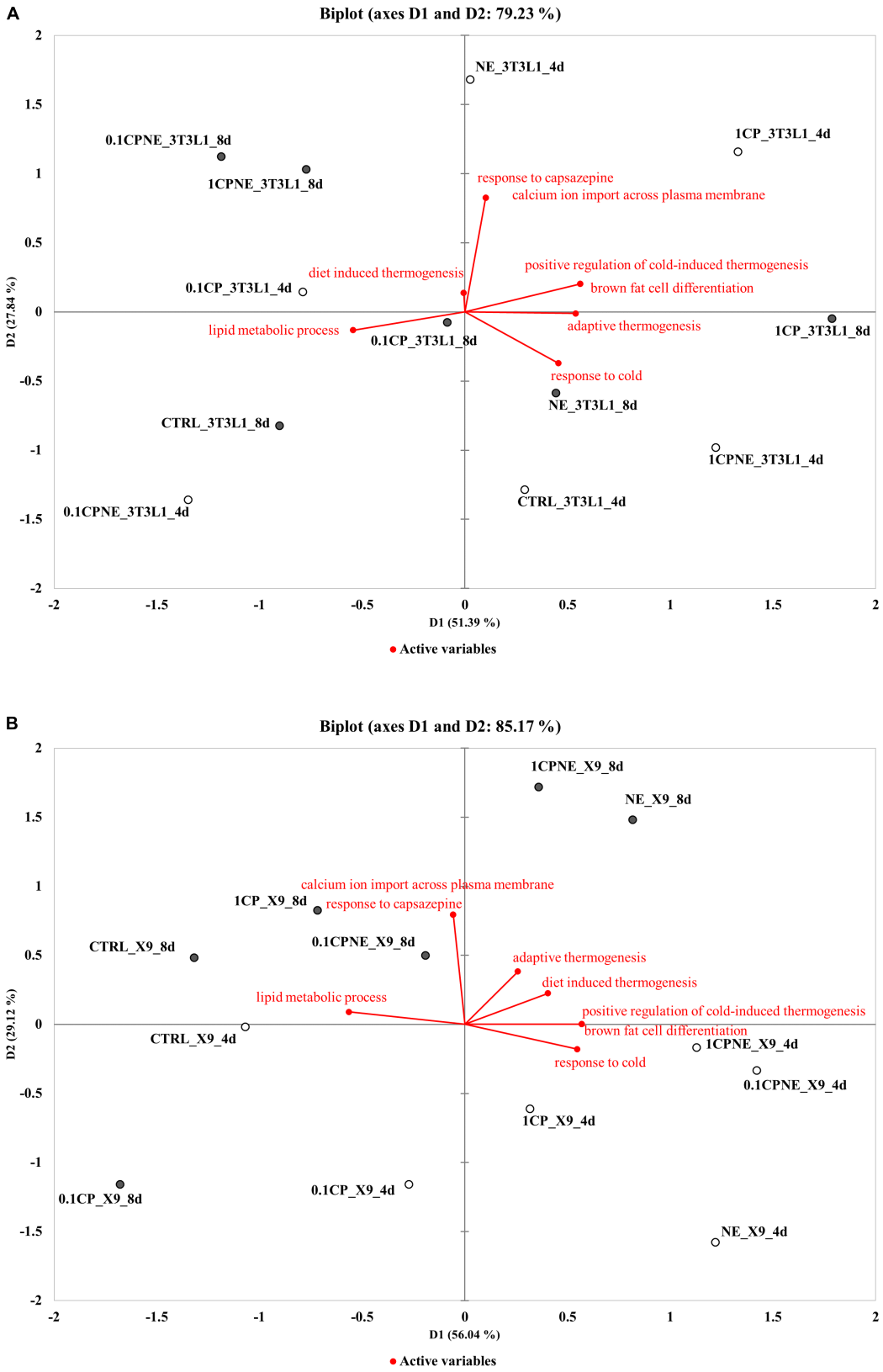

FIGURE 5 | Distance biplots of principal component analysis (PCA) to summarize and visualize the information of the data set containing the treatments (points, active observations) and biological process BPs (vectors, active variables) in **(A)** 3T3-L1 cells at 4 and 8 days and in **(B)** X9 cells at 4 and 8 days.

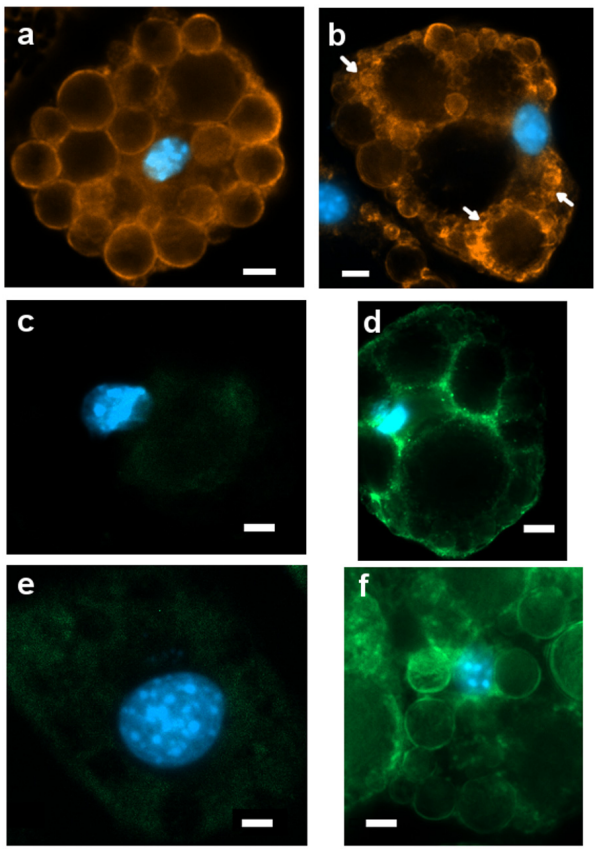

FIGURE 6 | Representative images (ROI) of immunoreactivity in CTRL and 1CP-treated 3T3-L1 cells after 8 days of differentiation (8d). **(a)** PLIN1 positivity along the large LDs in CTRL cells; **(b)** 1CP-treated cells showed PLIN1 immunoreactivity observed along the small and large LDs **(c)** no UCP1 immunoreaction was observed in CTRL cells **(d)** granular UCP1 cytoplasmic positivity in 1CP- treated cells; **(e)** no TRPV1 immunoreaction was observed in CTRL cells **(f)** 1CP-treated cells showed membrane and cytoplasmic TRPV1 immunostaining. Nuclear staining DAPI. Images are representative of n. 5 biological replicates. Scale bars: 5 μm.

and **Supplementary Movie S1**. No indicative fluorescence pulses were observed on cells treated with vehicle control or in X9 cells (data not shown).

DISCUSSION

This study aims to present the effects of different capsaicin treatments on 3T3-L1 and X9 cells, two metabolically distinct murine models, which differ in their functional role and browning response (White and Tchoukalova, 2014). X9 cells are composed of beige adipocytes, isolated from the subcutaneous inguinal adipose depot and display a more powerful response following β_3-adrenergic stimulation (Wu et al., 2012). While 3T3-L1 cells are an accurate model of WAT depots with visceral features, X9 can represent a subcutaneous pad, more prone to undergo browning. Although the effects of β_3-adrenergic stimulation appeared within few hours (Barneda et al., 2013), the treatment with NE was chosen to last as the capsaicin treatments (1 or 5 days) to compare the effects of the combination of NE and capsaicin at the same time.

Different functions of white and brown adipose tissues are reflected by LD morphology (Colitti et al., 2018), so the different response to browning of 3T3-L1 and X9 cells under capsaicin and NE treatment can be appreciated from the LD dynamic analysis.

Overall, in 3T3-L1 cells, NE and 1CPNE resulted the most effective treatment considering the LDs measurements. In terms of LDs area surface and MFD, NE treatment and the addition of capsaicin to NE (1CPNE and 0.1CPNE) were effective on 3T3-L1 cells. These results agreed with gene expression analysis recorded with 1CPNE and 0.1CPNE treatments after 4 days of differentiation (**Table 2**). According to Barneda et al. (2013), 3T3-L1 cells experiencing a β_3-adrenergic stimulation showed a LD size reduction due to lipolysis and a subsequent enlargement of newly formed LDs by a futile cycle of triglyceride hydrolysis and re-synthesis. The IOD value should be carefully considered, since the increase in triglyceride accumulation, evidenced by IOD value (Boschi et al., 2019) in all treatments and control, could be due to a *de novo* synthesis or by a triglyceride trafficking between LDs promoted by the CIDE proteins (Barneda et al., 2015).

Gene expression analysis performed on 3T3-L1 cells highlighted the administration of capsaicin 1 μM as the most powerful treatment on this cellular model, which displayed its greatest effects after 8 days of differentiation. 1CP-treated 3T3-L1 cells at 8 days promoted a significant expression of all brown markers as well as of *Trpv1*, indicating that exposure to capsaicin induced an up-regulation of its receptor. This observation has been confirmed by the detection of the intracellular flux of Ca^{2+} caused by TRPV1 activation. Interestingly, in X9 cells, intracellular flux of Ca^{2+} was not detected. It is known that in BAT TRPV1 activation leads to the SIRT1-mediated deacetylation of PPARγ and PRDM16, facilitating their interaction (Baskaran et al., 2017; Krishnan et al., 2019). Present results are coherent with the observation performed by Baboota et al. (2014), who stated that a 1 μM dose of capsaicin upregulates several thermogenic genes. Capsaicin 1 μM, increased the expression of *Ucp1*, *Tbx1*, *Prdm16*, *Ppargc1a* to trigger a beige phenotype. This was further confirmed by the immunostaining, which evidenced a positive immunoreaction of UCP1 in the cytoplasm of 1CP-treated cells at 8 days and corroborated by the expression of TRPV1 receptor. PLIN1 positivity was observed along small droplets surrounding the biggest ones during their dynamic rearrangement.

No other treatments administered to cultured 3T3-L1 cells produced any significant variation of the expression profile. Notably, NE-treated cells showed the lowest relative fold change values at both time points (**Table 2**), maybe due to the long NE exposure. In fact, rat epididymal adipose tissue minces exposed to various concentrations of catecholamine showed the highest expression of *Ppargc1a* after 2 h of treatment (Sutherland et al., 2009). On the other hand, it was demonstrated that chronic, but not acute exposure to catecholamine led 3T3-L1 adipocytes toward a brown adipocyte phenotype (Morrison and McGee, 2015). Possibly, the NE induction on gene expression was

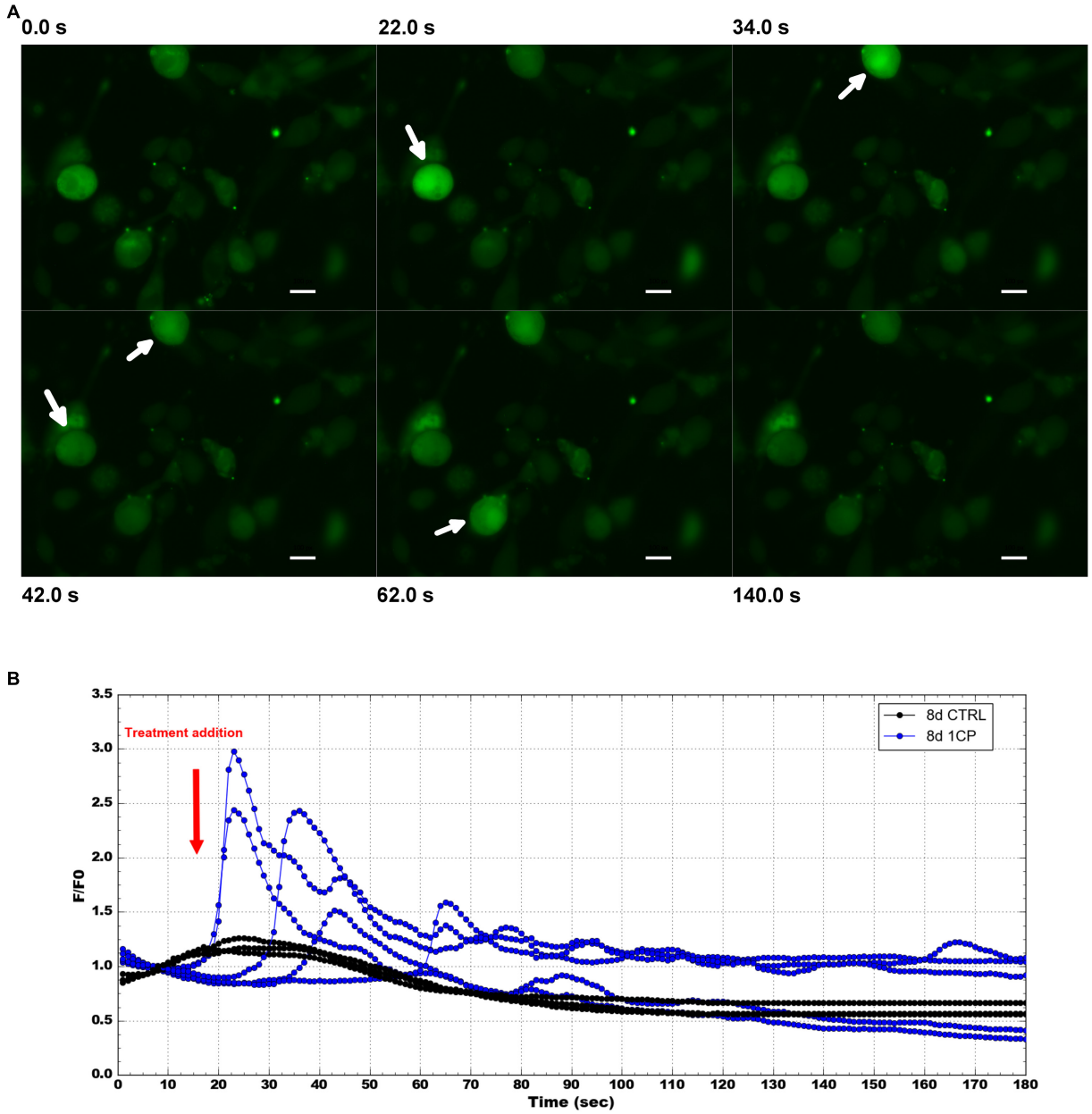

FIGURE 7 | Intracellular Ca^{2+} imaging and its fluorescence intensity changes on 3T3-L1 cells after 8 days of differentiation. **(A)** Selected images from Fluo-8 AM staining at different times before and after 1 μM capsaicin (1CP) or negative vehicle addition (CTRL) (at 12 s) Scale bars: 20 μm. **(B)** Plotted intracellular Ca^{2+} pulses expressed as the maximum fluorescence signal relative to its starting signal F/F0 and after background subtraction. Blue lines indicate fluorescence intensity after 1CP addition; black lines indicate fluorescence intensity after negative vehicle addition.

measured over time and may have induced a negative feedback on the cells (Higareda-Almaraz et al., 2018), thus inhibiting the typical brown-like gene expression profile. However, NE and 1CPNE treatments promoted LDs size reduction possibly activating a futile cycle of triglyceride hydrolysis (and re-synthesis). The up-regulation of *Cidea* relatively to *Cidec*, which did not show any significantly modulation among treatments at 4 days, could be related to the lack of LD fusion. In fact, while CIDEC is crucial for unilocular LD formation, CIDEA alone is not able to maintain the unilocular phenotype (Wu et al., 2014) and its mRNA expression increased during the cold-induced process independently of *Ucp1* expression (Barneda et al., 2013). Moreover, the over-expression of *Plin1* with a corresponding expression of *Cidec* at 8 days, facilitated the LDs enlargement in 1CP-treated 3T3-L1 cells, while CIDEA had a central role in packaging newly synthesized triglyceride in LDs for subsequent lipolysis and fatty acid oxidation useful in thermogenic cells. However, Nishimoto and Tamori (2017) claimed that FSP27β,

a novel isoform of CIDEC and abundantly expressed in BAT, is crucial in inhibiting the homodimerization of CIDEA and therefore in the formation of small multilocular LD.

To gain more insight into how capsaicin and NE regulate browning, we performed biological process enrichment analysis against UniProt mouse datasets. In this context, biological process involved in browning and capsaicin treatment were particularly enriched in 3T3-L1 cells at 8 days. The distance biplot of PCA highlighted these associations and, interestingly, 1CPNE and 1CP treatments were related to cold response and were opposite to lipid metabolism. This could suggest the efficacy of prolonged capsaicin treatments on 3T3-L1 cells, while adrenergic treatment was active after shorter stimulation.

The treatments that most affected the LDs dimensions in X9 cells were NE, 0.1CPNE and 1CPNE at both time points. Studies have demonstrated that lipogenesis and lipolysis are coupled in adipose tissue during chronic adrenergic stimulation (Mottillo et al., 2014). The significant decline in triglyceride content could account for the lipolysis, which is an essential prerequisite for UCP1 activation in brown and brite adipocytes (Braun et al., 2018) and in promoting energy dissipation in beige adipocytes independently of UCP1-mediated adaptive thermogenesis (Sepa-Kishi and Ceddia, 2018).

In terms of gene expression, browning markers were up-regulated by NE treatment in X9 cells, while capsaicin doses did not trigger a comparable variation of expression profile. This was confirmed by the fact that *Trpv1*, the membrane receptor for capsaicin, did not show a significant modulation at both time points. This is consistent with the proposed mechanism by which orally administered capsinoids bind to TRPV1 in the gut of mice and human activating a central signal through vagal nerves subsequently transmitted to inguinal WAT depots by the β_2-adrenoceptor (Snitker et al., 2009; Yoneshiro et al., 2013; Ohyama et al., 2016). Indeed, *Adrb3* was significantly up-regulated by NE at 4 days, activating the expression of browning marker genes. The combination of NE with capsaicin doses produced a significantly lower regulation of brown and brite markers, also in comparison to CTRL cells and to capsaicin treatments.

The distance biplot of PCA of X9 cells, obtained by enrichment analysis, depicted that BPs were involved in browning and response to cold and were associated to a cluster of treatments with NE (NE, 1CPNE, 0.1CPNE) at 4 days. They were negatively related to BPs involved in capsaicin response and lipid metabolism at 8 days. The response to NE observed in X9 cells mimed the cold mediated thermogenesis that stimulates sympathetic efferent (Beiroa et al., 2014), without involving TRPV1 induction, as observed by the lack of Ca^{2+} influx. Instead, in 3T3-L1 cells the observed positive response to browning at 8 days could be directly mediated by the TRPV1.

In terms of LDs dynamic on both cellular models and times of exposure, treatments with NE alone or in association with capsaicin produced a reduction of LDs area surface and size. It should be considered that LDs measurements were done on single cells snapshots in which the LDs remodeling cycle cannot be appreciated. For instance, in capsaicin-treated cells the larger size of LDs could be due to lipogenesis or lipid transference, while the reduction of LDs dimensions in NE-treated cells could be caused by the restart of lipolysis after LD enlargement process during futile cycle.

Present results achieved that *in vitro* chronic capsaicin treatment induced a brite phenotype in 3T3-L1 cells by direct stimulation of TRPV1 receptor. Capsaicin alone did not promote a browning effect on X9 cells, but beige adipocytes were activated, through ADRB3 receptor, only by NE or – to a lesser extent – by NE in association with capsaicin.

DATA AVAILABILITY STATEMENT

All the datasets for this study are available on request to the corresponding author.

AUTHOR CONTRIBUTIONS

TM and MC designed the study. TM performed the experiments and collected data. FB performed statistical analyses and assisted with data analysis. MC collected data measurements, prepared the figures and drafted the manuscript. All authors contributed in interpretation of results and in writing the manuscript.

SUPPLEMENTARY MATERIAL

The Supplementary Material for this article can be found online at: https://www.frontiersin.org/articles/10.3389/fphys.2019.01380/full#supplementary-material

FIGURE S1 | Modulation of MTT metabolism by treatments on 3T3-L1 cells **(A)** and X9 cells **(B)**. Differentiated adipocytes were incubated with different treatments. Values are reported as mean ± standard deviation (SD) of three independent experiments. CTRL = vehicle negative control; NE = 10 μM norepinephrine; 0.1CP = 0.1 μM capsaicin; 0.1CPNE = 0.1 μM capsaicin plus 10 μM norepinephrine; 1CP = 1 μM capsaicin; 1CPNE = 1 μM capsaicin plus 10 μM norepinephrine. 4d = at 4 days of differentiation; 8d = at 8 days of differentiation.

TABLE S1 | Lipid droplets measurements in 3T3-L1 cells after 4 (4d) days of differentiation and treated with different doses of compound. Total area surface (μm^2), MFD, Maximum Feret Diameter (μm); IOD = Intensity Optical Density (dimensionless). CTRL = vehicle negative control; NE = 10 μM norepinephrine; 0.1CP = 0.1 μM capsaicin; 0.1CPNE = 0.1 μM capsaicin plus 10 μM norepinephrine; 1CP = 1 μM capsaicin; 1CPNE = 1 μM capsaicin plus 10 μM norepinephrine. The data are shown as the mean ± standard deviation (SD). Significant pairwise comparisons are indicated in bold.

TABLE S2 | Lipid droplets measurements in 3T3-L1 cells after 8 (8d) days of differentiation and treated with different doses of compound. Total area surface (μm^2), MFD, Maximum Feret Diameter (μm); IOD = Intensity Optical Density (dimensionless). CTRL = vehicle negative control; NE = 10 μM norepinephrine; 0.1CP = 0.1 μM capsaicin; 0.1CPNE = 0.1 μM capsaicin plus 10 μM norepinephrine; 1CP = 1 μM capsaicin; 1CPNE = 1 μM capsaicin plus 10 μM norepinephrine. The data are shown as the mean ± standard deviation (SD). Significant pairwise comparisons are indicated in bold.

TABLE S3 | Lipid droplets measurements in X9 cells after 4 (4d) days of differentiation and treated with different doses of compound. Total area surface (μm^2), MFD, Maximum Feret Diameter (μm); IOD = Intensity Optical Density (dimensionless). CTRL = vehicle negative control; NE = 10 μM norepinephrine; 0.1CP = 0.1 μM capsaicin; 0.1CPNE = 0.1 μM capsaicin plus 10 μM norepinephrine; 1CP = 1 μM capsaicin; 1CPNE = 1 μM capsaicin plus 10 μM norepinephrine. The data are shown as the mean ± standard deviation (SD). Significant pairwise comparisons are indicated in bold.

TABLE S4 | Lipid droplets measurements in X9 cells after 8 (8d) days of differentiation and treated with different doses of compound. Total area surface (μm^2), MFD, Maximum Feret Diameter (μm); IOD = Intensity Optical Density (dimensionless). CTRL = vehicle negative control; NE = 10 μM norepinephrine; 0.1CP = 0.1 μM capsaicin; 0.1CPNE = 0.1 μM capsaicin plus 10 μM norepinephrine; 1CP = 1 μM capsaicin; 1CPNE = 1 μM capsaicin plus 10 μM norepinephrine. The data are shown as the mean ± standard deviation (SD). Significant pairwise comparisons are indicated in bold.

TABLE S5 | Enriched analysis of selected significant biological process performed by Funrich finding tool showing the percentage of annoated proteins in 3T3-L1 and X9 cell according to treatments and times. CTRL = vehicle negative control; NE = 10 μM norepinephrine; 0.1CP = 0.1 μM capsaicin; 0.1CPNE = 0.1 μM capsaicin plus 10 μM norepinephrine; 1CP = 1 μM capsaicin; 1CPNE = 1 μM capsaicin plus 10 μM norepinephrine. 4d = at 4 days of differentiation; 8d = at 8 days of differentiation.

MOVIE S1 | 3T3-L1 cells showing Ca^{2+} transients after capsaicin addition. Maximum fluorescence pulses were recorded at 20 and 42 s.

REFERENCES

Addinsoft (2017). *XLSTAT - Statistics Package for Excel, Paris*. Available at: http://www.xlstat.com (accessed December 18, 2018).

Baboota, R. K., Singh, D. P., Sarma, S. M., Kaur, J., Sandhir, R., Boparai, R. K., et al. (2014). Capsaicin induces "brite" phenotype in differentiating 3T3-L1 preadipocytes. *PLoS One* 9:e103093. doi: 10.1371/journal.pone.0103093

Bäcker, V. (2012). "ImageJ macro tool sets for biological image analysis," in *Proceedings of the ImageJ User and Developer Conference*, Luxembourg.

Barneda, D., and Christian, M. (2017). Lipid droplet growth: regulation of a dynamic organelle. *Curr. Opin. Cell Biol.* 47, 9–15. doi: 10.1016/j.ceb.2017.02.002

Barneda, D., Frontini, A., Cinti, S., and Christian, M. (2013). Dynamic changes in lipid droplet-associated proteins in the "browning" of white adipose tissues. *Biochim. Biophys. Acta* 1831, 924–933. doi: 10.1016/j.bbalip.2013.01.015

Barneda, D., Planas-Iglesias, J., Gaspar, M. L., Mohammadyani, D., Prasannan, S., Dormann, D., et al. (2015). The brown adipocyte protein CIDEA promotes lipid droplet fusion via a phosphatidic acid-binding amphipathic helix. *eLife* 4:e07485. doi: 10.7554/eLife.07485

Bartelt, A., and Heeren, J. (2014). Adipose tissue browning and metabolic health. *Nat. Rev. Endocrinol.* 10, 24–36. doi: 10.1038/nrendo.2013.204

Baskaran, P., Krishnan, V., Fettel, K., Gao, P., Zhu, Z., Ren, J., et al. (2017). TRPV1 activation counters diet-induced obesity through sirtuin-1 activation and PRDM-16 deacetylation in brown adipose tissue. *Int. J. Obes.* 41, 739–749. doi: 10.1038/ijo.2017.16

Baskaran, P., Krishnan, V., Ren, J., and Thyagarajan, B. (2016). Capsaicin induces browning of white adipose tissue and counters obesity by activating TRPV1 channel-dependent mechanisms. *Br. J. Pharmacol.* 173, 2369–2389. doi: 10.1111/bph.13514

Beiroa, D., Imbernon, M., Gallego, R., Senra, A., Herranz, D., Villarroya, F., et al. (2014). GLP-1 agonism stimulates brown adipose tissue thermogenesis and browning through hypothalamic AMPK. *Diabetes Metab. Res. Rev.* 63, 3346–3358. doi: 10.2337/db14-0302

Bevan, S., Quallo, T., and Andersson, D. A. (2014). TRPV1. *Handb. Exp. Pharmacol.* 222, 207–245. doi: 10.1007/978-3-642-54215-2_9

Bishnoi, M., Kondepudi, K. K., Gupta, A., Karmase, A., and Boparai, R. K. (2013). Expression of multiple transient receptor potential channel genes in murine 3T3-L1 cell lines and adipose tissue. *Pharmacol. Rep.* 65, 751–755. doi: 10.1016/s1734-1140(13)71055-7

Boschi, F., Rizzatti, V., Zoico, E., Montanari, T., Zamboni, M., Sbarbati, A., et al. (2019). Relationship between lipid droplets size and integrated optical density. *Eur. J. Histochem.* 63:3017. doi: 10.4081/ejh.2019.3017

Braun, K., Oeckl, J., Westermeier, J., Li, Y., and Klingenspor, M. (2018). Non-adrenergic control of lipolysis and thermogenesis in adipose tissues. *J. Exp. Biol.* 221:jeb165381. doi: 10.1242/jeb.165381

Cannon, B., and Nedergaard, J. (2004). Brown adipose tissue: function and physiological significance. *Physiol. Rev.* 84, 277–359. doi: 10.1152/physrev.00015.2003

Chu, D. T., Malinowska, E., Gawronska-Kozak, B., and Kozak, L. P. (2014). Expression of adipocyte biomarkers in a primary cell culture models reflects preweaning adipobiology. *J. Biol. Chem.* 289, 18478–18488. doi: 10.1074/jbc.M114.555821

Colitti, M., Boschi, F., and Montanari, T. (2018). Dynamic of lipid droplets and gene expression in response to β-aminoisobutyric acid treatment on 3T3-L1 cells. *Eur. J. Histochem.* 62:2984. doi: 10.4081/ejh.2018.2984

Cypess, A. M., Lehman, S., Williams, G., Tal, I., Rodman, D., Goldfine, A. B., et al. (2009). Identification and importance of brown adipose tissue in adult humans. *N. Engl. J. Med.* 360, 1509–1517. doi: 10.1056/NEJMoa0810780

El Hadi, H., Di Vincenzo, A., Vettor, R., and Rossato, M. (2019). Food ingredients involved in white-to-brown adipose tissue conversion and in calorie burning. *Front. Physiol.* 11:1954. doi: 10.3389/fphys.2018.01954

Gao, A. W., and Houtkooper, R. H. (2014). Mitochondrial fission: firing up mitochondria in brown adipose tissue. *EMBO J.* 33, 401–402. doi: 10.1002/embj.201487798

Gifford, A., Towse, T. F., Walker, R. C., Avison, M. J., and Welch, E. B. (2016). Characterizing active and inactive brown adipose tissue in adult humans using PET-CT and MR imaging. *Am. J. Physiol. Endocrinol. Metab.* 311, E95–E104. doi: 10.1152/ajpendo.00482.2015

Higareda-Almaraz, J. C., Karbiener, M., Giroud, M., Pauler, F. M., Gerhalter, T., Herzig, S., et al. (2018). Norepinephrine triggers an immediate-early regulatory network response in primary human white adipocytes. *BMC Genomics* 19:794. doi: 10.1186/s12864-018-5173-0

Krishnan, V., Baskaran, P., and Thyagarajan, B. (2019). Troglitazone activates TRPV1 and causes deacetylation of PPARγ in 3T3-L1 cells. *Biochim. Biophys. Acta* 1865, 445–453. doi: 10.1016/j.bbadis.2018.11.004

Livak, K. J., and Schmittgen, T. D. (2001). Analysis of relative gene expression data using real-time quantitative PCR and the 2-ΔΔCT method. *Methods* 25, 402–408. doi: 10.1006/meth.2001.1262

Montanari, T., and Colitti, M. (2018). Simpson-Golabi-Behmel syndrome human adipocytes reveal a changing phenotype throughout differentiation. *Histochem. Cell. Biol.* 149, 593–605. doi: 10.1007/s00418-018-1663-z

Montanari, T., Pošćić, N., and Colitti, M. (2017). Factors involved in white-to-brown adipose tissue conversion and in thermogenesis: a review. *Obes. Rev.* 18, 495–513. doi: 10.1111/obr.12520

Morrison, S., and McGee, S. L. (2015). 3T3-L1 adipocytes display phenotypic characteristics of multiple adipocyte lineages. *Adipocyte* 4, 295–302. doi: 10.1080/21623945.2015.1040612

Mottillo, E. P., Balasubramanian, P., Lee, Y. H., Weng, C., Kershaw, E. E., and Granneman, J. G. (2014). Coupling of lipolysis and de novo lipogenesis in brown, beige, and white adipose tissues during chronic β3-adrenergic receptor activation. *J. Lipid. Res.* 55, 2276–2286. doi: 10.1194/jlr.M050005

Muto, A., Ohkura, M., Abe, G., Nakai, J., and Kawakami, K. (2013). Real-time visualization of neuronal activity during perception. *Curr. Biol.* 23, 307–311. doi: 10.1016/j.cub.2012.12.040

Nishimoto, Y., and Tamori, Y. (2017). CIDE family-mediated unique lipid droplet morphology in white adipose tissue and brown adipose tissue determines the adipocyte energy metabolism. *J. Atheroscler. Thromb.* 24, 989–998. doi: 10.5551/jat.RV17011

Ohyama, K., Nogusa, Y., Shinoda, K., Suzuki, K., Bannai, M., and Kajimura, S. (2016). A synergistic antiobesity effect by a combination of capsinoids and cold temperature through promoting beige adipocyte biogenesis. *Diabetes Metab. Res. Rev.* 65, 1410–1423. doi: 10.2337/db15-0662

Pathan, M., Keerthikumar, S., Ang, C. S., Gangoda, L., Quek, C. Y., Williamson, N. A., et al. (2015). FunRich: an open access standalone functional enrichment and interaction network analysis tool. *Proteomics* 15, 2597–2601. doi: 10.1002/pmic.201400515

Peschechera, A., and Eckel, J. (2013). "Browning" of adipose tissue – regulation and therapeutic perspectives. *Arch. Physiol. Biochem.* 119, 151–160. doi: 10.3109/13813455.2013.796995

Reyes-Escogido Mde, L., Gonzalez-Mondragon, E. G., and Vazquez-Tzompantzi, E. (2011). Chemical and pharmacological aspects of capsaicin. *Molecules* 16, 1253–1270. doi: 10.3390/molecules16021253

Rozen, S., and Skaletsky, H. (2000). Primer3 on the WWW for general users and for biologist programmers. *Methods Mol. Biol.* 132, 365–386. doi: 10.1385/1-59259-192-2:365

Ruiz-Ojeda, F. J., Rupérez, A. I., Gomez-Llorente, C., Gil, A., and Aguilera, C. M. (2016). Cell models and their application for studying adipogenic differentiation in relation to obesity: a review. *Int. J. Mol. Sci.* 17:E1040. doi: 10.3390/ijms17071040

Sepa-Kishi, D. M., and Ceddia, R. B. (2018). White and beige adipocytes: are they metabolically distinct? *Horm. Mol. Biol. Clin. Investig.* 33:20180003. doi: 10.1515/hmbci-2018-2013

Snitker, S., Fujishima, Y., Shen, H., Ott, S., Pi-Sunyer, X., Furuhata, Y., et al. (2009). Effects of novel capsinoid treatment on fatness and energy metabolism in humans: possible pharmacogenetic implications. *Am. J. Clin. Nutr.* 89, 45–50. doi: 10.3945/ajcn.2008.26561

Sutherland, L. N., Bomhof, M. R., Capozzi, L. C., Basaraba, S. A., and Wright, D. C. (2009). Exercise and adrenaline increase PGC-1α mRNA expression in rat adipose tissue. *J. Physiol.* 587, 1607–1617. doi: 10.1113/jphysiol.2008.165464

White, U. A., and Tchoukalova, Y. D. (2014). Sex dimorphism and depot differences in adipose tissue function. *Biochim. Biophys. Acta* 1842, 377–392. doi: 10.1016/j.bbadis.2013.05.006

Wu, J., Boström, P., Sparks, L. M., Ye, L., Choi, J. H., Giang, A. H., et al. (2012). Beige adipocytes are a distinct type of thermogenic fat cell in mouse and human. *Cell* 150, 366–376. doi: 10.1016/j.cell.2012.05.016

Wu, L., and Xu, B. (2017). "Using thermogenic beige cells to identify biologically active small molecules and peptides," in *Thermogenic Fat: Methods and Protocols, Methods in Molecular Biology*, Vol. 1566, ed. J. Wu, (New York, NY: Humana Press), 203–212. doi: 10.1007/978-1-4939-6820-6_19

Wu, L., Zhou, L., Chen, C., Gong, J., Xu, L., Ye, J., et al. (2014). Cidea controls lipid droplet fusion and lipid storage in brown and white adipose tissue. *Sci. China Life Sci.* 57, 107–116. doi: 10.1007/s11427-013-4585-y

Yoneshiro, T., Aita, S., Matsushita, M., Kayahara, T., Kameya, T., Kawai, Y., et al. (2013). Recruited brown adipose tissue as an antiobesity agent in humans. *J. Clin. Invest.* 123, 3404–3408. doi: 10.1172/JCI67803

Yu, X., Yu, M., Liu, Y., and Yu, S. (2016). TRP channel functions in the gastrointestinal tract. *Semin. Immunopathol.* 38, 385–396. doi: 10.1007/s00281-015-0528-y

Conflict of Interest: The authors declare that the research was conducted in the absence of any commercial or financial relationships that could be construed as a potential conflict of interest.